VOLUME 81 JUNE 2, 1977 NUMBER 11

JPCHAx

THE JOURNAL OF PHYSICAL CHEMISTRY

PUBLISHED BIWEEKLY BY THE AMERICAN CHEMICAL SOCIETY

THE JOURNAL OF

PHYSICAL CHEMISTRY

Published by the
AMERICAN CHEMICAL SOCIETY
BOOKS AND JOURNALS DIVISION
D. H. Michael Bowen, Director
Marjorie Laflin, Assistant to the Director

Editorial Department: Charles R. Bertsch, Head; Marianne C. Brogan, Associate Head; Celia B. McFarland, Joseph E. Yurvati, Assistant Editors
Magazine and Production Department: Bacil Guiley, Head
Research and Development Department: Seldon W. Terrant, Head

Advertising Office: Centcom, Ltd., 25 Sylvan Road South, Westport, Conn. 06880.

Published biweekly by the American Chemical Society at 20th and Northampton Sts., Easton, Pennsylvania 18042. Second class postage paid at Washington, D.C. and at additional mailing offices.

Editorial Information

Instructions for authors are printed in the first issue of each volume. Please conform to these instructions when submitting manuscripts.

Manuscripts for publication should be submitted to *The Journal of Physical Chemistry*, Department of Chemistry, University of Minnesota, Minneapolis, Minn. 55455. Correspondence regarding **accepted papers and proofs** should be directed to the Editorial Department at the ACS Easton address.

Page charges of $60.00 per page may be paid for papers published in this journal. Ability to pay does not affect acceptance or scheduling of papers.

Bulk reprints or photocopies of individual articles are available. For information write to Business Operations, Books and Journals Division at the ACS Washington address.

Requests for **permission to reprint** should be directed to Permissions, Books and Journals Division at the ACS Washington address. The American Chemical Society and its Editors assume no responsibility for the statements and opinions advanced by contributors.

Subscription and Business Information

1977 Subscription rates—including surface postage

	U.S.	PUAS	Canada, Foreign
Member	$24.00	$33.00	$34.00
Nonmember	96.00	105.00	106.00
Supplementary material	15.00	19.00	20.00

Air mail and air freight rates are available from Membership & Subscription Services, at the ACS Columbus address.

New and renewal subscriptions should be sent with payment to the Office of the Controller at the ACS Washington address. **Changes of address** must include both old and new addresses with ZIP code and a recent mailing label. Send all address changes to the ACS Columbus address. Please allow six weeks for change to become effective. **Claims for missing numbers** will not be allowed if loss was due to failure of notice of change of address to be received in the time specified: if claim is dated (a) North America—more than 90 days beyond issue date, (b) all other foreign—more than 1 year beyond issue date; or if the reason given is "missing from files". Hard copy claims are handled at the ACS Columbus address.

Microfiche subscriptions are available at the same rates but are mailed first class to U.S. subscribers, air mail to the rest of the world. Direct all inquiries to Special Issues Sales, at the ACS Washington address or call (202) 872-4554. **Single issues** in hard copy and/or microfiche are available from Special Issues Sales at the ACS Washington address. Current year $4.75. Back issue rates available from Special Issues Sales. **Back volumes** are available in hard copy and/or microform. Write to Special Issues Sales at the ACS Washington address for further information. **Microfilm** editions of ACS periodical publications are available from volume 1 to the present. For further information, contact Special Issues Sales at the ACS Washington address. **Supplementary material** mentioned in the journal appears in the microfilm edition. Single copies may be ordered directly from Business Operations, Books and Journals Division, at the ACS Washington address.

	U.S.	PUAS, Canada	Other Foreign
Microfiche	$2.50	$3.00	$3.50
Photocopy			
1-7 pages	4.00	5.50	7.00
8-20 pages	5.00	6.50	8.00

Orders over 20 pages are available only on microfiche, 4 × 6 in., 24X, negative, silver halide. Orders must state photocopy or microfiche if both are available. Full bibliographic citation including names of all authors and prepayment are required. Prices are subject to change.

American Chemical Society
1155 16th Street, N.W.
Washington, D.C. 20036
(202) 872-4600

Member & Subscription Services
American Chemical Society
P.O. Box 3337
Columbus, Ohio 43210
(614) 421-7230

Editorial Department
American Chemical Society
20th and Northampton Sts.
Easton, Pennsylvania 18042
(215) 258-9111

Notice to Authors last printed in the issue of January 13, 1977

THE JOURNAL OF

PHYSICAL CHEMISTRY

Volume 81, Number 11 June 2, 1977

JPCHAx 81(11) 1031–1124 (1977)

ISSN 0022-3654

COMMUNICATIONS TO THE EDITOR

There is no supplementary material for this issue.

* In papers with more than one author, the asterisk indicates the name of the author to whom inquiries about the paper should be addressed.

AUTHOR INDEX

THE JOURNAL OF
PHYSICAL CHEMISTRY

VOLUME 81, NUMBER 11 JUNE 2, 1977

Products of the Gas Phase Reaction K + CF_3I

John R. Hardee and Philip R. Brooks*

Department of Chemistry, Rice University, Houston, Texas 77001 *(Received January 10, 1977)*

Publication costs assisted by the National Science Foundation

The reaction between K and CF_3I was studied in the milliTorr pressure range in a bell jar for comparison with molecular beam experiments. Macroscopic amounts of salt were collected and analyzed by wet chemical techniques. The relative amount of KI formed increased as the CF_3I pressure was raised, and it is concluded that KI is formed in gas phase collisions with a reactive cross section of roughly 15 $Å^2$ and that KF is formed by reaction at the surface of the bell jar.

I. Introduction

Molecular beam chemiluminescence and laser techniques have made possible the accumulation of a vast array of information concerning the intimate details of simple chemical reactions.[1] Indeed, for favorable cases one can almost routinely determine how much energy is channeled into product excitation, which product states are formed, how these states depend on the energy of the reagents, and how the products are distributed spatially. Ready availability of high speed digital computers allows comparison of calculated trajectories with experiment and enables one to make qualitative inferences about the potential-energy hypersurface governing the motion of the system.[2]

Despite the power inherent in these techniques, ambiguities still arise, the most serious of these being the inability to specify which reaction one is studying. For example, many molecular beam studies have been made using alkali metals because the product molecules can easily be detected with a surface ionization detector which selectively ionizes only molecules containing an alkali metal. Unfortunately, this detector does not discriminate between different alkali-containing molecules, such as KI or KF, if more than one product is possible.

In previous molecular beam experiments we studied the reaction of K atoms with CF_3I molecules which had been oriented prior to reaction.[3] An alkali-containing product, KX, was observed when K was incident on either the I end ("heads") or the CF_3 end ("tails") of the molecule, but because a surface ionization detector was used, it was impossible to distinguish between KI and KF and to thereby distinguish between the two possibilities

$$K + CF_3I \rightarrow KI + CF_3 \quad (1a)$$

$$\rightarrow KF + CF_2I \quad (1b)$$

The product KX is scattered into different center-of-mass (CM) angles depending on the original orientation of the CF_3I molecule. Backward scattering of KX is observed for reaction from the heads or I end, and since this is almost identical with the scattering from oriented CH_3I, we conclude that the product formed at the I end is KI.

In the tails configuration of the CF_3I molecule, K atom attack gives KX product forward scattered. If this product is KF, a complicated mechanism is suggested whereby KF is formed upon impact on the molecule and then the newly formed KF somehow passes the CF_2I group and is thrown forward. On the other hand, if KI were the product, one could postulate the K atom passing by (or through) the CF_3 end of the molecule and plucking off the I in a quasistripping reaction. Unfortunately, the limited thermodynamic data available suggest that both KF and KI are possibilities and, although formation of KI was strongly suggested, no definite conclusions can be reached about the identity of the product nor about the reaction mechanism.

In this note we describe experiments in which macroscopic amounts of salt formed from the K + CF_3I reaction were collected and analyzed by wet chemical techniques. Both KF and KI were found, but KF appeared to be formed by a surface reaction, and we conclude that the

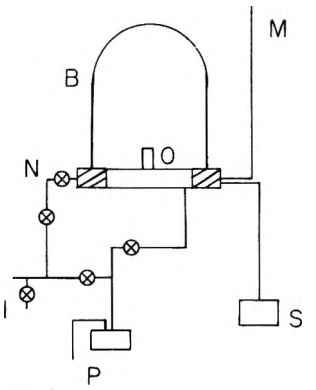

Figure 1. Schematic diagram of apparatus: (B) bell jar, (O) oven, (M) McLeod gauge, (N) needle valve, (I) gas inlet, (P) pumps, (S) oven heater power supply.

single collision molecular beam experiments yield solely KI.

II. Experimental Section

A schematic diagram of the apparatus[4] is shown in Figure 1. The reaction vessel is a 15 cm diameter × 30 cm bell jar evacuated through 1.5-cm diameter tubing by a cold trap and a 5-cm Cenco diffusion pump. Potassium atoms effuse from a 1.6-mm diameter orifice in a stainless steel oven heated to about 200 °C and mounted in the bell jar base plate. CF_3I was vacuum degassed, thermostatted at −78 °C in a dry ice–acetone bath, and introduced into the bell jar through the base plate. The steady-state pressure of CF_3I in the bell jar was controlled by a leak valve in the gas line and periodically throughout each run the pressure in the bell jar was measured with an untrapped mercury McLeod gauge; the pressure could be held constant to within ca. ±2 mTorr.

The CF_3I was admitted to the bell jar as the K oven was heated and the pressure stabilized at a value in the range 0.8–10 mTorr before the K oven reached its steady-state temperature. Reaction was allowed to proceed until a thin film of salt appeared on the sides of the bell jar. Reaction times (approximately the time the K oven was at its steady-state temperature) were on the order of 1 h. At higher pressures the oven orifice became clogged with salt before enough product was deposited on the bell jar walls for chemical analysis. This clogging was alleviated up to partial pressures of CF_3I of 12 mTorr by a steady-state pressure of N_2 of 0.04 Torr maintained in the bell jar by running dry N_2 into the top of the oven and through the orifice.

At the end of the reaction, the oven was cooled, the apparatus vented, and the products deposited on the bell jar were rinsed with water into a volumetric flask. Any contribution made by reaction on the surface of the molten potassium is thereby minimized because the potassium is contained in a separate oven and deposits inside the oven are not included in the analyses. Iodide concentrations were determined using a Volhard method[5] by adding a known excess of 0.02 M $AgNO_3$ and back titrating with 0.02 M KSCN using $FeNH_4(SO_4)_2$ as an indicator. Fluoride ion concentrations were determined using an Orion Model 94-09 specific fluoride ion electrode[6] by comparing the emf of the unknown solution to the emf of solution[5] of known concentration. Further details may be found in ref 4.

III. Results

The results obtained are given in Table I. Interpretation of these data in a traditional rate sense is complicated by uncertainties in (a) reaction times due to clogging of the oven orifice and (b) flux of K atoms due to small changes in oven temperature. For these reasons we focus our attention on the *ratio* of products, KI/KF.

TABLE I

P_{CF_3I}, m Torr	$[I^-]$, mmol	$[F^-]$, mmol	I^-/F^-	Time, h
0.8	0.084	0.24	0.35	1.25
1.8	0.12	0.19	0.63	1.5
2.0	0.10	0.14	0.71	2
4.0	0.13	0.025	5.2	1
7.4	0.23	0.031	7.4	1
11.0	0.24	0.021	11.4	1

Several experiments not shown in Table I demonstrated that KF was easily formed in surface reactions. Large amounts of KF were found in the early stages of these experiments as a result of reaction on the surface of Teflon-coated wires to give KF and visible carbon deposits. Teflon was therefore removed from the bell jar. In other experiments, a K film was plated out on the inside of the bell jar and then CF_3I (<10 mTorr) was admitted until the metallic film disappeared; the process was then repeated. For reaction on the metal surface, the KI/KF ratio ranged from 0.25 to 0.65, showing that KF was the dominant surface product.

The data in Table I clearly show that KI becomes the dominant product as the pressure is raised. Some KF is undoubtedly formed in secondary collisions of K atoms with CF_3 radicals produced in the KI formation, but even at the lowest pressures used, the concentration of CF_3 should only be about 5% of the concentration of CF_3I. Since the beam experiments show a reactive cross section of CF_3I near gas kinetic, it is unlikely that CF_3 is more reactive than CF_3I, so product from K–CF_3 collisions will not account for more than about 5% of that from K–CF_3I collisions. In addition, the mean free path at these pressures is comparable to the dimensions of the bell jar, making wall reactions likely. Since KF decreases with increasing pressure, we conclude that KF is formed on the walls and that KI is formed by K–CF_3I collisions. If the pressure is increased, fewer K atoms reach the surface of the bell jar and, instead, form KI in gas phase collisions.

The reactive cross section to form KI may be estimated by assuming that KI is formed only in gas phase collisions, and that each K atom hitting the bell jar reacts to form only KF. If F_0 is the flux of K atoms from the oven, the flux after passing a distance l through a gas of number density n of reactive cross section σ is $F = F_0 \exp(-nl\sigma)$, and can be equated to the rate of formation of KF on the surface. The flux which disappears, $F_0 - F = F_0[1 - \exp(-nl\sigma)]$, is the rate of formation of KI, and the ratio of KI to KF is given by

$$KI/KF = [1 - \exp(-nl\sigma)]/\exp(-nl\sigma)$$
$$= \exp(nl\sigma) - 1$$

independent of F_0. Figure 2 shows log (KI/KF + 1) plotted vs. P and is consistent with our earlier value,[3] KI/KF > 20, $P \sim 60$ mTorr. (In the earlier study KF was formed in amounts less than the limit of detectability.[7]) From the slope of the line we estimate σ to be 15 Å^2, but fluctuations in the pressure during the course of a run require that this number be regarded only as an estimate. Careful control of the pressure during reaction would make this method more reliable for determining rate constants, but the goal of this work was to determine which product, KI or KF, was formed.

IV. Conclusions

We conclude that the product of a gas phase K–CF_3I collision is predominantly (>90%) KI. A large body of

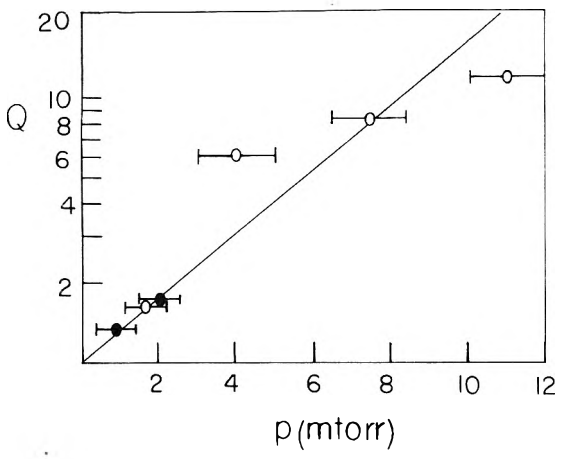

Figure 2. KI/KF + 1 ≡ Q plotted vs. CF_3I pressure in bell jar. Symbols are larger than errors in Q, and filled symbols represent runs in which N_2 was not admitted through the oven.

other evidence is consistent with this conclusion: In the early diffusion flame experiments, Polanyi[8] found that alkyl fluorides were orders-of-magnitude less reactive with sodium than alkyl iodides, presumably because the C–F bond is much stronger than the C–I bond (117 as compared to 56 kcal/mol).[9] Reaction to form KF is thus approximately thermoneutral whereas that to form KI is exoergic by 24 kcal/mol. Velocity analysis experiments show that about 10 kcal/mol of energy is converted to translational energy of the products,[10] strongly suggesting that the product cannot be KF. Unfortunately, uncertainties in the CF_2I–F bond energy do not unambiguously rule out formation of KF.

The oriented molecule experiments have been interpreted[3] by a charge-transfer or curve-crossing process in which the easily ionized alkali atom loses an electron to the electronegative CF_3I. The extra electron on CF_3I^- will be in the lowest unfilled orbital, centered mainly on I, and if the ion were unstable, it would decompose into CF_3 and I^-. Negative ion charge exchange experiments[11] on CF_3I at high energies show indeed that the CF_3I^- ion dissociates to I^-, and CF_3. Measurements near threshold for ion pair formation confirm this.[12] The I^- will be ejected from the CF_3I^- ion in the direction of the molecular axis, so forward KI scattering is consistent with tails orientation and backward KI scattering is consistent with heads orientation. In neither case should KF be formed.

Acknowledgment. This work was supported by the National Science Foundation. We wish to thank G. Marcelin, G. Young, and R. Davis for their early contributions to this study.

References and Notes

(1) J. M. Farrar and Y. T. Lee, *Annu. Rev. Phys. Chem.*, **25**, 357 (1974).
(2) R. N. Porter, *Annu. Rev. Phys. Chem.*, **25**, 317 (1974).
(3) P. R. Brooks, *Faraday Discuss. Chem. Soc.*, **55**, 299 (1973).
(4) J. R. Hardee, M.S. Thesis, Rice University, 1977.
(5) E. S. Gilreath, "Elementary Quantitative Analysis", W. H. Freeman, San Francisco, Calif., 1969.
(6) M. S. Frant and J. W. Ross, Jr., *Science*, **154**, 1553 (1966).
(7) Several exploratory experiments were done by G. Young in a Polanyi-type reactor (ref 8) at higher pressures (~40 mTorr). Ratios of KI to KF were found to be 400–2000, but uncertainties in analyzing fluoride were large and those results are consequently not shown. They do illustrate the strong preference for formation of KI and suggest that any "curvature" at high pressures in Figure 2 arises from experimental uncertainty.
(8) M. Polanyi, "Atomic Reactions", Williams and Norgate, London, 1932.
(9) S. W. Benson, *J. Chem. Educ.*, **42**, 502 (1963).
(10) A. M. Rulis, B. E. Wilcomb, and R. B. Bernstein, *J. Chem. Phys.*, **60**, 2822 (1974).
(11) E. W. Rothe, S. Y. Yang, and G. P. Reck, *Chem. Phys. Lett.*, **26**, 434 (1974).
(12) P. E. McNamee, K. Lachman, and D. R. Herschbach, *Faraday Discuss. Chem. Soc.*, **55**, 318 (1973).

Temperature Variation of Rate Constants for Atom Recombination

Neil S. Snider* and Derek G. Leaist

Department of Chemistry, Queen's University, Kingston, Ontario, Canada, K7L 3N6 *(Received November 11, 1976)*

Publication costs assisted by the National Research Council of Canada

A new two-parameter function (eq 3) was fitted to gas phase recombination rate constants k_r over wide temperature ranges for a number of diatomic molecules. The resulting curves were found in most cases to lie within the limits of experimental error of the data. The new function reproduces the observed variation of k_r with T somewhat better than do the Arrhenius and the inverse power functions which are customarily used to fit such data. The new function is based on a simple model. One of its adjustable parameters T^* is interpretable in terms of the model as the temperature above which the average internal energy gained (or lost) by the diatom in a collision with the third body is less than kT. For Br and I atom recombination with the rare gases as third bodies, T^* varies linearly with the polarizability of the third body. This correlation suggests that intermolecular attraction is important in determining the amount of energy transferred by collision to the rotational–vibrational degrees of freedom of the diatom.

Introduction

The rate constant k_r for the gas phase recombination of atoms to form diatomic molecules

$$2A \xrightarrow{M} A_2$$

is noteworthy in that it decreases with temperature. For purposes of expressing experimental values of k_r as a function of T, two equations have been employed. Each of these equations has two adjustable parameters. The one is an equation of the Arrhenius form

$$k_r = Ae^{-E_a/RT} \quad (1)$$

where E_a is sometimes referred to as a negative activation

energy. The other is the inverse power equation

$$k_r = B(T_0/T)^n \tag{2}$$

where T_0 is chosen arbitrarily and B and n are the adjustable parameters. Equation 1 has been found to usually give a better fit to the low temperature data whereas eq 2 is better at high temperatures.

Theory does not provide a compelling reason for choosing either (1) or (2). However, theoretical arguments can be brought forward in support of the following two-parameter equation:

$$k_r = C \sinh (T^*/T) \tag{3}$$

Although these arguments are speculative, they do provide a means for relating the temperature dependence of k_r to its underlying causes.

The work reported here has three objectives. The first is a theoretical justification, however limited, of eq 3. The second is a determination of which of eq 1–3 gives the best representation of k_r's measured over wide temperature ranges. A by-product of this portion of the investigation is the determination of a set of parameters (two for each equation) for each of the A_2–M pairs considered. The third objective is the correlation of values of C and T^* derived from the experimental data with other properties of the A_2–M pair to which the parameters correspond.

Theory

Recombination of diatomic molecules A_2 is now regarded as a multistep process which begins with the formation of A_2 in a highly excited rotational–vibrational state. The newly formed A_2 may redissociate in the next collision with the third body M, or it may be deactivated. The average amount of energy transferred in an A_2–M collision is typically of order kT. It is therefore small compared to the dissociation energy at temperatures for which experiments have been done. Hence, many collisions are required to deactivate A_2 to a level with an appreciable equilibrium population. Dissociation may be regarded as the reverse of this process. Hence, an adequate theory of diatom dissociation and recombination must include the formulation of detailed rate constants both for collisional transitions between states of the diatom and for transitions to and from states of the unbound atoms.

There is some theoretical evidence[1,2] to suggest that a fairly satisfactory model for these detailed rate constants is the separable exponential model. This model is based on an expression for $\mathbf{K}(y', y)\,dy'$, the rate constant for transitions between states of a given y and states in the interval y' to $y' + dy'$. The variable y is essentially the energy of the diatom divided by kT. For the separable exponential model $\mathbf{K}$ is given by

$$\begin{aligned}&\mathbf{K}(y', y)\,\rho(y)\\ &\quad = k_0 \exp[-y_d - (\beta - \alpha)y - \alpha(y - y')]\\ &\quad \text{for } y > y'\\ &\quad = k_0 \exp[-y_d - (\beta - \alpha)y' - \alpha(y' - y)]\\ &\quad \text{for } y < y'\end{aligned} \tag{4}$$

where $\rho(y)$ is the Boltzmann distribution function, y_d is the dissociation energy divided by kT, and k_0, α, β are parameters of the model. The parameter α is a measure of how rapidly the rate falls off with increasing separation of the energies of the initial and final states. The parameter difference $\beta - \alpha$ is a measure of how slowly the rate increases with increasing energy of the initial state at fixed separation of initial and final energies. The two trends characterized by α and $\beta - \alpha$ are probably the most important ones exhibited by the actual rate constants. It is worth emphasizing that kT is the unit of energy in this discussion.

We here make use of k_d, the dissociation rate constant for the separable exponential model. Also of interest is $k_d^{(e)}$, the rate constant for dissociation which would apply if the molecules were to maintain a Boltzmann distribution among their internal states. Derivations of these quantities have been presented in detail elsewhere.[3] Only the results need be cited here

$$k_d = \frac{k_0}{\alpha\beta}\left(1 - \frac{\alpha^2}{\beta^2}\right)e^{-y_d} = \frac{k_0}{\gamma\beta^2}(1 - \gamma^2)e^{-y_d} \tag{5a}$$

$$k_d^{(e)} = \frac{k_0}{\alpha\beta}e^{-y_d} = \frac{k_0}{\gamma\beta^2}e^{-y_d} \tag{5b}$$

where γ is α/β. We see that the rate constant is decreased by a factor $1 - \gamma^2$ because the molecules do not remain in a Boltzmann distribution during reaction. The recombination rate constant is obtained by dividing eq 4 by the equilibrium constant for dissociation. We write this equilibrium constant in the form

$$K = K_0 e^{-y_d}$$

Hence, we find k_r for the separable exponential model to be given by

$$k_r = {}^1/_2\, C(\gamma^{-1} - \gamma) \tag{6}$$

where C is defined to be $2k_0/K_0\beta^2$.

Theoretical studies of the temperature dependences of α and β are scarce. What evidence there is[2] indicates that β is temperature independent and that α approaches β as temperature increases. An expression for γ of the form

$$\gamma = \exp(-T^*/T) \tag{7}$$

where T^* is a constant, is consistent with these observations. In the harmonic oscillator-rigid rotor approximation K_0 is proportional to $T^{1/2}$ if kT is small compared to Planck's constant times the oscillator frequency. Furthermore, hard-sphere collision theory suggests a $T^{1/2}$ dependence for k_0. Hence, a first guess is that C is independent of T. Substitution of (7) in (6) gives (3)

$$k_r = C \sinh (T^*/T)$$

Note that for T much less than T^*, (3) reduces to (1) with E_a equal to $-RT^*$ and that for T much greater than T^* it reduces to (2) with n equal to one. It remains to be seen how well this equation fits the experimental data.

The Fitting Procedure

Experimental studies of dissociation and recombination are numerous for some A_2–M pairs. Furthermore, the temperature ranges of these studies are in some cases as large as several thousand degrees Kelvin. For the purpose of testing eq 1–3, two sets of data were used for any given A_2–M pair, a low temperature set derived from studies of recombination and a high temperature set derived from studies of dissociation. For the latter it was assumed that values of k_r obtained by division of the experimental k_d's by K could be compared with k_r's obtained for the same system at the lower temperatures. There is now a good deal of evidence, both experimental and theoretical, that this assumption is valid.

For a given system in either the low or high temperature range, only the data of a single investigation were used. Thus all of the tests reported here (and some not reported) make use of two sets of data for each A_2–M pair consid-

ered. In a number of cases a large temperature gap exists between the two sets. In such cases one might also regard eq 1–3 as interpolation formulas. The tests reported here make use of the most recent sets of data in most cases. For Br atom recombination, however, this policy has not been followed. Instead of the most recent recombination data[4] for Br_2, the results of a somewhat earlier study were employed[5] since these were obtained over much wider temperature ranges. Also for Br_2 dissociation the results of a study[6] which predates the most recent one[7] were used because in the former study results were obtained for rare gases other than argon as third bodies. Only data for temperatures above 1500 K were used because there is good cause to believe that the method by which these data were obtained is unreliable at lower temperatures.[7]

Standard least-squares techniques were used to fit the data. In the cases of eq 1 and 2 the best straight lines were sought for $\log k_r$ vs. T^{-1} and $\log k_r$ vs. $\log T$, respectively. For eq 3 an iterative procedure, described in the Appendix, was used to fit $\log k_r$ vs. T. In a number of shock tube studies the original method of data analysis was such that the final result for k_d emerged as a function of T. In these cases points generated from the reported function were used in the present analysis. Each data point for a given A_2–M pair was weighted according to the temperature interval I_i that it represented and the error σ_i assigned to it. The weighting factor w_i for the ith point was thus taken to be

$$w_i = \frac{I_i}{\sigma_i^2}\left[\sum_{i=1}^{N}\frac{I_i}{\sigma_i^2}\right]^{-1} \tag{8}$$

where σ_i is the logarithmic error[8] and N is the total number of points. To find I_i, the temperature range spanned by the subset of points to which point i belonged was divided by the total number of points in this subset.

In most cases error bounds were quoted by the investigators who made the measurements. In some cases these bounds were the limits of precision. Comparison of values of the same rate constants obtained in different investigations indicates that limits of accuracy may be wider. For a few shock tube studies no error bounds were reported. In these cases bounds were assigned on the basis of qualitative assessments by the investigators and/or on the basis of what was considered a typical error for such measurements. It has been assumed in the present study that the most recent investigations have yielded the most accurate results. Hence the conclusions of the present study are based largely on these investigations.

In studies of correlations of T^* and C with other properties of A_2 and M it is useful to have some estimate of the uncertainties in these parameters. The following formulas were employed for this purpose:

$$\delta T^* = \frac{\langle (y - \langle y\rangle)(\sigma - \langle\sigma\rangle)\rangle}{\langle (y - \langle y\rangle)^2\rangle} \tag{9a}$$

$$\delta\mu = \langle\sigma\rangle - \langle y\rangle\,\delta T^* \tag{9b}$$

where δ denotes uncertainty, μ is $\log C$, fences denote average with weighting factors given by eq 8, and y_i is given by

$$y_i = (T_i \ln 10)^{-1}\,\mathrm{ctnh}\,(T^*/T_i)$$

Equations 9 are derived in the Appendix. It is to be noted that y_i is always positive and decreasing with temperature. Thus the uncertainty in μ is amplified if the errors in the high temperature data are greater than those in the low temperature data.

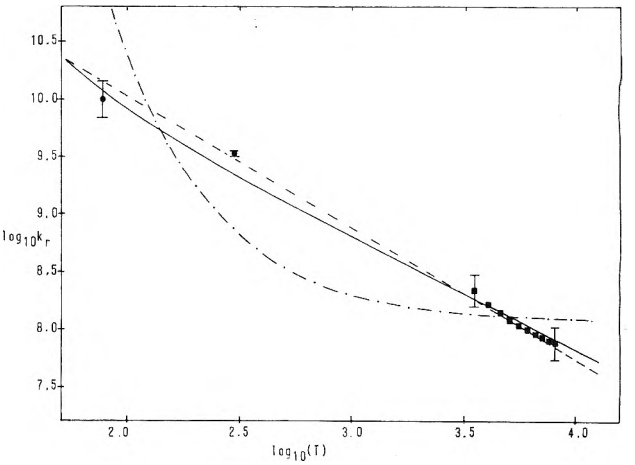

Figure 1. Fits of eq 1–3 to recombination rate constants for H_2 in Ar. Data points were obtained from ref *b* and *c* of Table I. Dot-dashed line represents eq 1, dashed line eq 2, and solid line eq 3. Circles represent low temperature measurements, squares represent high temperature measurements.

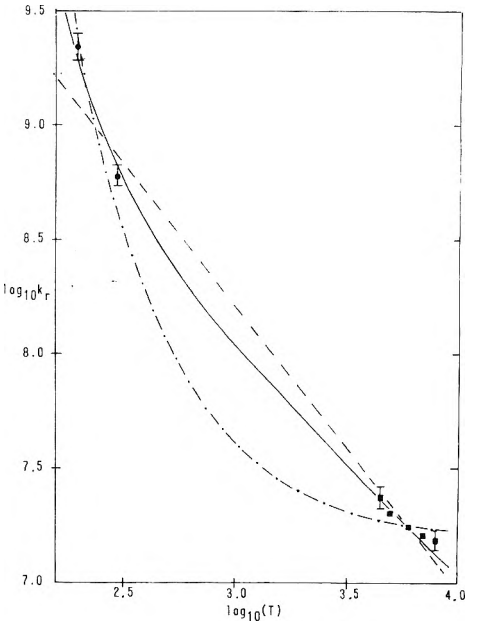

Figure 2. Fits of eq 1–3 to recombination rate constants for N_2 in Ar. Data points were obtained from ref *d* and *e* of Table I. Curves have the same significance as in Figure 1.

Results

Comparison of Fits. Equations 1–3 were fitted to combined low and high temperature data for H_2, N_2, O_2, Cl_2, Br_2, and I_2 with Ar as the third body as well as for Br_2 with He, Ne, Kr, and Xe as third bodies. The best fit values of the parameters and the rms deviations Δ of the respective curves from the experimental values of $\log k_r$ are presented in Table I. In the majority of cases the best fit, as indicated by the relative smallness of Δ, is provided by (3).

Visual comparisons of the fits are presented in Figures 1–6. None of the equations give curves which lie within the error bounds of all the experimental points. However, eq 3 does better in this regard than do eq 1 and 2. It is also to be noted that (1) and (3) provide better fits to the low temperature data whereas (2) is better for the high temperature data. On the other hand (1) usually gives a poor fit to the high temperature data, and (2) usually gives a poor fit to the low temperature data. The latter is even true for N_2 in Ar where (2) gives the best overall fit as indicated by the smallest value of Δ. Equation 3 on the

TABLE I: Results of Fitting Eq 1-3 to Recombination Rate Constants Over a Wide Temperature Range

			Best fit parameters and rms deviations									
			$A \exp(-E_a/RT)$			$B(1000/T)^n$			$C \sinh(T^*/T)$			
A_2	M	Temp range, K	A, 10^8L^2/mol^2 s	E_a, kcal/mol	Δ	B, 10^8L^2/mol^2 s	n	Δ	C, 10^8L^2/mol^2 s	T^*, K	Δ	Data ref[a]
H_2	Ar	77-8000	1.2	−1.0	0.29	8.0	1.1	0.03	60	110	0.07	*b, c*
N_2	Ar	196-15000	0.2	−2.1	0.14	4.7	1.2	0.04	7	440	0.05	*d, e*
O_2	Ar	196-8500	0.1	−2.0	0.06	1.7	1.2	0.06	2	630	0.04	*f, g*
Cl_2	Ar	195-2582	0.9	−2.4	0.11	4.8	2.0	0.12	3	1070	0.08	*h, i*
Br_2	He	300-2000	1.2	−1.4	0.10	2.9	1.2	0.07	6	420	0.07	*j, k*
Br_2	Ne	300-2000	1.2	−1.6	0.10	2.9	1.3	0.07	5	530	0.07	*j, k*
Br_2	Ar	300-2000	1.3	−1.8	0.08	3.6	1.4	0.08	4	710	0.06	*j, k*
Br_2	Kr	300-2000	1.1	−2.0	0.07	3.6	1.6	0.11	3	880	0.07	*j, k*
Br_2	Xe	300-2000	0.9	−2.3	0.06	3.4	1.8	0.14	2	1040	0.07	*l, k*
I_2	Ar	300-1600	2.2	−1.5	0.04	5.0	1.3	0.06	8	570	0.04	*m, n*

[a] In all cases the reference to the low temperature data is first. [b] D. W. Trainor, D. O. Ham, and F. Kaufman, *J. Chem. Phys.*, 58, 4599 (1973). [c] W. D. Breshears and P. F. Bird, *Symp. (Int.) Combust., [Proc.]*, 14, 211 (1972). [d] I. M. Campbell and B. A. Thrush, *Proc. R. Soc. London, Ser. A.*, 296, 201 (1967). [e] J. P. Appleton, M. Steinberg, and D. J. Liquornik, *J. Chem. Phys.*, 48, 599 (1968). [f] I. M. Campbell and B. A. Thrush, *Proc. R. Soc. London, Ser. A.*, 296, 222 (1967). [g] W. D. Breshears, P. F. Bird, and J. H. Kiefer, *J. Chem. Phys.*, 55, 4017 (1971). [h] R. P. Widman and B. A. DeGraff, *J. Phys. Chem.*, 77, 1325 (1973). [i] R. A. Carabetta and H. B. Palmer, *J. Chem. Phys.*, 46, 1333 (1967). [j] Reference 5. [k] Reference 6. Only data above 1500 K were used. [l] Reference 9. [m] Reference 10. [n] J. Troe and H. G. Wagner, *Z. Phys. Chem. (Frankfurt am Main)*, 55, 326 (1967).

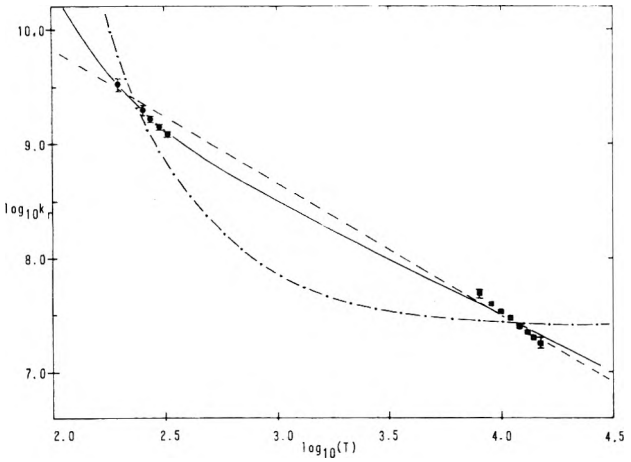

Figure 3. Fits of eq 1-3 to recombination rate constants for O_2 in Ar. Data points were obtained from ref *f* and *g* of Table I. Curves have the same significance as in Figure 1.

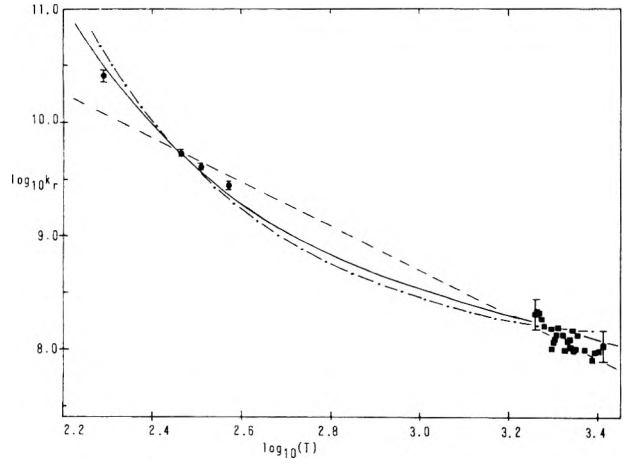

Figure 4. Fits of eq 1-3 to recombination rate constants for Cl_2 in Ar. Data points were obtained from ref *h* and *i* of Table I. Curves have the same significance as in Figure 1.

other hand always gives at least a fair fit to both high temperature and low temperature points.

Correlations of the Parameters. Values of k_r for Br_2 and I_2 have been measured over a temperature range of several

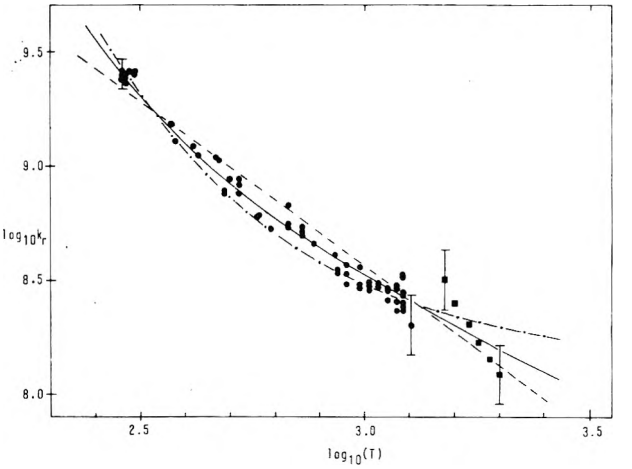

Figure 5. Fits of eq 1-3 to recombination rate constants for Br_2 in Ar. Data points were obtained from ref 5 and 6. Curves have the same significance as in Figure 1.

hundred degrees Kelvin for a fairly large number of third bodies.[5,9-11] Values of T^*_M correlate to some extent with the critical temperature of M and with its polarizability. It was not considered feasible to find correlations between C_M and other properties of M because of the very large uncertainties in the values of C_M which were extracted from the data. Experimental errors are higher at the higher temperatures. As mentioned above, this trend leads to enhanced uncertainty in log C. Values of the uncertainties in log C were found to exceed 0.4 in almost all cases. In other words we have little better than order of magnitude estimates for C.

In Table II are shown values of T^*_M for Br_2 and I_2 recombination. Also given are values of the polarizability α_M. To provide a consistent comparison, the values of T^*_M were in all cases derived from best fits to the low temperature data alone. In all cases for which T^* was also obtained over a wider temperature range the two values agree to within their calculated uncertainties. The literature values of the polarizabilities[12] which are listed in Table II were in most cases derived from the formula

$$\alpha = {}^1/_3 \operatorname{tr} \alpha \qquad (10)$$

where α is the polarizability tensor for the molecule. For

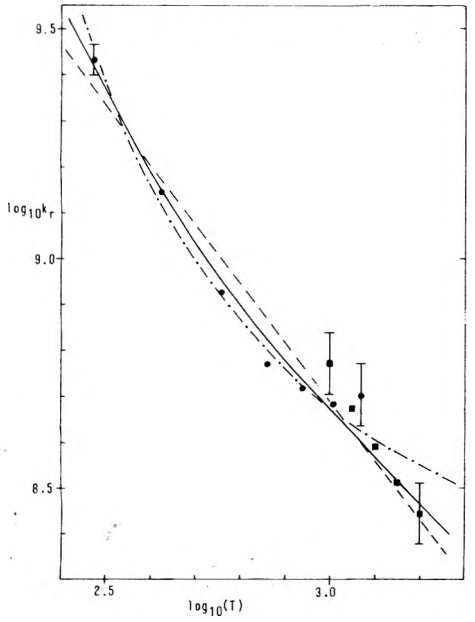

Figure 6. Fits of eq 1–3 to recombination rate constants for I_2 in Ar. Data points were obtained from ref 10 and from ref *n* of Table I. Curves have the same significance as in Figure 1.

TABLE II: Polarizabilities of Third Bodies and Values of T_M* from Studies of Br_2 and I_2 Recombination

M	T*, K: $A_2 = Br_2$	T*, K: $A_2 = I_2$	α, 10^{-30} m^3
He	450 ± 60[a]	410 ± 70[c]	0.21[e]
Ne	540 ± 60[a]	500 ± 50[d]	0.40[e]
Ar	730 ± 50[a]	600 ± 60[c]	1.63[e]
Kr	940 ± 40[a]	780 ± 40[d]	2.48[e]
Xe	1120 ± 40[b]	910 ± 50[c]	4.00[e]
N_2	800 ± 50[a]	760 ± 50[c]	1.76[f]
O_2	690 ± 50[a]		1.60[f]
CO		870 ± 50[c]	1.95[f]
HCl		1260 ± 40[d]	2.63[f]
HBr		1140 ± 20[d]	3.61[f]
CO_2		1180 ± 40[d]	2.65[f]
SO_2		1180 ± 40[d]	3.72[f]
CF_4	1300 ± 30[b]	1240 ± 40[d]	4.02[e]
SF_6	1240 ± 30[b]	1130 ± 30[d]	6.22[e]

[a] From data of ref 5. [b] From data of ref 9. [c] From data of ref 10. [d] From data of ref 11. [e] Derived from eq 11. [f] Derived from eq 10.

some of the spherical and nearly spherical molecules, ref 12 only gives α's derived from the formula

$$\alpha = \frac{3P}{4\pi N_0} \tag{11}$$

where P is the molar polarization of the gas and N_0 is Avogadro's number. However, for molecules which do not depart greatly from spherical symmetry, eq 10 and 11 give very nearly the same result.

The data for the rare gases in Table II are plotted in Figure 7. To within their calculated uncertainties, these points lie on two straight lines, one for Br_2 and one for I_2. If the points for the other third bodies in Table II had been plotted, they would mostly lie above the straight lines for the rare gases. Furthermore, they would not exhibit any sort of correlation.

Discussion

Of the equations considered, eq 3 provides the best fit to measured recombination rate constants over the full temperature range of the experiments. Furthermore, eq

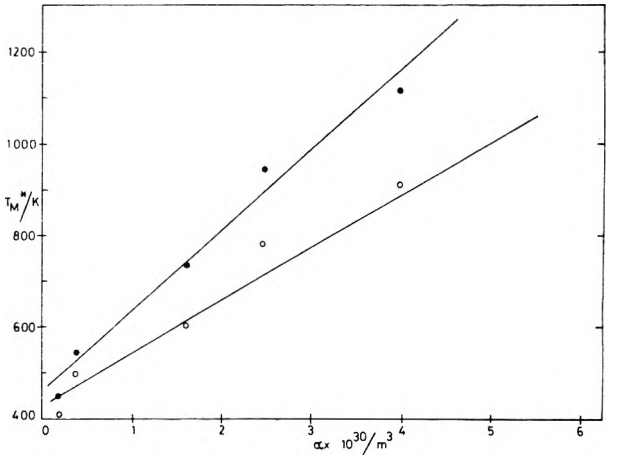

Figure 7. Plots of T^*_M for Br and I atom recombination in the rare gases vs. the polarizability of M. Filled circles correspond to bromine, open circles to iodine.

3 is based on a model, albeit a highly simplified one, of the process. However, it bears repeating that none of the equations which were investigated here give curves which lie within the limits of experimental error for all of the data which were analyzed. In practically all cases eq 3 gives a satisfactory fit to the low temperature data. However, it tends to deviate from the high temperature points in several of the cases shown. One might possibly conclude therefrom that the use of a three parameter equation is in order. However, such a sacrifice of simplicity is probably premature in view of large, not always resolved discrepancies between the results for (supposedly) identical systems.

Of the adjustable parameters in eq 3 only T* is satisfactorily determined from the data for halogen atom recombination. As has been mentioned in previous sections, the parameter dependence of the right side of (3) in conjunction with the prevailing pattern of experimental errors precludes the extraction of reliable values of C. The foregoing description of the model on which eq 3 is based indicated that C is the less interesting of the parameters in said equation. Hence, only T* is discussed in what follows.

In terms of the proposed model, T* can be interpreted on two levels. At the phenomenological level this parameter has a dual role. As seen from eq 5 and 7, the rate constant is reduced from what it would be if a Boltzmann distribution were maintained by a factor

$$1 - \exp(-2T^*/T)$$

Hence, one may interpret T* as the temperature above which the non-Boltzmann distribution of molecules among the reactive states has an appreciable effect on the rate. At low temperatures where k_r is very close to $k_r^{(e)}$, eq 3 has the same form as eq 1 with E_a equal to $-RT$*. In other words, T* is also related to an Arrhenius parameter. The connection between these roles is clarified by considerations at the second level of interpretation.

One may also interpret T* at the level of molecular collisions. From eq 7 and the definition of γ one obtains

$$\alpha = \beta \exp(-T^*/T)$$

where β is constant. As already pointed out, larger α implies less likelihood of transitions between states which differ by an energy on the order of kT or more. Hence, one can take T* to be roughly the temperature above which transitions take place almost entirely between states separated by an energy less than kT. In other words, the

larger T^*, the larger is the average amount of energy transferred to the internal degrees of freedom of A_2 in collisions with M.

The molecules have more tendency to maintain a Boltzmann distribution if the average energy transferred is large. This enhanced tendency is due to the widening of the range of reactive states and to the acceleration of the rate at which these states are replenished in dissociation or drained in recombination. The average energy transferred also represents a lowering of the effective dissociation energy since molecules which get this close to the actual dissociation energy are rapidly converted to atoms. This latter point provides an understanding of the relation between T^* and E_a.

The foregoing interpretation of T^* in conjunction with the correlation between T^* and α shown in Figure 7 suggests that attractive forces between A_2 and M may be important in determining the average amount of energy transferred, at least when M is a rare gas molecule. The attractive forces in this case are most likely dispersion forces, and polarizability provides a measure of the strength of such forces.[13] Thus Figure 7 may be regarded as a demonstration of the increase of a measure (T^*) of the average amount of energy transferred with an increase in a measure (α) of the strength of the attractive force between molecule and third body.

Because eq 3 reduces to the Arrhenius form at low temperatures, it might seem proper to associate kT^* with the binding energy of the radical molecule complex AM.[14] Such an interpretation does not clash with the one just given. The factors which determine whether or not M forms a tightly bound radical–molecule complex may coincide approximately with those which determine whether or not it transfers large amounts of energy in collisions with A_2. This point warrants investigation.

A final word of caution is in order. There is no reason to believe that the temperature dependence of k_r predicted by eq 3 is unique to the model proposed here. In other words, the interpretation of T^* which is given above is probably only one of several possible interpretations. More theoretical work is necessary to establish whether or not it is a valid interpretation.

Acknowledgment. We thank the National Research Council of Canada for financial support. One of us (N.S.S.) thanks Professors B. Widom and K. E. Russell for helpful discussions of this work.

Appendix. Determination of the Uncertainties in T^* and μ

Let $f(x)$ be a function which depends on parameters p_1, p_2, ... Suppose one wishes to fit f to a series of points $z(x_i)$ by the method of least squares. A standard procedure[15] for determining the appropriate values of the p_n's is to guess initial values $p_n^{(0)}$ and then to find improved values

$$p_n^{(1)} = p_n^{(0)} + \Delta p_n$$

where the Δp_n's are the components of the vector $\Delta\mathbf{p}$ given by

$$\Delta\mathbf{p} = \mathbf{A}^{-1}\mathbf{c} \tag{A1}$$

In eq A1 the elements of $\mathbf{A}$ are given by averages

$$A_{nm} = \Sigma_i w_i \left(\frac{\partial f}{\partial p_n}\right)_{x=x_i}\left(\frac{\partial f}{\partial p_m}\right)_{x=x_i} \equiv \left\langle \frac{\partial f}{\partial p_n}\frac{\partial f}{\partial p_m}\right\rangle \tag{A2}$$

and the components of $\mathbf{c}$ are given by similarly defined averages

$$c_m = \left\langle (z - f)\frac{\partial f}{\partial p_m}\right\rangle$$

One uses the $p_n^{(1)}$'s to construct a new $\mathbf{A}$ and $\mathbf{c}$ wherefrom one generates corrections to the $p_n^{(1)}$'s, again by means of eq A1. This procedure is iterated until the Δp_n's are sufficiently small.

Now suppose that each point has an error $\sigma(x_i)$ associated with it. This causes an uncertainty $\delta\mathbf{c}$ in $\mathbf{c}$

$$\delta c_m = \left\langle \sigma\frac{\partial f}{\partial p_m}\right\rangle \tag{A3}$$

Let $\mathbf{A}$ and $\delta\mathbf{c}$ be evaluated at the optimum values of the p_n's. From eq A1 we see that it is reasonable to take the uncertainty in the parameters to be given by

$$\delta\mathbf{p} = \mathbf{A}^{-1}\,\delta\mathbf{c} \tag{A4}$$

Equations 9 are a special case of eq A4.

In the problem at hand there are two p_n's, T^* and μ. The function f is given by

$$f = \mu + \log\sinh(T^*/T)$$

and its partial derivatives with respect to the parameters are given by

$$\left(\frac{\partial f}{\partial T}\right)_{T=T_i} = (T_i \ln 10)^{-1}\,\mathrm{ctnh}\,(T^*/T_i) \equiv y_i$$

$$\partial f/\partial\mu = 1$$

Substituting these expressions into (A2) and inverting the resulting matrix, we obtain

$$\mathbf{A}^{-1} = [\langle(y - \langle y\rangle)^2\rangle]^{-1}\begin{bmatrix} 1 & -\langle y\rangle \\ -\langle y\rangle & \langle y^2\rangle \end{bmatrix} \tag{A5}$$

From (A3) we obtain

$$\delta\mathbf{c} = \begin{bmatrix}\langle y\sigma\rangle \\ \langle\sigma\rangle\end{bmatrix} \tag{A6}$$

Equations 9 of the text follow readily from (A4), (A5), and (A6).

References and Notes

(1) J. C. Keck, *Adv. At. Mol. Phys.*, **8**, 39 (1972).
(2) V. H. Shui, *J. Chem. Phys.*, **58**, 4868 (1973).
(3) J. C. Keck and G. Carrier, *J. Chem. Phys.*, **43**, 2284 (1965); N. S. Snider, *ibid.*, **65**, 1800 (1976).
(4) B. A. DeGraff and K. J. Lang, *J. Phys. Chem.*, **74**, 4181 (1970).
(5) J. K. K. Ip and G. Burns, *J. Chem. Phys.*, **51**, 3414 (1969).
(6) M. Warshay, *J. Chem. Phys.*, **54**, 4060 (1971).
(7) R. K. Boyd, G. Burns, D. T. Chang, R. G. MacDonald, and W. H. Wong, *Symp. (Int.) Combust., [Proc.]*, **15**, 731 (1975).
(8) It was assumed that the temperature coordinates were known exactly and that all the uncertainty of the data was in k_r.
(9) S. K. Chang, A. G. Clarke, and G. Burns, *J. Chem. Phys.*, **54**, 1835 (1971).
(10) J. K. K. Ip and G. Burns, *J. Chem. Phys.*, **56**, 3155 (1971).
(11) H. W. Chang and G. Burns, *Can. J. Chem.*, **51**, 3394 (1973); *J. Chem. Phys.*, **62**, 2426 (1975).
(12) Landolt-Bornstein, "Zahlenwerte and Functionen", I Band, III Teil, Springer-Verlag, West Berlin, 1951.
(13) J. C. Slater and J. G. Kirkwood, *Phys. Rev.*, **37**, 682 (1931).
(14) G. Porter and J. A. Smith, *Nature (London)*, **184**, Suppl. 7, 446 (1959).
(15) H. Margenau and G. M. Murphy, "The Mathematics of Physics and Chemistry", Vol. 1, Van Nostrand, Princeton, N.J., 1956, pp 517–518.

Luminescence Quenching of Dicyanobis(2,2′-bipyridine)ruthenium(II) and Dicyanobis(1,10-phenanthroline)ruthenium(II) by Transition Metal Complexes

J. N. Demas,* J. W. Addington, Steven H. Peterson, and E. W. Harris

Chemistry Department, University of Virginia, Charlottesville, Virginia 22901 *(Received October 18, 1976)*

Publication costs assisted by the Petroleum Research Fund

Luminescence quenching of $Ru(bpy)_2(CN)_2$ and $Ru(phen)_2(CN)_2$ (bpy = 2,2′-bipyridine and phen = 1,10-phenanthroline) by 19 transition metal complexes is reported. The neutral cyano complexes have properties which permit them to supplement the widely used $[Ru(bpy)_3]^{2+}$ and $[Ru(phen)_3]^{2+}$ sensitizers. In addition to their intense, long-lived fluid solution emissions, the cyano complexes are free of ion-pairing problems and the large charge dependence of quenching rates with the tris complexes. The excited state energies of the cyano species can also be tuned significantly by solvent variation. Quenching is predominantly by diffusion. For Co^{2+}, Ni^{2+}, and Cu^{2+}, however, associational quenching by formation of a cyanide bridged species is important. Decay times, excited state energies, Stern–Volmer constants, bimolecular quenching constants, and association constants are reported. Quenching appears to be by energy and electron transfer.

Introduction

Luminescent Ru(II), Os(II), and Ir(III) complexes have proved to be nearly ideal photosensitizers.[1-20] They emit with long lifetimes in fluid solutions. They can transfer energy and undergo excited state electron transfer processes to a variety of organic and inorganic systems. They promise to be useful in solar energy conversion,[9] chemical actinometry of high power lasers,[11] and teaching experiments.[12]

To date most work has been done with the original sensitizer, $[Ru(bpy)_3]^{2+}$ (bpy = 2,2′-bipyridine) and with $[Ru(phen)_3]^{2+}$ (phen = 1,10-phenanthroline),[1-7,9-12] but work on analogous Os(II) and Ir(III) complexes is advancing rapidly.[8,9a,13,14] The latter complexes greatly extend the available excited state energies.[8] A disadvantage of the charged $[Ru(bpy)_3]^{2+}$ and related species is their tendency to form ion pairs or insoluble double salts with oppositely charged quenchers,[15,16] which can confuse or prevent quenching and sensitization studies.

The neutral $Ru(bpy)_2(CN)_2$ and $Ru(phen)_2(CN)_2$ have been used in energy transfer studies to O_2[13] and to some Cr(III) complexes.[17] In their protonated forms they also undergo unit efficiency excited state deprotonation reactions.[20] Their neutrality suggested they would prove very useful in sensitization studies with charged complexes. We present a survey of quenching of $Ru(bpy)_2(CN)_2$ and $Ru(phen)_2(CN)_2$ by a number of inorganic complexes which establishes their value in supplementing and extending the work with $[Ru(bpy)_3]^{2+}$ and $[Ru(phen)_3]^{2+}$.

Experimental Section

$Ru(phen)_2(CN)_2$[21] and $Ru(bpy)_2(CN)_2$[22] were prepared by procedures described elsewhere. All other reagents were the same as those described earlier.[15]

The luminescence intensity quenching measurements were carried out using the procedures and equipment described earlier;[15] data were corrected for the trivial absorption of exciting and emitted light by the quenchers.[23] Excitation and emission wavelengths were selected to minimize corrections (408-, 436-, 460-, and 480-nm excitation and 600- or 650-nm emission); correction factors rarely amounted to more than a few percent change in K_{sv}^{ϕ}. For the decay time, τ, measurements with $Ru(phen)_2(CN)_2$, the xenon flash apparatus described elsewhere was used.[12c] The strobe was, however, run at ~10 mJ which gave an ~0.7-μs duration, the phototube was an RCA 7164R, and photographic recording of the oscilloscope traces was used. For the decay time measurements with $Ru(bpy)_2(CN)_2$, a laser system described elsewhere[24] was used, except that the oscilloscope used a sampling plug-in setup as a scanning boxcar integrator; results were displayed directly on an x–y recorder.

TABLE I: Spectroscopic Properties of Sensitizers

	$Ru(bpy)_2(CN)_2$	$Ru(phen)_2(CN)_2$
$E_{5\%}(DMF)$,[a] μm^{-1}	1.736	1.768
$\tau_0(DMF)$,[b] μs	0.22	1.09
$E_{5\%}(CH_3OH)$,[a] μm^{-1}	1.830	1.830
$\tau_0(CH_3OH)$,[b] μs	0.40	1.58
$E_{5\%}(H_2O)$,[a] μm^{-1}	1.854	1.867
$\tau_0(H_2O)$,[b] μm^{-1}	0.27	0.71

[a] $E_{5\%}$'s are obtained from appropriate glasses at 77 K. [b] τ_0's are in the deoxygenated pure solvent at ~21 °C.

Low temperature emissions were measured in either ethanol–methanol (4/1 v/v), methanol–water (4/1 v/v), or dimethylformamide (DMF)–CH_2Cl_2 (9/1 v/v) glasses at 77 K. Emission data were not corrected for the spectral sensitivity of the system. Our phototube has a flat response in this region, however, and comparison of low temperature uncorrected spectra with corrected ones falling in the same region suggests that the spectral response is relatively flat, only falling off rapidly beyond 850 nm. Distortions should be mimimal, and errors in measurement on the sharp spectral features at 77 K should be insignificant.

Results

The room temperature absorption and emission spectra of $Ru(phen)_2(CN)_2$ and $Ru(bpy)_2(CN)_2$ are given in Figure 1. For the solvent series water, alcohols, DMF, the absorption and emission spectra show significant red shifts. The low temperature emission spectra in alcoholic and aqueous glasses are given in Figure 2; the pronounced red shift of the alcoholic vs. the aqueous glass is especially dramatic here because of the sharpness of the spectra. Visually the emission is orange in the aqueous glass, a distinct red in the alcoholic, and a deep, dull red in the DMF one.

At low temperatures the energy of the highest energy emission maximum is E_{max}. The energy at which the

TABLE II: Luminescence Quenching Data at ~21 °C

Quencher	$Ru(bpy)_2(CN)_2$ K_{SV}^{ϕ} (K_{SV}^{τ}), M^{-1}	$Ru(bpy)_2(CN)_2$ $10^{-9} k_2$, $M^{-1} s^{-1}$	$Ru(phen)_2(CN)_2$ K_{SV}^{ϕ} (K_{SV}^{τ}), M^{-1}	$Ru(phen)_2(CN)_2$ $10^{-9} k_2$, $M^{-1} s^{-1}$	$Ru(bpy)_3^{2+}$ or $Ru(phen)_3^{2+}$ [b] K_{SV}, M^{-1} [c]	$Ru(bpy)_3^{2+}$ or $Ru(phen)_3^{2+}$ [b] $10^{-9} k_2^0$, $M^{-1} s^{-1}$ [d]
$[Co(NH_3)_6](ClO_4)_3$ [a]	374 ± 9	1.39	1640 ± 50 (1500)	2.3	~10	~0.003
$[CoCl(NH_3)_5]Cl_2$ [a]	905 ± 33	3.35	2800 ± 150 (2800)	3.9	230	0.13
$CoCl_2$	14 ± 1 (1.73 ± 0.17)	0.0064	26.8 ± 1 (7.4 ± 1.8)	0.010	1	~0.0002
$CuSO_4$	378 ± 23 (104 ± 16)	0.39	770 ± 44 (340)	0.48	50	0.009
$NiSO_4$	14.1 ± 0.6 (2.5 ± 0.5)	0.009	55 ± 9 (14.3 ± 1.5)	0.020	4	0.007
$Ni(acac)_2$	55 ± 4	0.14	95 ± 2	0.060	21	0.042
$Co(acac)_3$	327 ± 19	0.82	1072 ± 11	0.68	400	0.86
$Co(acac)_2$	17 ± 2	0.043	128 ± 3	0.081	44	0.12
$Cr(acac)_3$	174 ± 2	0.44	1048 ± 27	0.66	230	0.54
$Cu(acac)_2$	427 ± 34	1.1	2420 ± 32 (2600)	1.5	840	1.6
NaI	0.41 ± 0.001	0.00015	0.28 ± 0.02	0.0004	0.3	0.001
$K[Cr(NH_3)_2(NCS)_4]$	525 ± 14	1.94	2310 ± 125 (2300)	3.3	ppt	ppt
$K_2[PtCl_4]$ [a]	161 ± 8	0.596	710 ± 30	1.00	20000	17
$K_2[Ni(CN)_4]$	1183 ± 9	4.38	3980 ± 130 (3900)	5.60	16000	28
$K_3[Co(C_2O_4)_3]$ [a]	804 ± 47	2.98	2300 ± 300 (2100)	3.24	27000	35
$K_3[Co(CN)_6]$	0.42 ± 0.27	0.0016	2.0 ± 0.1	0.0028	1	0.03
$K_3[Cr(C_2O_4)_3]$	50 ± 4	0.19	192 ± 10	0.27	16000	23
$K_3[Cr(CN)_6]$	82 ± 4	0.30	284 ± 10	0.40	17400	23
$K_3[Fe(CN)_6]$	1850 ± 150	6.9	4640 ± 30	6.54	36000	44
$K_4[Fe(CN)_6]$	165 ± 6	0.61	360 ± 30 (360)	0.51	44800	73

[a] Photosensitive with both donors. [b] All values for the acetylacetonato complexes and $[Ni(CN)_4]^{2-}$ are for $[Ru(bpy)_3]^{2+}$; all other data are for $[Ru(phen)_3]^{2+}$. [c] Observed values measured at low ionic strength with only donor and quencher present. Reference 15. [d] Evaluated at zero ionic strength.

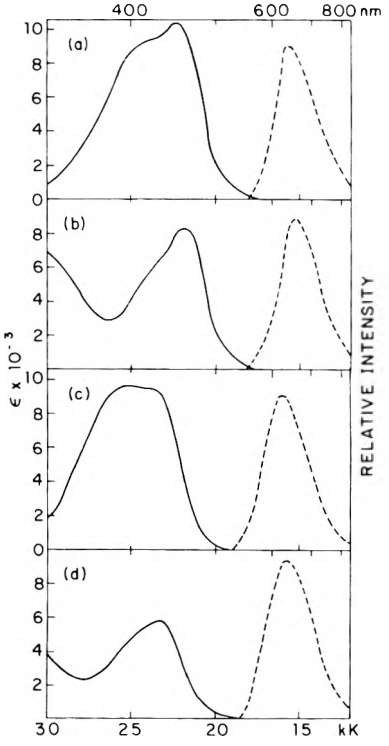

Figure 1. Room temperature absorption (—) and emission (----) spectra for (a) $Ru(phen)_2(CN)_2$ in methanol, (b) $Ru(bpy)_2(CN)_2$ in methanol, (c) $Ru(phen)_2(CN)_2$ in water, and (d) $Ru(bpy)_2(CN)_2$ in water.

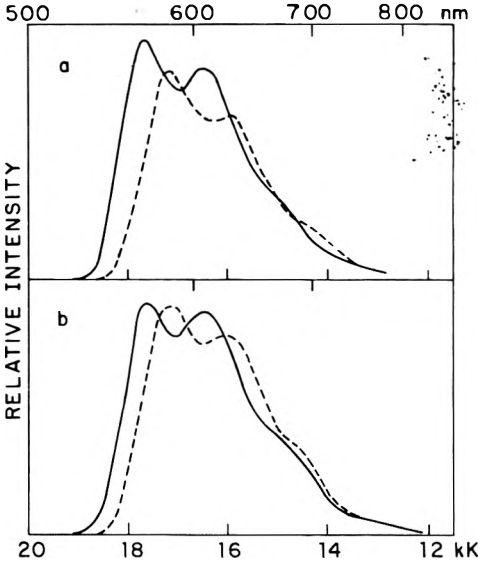

Figure 2. Low temperature (77 K) emission spectra of (a) $Ru(phen)_2(CN)_2$ and (b) $Ru(bpy)_2(CN)_2$ in methanol–water (—) and ethanol–methanol glasses (----).

emission intensity on the short wavelength side of E_{max} falls to 5% of the intensity at E_{max} is $E_{5\%}$; $E_{5\%}$ and E_{max} are tabulated in Table I for both sensitizers in the glasses at 77 K. Decay times, τ_0's, of the complexes in deoxygenated water, methanol, and DMF at ~21 °C are given also in Table I.

The intensity Stern–Volmer plots were linear except for Ni^{2+}, Co^{2+}, and Cu^{2+} which exhibited the upward curvature characteristic of a system showing both static and dynamic quenching.[10,25] Figure 3 shows typical $(\phi_0/\phi) - 1$ and $(\tau_0/\tau) - 1$ vs. [Q] plots for $Ru(phen)_2(CN)_2$ with Ni^{2+}. ϕ's and τ's are emission intensities and decay times, respectively. The subscript zero denotes values in the absence of quencher.

Table II summarizes our quenching results. All data were for aqueous solutions except for the acetylacetonato complex quenchers which used a methanol solvent. Intensity Stern–Volmer quenching constants, K_{sv}^{ϕ} ($=((\phi_0/\phi) - 1)/[Q]$), and for select systems the decay time Stern–Volmer quenching constants, K_{sv}^{τ} ($=((\tau_0/\tau) - 1)/[Q]$), are presented. Except in the cases of Ni^{2+}, Co^{2+}, and Cu^{2+}, K_{sv}^{ϕ} and K_{sv}^{τ} were equal within experimental error. Bimolecular quenching constants, k_2's, were computed from $k_2 = K_{sv}^{\phi}/\tau_0$ except for Ni^{2+}, Co^{2+}, and Cu^{2+} quenchers, where the correct form $k_2 = K_{sv}^{\tau}/\tau_0$ was used.

Systems exhibiting photosensitivity by changes of emission intensity with 1–2 min of irradiation are indicated in Table II. Other systems may be sensitive, but not detected by this procedure.

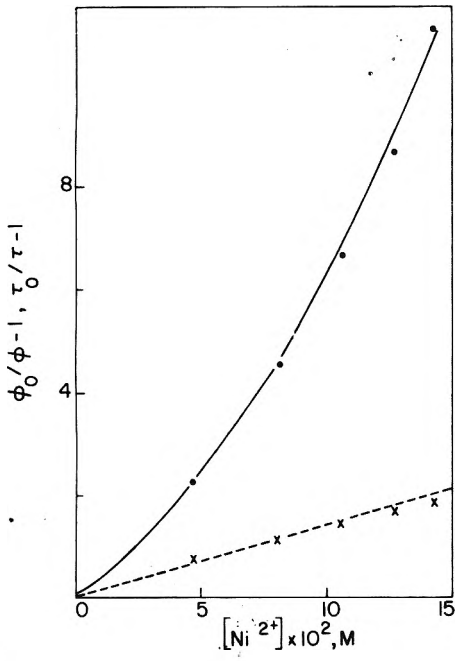

Figure 3. ϕ (●) and τ (×) Stern–Volmer plots for quenching of $Ru(phen)_2(CN)_2$ by Ni^{2+}. The dashed line is the calculated τ plot for $K_{SV}^{\tau} = 14.3\ M^{-1}$. The solid line is the calculated fit for $K_{SV}^{\tau} = 14.3\ M^{-1}$ and $K_{eq} = 12\ M^{-1}$.

Also indicated in Table II are the observed Stern–Volmer quenching constants and the k_2's for deactiviation at zero ionic strength for $[Ru(phen)_3]^{2+}$ or $[Ru(bpy)_3]^{2+}$. Data are reported for the sensitizers with the largest K_{sv}'s. With $[Ni(CN)_4]^{2-}$, $[Ru(phen)_3]^{2+}$ precipitated. With $[Cr(NH_3)_2(NCS)_4]^-$ both $[Ru(phen)_3]^{2+}$ and $[Ru(bpy)_3]^{2+}$ precipitated, and no data are available.

Discussion

In systems exhibiting both static and dynamic quenching the following equations are obeyed: [10,12c,25]

$$K_{SV}^{\tau} = ((\tau_0/\tau) - 1)/[Q] \quad (1)$$

$$K_{SV}^{\phi} = ((\phi_0/\phi) - 1)/[Q] = (K_{SV}^{\tau} + \beta K_{eq}) + K_{SV}^{\tau}(\beta K_{eq})[Q] \quad (2)$$

where [Q] is the quencher concentration and K_{eq} is the first association constant between donor and quencher. β varies from 1.000 to ϵ_{DQ}/ϵ_D for optically dilute to dense solutions where ϵ_D and ϵ_{DQ} are the molar extinction coefficients of donor and donor–quencher association pair, respectively, at the excitation wavelength. These expressions assume that the formal quencher concentration is always much greater than the donor concentration and that the association pair is not luminescent and cannot dissociate on excitation to give free excited donor. K_{sv}^{τ} equals $k_2\tau_0$, the normal Stern–Volmer quenching constant, under these conditions.

With Co^{2+}, Ni^{2+}, and Cu^{2+} where both dynamic and static quenching were present, $(K_{sv}^{\tau} + \beta K_{eq})$ was obtained from the intercepts of the K_{sv}^{ϕ} vs. [Q] plots which were linear within experimental error. Using K_{sv}^{τ} evaluated from τ measurements (eq 1), βK_{eq} was then calculated. $K_{sv}^{\tau}(\beta K_{eq})$ obtained from the slope of the K_{sv}^{ϕ} vs. [Q] plot agreed within experimental error with the product evaluated from the separately obtained terms. Since our experiments were always run under optically dilute conditions (<0.1), $\beta = 1$. The calculated K_{eq}'s are summarized in Table III.

We first consider the nature of the static quenching with Co^{2+}, Ni^{2+}, and Cu^{2+}. In the case of Cu^{2+}, spectral studies

TABLE III: Association Constants for Aqueous $Ru(phen)_2(CN)_2$ and $Ru(bpy)_2(CN)_2$ with Metal Ions at ~21 °C

	K_{eq}, M^{-1}	
	$Ru(bpy)_2(CN)_2$	$Ru(phen)_2(CN)_2$
Co^{2+}	12	18
Ni^{2+}	12	20
Cu^{2+}	200	270[a]

[a] From ref 25.

with $Ru(phen)_2(CN)_2$ clearly show the formation of at least two Cu^{2+}–donor ground state complexes, while $[Ru(bpy)_3]^{2+}$ is free of such species. Since CN's form bridging ligands, we have assigned the new species to $[Ru(phen)_2(CN)(CNCu)]^{2+}$ and $[Ru(phen)_2(CNCu)_2]^{4+}$ in analogy with the protonated CN species.[25,26] A roughly linear bonding scheme for the Ru(CN)Cu bonds seem most reasonable. We infer a similar static quenching mechanism for Cu^{2+} and $Ru(bpy)_2(CN)_2$ and for Ni^{2+} and Co^{2+} with both donors.

The K_{eq}'s for Cu^{2+}, Ni^{2+}, and Co^{2+} present an interesting picture. With both donors Cu^{2+} has substantially greater stability than Ni^{2+} and Co^{2+}. It is not possible to compare directly the association constants for free CN^- to Cu^{2+}, Ni^{2+}, and Co^{2+} with those for $Ru(phen)_2(CN)_2$ and $Ru(bpy)_2(CN)_2$; Cu^{2+}, Ni^{2+}, and Co^{2+} all form polycyano complexes of such great stability (β's $\geq 10^{12}$)[27] that it is impossible to measure the association constants for the first cyanides. It appears likely, however, that the affinity of Ru bonded CN is far less than a free cyanide for these three metal ions. Since Cu^{2+} is the only ion of the three which is readily reduced, a partial charge transfer stabilization of the association pair may be responsible for its greater stability compared to Ni^{2+} and Co^{2+}.

With both donors we find no evidence for static quenching with the remaining nonlabile quenchers. All intensity Stern–Volmer plots were linear with no evidence for upward curvature. Additionally, with $Ru(phen)_2(CN)_2$, ϕ and τ data show that nonlabile chloro, ammine, acetyacetonato, cyano, oxalato, and thiocyanato complexes all quench predominantly (>90%) by dynamic processes over the concentration ranges examined. The species studied included the open square-planar $[Ni(CN)_4]^{2-}$ and $Cu(acac)_2$ which conceivably could bond through their free trans sites. Thus, we infer that static quenching is at most a minor quenching component for all nonlabile quenchers with both donors.

For evaluating the detailed quenching mechanisms, knowledge of the energies of the donors' sensitizing levels is needed. The room temperature data do not give good information on this quantity. The emissions of the donors are broad and structureless, and their emitting states are too weak to resolve in absorption. We have, therefore, used low temperature emission spectra coupled with the Fleischauer criterion for estimating zero point excited state energies, E_0's.[28] Fleischauer et al. set E_0 equal to $E_{5\%}$. Thus, E_0's for the sensitizers in water, methanol, and DMF can be estimated from the $E_{5\%}$ values of Table I. These E_0's compare with the solvent independent E_0's of 1.80 and 1.84 μm^{-1} for $[Ru(bpy)_3]^{2+}$ and $[Ru(phen)_3]^{2+}$, respectively.[15] A word of caution is necessary. Measurements of E_0's based on low temperature emission spectra rest on the assumption that the metal complex and solvent reorganization energies following excitation are small. If this is not true, then at room temperature, where the solvent and donor can relax fully, the available excitation energy will be substantially less than that indicated from the low

temperature emission data. At 77 K the solvent and complex are clamped into a rigid environment that cannot relax during the lifetime of the excited state. We believe this to be a minor problem since the emission and absorption changes on going from room temperature to 77 K are very similar for both the cyanide complexes and $[Ru(bpy)_3]^{2+}$ and $[Ru(phen)_3]^{2+}$; the tris complexes being essentially spherical and having no permanent dipole moment will have much smaller reorganization energies. Further work involving time-resolved spectroscopy is in progress to answer this question with certainty.

In terms of the detailed diffusional quenching mechanisms, the results with $Ru(bpy)_2(CN)_2$ and $Ru(phen)_2(CN)_2$ are similar to and expand on our earlier studies with $[Ru(bpy)_3]^{2+}$ and $[Ru(phen)_3]^{2+}$. The essentially nonquenching nature of I^- demonstrates again that heavy atom quenching is unimportant in these heavy atom containing Ru(II) sensitizers. Further, the failure to find any consistent correlation between the degree of quencher paramagnetism and quenching ability seems to rule out the existence of paramagnetic quenching of the Ru(II) sensitizers. For example, the paramagnetic $Ni(acac)_2$, $Co(acac)_2$, Co^{2+}, and Ni^{2+} are substantially weaker quenchers than the diamagnetic $Co(acac)_3$ and $[Ni(CN)_4]^{2-}$. Finally $[Co(CN)_6]^{3-}$ is essentially a nonquencher indicating that the lowest d–d triplet of this complex is $>1.87\ \mu m^{-1}$, consistent with our early determination of $E_T > 1.84\ \mu m^{-1}$.[15]

Excluding heavy atom or paramagnetic quenching, there remain three basic diffusional quenching mechanisms possible for our systems: energy transfer ($^*D + Q \rightarrow D + {}^*Q$), oxidative electron-transfer quenching ($^*D + Q \rightarrow D^+ + Q^-$), and reductive electron-transfer quenching ($^*D + Q \rightarrow D^- + Q^+$). All have been observed unambiguously with $[Ru(bpy)_3]^{2+}$ [3,4,10] and are possible with $Ru(bpy)_2(CN)_2$ and $Ru(phen)_2(CN)_2$. Exciplex formation should not be possible on steric grounds, except possibly for the square-planar complex quenchers. We discount this possibility, however, because all those quenchers have low-lying energy levels which should promptly deactivate the donor before an exciplex could form.

The only quenching mechanism possible for Co^{2+}, Ni^{2+}, $Co(acac)_2$, $[PtCl_4]^{2-}$, and the Cr(III) complexes is energy transfer. Reduction or oxidation should be too difficult. We attribute all quenching in these cases to energy transfer into ligand field excited states.

$Cu(acac)_2$ and Cu^{2+} in addition to having low-lying d–d levels to act as energy transfer quenchers can be readily reduced[29,30] to Cu(I) species by the powerful reducing excited donors. With Cu^{2+} and $^*[Ru(bpy)_3]^{2+}$ flash photolysis shows a large component of oxidative quenching;[31] we infer that Cu^{2+} also quenches $Ru(bpy)_2(CN)_2$ and $Ru(phen)_2(CN)_2$ at least in part by oxidative quenching to yield Cu^+. $Cu(acac)_2$ is also very readily reduced, although the polarographic wave is irreversible.[30] We assume quenching in these cases is at least in part by electron transfer. For Cu^{2+} in water, the substantially higher k_2's compared to hexaaquo Co^{2+} and Ni^{2+} which can only quench by energy transfer to d–d states also support the presence of a large component of electron transfer quenching with Cu^{2+}. Similarly for $Cu(acac)_2$, k_2 is much larger than for $Ni(acac)_2$ and $Co(acac)_2$ which can only quench by energy transfer; this supports oxidative quenching by $Cu(acac)_2$. $[Co(NH_3)_6]^{3+}$, $[CoCl(NH_3)_5]^{2+}$, and $[Co(C_2O_4)_3]^{3-}$ are all photosensitive, and quench with much higher k_2's than most of the complexes which can quench by only energy transfer. We attribute a major quenching component in these systems to oxidative quenching to yield Co^{2+}, as has been established with quenching of $[Ru(bpy)_3]^{2-}$ by $[Co(NH_3)_6]^{3+}$, $[CoBr(NH_3)_5]^{2+}$, and $[Co(C_2O_4)_3]^{3-}$.[3,23] Since energy transfer quenching is possible in all these cases, however, some quenching by this pathway cannot be ruled out.

Thermodynamically $[Fe(CN)_6]^{3-}$ can quench $[Ru(bpy)_3]^{2+}$ and $[Ru(phen)_3]^{2+}$ by both energy and oxidative electron transfer,[15] this should also be true for the Ru–cyanide samples.[17] The essentially diffusion limited rate constant for quenching of $Ru(phen)_2(CN)_2$ and $Ru(bpy)_2(CN)_2$, however, is so much greater than for most observed energy transfer quenching processes that we believe electron transfer must be the dominant quenching pathway. For $[Fe(CN)_6]^{4-}$ with $[Ru(bpy)_3]^{2+}$ reductive quenching is possible[4c,d] and has been assigned as the major quenching pathway, but flash photolysis evidence for reductive quenching is negative.[31] Alternatively, we have suggested, based on the absence of any low temperature emission from $[Fe(CN)_6]^{4-}$, that a low-lying d–d state is responsible for deactivation. Although reductive quenching of $[Fe(CN)_6]^{4-}$ is possible for $Ru(bpy)_2(CN)_2$ (based on δ_0 from ref 17), and presumably also for $Ru(phen)_2(CN)_2$, we similarly suggest a mixture of energy and electron transfer as the quenching path for the cyanide donors.

For $[Ni(CN)_4]^{2-}$ with $[Ru(bpy)_3]^{2+}$ reductive quenching has also been postulated, although potentiometric data do not support this claim.[4c] Energy transfer quenching is possible from both cyanides to the $\sim 1.8\text{-}\mu m^{-1}$ lowest triplet of $[Ni(CN)_4]^{2-}$.[15] The k_2's for $Ru(bpy)_2(CN)_2$ and $Ru(phen)_2(CN)_2$ seem anomalously high for energy transfer to a ligand field excited state, approaching the diffusion limit. The open trans positions may be responsible for the lesser shielding of the d levels. Also for $[Cr(NH_3)_2(NCS)_4]^-$ k_2 is quite large even though energy transfer is presumably involved. We hope by means of flash photolysis to determine the quenching mechanisms in these systems unambiguously.

In terms of using $Ru(bpy)_2(CN)_2$ and $Ru(phen)_2(CN)_2$ as luminescent photosensitizers, Figure 1 and Tables I and II reveal interesting features. Unlike the previously very successful and widely used $[Ru(bpy)_3]^{2+}$ and the related $[Ru(phen)_3]^{2+}$, both cyanide complexes exhibit strongly solvatochromic shifts on their absorption spectra and the energy of their sensitizing emitting states. A significant and useful $1\text{–}1.3\text{-}\mu m^{-1}$ (3–4 kcal) variation of the excited state energy arises on going from water to DMF; continuous tunability by use of mixed solvents should be possible. Thus, for detailed probing of acceptor excited state properties, a single donor could be used over a substantial and essentially continuous energy range merely by varying the solvent.

Unlike $[Ru(bpy)_3]^{2+}$ and $[Ru(phen)_3]^{2+}$, the cyanide complexes are also free of ion-pairing and electrostatic repulsion problems associated with the use of the charged complexes with charged quenchers. The absence of repulsions with like charged quenchers can manifest itself by enormous increases in K_{sv}'s when one of the charged sensitizers is replaced with the neutral cyanides. Improvements in K_{sv}'s of ~40–160 exist for $[Co(NH_3)_6]^{3+}$ and ~4–10 exist for $[CoCl(NH_3)_6]^{2+}$ run at low ionic strengths. For the neutral quenchers in methanol, however, the k_2's differ little and in no systematic way for the charged vs. uncharged donors; the τ_0's largely determine the relative K_{sv}'s. Based on the K_{sv}'s, $Ru(bpy)_2(CN)_2$ in methanol is generally somewhat inferior to $[Ru(bpy)_3]^{2+}$, but $Ru(phen)_2^+(CN)_2$ is superior to $[Ru(bpy)_3]^{2-}$ with K_{sv}'s two to four times larger. This is a very significant improvement

for example in flash photolysis experiments where the quencher absorbance can obscure the signal of interest. Although we do not have quenching data in DMF, based on the τ_0's $Ru(phen)_2(CN)_2$ appears far superior to $Ru(bpy)_2(CN)_2$.

For anionic quenchers where electrostatic attractions aid K_{sv}'s for the cationic donors, the cationic donors give larger K_{sv}'s at low ionic strengths. Nevertheless, the cyanide complexes generally exhibit quite large and useful K_{sv}'s and, for experiments run at high ionic strengths, the differences between the neutral and charged donors will be substantially narrowed. Also, not all anionic species can be studied with $[Ru(bpy)_3]^{2+}$ and $[Ru(phen)_3]^{2+}$ because of formation of insoluble double salts (e.g., $[Cr(NH_3)_2(NCS)_4]^-$) which prevents data collection; the neutral cyanides give excellent data.

Both cyano complexes also have very high efficiencies of population of their sensitizing states. Singlet oxygen production efficiencies in methanol set lower bounds of 0.68 and 0.80 for $Ru(phen)_2(CN)_2$ and $Ru(bpy)_2(CN)_2$, respectively.[13] Also in methanol at room temperature $Ru(bpy)_2(CN)_2$ shows no variation in luminescence yield on going from the principal CT band to below the zero point energy of the excited state.[32]

Acknowledgment. Acknowledgment is gratefully made to the National Science Foundation (CHE-74-17916), the Research Corporation, the donors of the Petroleum Research Fund, administered by the American Chemical Society, and the NIH (Biomedical Science Support Grant administered by the University of Virginia) for support of this work. We thank V. Balzani for a preprint and R. B. Martín for the use of his Cary 14.

References and Notes

(1) J. N. Demas and A. W. Adamson, *J. Am. Chem. Soc.*, **93**, 1800 (1971).
(2) P. Natarajan and J. F. Endicott, *J. Am. Chem. Soc.*, **94**, 3635 (1972).
(3) (a) H. Gafney and A. W. Adamson, *J. Am. Chem. Soc.*, **94**, 8238 (1972); (b) G. Navon and N. Sutin, *Inorg. Chem.*, **13**, 2159 (1974); (c) H. Gafney and A. W. Adamson, submitted for publication.
(4) (a) C. R. Bock, T. J. Meyer, and D. G. Whitten, *J. Am. Chem. Soc.*, **96**, 4710 (1974); (b) *ibid.*, **97**, 2909 (1975); (c) A. Juris, M. T. Gandolfi, M. F. Manfrin, and V. Balzani, *ibid.*, **98**, 1047 (1976); (d) C. Creutz and N. Sutin, *Inorg. Chem.*, **15**, 496 (1976); (e) *J. Am. Chem. Soc.*, **98**, 6384 (1976).
(5) G. S. Laurence and V. Balzani, *Inorg. Chem.*, **13**, 2976 (1974).
(6) M. Wrighton and J. Markham, *J. Phys. Chem.*, **77**, 3042 (1973).
(7) J. N. Demas, D. Diemente, and E. W. Harris, *J. Am. Chem. Soc.*, **95**, 6864 (1973).
(8) J. N. Demas, E. W. Harris, C. M. Flynn, Jr., and D. Diemente, *J. Am. Chem. Soc.*, **97**, 3838 (1975).
(9) (a) C. Lin and N. Sutin, *J. Phys. Chem.*, **80**, 97 (1976); (b) G. Sprintschnik, H. W. Sprintschnik, P. P. Kirsch, and D. G. Whitten, *J. Am. Chem. Soc.*, **98**, 2337 (1976); (c) C. T. Lin, M. Chou, C. Creutz, and N. Sutin, *ibid.*, **98**, 6536 (1976).
(10) V. Balzani, L. Moggi, M. F. Manfrin, F. Bolletta, and G. S. Laurence, *Coord. Chem. Rev.*, **15**, 321 (1975).
(11) (a) J. N. Demas, R. P. McBride, and E. W. Harris, "Lasers in Physical Chemistry and Biophysics", J. Joussot-Dubien, Ed., Elsevier, New York, N.Y., 1975, p. 477; (b) J. N. Demas, R. P. McBride, and E. W. Harris, *J. Phys. Chem.*, **80**, 2248 (1976).
(12) (a) J. N. Demas, *J. Chem. Educ.*, **52**, 677 (1975); (b) H. D. Gafney and A. W. Adamson, *ibid.*, **52**, 480 (1975); (c) J. N. Demas, *ibid.*, **53**, 657 (1976).
(13) J. N. Demas, E. W. Harris, and R. P. McBride, *J. Am. Chem. Soc.*, in press.
(14) (a) P. Sisher, E. Finkenberg, and H. D. Gafney, "The 12th Informal Conference on Photochemistry. Extended Abstracts", National Bureau of Standards, Gaithersberg, Md., G7, 1976; (b) P. K. Lam, A. W. Adamson, and H. D. Gafney, submitted for publication.
(15) J. N. Demas and J. W. Addington, *J. Am. Chem. Soc.*, **98**, 5800 (1976).
(16) F. Bolletta, M. Maestri, L. Moggi, and V. Balzani, *J. Phys. Chem.*, **78**, 1374 (1974).
(17) F. Bolletta, M. Maestri, and V. Balzani, *J. Phys. Chem.*, **80**, 2499 (1976).
(18) N. Sabbatini, M. A. Scandola, and V. Balzani, *J. Phys. Chem.*, **78**, 541 (1974).
(19) I. Fujita and H. Kobayashi, *J. Chem. Phys.*, **59**, 2902 (1973).
(20) (a) S. H. Peterson and J. N. Demas, *J. Am. Chem. Soc.*, **98**, 7880 (1976); (b) *ibid.*, manuscript in preparation.
(21) J. N. Demas, M. W. Weiss, D. Diemente, A. McNutt, and C. M. Flynn, Jr., manuscript in preparation.
(22) J. N. Demas, T. F. Turner, and G. A. Crosby, *J. Inorg. Chem.*, **8**, 674 (1969).
(23) J. N. Demas and A. W. Adamson, *J. Am. Chem. Soc.*, **95**, 5159 (1973).
(24) J. N. Demas and C. M. Flynn, Jr., *Anal. Chem.* **48**, 353 (1976).
(25) J. N. Demas and J. W. Addington, *J. Am. Chem. Soc.*, **96**, 3663 (1974).
(26) A. A. Schilt, *J. Am. Chem. Soc.*, **85**, 904 (1963).
(27) "Stability Constants of Metal-Ion Complexes", *Chem. Soc., Spec. Publ.*, **No. 17** (1964).
(28) P. D. Fleischauer, A. W. Adamson, and G. Sastori, "Inorganic Reaction Mechanisms", Part II, J. O. Edwards, Ed., Wiley, New York, N.Y., 1972, p 1.
(29) J. H. Esperson, K. Shaw, and O. J. Parker, *J. Am. Chem. Soc.*, **89**, 5730 (1967).
(30) H. F. Holtzclaw, Jr., K. W. R. Johnson, and F. W. Hengeveld, *J. Am. Chem. Soc.*, **74**, 3776 (1952).
(31) B. A. DeGraff and J. N. Demas, work in progress.
(32) D. G. Taylor, M. S. Thesis, University of Virginia, 1976.

Kinetics and Mechanism of the Ruthenium(III) Chloride Catalyzed Oxidation of Butan-2-ol and 2-Methyl-1-propanol by the Hexacyanoferrate(III) Ion in an Aqueous Alkaline Medium

H. S. Singh,* R. K. Singh, S. M. Singh, and A. K. Sisodia

Chemical Laboratories, University of Allahabad, Allahabad, India *(Received August 17, 1976; Revised Manuscript Received March 4, 1977)*

Studies of the kinetics of ruthenium(III) chloride catalyzed oxidation of butan-2-ol and 2-methyl-1-propanol by aqueous alkaline potassium hexacyanoferrate(III) were made at constant ionic strength. The results show that complex formation between the ruthenium(III) species and the alcohol molecule takes place with the possible exchange of a hydroxide ion. The complex thus formed undergoes disproportionation yielding the carbonium ion derived from the alcohol molecule as an intermediate and the ruthenium(III) hydride species. The carbonium ion rapidly goes to an aldehyde (or ketone with secondary alcohol) with one molecule of hydroxide ion. The Ru(III) hydride thus produced is oxidized rapidly to Ru(III) with the hexacyanoferrate(III) ion. The oxidation products are confirmed and a probable reaction path is given.

Introduction

There have been only very few investigations concerning the ruthenium tetroxide or ruthenium trichloride catalyzed oxidation of organic compounds with some cooxidants in acid or alkaline medium. Recently, it has been reported that the oxidation of α diols under alkaline condition gives extensive carbon–carbon bond cleavage, i.e., adipic acid was obtained in 80–90% yields from the oxidation of cyclohexane-1,2-diol using a catalytic amount of ruthenium trichloride along with sodium hypochlorite as a cooxidant in an aqueous medium.[1] However, the kinetics of the problem are still unknown. Thus, this study was undertaken to investigate the kinetic features of the ruthenium trichloride catalyzed oxidation of butan-2-ol and 2-methyl-1-propanol by the hexacyanoferrate(III) ion in an aqueous alkaline medium.

Accordingly, the details of the results are presented and a probable reaction mechanism has been proposed.

Results and Discussion

The reduction of hexacyanoferrate(III) by butan-2-ol and 2-methyl-1-propanol in the presence of ruthenium(III) chloride as a homogeneous catalyst was investigated at varying initial concentration of hexacyanoferrate(III). The details of the kinetic data are presented in Tables I–III. The standard zero-order rate constants (k_s) presented in these tables are the averages from a particular run.

A typical zero-order plot for the rate of oxidation of butan-2-ol and 2-methyl-1-propanol is shown in Figure 1. It is obvious from these plots that the reaction velocity follows zero-order kinetics even up to the end of the reaction. A close examination of Table I clearly indicates that the k_s values are practically constant indicating zero-order kinetics with respect to the oxidant. The results presented in Table IIA and B contain the standard zero-order rate constants at varying concentrations of organic substrates, and from k_s/[alcohol] values it is quite obvious that the k_s values obtained for molar concentration of organic substrates continue to decrease with its increasing concentration. Thus the results presented in Figure 2 indicate the direct proportionality of the reaction rate on the low alcohol concentration and it tends toward zero order at higher concentrations.

The oxidation kinetics of these alcohols have been found to depend on the hydroxide ion concentration. A plot of k_s values against hydroxide ion concentration showed that the k_s values decrease with its increasing concentration, i.e., it suggests an approximate inverse proportionality of the reaction rate on hydroxide ion concentration (Figure 3).

TABLE I: Effect of Hexacyanoferrate(III) on the Rate of Oxidation

A

[2-Methyl-1-propanol] = 2.0×10^{-2} M, [NaOH] = 2.0×10^{-2} M, [Ru(III)] = 1.20×10^{-6} M

$[K_3Fe(CN)_6] \times 10^3$ M = 1.0, 2.0, 3.0, 4.0, 5.0

$k_s \times 10^5$ M min^{-1} = 2.65, 2.81, 3.18, 3.28, 3.07

B

[Butan-2-ol] = 5.0×10^{-2} M, [NaOH] = 2.0×10^{-2} M, [Ru(III)] = 1.20×10^{-6} M

$[K_3Fe(CN)_6] \times 10^3$ M = 0.50, 1.0, 2.0, 3.0, 4.0, 5.0

$k_s \times 10^5$ M min^{-1} = 1.53, 1.50, 1.58, 1.85, 1.91, 1.77

TABLE II: Effect of Variation of the Alcohol Concentration on the Rate of Oxidation

A

$[K_3Fe(CN)_6]$ = 2.0×10^{-3} M, [NaOH] = 8.0×10^{-2} M, [Ru(III)] = 1.20×10^{-6} M

[2-Methyl-1-propanol] $\times 10^2$ M = 1.0, 2.0, 3.0, 4.0, 5.0, 6.0, 8.0, 10.0

$k_s \times 10^5$ M min^{-1} = 0.77, 1.33, 1.88, 2.30, 2.71, 3.03, 3.94, 4.64

$\{k_s/[2\text{-methyl-1-propanol}]\} \times 10^3$ min^{-1} = 0.77, 0.66, 0.62, 0.57, 0.54, 0.50, 0.49, 0.46

B

$[K_3Fe(CN)_6]$ = 2.0×10^{-3} M, [NaOH] = 2.0×10^{-2} M, [Ru(III)] = 4.80×10^{-6} M

[Butan-2-ol] $\times 10^2$ M = 1.0, 2.0, 3.0, 5.0, 6.0, 7.0, 8.0, 10.0

$k_s \times 10^5$ M min^{-1} = 2.47, 4.59, 6.60, 9.70, 11.85, 12.59, 13.91, 16.12

$\{k_s/[\text{butan-2-ol}]\} \times 10^3$ min^{-1} = 2.47, 2.29, 2.29, 1.94, 1.97, 1.79, 1.74, 1.61

Table IIIA and B presents the effect of the variation of ruthenium(III) chloride concentration on the reaction rate. Again, the values of k_s calculated for molar concentration of the catalyst are fairly constant for about a tenfold variation, so it is concluded that the order with respect to ruthenium(III) chloride is unity.

Now on the basis of these results the following rate expression is proposed:

$$-\frac{d[Fe(CN)_6]^{3-}}{dt} = \frac{k_a[\text{ruthenium(III)}][\text{alcohol}]}{k_b[OH^-] + k_c[\text{alcohol}]} \quad (1)$$

TABLE III: Effect of Variation of the Ru(III) Concentration on the Rate of Oxidation

A

$[K_3Fe(CN)_6] = 2.0 \times 10^{-3}$ M, [2-methyl-1-propanol] = 2.0×10^{-2} M, [NaOH] = 8.0×10^{-2} M

[Ru(III)] $\times 10^6$ M = 0.48, 0.96, 1.44, 1.92, 2.40, 3.12, 3.60, 4.32, 4.80

$k_s \times 10^5$ M min^{-1} = 0.53, 1.02, 1.42, 1.73, 2.62, 3.40, 3.64, 4.27, 4.92

$\{k_s/[Ru(III)]\} \times 10^{-1}$ min^{-1} = 1.10, 1.06, 0.98, 0.90, 1.09, 1.08, 1.01, 0.98, 1.02

B

$[K_3Fe(CN)_6] = 2.0 \times 10^{-3}$ M, [butan-2-ol] = 2.0×10^{-2} M, [NaOH] = 2.0×10^{-2} M

[Ru(III)] $\times 10^6$ M = 0.48, 0.96, 1.20, 1.44, 1.92, 2.40, 3.60, 4.80

$k_s \times 10^5$ M min^{-1} = 0.86, 1.61, 2.00, 2.33, 3.01, 3.62, 5.21, 7.29

$\{k_s/[Ru(III)]\} \times 10^{-1}$ min^{-1} = 1.79, 1.67, 1.66, 1.61, 1.61, 1.50, 1.44, 1.51

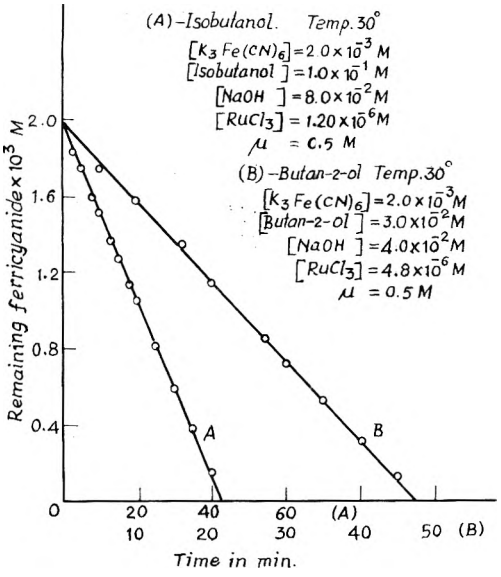

Figure 1.

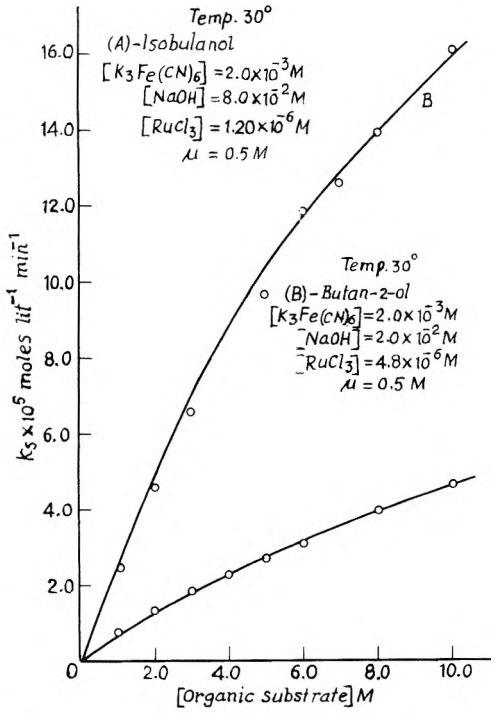

Figure 2.

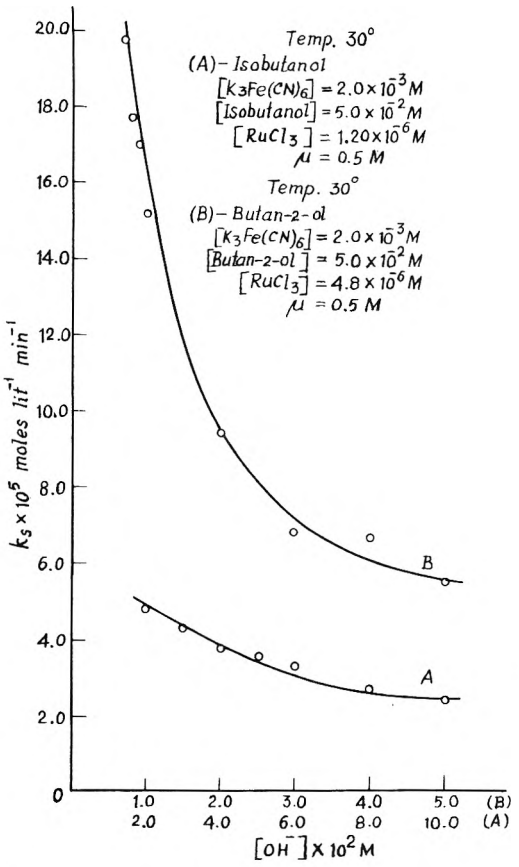

Figure 3.

where k_a, k_b, and k_c are constants.

Before presenting the probable oxidation scheme, it is interesting to know the probable species of ruthenium(III) chloride in the alkaline medium. Electronic spectra studies have confirmed that the ruthenium(III) chloride exists in the hydrated[2] form as $[Ru(H_2O)_6]^{3+}$. Metal ions[3a] of the form $[Ru(H_2O)_6]^{3+}$ are also known to exist as $[Ru(H_2O)_5(OH)]^{2+}$ in an alkaline medium.

In the present study it is quite probable that the species $[Ru(H_2O)_5OH]^{2+}$ might assume the general form $[Ru(III)(OH)_x]^{3-x}$. The value of x would always be less than six because there are no definite reports of any hexahydroxy species[3b] of ruthenium. The remainder of the coordination sphere will be filled up by water molecules.

Thus, all ruthenium(III) chloride existing in the above form in an aqueous alkaline medium will be the actual reacting species. It has frequently been observed that transition metal complexes are a good abstracting agent for the hydride ion.[4,5] They can adequately abstract a hydride ion even from a hydrogen molecule. In acidic medium the abstraction of a hydride ion from the α-carbon atom of the 2-propanol has also been observed.[6] In a similar manner studies have been performed and it was concluded that hydride ion transfer takes place from the α-carbon atom of the alcohol or alkoxide ion to the metal atom.[7] This gives sufficient evidence that hydride ion transfer will take place during the course of the oxidation of the above-mentioned alcohols by the hexacyanoferrate(III) ion in aqueous alkaline medium using ruthenium(III) chloride as a homogeneous catalyst.

On the basis of the above evidence, the oxidation of these alcohols might be described as shown in Scheme I.

The proposed mechanism apparently shows that complex formation between the ruthenium(III) species and the alcohol molecule takes place with the possible exchange of an hydroxide ion coordinated with the central metal ion.

Scheme I

$$[Ru(III)(OH)]^{2+} + H_3C\text{-}\underset{\text{alcohol}}{\underset{|}{CH_3}}\text{-}CH\text{-}CH_2OH \rightleftharpoons [Ru(III)\text{-}HOH_2C\text{-}\underset{|}{CH_3}\text{-}CH\text{-}CH_3]^{3+} + OH^- \quad (I)$$

(k_1, k_{-1}; complex C_1)

$$[complex]^{3+} \xrightarrow{k_2} H_3C\text{-}\underset{|}{CH_3}\text{-}CH\text{-}C^{\cdot}CHOH + [Ru(III)(H)]^{2+} \quad (II)$$

$$[Ru(III)(H)]^{2+} + 2OH^- + 2Fe(CN)_6^{3-} \xrightarrow{fast} [Ru(III)(OH)]^{2+} + 2Fe(CN)_6^{4-} + H_2O \quad (III)$$

$$H_3C\text{-}\underset{|}{CH_3}\text{-}CH\text{-}C^{\cdot}HOH + OH^- \xrightarrow{fast} H_3C\text{-}\underset{|}{CH_3}\text{-}CH\text{-}CHO + H_2O \quad (IV)$$

(2-methylpropionaldehyde)

The water molecule coordinated with it has been omitted for the sake of simplicity.

The complex thus formed undergoes disproportionation yielding a carbonium ion via hydride ion abstraction from the α-carbon atom of the alcohol by the ruthenium(III) species. The metal hydride then undergoes rapid oxidation with ferricyanide in the subsequent step, yielding the initial ruthenium(III) species and the ferrocyanide ion. Although the oxidation of the metal hydride would take place in one-electron abstraction steps, for the sake of simplicity only one step in the stoichiometric equation has been given. The carbonium ion thus produced in the system will react rapidly with the hydroxide ion producing an aldehyde (or ketone with secondary alcohol) and a water molecule.

If we assume a steady state condition for the concentration of complex C_1 we have

$$[C_1] = \frac{k_1[Ru(III)(OH)]^{2+}[alcohol]}{k_2 + k_{-1}[OH^-]} \quad (2)$$

The total ruthenium(III) concentration could be obtained from

$$[Ru(III)]_T = [Ru(III)(OH)]^{2+} + [complex\ C_1] \quad (3)$$

Substituting the value for the complex C_1 in eq 3 and solving for $[Ru(III)(OH)]^{2+}$, we have

$$[Ru(III)(OH)]^{2+} = \frac{[Ru(III)]_T(k_2 + k_{-1}[OH^-])}{k_2 + k_{-1}[OH^-] + k_1[alcohol]} \quad (4)$$

Now the final rate law in terms of decreasing concentration of the hexacyanoferrate(III) would be

$$-\frac{d[Fe(CN)_6]^{3-}}{dt} = \frac{2k_1k_2[alcohol][Ru(III)]_T}{k_2 + k_{-1}[OH^-] + k_1[alcohol]} \quad (5)$$

This rate law (eq 5) apparently accounts for pseudo-first-order kinetics with respect to ruthenium(III) concentration. The retarding trend due to hydroxide ion is also quite obvious from eq 5.

At high hydroxide ion and low alcohol concentration the inequality $k_2 + k_{-1}[OH^-] \gg k_1[alcohol]$ would be evident and eq 5 reduces to

$$\frac{-d[Fe(CN)_6]^{3-}}{dt} = \frac{2k_1k_2[alcohol][Ru(III)]_T}{k_2 + k_{-1}[OH^-]} \quad (6)$$

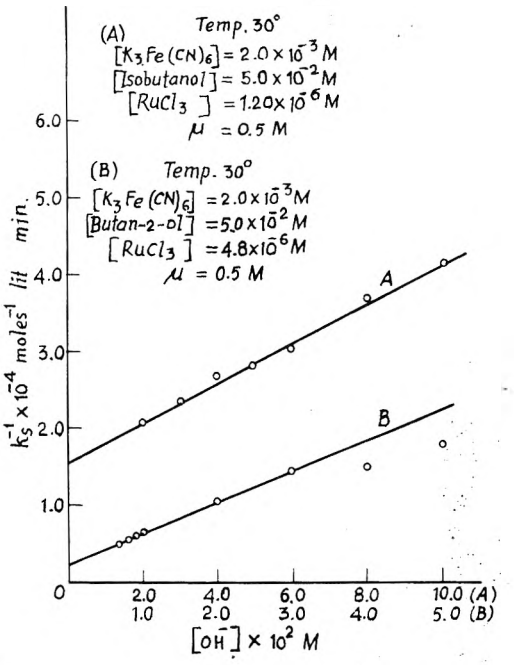

Figure 4.

This rate law (eq 6) clearly explains the first-order kinetics with respect to alcohol at low concentrations.

Further verification of rate expression 5 might be made on rearranging it as

$$\frac{1}{V_i} = \frac{1}{2k_1[alcohol][Ru(III)]_T} + \frac{k_{-1}[OH^-]}{2k_1k_2[alcohol][Ru(III)]_T} + \frac{1}{2k_2[Ru(III)]_T} \quad (7)$$

where $V_i = -d[Fe(CN)_6]^{3-}/dt$. According to eq 7, a plot of $1/V_i$ vs. $[OH^-]$ gives a straight line (Figure 4) and supports the validity of eq 5. The slope gives values for K_1k_2 as 5.1 and 32.3 for butan-2-ol and 2-methyl-1-propanol at 30 °C (where $K_1 = k_1/k_{-1}$), respectively. Similarly, a plot of $1/V_i$ vs. $1/[alcohol]$ gives a straight line (Figure 5) with a positive intercept at the $1/V_i$ axis. These straight lines again support the validity of rate law 5. From the intercept the value of k_2 is 52.1 min^{-1} for butan-2-ol and 2-methyl-1-propanol both at 30 °C. Now the value of K_1 is 9.5×10^{-2} and 59×10^{-2} for butan-2-ol and 2-methyl-1-propanol, respectively, at 30 °C.

A close examination of K_1 values clearly reveals that the rate of complex formation (k_1) is slower than the reverse process, i.e., k_{-1}, and for this reason the value of K_1 is quite small. It is quite remarkable to note that the rate of complex formation of butan-2-ol and 2-methyl-1-porpanol is in the following order: butan-2-ol < 2-methyl-1-propanol. The value of k_2 obtained for these two alcohols clearly reveals that the rate of disproportion is of the same order.

From the experimental results, it becomes apparent that for one molecule of alcohol two molecules of hexacyanoferrate(III) are consumed. Thus, the actual amount of aldehyde or ketone produced in a particular run will be half of the initial hexacyanoferrate(III) concentration and the stoichiometry of the reaction might be represented as

$$CH_3\text{-}\underset{|}{CH_3}\text{-}CH\text{-}CH_2OH + 2OH^- + 2Fe(CN)_6^{3-} \rightarrow CH_3\text{-}\underset{|}{CH_3}\text{-}CH\text{-}CHO + 2Fe(CN)_6^{4-} + 2H_2O$$

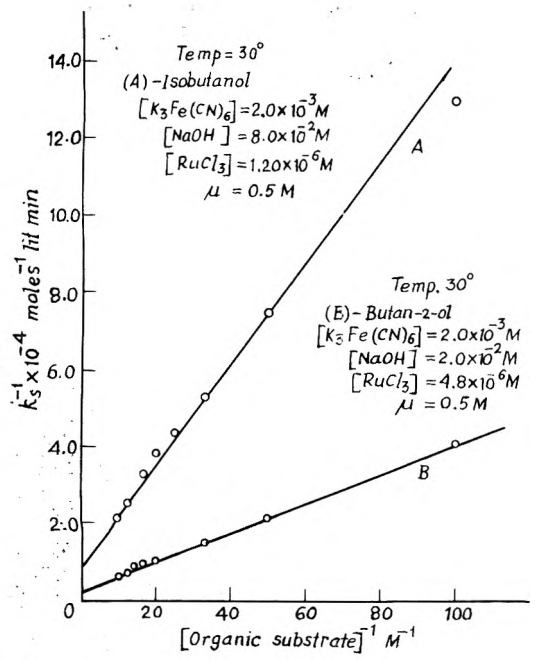

Figure 5.

A similar equation can be written for butan-2-ol.

In the above-mentioned reaction mechanism the complex formed in step I disproportionates into the ruthenium(III) hydride and the corresponding carbonium ion. The carbonium ion thus formed reacts with one molecule of hydroxide ion with the fast process resulting in the corresponding aldehyde or ketone and a water molecule. Another possibility which might be assumed is that the complex formed in step I would disproportionate in the subsequent step yielding the ruthenium(III) hydride and the corresponding aldehyde or ketone. The steps then would be as shown in Scheme II. Now, considering the general form of ruthenium(III) chloride, the probable steps then would be as shown in Scheme II. The coordinated hydroxide ions are given an unknown number x. Applying a steady state conditions, the rate law for this sequence of steps is

$$\frac{-d[Fe(CN)_6]^{3-}}{dt} = \frac{2k_1k_2[Ru(III)]_T[alcohol]}{k_2 + k_1[alcohol] + k_{-1}[OH^-]} \quad (8)$$

Rate laws 5 and 8 are the same although they have been derived from two different reaction schemes. Thus, the validity of Scheme II is again obvious.

Experimental Section

Analar (BDH) grade samples of butan-2-ol and 2-methyl-1-propanol were employed and were redistilled before use. The solution of ruthenium trichloride was prepared by dissolving the sample in very dilute hydrochloric acid with the final strength of HCl and that of ruthenium trichloride kept at 16.38×10^{-2} M and 4.8×10^{-3} M, respectively. The sample of NaOH was of AR (BDH) grade but that of potassium hexacyanoferrate(III) was of GR (S. Merck) grade.

Scheme II

$$[Ru(OH)_x]^{3-x} + H_3C\text{-}\underset{CH_3}{CH}\text{-}CH_2OH \underset{k_{-1}}{\overset{k_1}{\rightleftharpoons}} [complex]^{4-x} + OH^-$$

$$[complex]^{4-x} \xrightarrow{k_2} [(HO)_{x-2}\underset{OH_2}{Ru(III)}H]^{4-x} + H_3C\text{-}\underset{CH_3}{CH}\,CHO$$

$$[\underset{OH_2}{Ru}(OH)_{x-2}(H)]^{4-x} + 3OH^- + 2Fe(CN)_6^{3-} \xrightarrow{fast} [Ru(OH)_x]^{3-x} + 2H_2O + 2Fe(CN)_6^{4-}$$

The initiation of the reaction is carried out by mixing the requisite quantity of alcohol solution maintained at a constant temperature into a solution of $K_3Fe(CN)_6$, NaOH, and $RuCl_3$ kept in a reaction bottle at the same temperature. The temperature of the reaction mixture was kept constant with an electrically operated thermostat with an accuracy of ±0.1 °C.

The progress of reaction was followed by estimating the amount of hexacyanoferrate(II) ion produced after definite time intervals with a standard solution of ceric(IV) sulfate using ferroin as a redox indicator.[8] The method always gave reproducible results. This clearly confirms that ceric(IV) does not react with the alcohols under the present experimental conditions. In a separate set of experiments methyl ethyl ketone and 2-methylpropionaldehyde were confirmed as the main oxidation products via the catalytic route using chromatography.

Acknowledgment. One of the authors (R. K. Singh) wishes to express his thanks to U.G.C. (New Delhi) for financing the project.

References and Notes

(1) S. Wolfe, S. K. Hasan, and J. R. Campbell, *J. Chem. Soc. D*, 1420 (1970).
(2) R. E. Connick and D. A. Fine, *J. Am. Chem. Soc.*, **82**, 4187 (1960).
(3) (a) F. A. Cotton and G. Wilkinson, "Advanced Inorganic Chemistry", 2nd ed, Wiley, New York, N.Y., p 153; (b) W. P. Griffith, "The Chemistry of the Rarer Platinum Metals", Interscience, New York, N.Y., 1967, p 27.
(4) J. F. Harrod, S. Ciccone, and J. Halpern, *Can. J. Chem.*, **39**, 1372 (1961).
(5) (a) G. Lee Donald and V. D. E. Mathus, *Can. J. Chem.*, **50**, 2000, 3129 (1972); (b) S. Yoel and R. Garryl, *ibid.*, **52**, 3825 (1974).
(6) H. B. Charman, *J. Chem. Soc. B*, 629 (1967).
(7) J. Chatt and B. L. Shah, *Chem. Ind.*, 290 (1961).
(8) V. N. Singh, H. S. Singh, and B. B. L. Saxena, *J. Am. Chem. Soc.*, **91**, 2643 (1969).

Mechanism of the Disproportionation of Superoxide Radicals[1]

Benon H. J. Bielski* and Augustine O. Allen

Chemistry Department, Brookhaven National Laboratory, Upton, New York 11973 *(Received February 4, 1977)*

Publication costs assisted by Brookhaven National Laboratory

New measurements are reported on the rate of the spontaneous uncatalyzed second-order decay of the superoxide radical in aqueous solution at 23 °C. By extreme purification of reagents, and addition of small amounts of EDTA to sequester traces of catalytic metal ions, purely second-order kinetics were found up to pH 13.2. The pH effects clearly show that the ionic form O_2^- never reacts with itself but only with the HO_2 in equilibrium with it, even when the ratio HO_2/O_2^- is as small as 2×10^{-8}; the rate constant for $O_2^- + O_2^-$ is less than 0.3 M^{-1} s^{-1}. The pK of HO_2 was determined as 4.75 ± 0.08, and the bimolecular rate constants were $k_1 = (7.61 \pm 0.55) \times 10^5$ M^{-1} s^{-1} for $HO_2 + HO_2$ and $k_2 = (8.86 \pm 0.43) \times 10^7$ M^{-1} s^{-1} for $HO_2 + O_2^-$, all in good agreement with published values. The change in the spontaneous decay of superoxide radicals with pH follows the equation $k_{obsd} = [k_1 + k_2 K_{HO_2}/(H^+)]/[1 + K_{HO_2}/(H^+)]^2$. The optical extinction coefficients of hydrogen peroxide were determined over the pH range 6.1–13.8 at wavelengths from 280 to 230 nm.

In the course of developing techniques for studying the chemical reactions of radiation-generated superoxide radicals, we have obtained considerable data on their spontaneous decay, which is due to their disproportionation to form oxygen and hydrogen peroxide. Our measurement techniques include pulse radiolysis and the recently described method of stopped-flow radiolysis;[2] but equally important are the techniques of purification of reagents. Although the disproportionation of these radicals should be a purely second-order reaction, previous workers[3,4] have found that in an alkaline solution a first-order component, attributed to the presence of catalytic impurities, was superimposed on the second-order reaction. By reducing heavy metal impurities in our solutions to the order of a few parts per billion, and working always in the presence of ethylenediaminetetraacetic acid (EDTA) to sequester the remaining traces of metals, we have been able to carry the determinations of reaction rate to a higher pH than previous workers. The results indicate that the disproportionation of the ionic form O_2^- in aqueous solution appears always to occur by reaction with the small quantity of HO_2 present in equilibrium, and there is no evidence that the ionic form O_2^- is capable of reacting directly with itself.

Experimental Section

Materials. Ordinary distilled water was purified by a Milli-Q reagent grade water system obtained from the Millipore Corporation of Bedford, Mass. This treatment, consisting of deionization followed by ultrafiltration, was found to produce water more nearly free of catalytic heavy metal impurities than the formerly used multiply distilled water. Reagent grade EDTA, purchased as the disodium salt, was dissolved in water and precipitated in the acid form by addition of perchloric acid. The acid form was then recrystallized directly from hot water. Analysis showed that the original product contained 10 ppm of Fe which was reduced to 0.037 ppm by two recrystallizations. The product was always recrystallized at least three times before use. Perchloric acid was the double vacuum distilled product from G. Frederick Smith Chemical Co., guaranteed to contain less than 0.01 ppm of iron or heavy metals. Trisodium phosphate and sodium formate were recrystallized from water containing EDTA and then twice more from pure water. Baker Analyzed Reagent grade sodium hydroxide was made into a 50% slurry in water, cooled in an ice bath, and filtered through ultra-fine sintered glass. It was then diluted with purified water to a concentration of about 1.5 M and was then filtered through a "fluoropore" cartridge (Millipore Corporation) having a pore size of 0.2 μm. Water and all solutions were stored in carefully cleaned vessels of fused silica.

Solutions Used. All irradiated solutions were saturated with air or oxygen and contained formic acid or sodium formate in concentration ranging from 0.01 to 0.1 M, together with EDTA to a concentration 0.01 of that of the formate. Presence of these solutes converts all the primary radicals, e^-, H, and OH to the form HO_2 or O_2^-.[3,4] A 100-fold excess of formate over EDTA is sufficient to protect the latter from attack by OH radicals.

Procedures. Four different irradiation procedures were used depending upon the pH and the rates of radical decay to be measured. In every case the measurement consisted of determining the rate of decline of the optical density at 250–270 nm and 23 °C due to HO_2 or O_2^-.

(a) *Pulse Radiolysis.* This was the standard pulse radiolysis method for HO_2 detection described for example by Bielski and Schwarz.[5]

(b) *Stopped-Flow Radiolysis.* This method (described by Bielski and Richter[2]) uses a fast kinetics spectrophotometer (Durrham Instrument Co. Model D110) modified so that one of the flowing solutions passes through a 2-MeV electron beam produced by a Van de Graaff generator. This solution was always adjusted to pH 9.5 with trisodium phosphate. In the fast mixing chamber the solution was mixed with one containing acid or buffer to produce the desired pH, and then entered a spectrophotometer where, after the flow stopped, the decay of the radical was monitored. The optical cell in this setup has an internal diameter of only 2 mm, and it was found that for reactions lasting longer than 1 min the kinetics became distorted by wall reactions which led to introduction of a first-order component superimposed on the second-order decay reaction.

(c) *Continuous-Flow Radiolysis.* For systems in which the first half-life of the radicals was longer than 1 min, instead of stopping the flow the entire irradiated mixed solution was collected in a test tube and was then poured into an optical cell which was placed in a Cary 14 spectrophotometer, and the optical density was read out as a function of time on a recorder. The optical cells used in the spectrophotometer are 2 cm in diameter and no de-

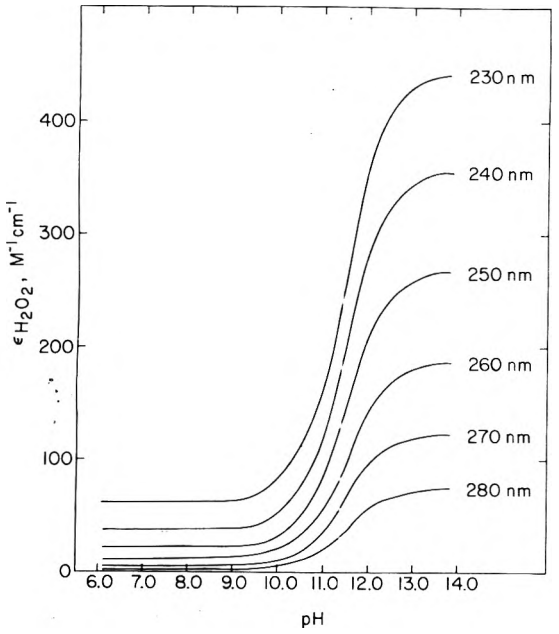

Figure 1. Optical extinction coefficients for alkaline aqueous hydrogen peroxide solutions.

tectable wall reaction occurs in these cells in the course of 2 h.

(d) γ *Ray Radiolysis.* When the decay of the radicals was very slow (at pH >10) the solutions were irradiated with γ rays which resulted in building up the concentration of radicals to a higher level than was obtained in the other methods. The solutions were allowed to stay in the γ-ray source until an optical density of the order of unity due to the radicals had been built up. Depending on the concentration, cells of optical path lengths of 10, 5, or 1.8 cm were used. These solutions contained 0.01 M HCOONa, 10^{-4} M EDTA, and the pH was adjusted with NaOH.

Extinction Coefficients. The extinction coefficients of HO_2 (ϵ_{250nm} 800 M^{-1} cm^{-1}; ϵ_{260nm} 495 M^{-1} cm^{-1}; ϵ_{270nm} 260 M^{-1} cm^{-1}) and O_2^- (ϵ_{250nm} 1930 M^{-1} cm^{-1}; ϵ_{260nm} 1680 M^{-1} cm^{-1}; ϵ_{270nm} 1330 M^{-1} cm^{-1}) were taken from the work of Behar et al.[4] At any pH the ratio of O_2^- to HO_2 is determined by the equilibrium constant $K = (H^+)(O_2^-)/(HO_2)$. We set $K/(H^+) = X$ so that $\log X = pH - pK$. The ratio $(O_2^-)/(HO_2) = X$ and the total radical concentration $(R) = (HO_2) + (O_2^-) = (HO_2)(1 + X)$. Then to determine the effective extinction coefficient of the total radical concentration, ϵ_R, at any pH, we note that the optical absorbance $A = \epsilon_R(R) = \epsilon_{HO_2}(HO_2) + \epsilon_{O_2^-}(O_2^-) = (HO_2)(\epsilon_{HO_2} + \epsilon_{O_2^-}X)$. Hence

$$\epsilon_R = (\epsilon_{HO_2} + \epsilon_{O_2^-}X)/(1 + X) \qquad (A)$$

For the decay study, however, the extinction coefficient to be used must be corrected for the absorption from the H_2O_2 formed in the reaction. Since each radical disappearing forms one-half molecule of H_2O_2, the loss in absorbance will correspond to the difference $\epsilon_R - {}^1/_2\epsilon_{H_2O_2}$. Although the peroxide correction is small it is not entirely negligible and since we could not find appropriate values in the literature we determined them. A stock solution of hydrogen peroxide was made by dilution with pure water of the Mallinckrodt analytical reagent 30% solution, and its concentration was determined by the modified Ghormley iodometric method.[6] The stock solution (0.063 M) was then diluted to 50 times its volume with various buffers and the optical density was read on the Cary 14 spectrophotometer. Although peroxide is somewhat unstable in alkaline solution the determinations were fast enough so that the concentrations were found not to change noticeably during the time required for dilution and measurement.

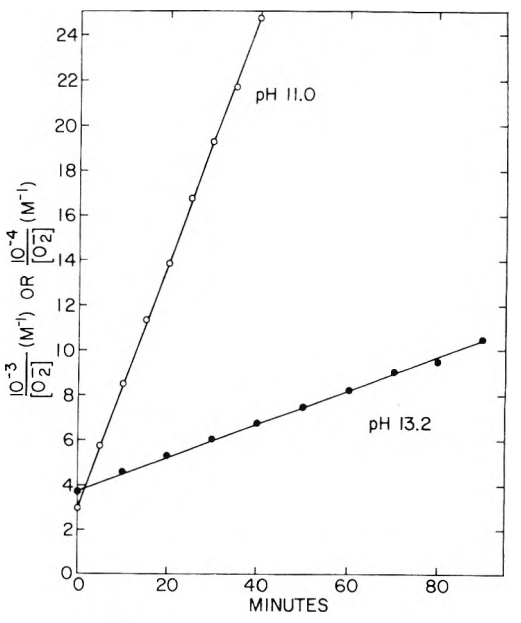

Figure 2. Typical runs showing second-order decay of O_2^- at high pH. Ordinate: $10^{-3}/[O_2^-]$ for pH 13.2; $10^{-4}/[O_2^-]$ for pH 11.0.

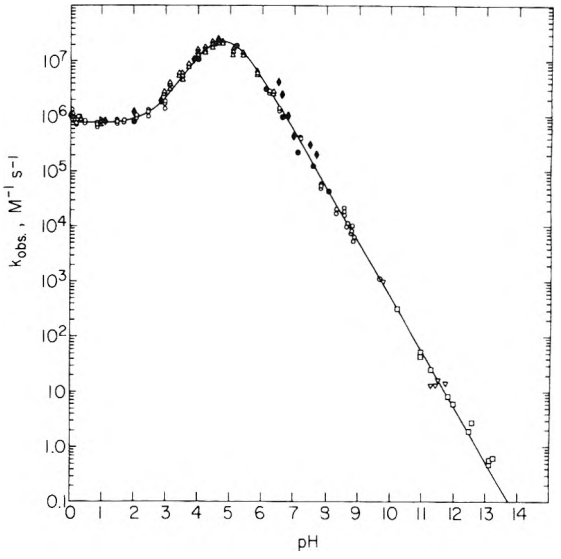

Figure 3. Observed second-order rate constants for the decay of superoxide radical plotted vs. pH. The curve gives the function $k_{obsd} = [7.61 \times 10^5 + 1.58 \times 10^{pH+3}][1 + 1.78 \times 10^{pH-5}]^{-2}$: O, stopped flow; △, pulse radiolysis; ▽, continuous flow; □, γ rays; ▷, $NaClO_4$ added; ◆, ref 4; ●, ref 3.

Results

The extinction coefficients of hydrogen peroxide are shown in Figure 1. The increase in $\epsilon_{H_2O_2}$ in alkaline solutions is due to the ionization of H_2O_2 to form HO_2^- which has higher extinction coefficients. The results on the acid side are in good agreement with the literature values.[7]

All runs reported here showed strictly second-order decay of the radical as indicated by the linearity of plots of the reciprocal of the optical density against time. Typical results at high alkalinity are shown in Figure 2. If any deviation from linearity appeared the result was rejected, and it was always found that such deviation was due to the presence of impurities, so that when more rigorous precautions to eliminate impurities were taken

these plots straightened out.

The bimolecular rate constants for superoxide radical decay which we have obtained by least-squares treatment of each run are assembled in Figure 3, which also includes results taken from the literature.[3,4] The solid curve in the figure is given by a theoretical expression discussed below. Agreement with the theory is extremely good except at the lowest pH where a rise in the decay rate occurs at a place where the theoretical expression has leveled off to a plateau. To see whether this rise could be due to the increase in ionic strength resulting from the addition of perchloric acid necessary to reduce the pH to near-zero values, runs were made at pH 0.92 with the addition of approximately 1 M $NaClO_4$. This change in ionic strength had no detectable effect on the rate.

Discussion

The decay of superoxide radicals has been explained[3] by the occurrence of three bimolecular reactions between the neutral and ionic forms:

$$HO_2 + HO_2 \rightarrow O_2 + H_2O_2 \quad (1)$$

$$HO_2 + O_2^- \rightarrow O_2 + HO_2^- \xrightarrow{(H_2O)} O_2 + H_2O_2 + OH^- \quad (2)$$

$$O_2^- + O_2^- \rightarrow O_2 + O_2^{2-} \xrightarrow{(2H_2O)} O_2 + H_2O_2 + 2OH^- \quad (3)$$

The observed rate of decline of the total radical concentration (R) = $(HO_2) + (O_2^-)$ is given (if reaction (3) is neglected) by

$$-d(R)/dt = k_{obsd}(R)^2 = k_1(HO_2)^2 + k_2(HO_2)(O_2^-) \quad (B)$$

Since O_2^- and HO_2 are in equilibrium with H^+, we have $(O_2^-) = (HO_2)K/(H^+) = (HO_2)X$ and $(R) = (HO_2)(1 + X)$, where $X = K/(H^+)$ and $\log X = pH - pK$, with $pH = -\log (H^+)$ and $pK = -\log K$. Substituting in (B), one finds[4]

$$k_{obsd} = \frac{k_1 + k_2X}{(1 + X)^2} \quad (C)$$

The best fit of this expression to our data gave the curve shown in Figure 3.

At large X (high pH) the first terms in both numerator and denominator become negligible and $k_{obsd} = k_2(H^+)/K$; $\log k_{obsd} = -pH + pK + \log k_2$. Thus a plot of $\log k_{obsd}$ vs. pH is a line of slope −1 and intercept (at $k_{obsd} = 1\ M^{-1}\ s^{-1}$) of $\log (k_2/K)$. Figure 3 shows that a line of slope −1 fits our data over a range of seven orders of magnitude in k_{obsd}; a least-squares fit to 28 data points between pH 7 and 12 yielded $k_2/K = (4.98 \pm 0.24) \times 10^{-12}$. An average of 8 data points between pH 0.9 and 1.7 gave $k_1 = (7.61 \pm 0.55) \times 10^5\ M^{-1}\ s^{-1}$. With these values for k_1 and k_2/K, K was calculated from eq C for each of 49 data points between pH 2 and 6.5. The average yielded $K_{HO_2} = 1.78 \pm 0.34 \times 10^{-5}$ M, $pK_{HO_2} = 4.75 \pm 0.08$; $k_2 = (8.86 \pm 0.43) \times 10^7\ M^{-1}\ s^{-1}$ compared to the earlier reported values of $K = 1.32 \times 10^{-5}$ M, $pK_{HO_2} = 4.88 \pm 0.10$; $k_2 = 8.5 \times 10^7\ M^{-1}\ s^{-1}$, and $k_1 = 7.6 \times 10^5\ M^{-1}\ s^{-1}$.[4] We have extended the study to pH >13 without finding any deviation from eq C. The effect of reaction 3 would be to increase points at high pH, with a k_{obsd} leveling off at a value equal to k_3. No such effect is seen, and we can say definitely that k_3 is less than $0.3\ M^{-1}\ s^{-1}$. Behar et al.[4] found $k_3 < 100\ M^{-1}\ s^{-1}$; a more recent article[8] claims $k_3 = 6\ M^{-1}\ s^{-1}$ at pH >12. These results must have been affected by traces of impurity in the solutions used.

Certainly the direct reaction of O_2^- with itself plays no role in the behavior of the radical ion in aqueous solution under any ordinary conditions, and O_2^- disappears only by reaction with the HO_2 which exists in equilibrium, or by reaction with catalysts. We suggest that the self-disproportionation cannot occur at all, as shown by the reported stability of O_2^- in aprotic solvents. Thus, a 0.15 M solution of KO_2 in dimethyl sulfoxide, stabilized by a crown ether, showed[9] less than 10% decomposition in 1 day at room temperature. Discussions[10] of the supposed self-reaction of O_2^- and the state of the O_2 formed from it have little relevance to real situations.

The weak acid catalysis shown by the rise in k_{obsd} at pH values below 1 is real and not due to ionic strength effects.

References and Notes

(1) Research carried out at Brookhaven National Laboratory under contract with the U.S. Energy Research and Development Administration and supported by its Division of Physical Research.
(2) B. H. J. Bielski and H. W. Richter, *J. Am. Chem. Soc.*, submitted for publication.
(3) J. Rabani and S. O. Nielsen, *J. Phys. Chem.*, **73**, 3736 (1969).
(4) D. Behar, G. Czapski, J. Rabani, L. M. Dorfman, and H. A. Schwarz, *J. Phys. Chem.*, **74**, 3209 (1970).
(5) B. H. J. Bielski and H. A. Schwarz, *J. Phys. Chem.*, **72**, 3836 (1968).
(6) B. H. J. Bielski and A. O. Allen, *Int. J. Radiat. Phys. Chem.*, **1**, 153 (1969).
(7) W. C. Schumb, C. N. Satterfield, and R. N. Wentworth, "Hydrogen Peroxide", Reinhold, New York, N.Y., 1955, p 287.
(8) J. Divišek and B. Kastening, *J. Electroanal. Chem.*, **65**, 603 (1975).
(9) J. S. Valentine and A. B. Curtis, *J. Am. Chem. Soc.*, **97**, 224 (1975).
(10) A. U. Khan, *J. Phys. Chem.*, **80**, 2219 (1976).

Radiation-Induced Homolytic Aromatic Substitution. 6. The Effect of Metal Ions on the Hydroxylation of Benzonitrile, Anisole, and Fluorobenzene

Manfred K. Eberhardt

Puerto Rico Nuclear Center,[1] Caparra Heights Station, San Juan, Puerto Rico 00935 *(Received October 27, 1976)*

Publication costs assisted by the Center for Energy and Environment Research[†]

The radiation-induced hydroxylation of benzonitrile, anisole, and fluorobenzene has been investigated. In absence of oxidizing agents (O_2, metal salts) only trace amounts of substituted phenols are formed. Some metal salts ($Fe(CN)_6^{3-}$, Fe^{3+}, $Cr_2O_7^{2-}$) oxidize the intermediate hydroxycyclohexadienyl radicals and give a very high conversion of OH radicals to phenols, whose isomer distribution is dependent on the metal salts. With Cu^{2+} salts ($Cu(ClO_4)_2$, $CuSO_4$, $CuCl_2$) no oxidation of the hydroxycyanocyclohexadienyl radicals was observed. Oxidation with $K_3Fe(CN)_6$ leads in a quantitative way to the corresponding phenols. We have shown that in the hydroxylation of anisole, fluorobenzene, bromobenzene, toluene, benzonitrile, and nitrobenzene a linear relationship exists between log $2k_m/2k_o + 2k_m + k_p$ and log k_p/k_m and σ_M values. Electron-withdrawing substituents give a high percentage of meta hydroxylation, whereas electron-donating substitients give a low percentage of meta hydroxylation. This is due to the increasing electron density at the ortho and para positions and the decreasing electron density at the meta position with increasing +M effect. With strong electron-withdrawing substituents the OH radicals attack in a statistical fashion. As the difference in electron density between ortho and meta position increases the electrophilic OH radicals attack preferentially at the ortho and para positions. From our results we conclude that dehydration from the initially formed hydroxycyclohexadienyl radicals takes place only if the substituent is electron donating (+M effect), but not if the substituent is electron withdrawing (NO_2, CN). The reversible dehydration of the isomeric hydroxyfluorocyclohexadienyl radicals gives phenol indicating the fluorobenzene radical cation as intermediate. For the rate of oxidation of the hydroxyfluorocyclohexadienyl radicals the following sequence was established: $Fe(CN)_6^{3-} > Cu^{2+} > Fe^{3+}$.

Introduction

The radiolysis of water is a convenient way to produce an accurately known amount of OH radicals and study their reactions. In the radiolysis of aqueous benzene solutions the following mechanism is generally accepted:

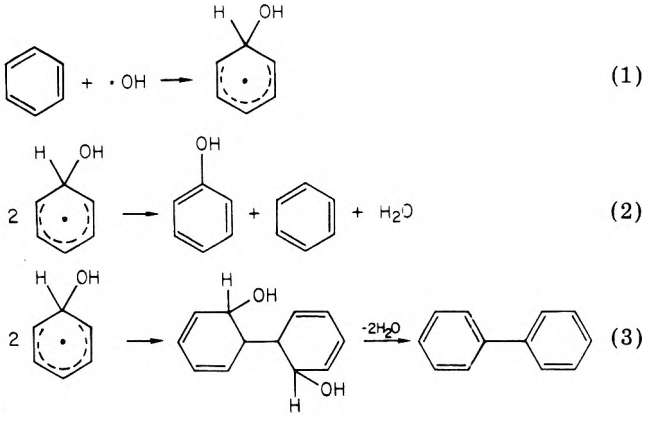

The hydroxycyclohexadienyl radical undergoes disproportionation and dimerization. In some cases (anisole,[2,3] fluorobenzene,[2] toluene,[3-5] phenylacetic acid,[5] phenol,[6] and benzene) the hydroxycyclohexadienyl radicals have been found to undergo acid-catalyzed dehydration. In the radiolysis of benzene the hydroxycyclohexadienyl radical was also found to recombine with the H· atom adduct to benzene to form phenylcyclohexadienes.[7] All of the above reactions contribute to the low yield of phenols observed in the radiation induced hydroxylation of aromatics. Oxidizing agents (such as oxygen[8] and metal salts[9]) have been used to oxidize the intermediate hydroxycyclohexadienyl radicals and increase the yield of phenols. In a recent study on the hydroxylation of nitrobenzene[10] and toluene[11] we have shown that in presence of several metal salts a high conversion of OH radicals to substituted phenols can be obtained. In both cases $K_3Fe(CN)_6$ and $K_2Cr_2O_7$ were found to be the most effective oxidizing agents. The effectiveness of $K_3Fe(CN)_6$ was also observed in the hydroxylation of benzene[12] and benzoic acid.[13] In the hydroxylation of nitrobenzene[10] and toluene[11] we have observed a drastic change in isomer distribution depending on the oxidizing metal salts and in the case of toluene with pH. In order to predict the relative reactivity of the ortho, meta, and para positions toward OH radical attack from the final product distribution one has to make sure that the oxidation of the intermediate hydroxycyclohexadienyl radicals is fast compared to the other radical termination processes mentioned above. Since $K_3Fe(CN)_6$ seems to be the most effective oxidizing agent we have suggested that in the hydroxylation of nitrobenzene at low pH and of toluene the isomer distribution of the nitrophenols and cresols is a direct measure of the relative reactivities at the ortho, meta, and para positions. In order to learn more about the reactivity of OH radicals toward aromatics we have investigated the hydroxylation of benzonitrile, anisole, and fluorobenzene.

Results

Fluorobenzene. The products in the hydroxylation of fluorobenzene are phenol and the three isomeric fluorophenols. Bielski and Allen[14] have determined that in the radiolysis of water $G(\cdot OH) = 2.74 \pm 0.08$ at pH 7. The results summarized in Table I show that in presence of metal salts an excellent material balance is obtained, whereas in absence of oxidizing agents only trace amounts of fluorophenols and a small amount of phenol ($G = 0.7$) are formed. The relative yield of phenol to fluorophenols depends on the metal salts and the pH. With $K_3Fe(CN)_6$ we obtain the highest (almost quantitative) conversion of OH radicals to fluorophenols. In presence of $K_3Fe(CN)_6$

[†] Formerly the Puerto Rico Nuclear Center.

TABLE I: Fluorophenol and Phenol Yields in the Radiolysis of Aqueous Fluorobenzene Solutions[a]

Expt no.	Conditions	G values				%			
		Ortho	Meta	Para	Total	PhOH	Ortho	Meta	Para
1	$K_3Fe(CN)_6$ 5×10^{-4} M	1.12	0.53	0.93	2.58	0.30	43.4	20.5	36.1
2	10^{-3} M	1.12	0.54	0.90	2.56	0.27	43.7	21.1	35.2
3	2×10^{-3} M	1.18	0.57	0.98	2.73	0.28	43.2	20.9	35.9
4	5×10^{-3} M	1.12	0.54	0.92	2.58	0.25	43.4	20.9	35.7
5	10^{-2} M	1.11	0.53	0.92	2.56	0.26	43.4	20.7	35.9
6	5×10^{-4} M, pH 1.6[b]	1.14	0.27	1.06	2.47	0.74	46.2	10.9	42.9
7	5×10^{-3} M, pH 1.6[b]	1.20	0.49	1.00	2.69	0.29	44.6	18.2	37.2
8	$CuSO_4$ 10^{-3} M	0.55	Tr[c]	0.72	1.27	0.38	43.3		56.7
9	5×10^{-3} M	0.98	Tr	1.02	2.00	0.36	49.0		51.0
10	5×10^{-2} M	0.94	Tr	0.81	1.75	0.25	53.7		46.3
11	Argon satd	Tr	Tr	Tr		0.70			
12	Oxygen (10^{-3} M)	Tr	0.32	0.56	0.88	0.24		36.4	63.6
13	Argon satd + 0.1 M $HClO_4$, pH 1.7	None	None	None	None	2.35			
14	$FeNH_4(SO_4)_2$ 5×10^{-4} M, pH 3.05	Tr	Tr	Tr	Tr	2.0			
15	2×10^{-3} M, pH 2.85	0.1	Tr	0.1	0.2	2.15	50.0		50.0
16	5×10^{-3} M, pH 2.70	0.23	Tr	0.22	0.45	2.0	51.1		48.9
17	2×10^{-2} M, pH 2.50	0.43	Tr	0.46	0.89	2.2	48.3		51.7
18	5×10^{-2} M, pH 2.70	0.54	Tr	0.55	1.09	1.9	49.5		50.5
19	$CuSO_4$ 5×10^{-3} M, pH 4.6	0.95	Tr	0.98	1.93	0.36	49.2		50.8
20	5×10^{-3} M, pH 3.1[b]	0.84	Tr	0.80	1.64	0.61	51.2		48.8
21	5×10^{-3} M, pH 2.7[b]	0.70	Tr	0.58	1.28	1.00	54.7		45.3
22	5×10^{-3} M, pH 2.3[b]	0.40	Tr	0.34	0.74	1.70	54.1		45.9
23	5×10^{-3} M, pH 1.7[b]	Tr	Tr	Tr	Tr	3.0			

[a] All solutions were deoxygenated (except experiment no. 12) solutions (5×10^{-3} M fluorobenzene) irradiated at a dose rate of 2.06×10^{16} eV/g min, and a total dose of 1.54×10^{18} eV/g. [b] The pH in these experiments was adjusted with $HClO_4$. [c] Tr = trace.

TABLE II: Hydroxyanisole and Phenol Yields in the Radiolysis of Aqueous Anisole Solutions[a]

Expt no.	Conditions	G values				%			
		Ortho	Meta	Para	Total	PhOH	Ortho	Meta	Para
1	$K_3Fe(CN)_6$ 5×10^{-4} M	1.35	0.26	0.98	2.59	0.14	52.1	10.0	37.8
2	10^{-3} M	1.29	0.25	0.96	2.50	0.16	51.6	10.0	38.4
3	2×10^{-3} M	1.34	0.26	1.00	2.60	0.18	51.5	10.0	38.5
4	5×10^{-3} M	1.30	0.26	0.97	2.53	0.16	51.4	10.3	38.3
5	10^{-2} M	1.34	0.26	0.98	2.58	0.18	51.9	10.1	38.0
6	5×10^{-2} M	1.28	0.27	0.90	2.45	0.14	52.2	11.0	36.7
7	5×10^{-4} M, pH 1.6[b]	0.38	Tr	Tr	0.38	0.18	100		
8	$K_3Fe(CN)_6$ 5×10^{-3} M, pH 1.0[b]	1.05	Tr	0.20	1.25	0.15	84.0		16.0
9	$K_3Fe(CN)_6$ 5×10^{-3} M, pH 2.4[b]	1.05	0.05	0.52	1.02	0.15	65.0	8.0	32.0
10	$K_3Fe(CN)_6$ 5×10^{-3} M, pH 3.2[b]	1.10	0.20	0.85	2.15	0.15	51.2	9.3	39.5
11	$CuSO_4$ 5×10^{-3} M	1.29	Tr	0.48	1.77	0.20	72.0		27.1
12	5×10^{-2} M	1.36	0.1	0.80	2.26	0.20	60.2	4.4	34.4
13	Argon	Tr	Tr	Tr	Tr	0.64			
14	O_2 (10^{-3} M)	0.28	Tr	0.49	0.77	0.22	36.4		63.6
15	Argon, pH 1.4[b]	Tr	Tr	Tr		Tr			

[a] All solutions were deoxygenated (except expt no. 14) solutions of anisole (5×10^{-3} M) irradiated at a dose rate of 2.06×10^{16} eV/g min, and a total of 1.54×10^{18} eV/g. [b] The pH in these experiments was adjusted with $HClO_4$.

the total yield of fluorophenols as well as the isomeric distribution is constant over a wide range of concentration. This observation was made previously by us in the hydroxylation of nitrobenzene,[10] and by Schuler et al.[13] in the hydroxylation of benzoic acid. With Cu^{2+} and Fe^{3+} as oxidizing agents we obtain much less fluorophenols and more phenol, whose percentage is increasing with decreasing pH in agreement with previous observations in the hydroxylation with Fenton's reagent.[2] Particularly interesting with Cu^{2+} and Fe^{3+} is the almost complete absence of *m*-fluorophenol. In absence of any oxidizing agent, we observe an especially dramatic pH effect. In neutral solution (expt 11) very little phenol is formed, but at pH 1.7 (expt 13) we obtain a very high conversion (ca. 85%) of OH radicals to phenol.

Anisole. The results on the hydroxylation of anisole show essentially the same characteristic patterns as those on fluorobenzene (see Table II). The products are hydroxyanisoles and phenol. A quantitative material balance is obtained with $K_3Fe(CN)_6$, and the isomer ratio stays constant over a wide range of concentration. With decreasing pH the *G*(meta) and *G*(para) decrease considerably, while *G*(ortho) changes very little. With Cu^{2+} the *G*(hydroxyanisole) is smaller and so is the percentage of *m*-hydroxyanisole. A most interesting observation is that even in presence of $K_3Fe(CN)_6$, when we obtain an almost quantitative conversion of OH radicals to hydroxyanisole, we obtain only a small percentage of meta hydroxylation. The same observations were made in the hydroxylation with Fenton's reagent.[3] In absence of metal salts only trace amounts of hydroxyanisoles were obtained.

An important difference to the fluorobenzene results is the observation that with decreasing pH value the decrease in hydroxyanisoles is not accompanied by an equivalent increase in the yield of phenol.

Benzonitrile. No study on the homolytic hydroxylation of benzonitrile has been reported. Our results (Table III) show that in presence of $K_2Cr_2O_7$ or $K_3Fe(CN)_6$ high conversions of OH radicals to hydroxybenzonitriles are obtained, while in absence of metal salts only trace am-

TABLE III: Hydroxybenzonitrile Yields in the Radiolysis of Aqueous Benzonitrile Solutions[a]

Expt no.	Conditions		G values[b]				%		
			Ortho	Meta	Para	Total	Ortho	Meta	Para
1	$K_2Cr_2O_7$	5×10^{-4} M	1.22	0.63	0.60	2.45	49.8	25.7	24.5
2		5×10^{-3} M	1.25	0.87	0.58	2.70	46.3	32.2	21.5
3		5×10^{-2} M	1.40	1.13	0.77	3.30	42.4	34.2	23.3
4	$K_3Fe(CN)_6$	5×10^{-4} M	1.08	0.76	0.55	2.39	45.2	31.8	23.0
5		5×10^{-3} M	1.07	0.80	0.52	2.39	44.8	33.5	21.8
6		5×10^{-2} M	1.03	0.75	0.49	2.27	45.4	33.0	21.6
7	$K_3Fe(CN)_6$ + $K_4Fe(CN)_6$	5×10^{-4} M 5×10^{-4} M	0.82	0.63	0.42	1.87	43.8	33.7	22.5
8	$K_3Fe(CN)_6$	5×10^{-4} M, pH 1.4[c]	1.10	0.80	0.55	2.45	44.9	32.6	22.5
9		5×10^{-3} M, pH 1.4[c]	1.12	0.82	0.55	2.49	45.0	32.9	22.1
10		5×10^{-2} M, pH 1.4[c]	1.08	0.80	0.55	2.43	44.4	32.9	22.6
11	$K_3Fe(CN)_6$ + $K_4Fe(CN)_6$	5×10^{-4} M 5×10^{-4} M, pH 1.4[c]	1.05	0.78	0.55	2.38	44.1	32.8	23.1
12	$Fe(ClO_4)_3$	5×10^{-4} M, pH 2.8	Tr	Tr	Tr				
13		5×10^{-3} M pH 2.2	0.46	0.11	0.25	0.82	56.1	13.4	30.5
14		5×10^{-3} M pH 1.6	1.30	0.33	0.66	2.29	56.8	14.4	28.8
15	Argon satd		Tr	Tr	Tr	>0.1			
16	Oxygen 10^{-3} M		0.93	0.33	0.42	1.68	55.4	19.6	25.0

[a] All solutions were deoxygenated (except experiment no. 16) solutions (5×10^{-3} M benzonitrile) irradiated at a dose rate of 2.44×10^{16} eV/g min, and a total dose of 1.46×10^{18} eV/g. [b] The G value is defined as the number of molecules produced per 100 eV of energy absorbed. [c] The pH in these experiments (no. 8, 9, 10 and 11) was adjusted with H_2SO_4.

ounts of phenols are produced. With $K_2Cr_2O_7$ at a concentration of 5×10^{-2} M (expt 3) we observe a somewhat higher yield of hydroxybenzonitrile than G(·OH). This result was also obtained by us in the hydroxylation of nitrobenzene,[10] and by Bhatia and Schuler[12] in the hydroxylation of benzene. The latter authors have pointed out that this effect may be due to a reaction of reduced metal ion with H_2O_2, which is formed in the irradiation of water. This could increase the G(·OH) by as much as the yield of H_2O_2 (G = 0.7).

The isomer distribution again is dependent on the metal salts. Comparing experiment 10 ($K_3Fe(CN)_6$) with 14 ($Fe(ClO_4)_3$) we observe very little change in the total yield of hydroxybenzonitrile, but with Fe^{3+} the yield of meta isomer is lower, whereas the yield of ortho and para isomers is higher.

There are several characteristic differences in the hydroxylation of benzonitrile as compared to fluorobenzene and anisole: (1) The effect of pH: in presence of $K_3Fe(CN)_6$ at pH 1.4 (Table III, expt 8–10) we obtain the same G(total hydroxybenzonitrile) and the same isomer distribution as in neutral solution (Table III, expt 3–6). (2) In the hydroxylation of benzonitrile in presence of metal salts no phenol was detected. (3) A high percentage of metahydroxylation. These observations seem to be characteristic of aromatics with electron-withdrawing substituents, since similar results were obtained in the radiation-induced hydroxylation of nitrobenzene.

In the hydroxylation of nitrobenzene we reported a selective reduction of the ortho and para OH radicals adducts by $Fe(CN)_6^{4-}$. This selective reduction is not observed with benzonitrile (expt 7 and 11). The decrease in G(hydroxybenzonitriles) in experiment 7 is due to a competition between $Fe(CN)_6^{4-}$ and benzonitrile for OH radicals ($k = 1.1 \times 10^{10}$ M^{-1} s^{-1} and $k = 4.9 \times 10^9$ M^{-1} s^{-1}, respectively).[15] On the basis of the rate constants one would expect in expt 7 a G(total) = 1.95, which is in fair agreement with the observed value.

All attempts to oxidize the intermediate hydroxycyanocyclohexadienyl radicals by Cu^{2+} ($Cu(ClO_4)_2$, $CuSO_4$, $CuCl_2$) failed. Only trace amounts of hydroxybenzonitriles were obtained. This is analogous to the behavior of the hydroxynitrocyclohexadienyl radicals, and is probably due to the higher oxidation potential of these intermediates as compared to the hydroxycyclohexadienyl radicals with electron-donating substituents.

Discussion

From our results in Tables I–III we can see that in presence of metal salts we obtain in most cases a quantitative conversion of OH radicals to phenols, whereas in absence of oxidizing agents we observe only trace amounts of substituted phenols. It is generally accepted that the first step in the homolytic hydroxylation is addition to the aromatic ring.[8] These addition reactions proceed with very high rate constants (10^9–10^{10} M^{-1} s^{-1})[15] as determined by pulse radiolysis. An electron transfer to form OH^- and a radical cation has been discussed,[16] but was rejected by Walling and Johnson[5] on energetic grounds. In the hydroxylation of fluorobenzene Köster and Asmus[17] have observed the hydroxyfluorocyclohexadienyl radical by pulse radiolysis (rate constant, 8×10^9 M^{-1} s^{-1}). Conductivity measurements carried out simultaneously showed that ionic species are formed to an almost negligible extent in this reaction. The initially formed hydroxycyclohexadienyl radicals are oxidized by metal ions to the substituted phenols. This oxidation competes with other radical termination processes. With $K_3Fe(CN)_6$ neither the isomer distribution nor the total G(phenols) changes over a wide range of concentration (Table I, expt 4–6; Table II, expt 1–6; Table III, expt 1–5). These results indicate that $Fe(CN)_6^{3-}$ oxidizes the intermediate hydroxycyclohexadienyl radicals fast enough to compete effectively with other radical termination processes at concentrations as low as 5×10^{-4} M. This is in agreement with our previous observations in the hydroxylation of nitrobenzene and toluene and with recent results of Schuler and coworkers[13] on the hydroxylation of benzoic acid. Schuler et al. have actually demonstrated that the isomer distribution obtained in the hydroxylation of benzoic acid in presence of $K_3Fe(CN)_6$ is identical with the isomer distribution of the hydroxycarboxycyclohexadienyl radicals as determined by ESR measurements. We therefore suggest that the isomer distribution in presence of $Fe(CN)_6^{3-}$ represents the relative reactivity at the different positions. The percentage of meta hydroxylation is then equal to

$$\frac{2k_m}{2k_o + 2k_m + k_p} 100\%$$

TABLE IV: *G* Values and Reactivity Ratios in the Hydroxylation of Some Substituted Benzenes in the Presence of 5×10^{-3} M $K_3Fe(CN)_6$

	OCH_3	F	Br[a]	CH_3[b]	CN	NO_2[c]
G(ortho)	1.30	1.12	1.9	1.12	1.07	1.10
G(meta)	0.26	0.54	0.9	0.54	0.80	1.08
G(para)	0.97	0.92	1.1	0.60	0.52	0.50
$[2k_m/(2k_o + 2k_m + k_p)]$ 100%	10.3	20.9	23.1	23.9	33.5	39.3
k_p/k_m	7.46	3.41	2.45	2.22	1.30	0.93
σ_M[+]	−0.50	−0.45	−0.22	−0.13	+0.07	+0.15

[a] Reference 12. These experiments were carried out in N_2O saturated solutions in presence of 5×10^{-4} M $K_3Fe(CN)_6$. Note that under these conditions $G(OH) = 5.8$. [b] Reference 11. [c] Reference 10. [d] Reference 15.

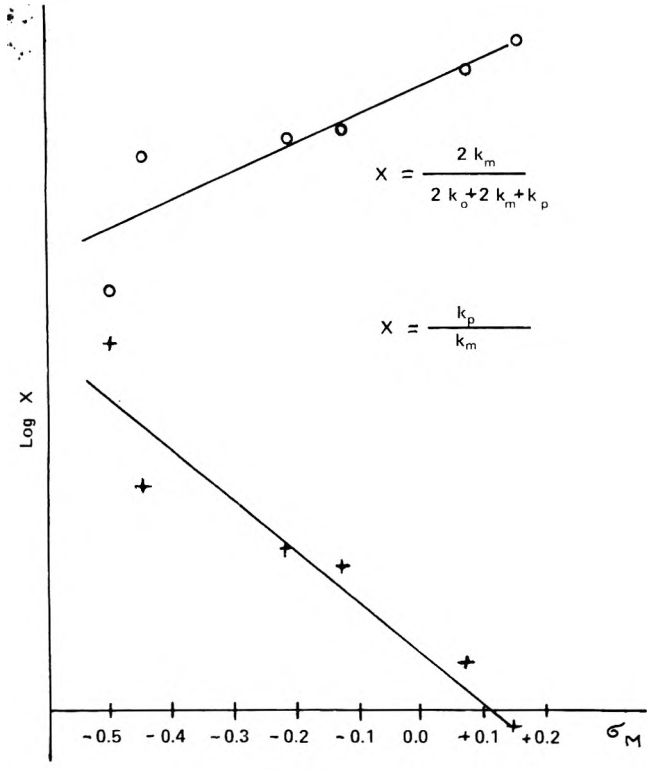

Figure 1. Hammett plot (log *X* vs. σ_M).

These values and k_p/k_m for anisole, fluorobenzene, bromobenzene, toluene, benzonitrile, and nitrobenzene are summarized in Table IV. We have plotted the logarithm of these values vs. σ values. The best linear plots were obtained with σ_M[18] (see Figure 1) and $\sigma_p - \sigma_m$, which is linearly related to σ_M[18]. By definition $\sigma_M = \sigma_{para} - \sigma_I$. According to Taft the σ_{meta} constants are related to σ_I and σ_M by the following empirical relationship: $\sigma_{meta} = \sigma_I + 0.33\sigma_M$. From the above two equations follows: $\sigma_{para} - \sigma_{meta} = 0.67\sigma_M$. σ_M values are a measure of the mesomeric effect of substituents. The greater the +M effect of the substituent ($CH_3 < F < OCH_3$) the smaller is the percentage of meta hydroxylation, and with increasing −M effect ($CN < NO_2$) we observe an increase in meta hydroxylation, and a decrease in k_p/k_m. With strong electron-withdrawing substituents the difference in electron density at the ortho and para positions compared to the meta position is small. In this case the electrophilic ·OH radical is unselective and the result is a close to statistical isomer distribution.[10] With increasing +M effect the electron densities increase at the ortho and para positions, and the difference to the electron density at the meta position becomes large, and

Scheme I

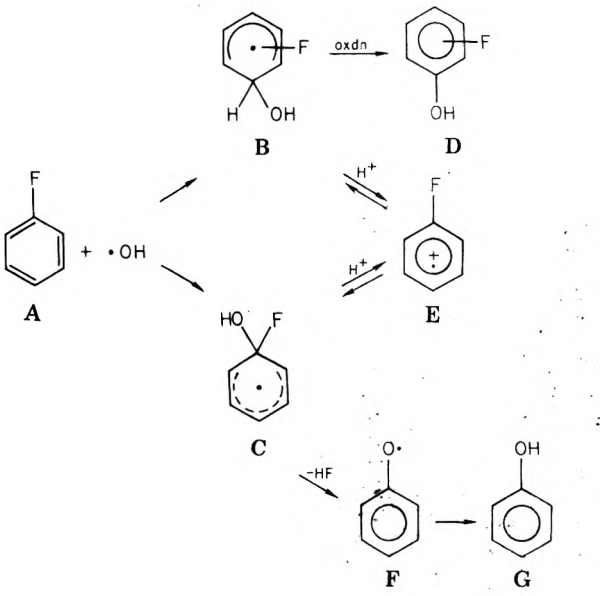

the ·OH radicals react more selectively at the ortho and para positions. SCF–MO calculations (CNDO-2) on phenol,[19] anisole,[19] toluene,[20] and nitrobenzene,[20] which we have reported previously, indeed show a linear relationship between σ_M values and the difference in total electron densities between ortho and meta positions and between meta and para positions. This type of relationship between σ values and electron densities using the Hückel MO method have been demonstrated previously.[21,22] The particular significance of the mesomeric effect of substituents was also observed by Peters[23] in the radical phenylation of substituted benzenes. The relationship shown in Figure 1 demonstrates the electrophilic character of ·OH radicals, and justifies our assumption that in presence of $K_3Fe(CN)_6$ the final product distribution represents the initial positions of OH radical attack.

Fluorobenzene. The mechanism of fluorobenzene hydroxylation is summarized in Scheme I. An important process which competes with oxidation is acid-catalyzed dehydration. It has first been observed in the Fenton's reagent hydroxylation of anisole,[2] toluene,[3] and fluorobenzene,[2] and was later also observed in the radiation induced hydroxylation of phenol[6] and toluene.[4] On the basis of this competition one can determine the relative rates of oxidation by different metal salts. In the hydroxylation of toluene[11] the following sequence for *k*(oxidation) was established: $Fe(CN)_6^{3-} > Cu^{2+} > Fe^{3+}$. The same sequence can be deduced from our results on fluorobenzene (Table I). At a metal salt concentration of 5×10^{-3} M and low pH we obtain with $Fe(CN)_6^{3-}$ (assuming a $G(\cdot OH)$ of approximately 3) a 90% conversion of ·OH radicals to fluorophenols (expt 7), but with Cu^{2+} and Fe^{3+} at pH 2.7 we obtain only a 43 and 15% conversion, respectively (experiments 21 and 16).

The results of Shevchuk and Vysotskaya[24] on the ^{18}O incorporation in the Fenton's reagent hydroxylation in ^{18}O enriched water indicated the possibility of a reversible dehydration in the hydroxylation of benzene and fluorobenzene. No ^{18}O incorporation however was observed with nitrobenzene, anisole, phenol, and chlorobenzene. Dehydration in the hydroxylation of anisole and phenol is well established, so in these cases the dehydration is irreversible. This can be seen from our results on anisole (Table II, compare experiment 1 with 7). At low pH we observe only small amounts of methoxyphenols. Recently evidence for a reversible dehydration in the hydroxylation

of benzene and toluene with $SO_4^-\cdot$ was reported by Walling and Camaioni.[25] A reversible dehydration could lead to isomerization.

The mechanism of dehydration leading to phenol has been discussed previously.[2,24b] A conversion of B to C bypassing the radical cation E (Scheme I) has been proposed by Shevchuk and Vysotskaya:

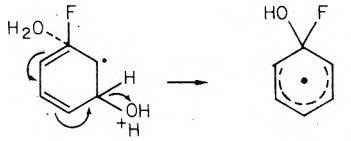

(4)

This low energy pathway is only available from the *m*-hydroxyl radical adduct. Our experiments have the advantage over previous experiments with Fenton's reagent, that we obtain a complete accounting of the OH radicals. This quantitative conversion of OH radicals to product allows us to draw more reliable mechanistic conclusions. Depending on the pH and oxidizing agent we produce either quantitatively fluorophenols (Table I, expt 1–5) or phenol (Table I, expt 23). This observation demonstrates that phenol is formed not only from the *m*-hydroxyl adduct according to reaction 4, but also from the *o*- and *p*-hydroxyl adduct, indicating the formation of a common intermediate from all isomeric hydroxyfluorocyclohexadienyl radicals. This intermediate is the radical cation E. At low pH in presence of $K_3Fe(CN)_6$ (Table I, expt 6) we observe a decrease in *m*-fluorophenol and an increase in phenol. This observation gives us the following relationship:

$$\left(\frac{\text{rate of oxidation}}{\text{rate of dehydration}}\right)_{o,p} > \left(\frac{\text{rate of oxidation}}{\text{rate of dehydration}}\right)_{m} \quad (5)$$

This inequality is fulfilled if (rate of oxidation)$_{o,p}$ > (rate of oxidation)$_m$ or (rate of dehydration)$_{o,p}$ < (rate of dehydration)$_m$. Although the present data do not permit us to decide between these two possibilities, we are inclined toward the latter inequality because of the lower energy pathway for dehydration available from the meta adduct as shown in eq 4.

Our results also provide evidence for reaction A → C. In presence of $K_3Fe(CN)_6$ we obtain a small G(phenol) which remains constant over a wide range of concentration. If this phenol is formed via dehydration we would expect a decrease with increasing $K_3Fe(CN)_6$ concentration. This phenol with an average G(phenol) = 0.27 is formed by direct attack at the α position (A → C). This mechanism would require that the intermediate C is not oxidized by $Fe(CN)_6^{3-}$, which may be due to a short lifetime of this species. Pulse radiolysis work on fluorinated benzenes have indeed provided evidence for a short lifetime of 1-hydroxy-1-fluorocyclohexadienyl radicals.[17] The independence of G(phenol) from the $K_3Fe(CN)_6$ concentration may also be due to the fact that this small amount of phenol is formed inside a spur. In the study of Vysotskaya and Shevchuk phenol formed via E and eq 4 would incorporate ^{18}O, whereas phenol formed by reaction (A → C → F) would not. They found at pH 5 a 64–66% and at pH 1.5 a 77–83% ^{18}O incorporation into the phenol. Our results indicate that in unbuffered solutions (Table I, expt 11) about 61.5% ([(0.70 − 0.27)/0.70] 100%) of the phenol is formed via the radical cation E and eq 4, whereas at low pH (3.05–1.7) in absence and in presence of Fe^{3+} the percentage varies from 86 to 89% (Table I, expt 13–18).

Considering the different experimental approaches the conclusions reached from our results are in excellent quantitative agreement with those of the Russian workers. The reduction of PhO· to PhOH (F → G) may proceed via several possible pathways. In the reaction of fluorobenzene with e_{aq}^- Köster and Asmus have suggested the formation of the following intermediates:

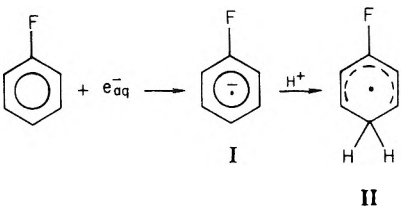

(6)

I II

PhO· can react with I or II to yield phenolate anion or phenol. In presence of oxidizing metal ions the reduced form (Fe^{2+} or $Fe(CN)_6^{4-}$), which is formed during the reaction, can also reduce phenoxy radical to phenolate.

The reversible dehydration of the isomeric hydroxyfluorocyclohexadienyl radicals leads exclusively to phenol in absence of oxidizing agent (Table I, expt 13). Hydration of the radical cation E will lead to C and phenol. In the hydroxylation of fluorobenzene with $SO_4^-\cdot$ we recently obtained evidence showing that the fluorobenzene radical cation not only becomes hydrated to give C and phenol, but also to a large extent gives *p*-hydroxyfluorocyclohexadienyl radical and to an insignificant extent *o*-hydroxyfluorocyclohexadienyl radical.[26] In this case the reversible dehydration will lead to isomerization.

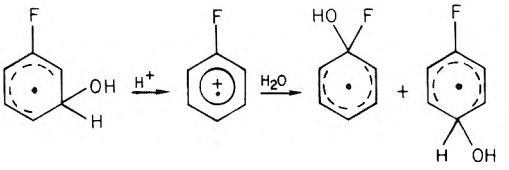

(7)

In the presence of metal ions such as Cu^{2+} or Fe^{3+}, which have a smaller k(oxidation) values than $Fe(CN)_6^{3-}$ we therefore expect a decrease in the percentage of *m*-fluorophenol and an increase in *p*-fluorophenol and phenol, in agreement with our experimental observations (Table I, compare experiments 1–5 with 8–10). In absence of oxidizing agents the hydroxyfluorocyclohexadienyl radicals however eventually all wind up as phenol (Table I, expt 13).

Anisole. The most striking result in the hydroxylation of anisole (Table II) is the small percentage of meta hydroxylation. This is due to the strong ortho–para directing +M effect of the methoxy group. Previous work has established that the hydroxymethoxycyclohexadienyl radical undergoes acid-catalyzed dehydration to produce the anisole radical cation.[27] Recent results in our laboratory on the reaction of $SO_4^-\cdot$ with anisole have shown that the anisole radical cation does not undergo water addition to give hydroxymethoxycyclohexadienyl radicals. The irreversibility of the dehydration can also be deduced from our results in Table II (compare experiment 1 with 7) in agreement with the ^{18}O exchange experiments of Shevchuk and Vysotskaya. Comparing experiment 7 with 1 we see that the decrease in methoxyphenols is not accompanied by an increase in phenol as was observed in the hydroxylation of fluorobenzene (Table I). The small amount of phenol is therefore not produced via a radical cation intermediate, but most likely by direct attack of OH radical at the α position. Our results show that in presence of $K_3Fe(CN)_6$ the yield of phenol decreases (compare experiment 13 with 1–6). This observation may be explained

by oxidation of the 1-hydroxy-1-methoxycyclohexadienyl radical to a carbonium ion, followed by rearrangement to give *o*-methoxyphenol. The small amount of phenol formed in presence of $K_3Fe(CN)_6$ is independent of its concentration, and is therefore very likely formed inside a spur.

Benzonitrile. In the hydroxylation of benzonitrile in presence of $K_3Fe(CN)_6$ there is no pH effect contrary to the results obtained with fluorobenzene, anisole, and toluene. Considering also previous results on nitrobenzene[10,28] we conclude that dehydration from the initially formed hydroxycyclohexadienyl radicals does not take place if the substituent is electron withdrawing (NO_2, CN) or at least takes place at a much slower rate than if the substituent is electron donating (+M effect). This conclusion is reasonable on energetics grounds, since it is more difficult to eliminate OH^- from an already electron-deficient aromatic system.

In the hydroxylation of benzonitrile we observe a considerable difference in isomer distribution with $Fe(CN)_6^{3-}$ or Fe^{3+} (Table III, expt 6, 10, 14), which is a general phenomenon in aromatic hydroxylation. With identical metal salt concentration (5×10^{-2} M) and the same pH (1.4–1.6) we obtain almost the same G(total hydroxybenzonitriles) but a much lower G(meta) in the experiment with Fe^{3+}. This behavior suggests an isomerization in the oxidation with Fe^{3+}. This isomerization can a priori take place either before or after the oxidation step:

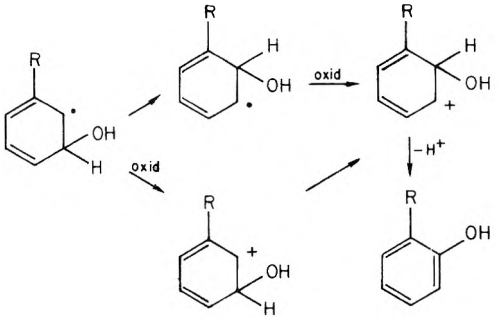

(8)

In previous work on nitrobenzene[10] and toluene[11] we have suggested the first possibility, whereas Walling and Johnson[5] in the hydroxylation of toluene have proposed the second possibility involving a carbonium ion. Since $Fe(CN)_6^{3-}$ like Fe^{3+} is a one electron transfer agent,[29] it is difficult to accept the formation of a carbonium ion in one case but not in the other. We therefore believe that no carbonium ions are formed in either of the two cases. Evidence which indicates that electron transfer and deprotonation occur synchronously has been presented by Norman et al.[3] The isomerization must therefore take place before the oxidation step, which in some cases may proceed via a reversible dehydration, as we have shown for fluorobenzene. In the hydroxylation of nitrobenzene and benzonitrile, where dehydration has not been demonstrated and appears unlikely from the presently available evidence, the reason for the difference in isomer distribution with $Fe(CN)_6^{3-}$ and Fe^{3+} remains open to speculation.[20]

Experimental Section

Materials. All solutions were prepared using water which was doubly distilled from an all glass still. Then it was further distilled over alkaline permanganate, acidic dichromate, and one final distillation. Benzonitrile was spectrograde quality (Eastman). Anisole and fluorobenzene (Aldrich Chemical Co.) were distilled prior to use. All metal salts were of reagent grade quality. The aqueous solutions were deoxygenated by bubbling argon through 1 L of the solution for 1 h. The saturation was enhanced by frequent shaking.

Irradiations. Irradiation were carried out with a ^{60}Co source on 1 L solutions. Dose rates and total doses are given in the tables (determined by Fricke dosimetry with $G(Fe^{3+}) = 15.5$). The dosimetry was carried out by using the same bottles and volume as the irradiated solutions.

Analytical Procedure. Immediately after the irradiation the solution (1 L) was extracted once with 200 mL of ether and four times with 100 mL of ether. The ether extract was dried over 80 g of Na_2SO_4 for about 24 h, and was then concentrated to about 30 mL and 20 mL of a diazomethane solution (prepared from Diazald, Aldrich Chemical Co.) was added. After 2 days the solution was concentrated to 10 mL and analyzed by vapor phase chromatography using a hydrogen flame detector. The column was a 6 ft FFAP (Varian 5% liquid phase on Chromosorb W-AW-DMCS (100–120 mesh) column at 180 °C and a flow of about 25 mL of He/min. The products appeared in the following sequence: *m*-methoxybenzonitrile (8.2 min), *p*-methoxybenzonitrile (12.0 min), *o*-methoxybenzonitrile (13.3 min). The fluorophenols, phenol, and methoxyphenols could be analyzed without prior methylation. The fluorophenols and phenol were analyzed on the same column under the same conditions. The products appeared in the following sequence: *o*-fluorophenol (4.0 min), phenol (8.2 min), *p*-fluorophenol (11.2 min), *m*-fluorophenol (12.4 min). The methoxyphenols were analyzed on the same column at 200 °C and appeared as follows: *o*-methoxyphenol (3.4 min), phenol (4.8 min), *p*-methoxyphenol (15.2 min), *m*-methoxyphenol (17.2 min). Standard aqueous substituted phenol solutions were prepared containing amounts of phenols which were very close to the amounts present in the irradiated solutions and worked up in the same way. All experiments were carried out in duplicate and were found to be reproducible within the limits of the analytical technique (±5%).

References and Notes

(1) This paper was prepared in connection with work under Contract No. E-(40-1)-1833 with the U.S. Energy Research and Development Administration (ERDA).
(2) C. R. E. Jefcoate and R. O. C. Norman, *J. Chem. Soc. B*, 48 (1968).
(3) C. R. E. Jefcoate, J. R. Lindsay-Smith, and R. O. C. Norman, *J. Chem. Soc. B*, 1013 (1969).
(4) (a) H. C. Christensen and R. Gustafson, *Acta Chem. Scand.*, **26**, 937 (1972); (b) H. C. Christensen, K. Sehested, and E. J. Hart, *J. Phys. Chem.*, **77**, 983 (1973).
(5) C. Walling and R. A. Johnson, *J. Am. Chem. Soc.*, **97**, 363 (1975).
(6) E. J. Land and M. Ebert, *Trans. Faraday Soc.*, **63**, 1181 (1967).
(7) M. K. Eberhardt, *J. Phys. Chem.*, **78**, 1795 (1974).
(8) L. M. Dorfman, I. A. Taub, and R. E. Buhler, *J. Chem. Phys.*, **36**, 3051 (1962).
(9) J. H. Baxendale and D. Smithies, *J. Chem. Soc.*, 799, (1959).
(10) M. K. Eberhardt, *J. Phys. Chem.*, 79, 1913 (1975).
(11) M. K. Eberhardt and M. I. Martinez, *J. Phys. Chem.*, **79**, 1917 (1975).
(12) K. Bhatia and R. H. Schuler, *J. Phys. Chem.*, **78**, 2335 (1974).
(13) G. W. Klein, K. Bhatia, V. Madhavan, and R. H. Schuler, *J. Phys. Chem.*, **79**, 1767 (1975).
(14) B. H. J. Bielski and A. O. Allen, *Int. J. Radiat. Phys. Chem.*, **1 (2)**, 153 (1969).
(15) L. M. Dorfman and G. E. Adams, *Natl. Stand. Ref. Data Ser., Natl. Bur. Stand.*, **No. 40** (1973).
(16) M. E. Snook and G. A. Hamilton, *J. Am. Chem. Soc.*, 96, 860 (1974).
(17) R. Köster and K. D. Asmus, *J. Phys. Chem.*, **77**, 749 (1973).
(18) (a) H. A. Staab in "Einfuhrung in die theoretische organische Chemie", Verlag Chemie, Weinheim Bergstr., 1966, p 586. (b) R. W. Taft, Jr., in "Steric Effects in Organic Chemistry", M. S. Newman, Ed., Wiley, New York, N.Y., 1956, pp 594–597.
(19) M. K. Eberhardt and G. Chuchani, *J. Org. Chem.*, **37**, 3654 (1972).
(20) M. K. Eberhardt and M. Yoshida, *J. Phys. Chem.*, **77**, 589 (1973).
(21) H. H. Jaffé, *J. Chem. Phys.*, **20**, 279 (1952); *J. Am. Chem. Soc.*, **76**, 5843 (1954); **77**, 274 (1955).
(22) D. Peters, *J. Chem. Soc.*, 2654 (1957).
(23) D. Peters, unpublished results, cited in ref 22.
(24) (a) L. G. Shevchuk and N. A. Vysotskaya *Zh. Org. Khim.*, **4**, 1936 (1968); (b) N. A. Vysotskaya and L. G. Shevchuk, *ibid.*, **9**, 2080 (1973).

(25) C. Walling and D. M. Camaioni, *J. Am. Chem. Soc.*, **97**, 1603 (1975).
(26) M. K. Eberhardt, *J. Org. Chem.*, **42**, 832 (1977).
(27) P. O'Neill, S. Steenken, and D. Schulte-Frohlinde, *J. Phys. Chem.*, **79**, 2773 (1975).
(28) See also J. H. Fendler and G. L. Gasowski, *J. Org. Chem.*, **33**, 1865 (1968). These authors found, in the radiation induced hydroxylation of nitrobenzene in absence of oxidizing agents, no change in total nitrophenols nor isomer distribution with changing pH.
(29) R. Stewart in "Oxidation Mechanisms", W. A. Benjamin, New York, N.Y., 1964, p 84 *ff*.

Rate of Energy Transfer from Excited Cyclohexane to Solutes in the Liquid Phase

Toshinori Wada and Yoshihiko Hatano*

Laboratory of Physical Chemistry, Tokyo Institute of Technology, Meguro-ku, Tokyo 152, Japan *(Received July 6, 1976; Revised Manuscript Received January 24, 1977)*

Photolysis of liquid cyclohexane in the presence of solutes, most of which are used as electron scavengers in radiation chemistry, has been carried out at 163 nm. The yield of hydrogen which is a main product in the photolysis of pure cyclohexane is reduced upon the addition of a solute, which is attributed to energy transfer from excited cyclohexane to the solute. The rate constant of the energy transfer k_t for various solutes was determined to be $(5\sim14) \times 10^{10}$ M^{-1} s^{-1} (at 15 °C), which is a factor of 9~24 larger than that expected for an ordinary diffusion-controlled rate. The temperature dependence of k_t, however, indicates that the energy transfer is controlled by the diffusive motion of the reacting species. This apparent anomaly is explained in terms of excited cyclohexane with a large effective interaction radius in the liquid phase which is estimated to be 10~20 Å.

Introduction

The elucidation of excitation and ionization in liquid alkanes is one of the important problems in radiation chemistry. Photochemical studies of liquid alkanes with photons of energies near, or slightly above, the ionization potentials may yield important viewpoints for understanding excitation and ionization in liquid alkanes.

It has been shown in liquid-phase photolysis of cyclohexane[1] and steady-state quenching of cyclohexane fluorescence[2] that electronically excited cyclohexane, produced by 147-nm excitation, transfers its excitation energy to various solutes such as aromatic compounds and electron scavengers. The energy transfer efficiencies, $\alpha_t = k_t\tau$, have been reported, where k_t is the rate constant of energy transfer and τ is the lifetime of excited cyclohexane. Subsequently the values of τ and k_t have separately been measured from cyclohexane fluorescence decay time[3] and energy-transfer experiments[4] using, respectively, x-ray excitation and pulse radiolysis techniques. In liquid-phase photolysis of cyclohexane solutions at 163 nm the values of k_t for CCl_4, SF_6, and N_2O have also been determined and demonstrated to be much larger than that expected as for an ordinary diffusion-controlled rate.[5] Consistent with this result, it has been reported that the lifetime of the cyclohexane fluorescence state, estimated from the values of α_t obtained in steady-state quenching and the rate constant calculated from the Stokes–Einstein–Smoluchowski (SES) equation, is an order of magnitude longer than that measured directly.[6]

Thus unusually high rates of energy transfer from excited alkanes to solutes have been reported by some groups.[4-8] However, an explicit explanation for the process of energy transfer has still not been presented. As a plausible explanation it has been assumed[5b] that excited cyclohexane has a large effective interaction radius compared with the geometrical radius in the ground state. In liquid alkanes it seems difficult to draw a clear distinction between highly excited molecules and so-called geminate ion pairs. Further investigations into the behavior of excited alkanes in the liquid phase are necessitated. In this work photolysis of liquid cyclohexane at 163 nm is carried out in the presence of various solutes where the values of k_t and their temperature dependence are investigated.

Experimental Section

Cyclohexane (>99.99 mol %) was a Phillips Research Grade material. Olefin impurities, such as cyclohexene, were not detected by a gas chromatograph with a flame ionization detector.[9] This material was used after usual degassing and trap-to-trap distillations in vacuo. Pure CCl_4, SF_6, N_2O, CO_2, CH_3Br, CH_3I, C_2H_5Br, and benzene were used as additives after usual degassing.

The 163-nm light source was an electrodeless discharge bromine lamp. The photolysis apparatus and the lamp emission spectrum have been illustrated in previous papers.[5] The lamp intensity through the Suprasil quartz window was about 2×10^{-8} einstein s^{-1} and it remained constant within 5% for at least one experiment. Solutions were prepared by the addition of known amounts of solutes to 8 mL of degassed cyclohexane in the reaction cell and mixing thoroughly. The concentrations of SF_6, N_2O, and CO_2 in the liquid phase were calculated using the Ostwald absorption coefficients of 1.3, 3.3, and 1.8 in cyclohexane,[10] respectively. Other solutes were assumed to dissolve completely in the liquid phase. Photolysis of a solution was carried out with stirring for 3 min for which the solution was cooled to (15 ± 1) °C by means of a water bath. Solutions of CCl_4 were photolyzed at water bath temperatures in the range of 10~35 °C. Photolysis was repeated for a solution at several concentrations and the total amount of conversion was less than 0.02%. After a photolysis noncondensable gases at 77 K were collected to a calibrated the volume and the pressure was measured. The gases were identified by mass spectrometry. The hydrogen yield was confirmed quantitatively by a gas chromatograph with a 5 A molecular sieve column.

Results and Discussion

The photolysis of pure liquid cyclohexane at 163 nm is detailed in previous papers.[5] The major photoproducts are hydrogen and cyclohexene. Bicyclohexyl is a minor

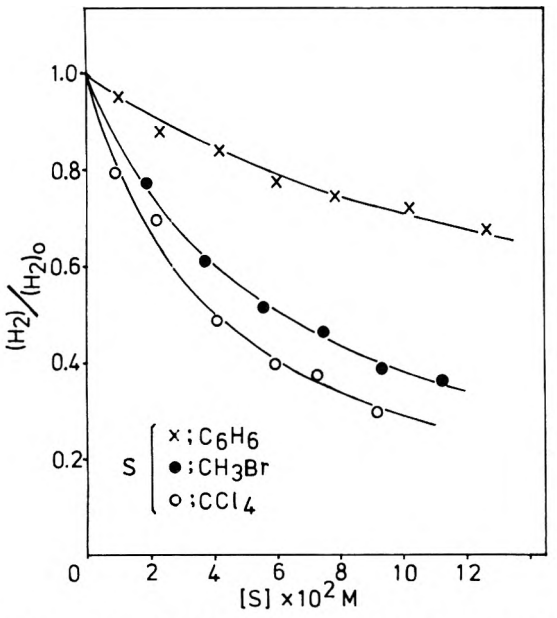

Figure 1. Effect of the addition of C_6H_6, CH_3Br, and CCl_4 on hydrogen yield.

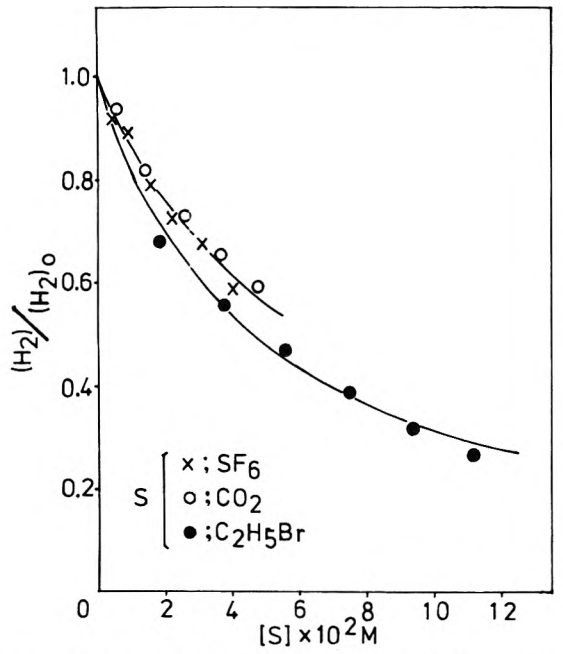

Figure 2. Effect of the addition of SF_6, CO_2, and C_2H_5Br on hydrogen yield.

product. The yield of hydrogen balances the sum of the yields of cyclohexene and bicyclohexyl. The quantum yield of hydrogen formation $\Phi(H_2)$ is determined to be 1.0 ± 0.1 using ethylene as a chemical actinometer. The main process of hydrogen formation is molecular detachment of hydrogen from excited cyclohexane. The atomic detachment process is minor.

Figures 1, 2, and 3 show the effects of the additives on the yield of hydrogen. The hydrogen yield decreases with increasing concentration of solute. The addition of N_2O or CH_3I in Figure 3 reduces the hydrogen yield to a constant value, which is different from the effect of other additives in Figures 1 and 2. When the solutes N_2O, CO_2, and methyl halides are added, noncondensable gases at 77 K, N_2, CO, and CH_4, respectively, are produced together with hydrogen. The formation of N_2 compensates precisely for the decrease in hydrogen yield,[5b] while the yield of CO is about one third of the decrement of hydrogen yield. The

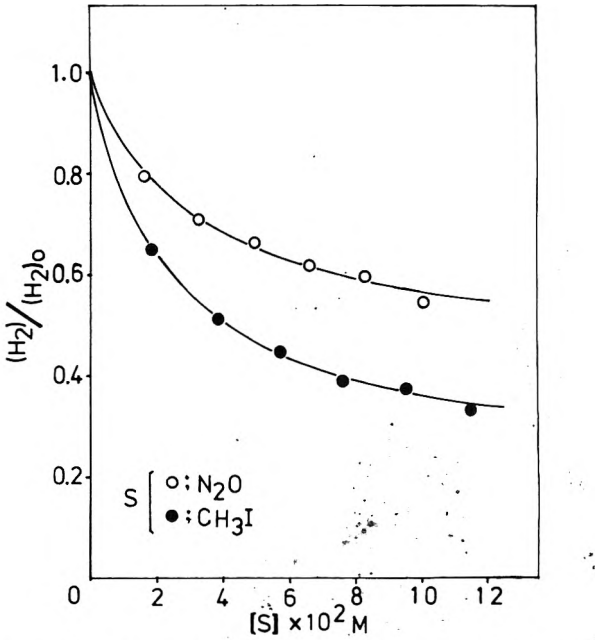

Figure 3. Effect of the addition of N_2O and CH_3I on hydrogen yield.

yield of CH_4 is relatively low. For solutions of CH_3I and benzene a slight correction for the direct absorption of exciting light by the solute is made using the absorption coefficients for CH_3I (17 000 M^{-1} cm^{-1}),[11] benzene (9000 M^{-1} cm^{-1}),[12] and cyclohexane (2000 M^{-1} cm^{-1})[13] in the gas phase at 163 nm. For other solutions the fraction of exciting light absorbed by solutes at the concentrations used in this experiment was negligible.[14] The effects of additives in Figures 1–3 are attributed, as discussed previously,[5] to energy transfer from excited cyclohexane to solutes.

The following reaction scheme accounts for the observed results in Figures 1 and 2:

$$c\text{-}C_6H_{12} + h\nu \rightarrow c\text{-}C_6H_{12}^{*\prime} \quad (0)$$

$$c\text{-}C_6H_{12}^{*\prime} \xrightarrow{k_i} c\text{-}C_6H_{12}^{*} \quad (1)$$

$$c\text{-}C_6H_{12}^{*} \xrightarrow{k_2} H_2 + c\text{-}C_6H_{10} \quad (2)$$

$$c\text{-}C_6H_{12}^{*} \xrightarrow{k_f} c\text{-}C_6H_{12} + h\nu' \quad (3)$$

$$c\text{-}C_6H_{12}^{*} + S \xrightarrow{k_t} c\text{-}C_6H_{12} + S^{*} \quad (4)$$

where $c\text{-}C_6H_{12}^{*\prime}$ and $c\text{-}C_6H_{12}^{*}$ represent, respectively, a highly excited state and the first excited singlet state of cyclohexane. The lower excited state is the source of hydrogen formation as well as the fluorescence of low yield ($\Phi_f = 8.8 \times 10^{-3}$ at 165-nm excitation).[6] Energy transfer from $c\text{-}C_6H_{12}^{*}$ to a solute S with a rate constant k_t causes the reduction in hydrogen yield and quenching of the fluorescence. On steady-state treatment of reactions 0–4 the following equation is given:

$$(H_2)_0/(H_2) = 1 + \alpha_t[S] \quad (I)$$

where $(H_2)_0$ and (H_2) represent, respectively, the hydrogen yield in the photolysis of cyclohexane in the pure state and in the presence of a solute S with a concentration of [S], and the energy transfer efficiency α_t is equal to $k_t/(k_2 + k_f)$. The plots of $(H_2)_0/(H_2)$ vs. [S] for the data in Figures 1 and 2 show a linear relation and values of α_t are obtained from the slopes of straight lines with errors of about ±10%.

For the data of N_2O and CH_3I in Figure 3, however, analysis of the above reaction is not adequate. In the process of hydrogen formation there seems to be a path

TABLE I: Summary of the Energy Transfer Efficiency α_t and the Rate Constant k_t for Various Solutes

Solute	α, M^{-1}	$k_t \times 10^{-10}$ M^{-1} s^{-1}
CCl_4	25	8.2
SF_6	16	5.4
CO_2	15	5.1
N_2O	31	10.2
CH_3I	43	14.3
CH_3Br	16	5.4
C_2H_5Br	22	7.2
C_6H_6	4	1.3

which is unaffected by the addition of N_2O or CH_3I. A fraction of c-C_6H_{12}*′ does not convert into c-C_6H_{12}* but decomposes to yield hydrogen, which has been detailed for the result of N_2O in a previous paper.[5b] The following equation was used for the data in Figure 3:

$$\frac{(H_2)_0 - (H_2)_{unq}}{(H_2) - (H_2)_{unq}} = 1 + \alpha_t[S] \qquad \text{(II)}$$

where $(H_2)_{unq}$ represents the amount of hydrogen which is unquenched by additives at infinite concentration. The values of $(H_2)_{unq}/(H_2)_0$ for N_2O and CH_3I are evaluated to be 0.43 and 0.22, respectively. Plots of eq II give straight lines and α_ts are obtained from values of the slopes. The difference between the effect of the addition of N_2O or CH_3I and that of other solutes cannot be clearly explained. It may be suggested that excited states of cyclohexane taking part in energy transfer vary according to the properties of the additives. Experiments on competitive energy transfer of N_2O with other additives will be necessary to clarify the situation.

The values of α_t obtained are summarized in Table I. The values of α_t for CCl_4 and SF_6 are lower than those reported previously,[5a] which is due to a difference in reaction temperature. In this work the temperature of the sample is controlled at (15 ± 1) °C by means of a water bath, while in previous work the reaction temperature was not controlled and was somewhat higher than room temperature because the reaction cell is near the sources of heat such as the microwave cavity and the heating tape. The value of α_t for benzene (4 M^{-1}) is exceptionally lower than those for electron scavengers. The similarly low α_t value for benzene has been reported by Holroyd et al.[1a] in the photolysis of cyclohexane solutions at 147 nm. In the steady-state quenching of fluorescence and direct measurements of k_t, however, the values of α_t for benzene and other aromatics have been determined to be much higher (70–80 M^{-1}).[2,4,8] The reason for the large difference between these values is not clear.

The lifetime of excited cyclohexane, τ, has been directly determined to be 0.3 ns by Henry and Helman[3] in fluorescence decay time measurements and by Beck and Thomas[4] in energy transfer measurements. The cyclohexane fluorescence spectrum and values of α_t obtained in x-ray excitation[3] and pulse radiolysis[4,8] agree with those in photochemical experiments,[2,5,6] which indicates that the same excited species is treated in both studies. Based on these facts $(k_2 + k_f)^{-1}$ is equated to τ = 0.3 ns. The rate constants of energy transfer k_t are then obtained from the values of α_t, which are summarized in Table I. The values of k_t for electron scavengers, (5∼14) × 10^{10} M^{-1} s^{-1}, are a factor of 9∼24 larger than the rate constant 0.6 × 10^{10} M^{-1} s^{-1} (at 15 °C) expected for an ordinary diffusion-controlled reaction in liquid, which is calculated from the Stokes–Einstein–Smoluchowski (SES) equation

$$k_{SES} = 8RT/3000\eta \ M^{-1} \ s^{-1} \qquad \text{(III)}$$

where η is the viscosity of liquid cyclohexane at an absolute temperature T and R is the gas constant. Thus the SES equation may not be applicable to the reaction of excited cyclohexane with electron scavengers, though the value of k_t for benzene is not too different from eq III. The above inapplicability is in marked contrast to the fact that the SES equation has successfully been applied to many reactions of excited aromatic molecules in different solvents.[15] The failure of eq III to predict the rate of energy transfer from excited cyclohexane to electron scavengers seems to indicate a peculiarity of the excited alkane molecules in the liquid phase. Using 0.68 ns as a value of τ,[16] which has been determined using a single photon instrument with 156-nm excitation, one obtains qualitatively the same conclusion as those described above.

TABLE II: Temperature (or Viscosity) Dependence of α_t and k_t for the Cyclohexane-CCl_4 System

T, °C	η, cP	α, M^{-1}	$k_t \times 10^{-10}$ M^{-1} s^{-1}	$(k_t\eta/T) \times 10^{-5}$ erg mol^{-1} deg^{-1}
10	1.16	21	7.1	29
15	1.06	25	8.2	30
22	0.94	26	8.6	27
35	0.76	32	10.6	26

As a possible explanation for the unusually high rates it may not be impossible to assume that energy transfer to electron scavengers takes place through a process such as Förster-type transfer, for which the treatment for a diffusion-controlled reaction is inapplicable. In order to decide whether the process of energy transfer is diffusion controlled or not, we investigated the temperature (or viscosity) dependence of k_t for the cyclohexane–CCl_4 system. The results are summarized in Table II. Though the measurements are limited to the temperature range 10∼35 °C, the values of α_t and derived k_t increase with increasing temperature (or decreasing viscosity). An Arrhenius plot of k_t gives an apparent activation energy of 2.8 kcal/mol, for which the temperature dependence of the viscosity η[17] is responsible. If the process of the energy transfer to CCl_4 is diffusion controlled, k_t should depend on both the temperature and the viscosity as indicated by eq III. The ratio of k_t to T/η is then calculated, which is given in the last column of Table II. The value of $k_t\eta/T$ is constant, (2.8 ± 2) × 10^6 erg mol^{-1} deg^{-1}, in the temperature range in this work. However, it is still a factor of 13 larger than $k_{SES}\eta/T$ = 2.2 × 10^5 erg mol^{-1} deg^{-1}. Helman[7] has measured the specific rates (k_q) for quenching of fluorescence of decalin and dodecane in a wider range of temperature, and reported that the value of $k_q\eta/T$, (10 ± 1) × 10^5 erg mol^{-1} deg^{-1}, is temperature independent and a factor of 4.5 larger than $8R/3000$. Consequently, it is considered that the rate of energy transfer from excited cyclohexane to electron scavengers is controlled by diffusion of the reacting species in a sense that k_t is in proportion to T/η, though the large rate constant is not predicted from the SES equation.

An examination in the derivation of the SES equation is necessary to elucidate the reason for its inapplicability to energy transfer. When a reaction of excited molecules with solutes is diffusion controlled, the rate constant is generally given by[15,18]

$$k = \frac{4\pi\rho D'N}{1000}\left(1 + \frac{\rho}{\sqrt{D'\tau}}\right) M^{-1} \ s^{-1} \qquad \text{(IV)}$$

where ρ is the sum of the interaction radii of reacting molecules ($r_{ex} + r_s$), D' is the sum of the diffusion coefficients ($D_{ex} + D_s$), τ is the lifetime of the excited molecule, and N is Avogadro's number. For $\tau > 10^{-8}$ s and a moderate value of D', the second term in the parentheses

(transient term) is negligible and the steady-state rate constant is given as $k = 4\pi\rho D'N/1000$, which is the Smoluchowski equation. The diffusion coefficient can be estimated from the Stokes–Einstein equation, $D = kT/6\pi\eta(d/2)$, where $d/2$ is the geometrical radius in the diffusive motion in the solvent of reacting molecules (Stokes' radius) and k is the Boltzmann constant. The SES equation is derived by applying the Stokes–Einstein equation to the Smoluchowski equation with an assumption that the interaction radii and the Stokes' radii of reacting molecules are equal to one another, $r_{ex} = r_s = d_{ex}/2 = d_s/2$, so the two composite radii cancel. The SES equation thus derived is very simple as indicated by eq III. A comparison between k_{SES} and the experimental rate constant is easily possible only with a knowledge of viscosity. However, some approximations and assumptions in the above derivation seem to be inadequate for the reaction of excited cyclohexane. The transient term in eq IV is not negligible because of the short lifetime of excited cyclohexane (0.3 ns). It has been pointed out that the diffusion coefficient calculated from the Stokes–Einstein equation is a factor of 2 or 3 smaller than that measured in cyclohexane solvent.[15] Using eq IV including transient term, one predicts a rate constant three times larger than k_{SES} using $\rho = 5$ Å estimated from geometrical radii and $D' \simeq 3 \times 10^{-5}$ cm^2 s^{-1} measured experimentally.[15,19] The unusually high rate of energy transfer is still not sufficiently explained by inclusion of the transient term only. Other factors in the energy transfer should be considered, which may be attributed to either a larger D' or a larger ρ. An apparently large D' due to energy migration between cyclohexane molecules, however, may not be expected because of the large Stokes shift (0.8 eV)[6] between the absorption spectrum and the emission spectrum. In practice Lipsky et al.[6] have reported negative evidence for energy migration through alkane solvent. On the other hand, it seems plausible that the effective interaction radius ρ at which energy transfer occurs from excited cyclohexane to electron scavengers is larger than the sum of the geometrical radii of stable cyclohexane and a solute molecule. Large nuclear displacement in the excited state of cyclohexane can be conjectured from such facts as the large Stokes shift and the structureless appearance of the absorption[13] and the emission[6] spectra. The large effective interaction radius implies noncancellation of the two composite radii (interaction radii and Stokes' radii) and the constant and large value of $k_t\eta/T$, i.e., the inapplicability of the SES equation. The value of ρ is conversely estimated from the derived k_t in Table I using eq IV as 10∼20 Å for energy transfer to electron scavengers. Thus we consider that an expanded cyclohexane excited state in the liquid phase is a significant factor responsible for the unusually high rate of energy transfer.

From the inspection of excited cyclohexane obtained through this work, we inquire into the problem of excitation and ionization in liquid alkanes. An electron orbital of excited cyclohexane is imagined to smear out over several molecules in the liquid phase. It seems to be difficult to distinguish essentially the expanded cyclohexane excited state from the so-called geminate ion pair which are attracted to each other to recombine after the electron removed by ionization has thermalized in the liquid. Though the most probable thermalization distance in liquid cyclohexane has been estimated to be about 70 Å,[20] there is some degree of probability that electrons thermalize at the interpair distance of 10∼20 Å. The excitation and ionization phenomena in the liquids should not be described by conceptions in an isolated system but those in a disordered condensed system. Energy levels of excited states seem to become blurred and overlap with the beginning of ionized states. As to the reactivity of excited cyclohexane, the values of k_t for electron scavengers in Table I lie between the ordinary diffusion-controlled rate constant (∼10^{10} M^{-1} s^{-1}) and the estimated rate constant of geminate electron scavenging (2×10^{11}–10^{13} M^{-1} s^{-1}),[21] which may suggest a possibility of charge transfer from excited cyclohexane to solutes even if the donor is not necessarily in an ionized state.

Photochemical studies of cyclohexane with a photon energy of 7.6 eV have been carried out to study the behavior of excited cyclohexane in the liquid phase. Further work on liquid cyclohexane at higher photon energies such as those from Xe and Kr resonance lamps as well as work with other solutes such as aromatic compounds are required. A similar experiment on other alkane solvents will provide an attempt to correlate the values of ρ with those of electron mobilities. The measurements of the lifetime τ for various hydrocarbon solvents as well as a more reliable τ for cyclohexane, which might be possible using synchrotron radiation, are greatly needed for better substantiation of our conclusion.

References and Notes

(1) (a) J. Y. Yang, F. M. Servedio, and R. A. Holroyd, *J. Chem. Phys.*, **48**, 1331 (1968); (b) R. A. Holroyd, *Adv. Chem. Ser.*, **No. 82**, 488 (1968).
(2) F. Hirayama and S. Lipsky in "Organic Scintillators", D. L. Horrocks, Ed., Academic Press, New York, N.Y., 1970, p 205.
(3) M. S. Henry and W. P. Helman, *J. Chem. Phys.*, **56**, 5734 (1972).
(4) G. Beck and J. K. Thomas, *J. Phys. Chem.*, **76**, 3856 (1972).
(5) (a) J. Nafisi-Movaghar and Y. Hatano, *J. Phys. Chem.*, **78**, 1899 (1974); (b) T. Wada and Y. Hatano, *ibid.*, **79**, 2210 (1975).
(6) (a) F. Hirayama and S. Lipsky, *J. Chem. Phys.*, **51**, 3616 (1969); (b) W. Rothman, F. Hirayama, and S. Lipsky, *ibid.*, **58**, 1300 (1973).
(7) W. P. Helman, *Chem. Phys. Lett.*, **17**, 306 (1972).
(8) J. H. Baxendale and J. Mayer, *Chem. Phys. Lett.*, **17**, 458 (1972).
(9) Y. Hatano, K. Takeuchi, and S. Takao, *J. Phys. Chem.*, **77**, 586 (1973).
(10) T. Saito, K. Takahashi, and S. Sato, *Bull. Chem. Soc. Jpn.*, **41**, 2603 (1968).
(11) P. Hochmann, P. H. Templet, H.-t. Wang, and S. P. McGlynn, *J. Chem. Phys.*, **62**, 2588 (1975).
(12) L. W. Pickett, M. Muntz, and E. M. McPherson, *J. Am. Chem. Soc.*, **73**, 4862 (1951).
(13) (a) J. W. Raymonda and W. T. Simpson, *J. Chem. Phys.*, **47**, 430 (1967); (b) B. A. Lombos, P. Sauvageau, and C. Sandorfy, *J. Mol. Spectrosc.*, **24**, 253 (1967).
(14) (a) E. D. Nostrand and A. B. F. Duncan, *J. Am. Chem. Soc.*, **76**, 3377 (1954); (b) J. R. McNesby and H. Okabe, *Adv. Photochem.*, **1**, 185 (1964).
(15) A. H. Alwattar, M. D. Lumb, and J. B. Birks in "Organic Molecular Photophysics", Vol. 1, J. B. Birks, Ed., Wiley-Interscience, New York, N.Y., 1973, pp 403–456, and references therein.
(16) W. R. Ware and R. L. Lyke, *Chem. Phys. Lett.*, **24**, 195 (1974).
(17) (a) Landolt-Börnstein, "Zahlenwerte und Funktionen aus Physik, Chemie, Astronomie, Geophysik und Technik", Sechste Auflage, II Band, "Eigenschafter der Materie in Ihren Aggregatzuständen", 5 Teil, Bandteil a, Transportphänomene I (Viskosität und Diffusion), Springer-Verlag, West Berlin, 1969, p 157. (b) "International Critical Tables of Numerical Data, Physics, Chemistry and Technology", Vol. VII, 1930, p 217.
(18) (a) B. Sveshnikoff, *Acta Physicochim. USSR*, 3, 257 (1935); (b) J. Q. Umberger and V. K. LaMer, *J. Am. Chem. Soc.*, **67**, 1099 (1945); (c) W. R. Ware and J. S. Novros, *J. Phys. Chem.*, **70**, 3246 (1966).
(19) I. Kamal and E. McLaughlin, *Trans. Faraday Soc.*, **62**, 1762 (1966).
(20) (a) W. F. Schmidt and A. O. Allen, *J. Chem. Phys.*, **52**, 2345 (1970); (b) J.-P. Dodelet, K. Shinsaka, U. Kortsch, and G. R. Freeman, *ibid.*, **59**, 2376 (1973).
(21) G. W. Klein and R. H. Schuler, *J. Phys. Chem.*, **77**, 978 (1973).

Ferric Hydrous Oxide Sols. 2. Thermodynamics of Aqueous Hydroxo and Sulfato Ferric Complexes[1,2]

Ronald S. Sapieszko,[3] Ramesh C. Patel, and Egon Matijević*

Department of Chemistry and the Institute of Colloid and Surface Science, Clarkson College of Technology, Potsdam, New York 13676
(Received November 15, 1976)

Publication costs assisted by the American Iron and Steel Institute

Ferric ion hydrolysis and complexation by sulfate ion were extensively studied by spectrophotometric, potentiometric, and combined stopped-flow temperature jump techniques. Results were analyzed by applying both graphical and computerized general multiparametric curve-fitting procedures. Equilibrium constants for the following reactions were determined over the temperature range from 25 to 80 °C and, in some cases, over a range of ionic strengths: $Fe^{3+} \rightleftharpoons FeOH^{2+} + H^+$, K_1; $Fe^{3+} \rightleftharpoons Fe(OH)_2^+ + 2H^+$, K_2; $2Fe^{3+} \rightleftharpoons Fe_2(OH)_2^{4+} + 2H^+$, K_{22}; $Fe^{3+} + SO_4^{2-} \rightleftharpoons FeSO_4^+$, K_{ML}. In addition, the equilibrium constants for HSO_4^- dissociation, $NaSO_4^-$ ion pair formation, and $FeHSO_4^{2+}$ complex formation were obtained. The formation constants were used to construct species distribution diagrams in the absence and in the presence of sulfate ions at 25, 55, and 80 °C. Changes in concentration of the various ferric complexes with increasing temperature indicated possible mechanisms explaining the formation of monodispersed basic ferric sulfate hydrosols. Application of the study to an analysis of atmospheric steel corrosion in the presence of sulfate ions is discussed.

Introduction

Iron (hydrous) oxides appear in the form of different minerals and they are widely used as pigments, catalysts, and in many other applications. In addition, corrosion of iron and steel results in rust which consists of colloidal aggregates of ferric hydroxides and of magnetite. Despite many important aspects of this family of compounds no mechanism of formation of different ferric (hydrous) oxides has yet been developed. It is obvious that the precipitation process must be preceded by ferric ion complexation which involves hydroxyl ions and, in some cases, other anions such as sulfate or phosphate. Indeed, it is now well established that corrosion of iron is strongly accelerated by the presence of sulfate ions.[4-7] On the other hand, there is evidence that some metal basic sulfates may actually act as an inorganic "glue" which binds the rust to the clean metal substrate producing a self-protecting coating.[8,9]

Obviously, if one is to explain the mechanism of iron corrosion, or the formation of different iron (hydrous) oxides in nature or for various applications, it is essential that the composition of the solution environment, in which these systems precipitate, is completely elucidated. This involves a qualitative and quantitative identification of all solute complexes during the prenucleation, nucleation, and particle growth stages.

The only way one may expect to answer the as yet unresolved question of the chemical processes involved in iron (hydrous) oxide formation is to carry out controlled precipitation reactions which would yield particles perfectly well defined in terms of composition, structure, size, and other characteristics. No such attempts have been successful in the past. Recently, we have developed a technique which yields colloidal particles of basic ferric sulfate of exceedingly uniform morphology and dimensions.[2] These sols were reproducibly obtained by forced hydrolysis, at elevated temperatures, of ferric salt solutions to which alkali metal sulfates were added. As an example, Figure 1 gives transmission and scanning electron micrographs of colloidal dispersions with the chemical composition of the particles being $Fe_3(SO_4)_2(OH)_5 \cdot 2H_2O$. Interestingly, the x-ray determined structure and the stoichiometry of these particles showed them to be identical with the naturally occurring alunite type minerals.[10,11]

Our ultimate aim is to explain the mechanism of formation of such well-defined basic ferric sulfate systems, especially since this would help in the understanding of iron and steel corrosion. Indeed, the conditions required for the formation of particles illustrated in Figure 1 are rather akin to those which prevail on a corroding steel surface when sulfate ions are present. This task would be feasible if the thermodynamic data on ferric complexes with hydroxyl and sulfate ions were available. The information in the literature is essentially restricted to monomeric ferric hydrolysis products at room temperature. There is considerable disagreement in the available formation constants for the polynuclear complexes. Only one report deals with the hydrolysis of ferric ions at a temperature as high as 51 °C, and this is over 20 years old.[12]

The present study has been undertaken to establish the composition and the thermodynamic properties of ferric hydrolysis products in the absence and in the presence of sulfate ions at different ionic strengths. The data were obtained for the temperature range of 25–80 °C at low pH and complete species distribution diagrams are offered for these conditions.

Spectrophotometric, potentiometric, and combined stopped-flow temperature jump techniques were used. In some cases, more than one method was employed to obtain the same information and excellent agreement was found.

Establishing the thermodynamic quantities of ferric species in aqueous solution is by no means a trivial problem. This is best attested to by the inordinate amount of work applied to determinations at 25 °C only, where the complications are considerably less than those encountered at elevated temperatures. The latter information is of importance in various applications, such as in explaining the corrosion processes in water-cooled nuclear reactors or steam generators.

Using the thermodynamic data obtained, an overall mechanism for the formation of basic ferric sulfate is suggested which will have to be substantiated by kinetic measurements.

Experimental Section

1. *Solutions.* To prepare the appropriate stock solutions $Fe(NO_3)_3 \cdot 9H_2O$, $Fe(ClO_4)_3 \cdot 9H_2O$, or $Fe(ClO_4)_2 \cdot 6H_2O$ salts were dissolved in doubly distilled water and passed

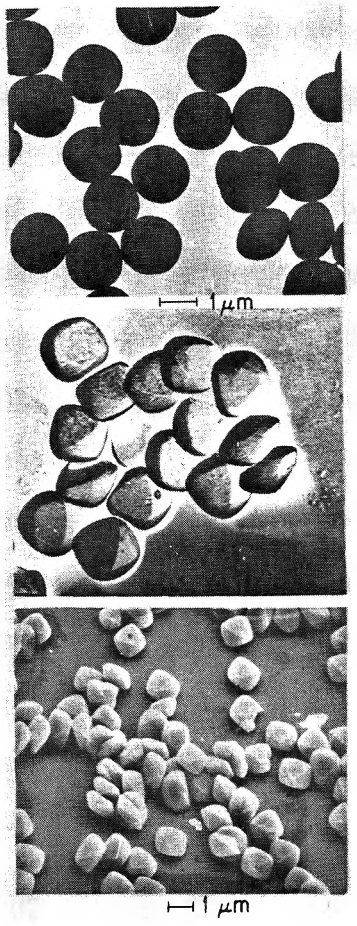

Figure 1. (Top) Transmission electron micrograph of a basic ferric sulfate hydrosol prepared from a solution 0.18 M in $Fe(NO_3)_3$ and 0.53 M in Na_2SO_4 heated from room temperature to 80 °C at 1.5 °C/min in an oil bath. Total aging time at 80 °C was 60 min. (Center) Carbon replica of the basic ferric sulfate hydrosol described above. (Bottom) Scanning electron micrograph of a basic ferric sulfate hydrosol prepared as described above except that K_2SO_4 was used instead of Na_2SO_4.

through 0.45-μm Millipore filters prior to use. Such solutions were stable over extended periods of time, either in highly concentrated state (>2 M) or if the ratio of $[Fe^{3+}]$ to added $[H^+]$ was at least 1:10, as indicated by the constancy of absorbance readings on diluted solutions which showed no change for several weeks. To prevent oxidation, iron(II) salt solutions were stored under nitrogen.

All glassware was soaked in 6 M HCl for ~12 h prior to regular cleaning procedures to remove possible iron deposits on the walls.

The ferric perchlorate solutions (ionic strength 2.67 M) were standardized by the spectrophotometric determination[13] of ferric ions as the thiocyanate complex in acidic media.

Throughout this work the order of mixing was as follows: Fe(III) solution, acid, SO_4^{2-} (if any), $NaClO_4$, and filtered, doubly distilled water. This was necessary, particularly at lower acidities, to prevent formation of polynuclear complexes or precipitation of the hydroxide. In all experiments, samples were allowed to equilibrate at room temperature for at least 6 (in most cases 12) h prior to any measurements.

Tetramethylammonium chloride (Eastman) was recrystallized once from distilled water and oven dried at 120 °C. All other chemicals were of the highest available purity grade and were used without further treatment.

2. *Methods.* a. *Spectrophotometry.* Quantitative absorbance measurements were obtained with a Zeiss Model PMQ3 spectrophotometer equipped with a Zeiss Model PMI photometer-indicator-with digital readout. The latter device permitted the determination of absorbance values to three decimal places. A thermostated cell holder was temperature controlled to ±0.1 °C by means of a Haake Model FK external circulating water bath. Matched 1-cm quartz (Hellma) or Pyrex (Coleman) cells were tightly stoppered to prevent evaporation losses, particularly at higher temperatures. Since no mechanical agitation was employed to stir the contents of the cells, a minimum of 20 min was allowed for equilibration.

b. *Potentiometric Titrations.* The study of Fe^{3+} hydrolysis by potentiometric titrations was carried out by the procedure described by Hedström,[14] which was extended to temperatures of 55 and 80 °C. To prevent interference from CO_2, the systems were continuously purged with nitrogen during the titrations at 25 °C. At 55 and 80 °C the flow of N_2 gas caused considerable losses due to evaporation and for that reason no purging was done. In view of the smaller solubility of CO_2 at higher temperatures no detrimental effect was observed. Also, it was shown that Fe^{3+} complexation by CO_3^{2-} does not occur to any appreciable extent in acidic solutions.[14,15]

In the interpretation of ferric ion hydrolysis in the presence of sulfate ions in highly acidic solutions, the stability data for the bisulfate ion at the corresponding temperatures were necessary. Since this information was not available in the literature, titrations of Na_2SO_4 with perchloric acid at constant ionic strengths (as adjusted with $NaClO_4$) were carried out at 25, 55, and 80 °C using glass electrodes. The evaluation of the dissociation constant of the HSO_4^- ion required the knowledge of the extent of $NaSO_4^-$ ion pairing, particularly in solutions of high ionic strength. The latter was determined with a sodium ion selective electrode (Orion) which was used to measure the potentials due to the activity of free Na^+ ion in solutions of Na_2SO_4 at constant ionic strength (as adjusted with tetramethylammonium chloride). The corresponding concentrations of free Na^+ were obtained by graphical interpolation from a calibration plot established with NaCl solutions of known concentrations, assuming that ion pairing between Na^+ and Cl^- was negligible.

c. *Temperature Jump and Stopped Flow.* A combined stopped-flow temperature jump apparatus described in detail elsewhere[16] was used to obtain corroborating thermodynamic data for the first hydrolysis step. Preliminary kinetic studies on the formation of complexes in solutions from which basic ferric sulfate precipitated were also carried out.

Data Treatment and Calculations

1. *Spectrophotometric Determinations.* (a) $FeOH^{2+}$. The first hydrolysis step of Fe^{3+} represented by

$$Fe^{3+} \xrightarrow{K_1} FeOH^{2+} + H^+ \qquad (1)$$

was investigated in a manner identical with that of Siddall and Vosburgh[17] who derived the following relationship:

$$1/A = \frac{1}{[Fe^{3+}]_{tot}\epsilon_{FeOH^{2+}}} + \frac{[H^+]}{[Fe^{3+}]_{tot}\epsilon_{FeOH^{2+}}K_1} \qquad (2)$$

in which A is the absorbance and $\epsilon_{FeOH^{2+}}$ is the extinction coefficient for the first hydrolysis complex and $[Fe^{3+}]_{tot}$ is the weighed-in concentration of the ferric ions. A plot of $1/A$ vs. $[H^+]$ should yield a straight line from which K_1 or ϵ could be calculated in the absence of other hydrolysis complexes.

Data at different temperatures were then used to calculate the enthalpy of formation of the $FeOH^{2+}$ complex.

(b) $FeSO_4^+$. Experiments designed after those of Lister and Rivington[18] were conducted in order to evaluate the complex formation constants K_{ML} and K_{MHL} for the reactions between Fe^{3+} and SO_4^{2-} and HSO_4^-, respectively, according to

$$Fe^{3+} + SO_4^{2-} \overset{K_{ML}}{\rightleftharpoons} FeSO_4^+ \quad (3)$$

$$Fe^{3+} + HSO_4^- \overset{K_{MHL}}{\rightleftharpoons} FeHSO_4^{2+} \quad (4)$$

However, the graphical analysis as carried out by these authors proved to be inadequate, especially for the data obtained at elevated temperatures. Instead the following procedure was adopted.

The total absorbance of a solution (A_T) composed of Fe^{3+} and SO_4^{2-} at high acidity with $[Fe^{3+}]$ always in excess over $[SO_4^{2-}]$ is given as

$$A_T = \epsilon_{Fe^{3+}}[Fe^{3+}] + \epsilon_{FeOH^{2+}}[FeOH^{2+}] + \epsilon_{FeSO_4^+}[FeSO_4^+] + \epsilon_{FeHSO_4^{2+}}[FeHSO_4^{2+}] \quad (5)$$

The total analytical concentrations of Fe^{3+} (C_M^0) and SO_4^{2-} (C_L^0) are expressed as

$$C_M^0 = [Fe^{3+}] + [FeOH^{2+}] + [FeSO_4^+] + [FeHSO_4^{2+}] \quad (6)$$

$$C_L^0 = [SO_4^{2-}] + [HSO_4^-] + [FeSO_4^+] + [FeHSO_4^{2+}] \quad (7)$$

Under the rather acidic conditions of these experiments, the sulfate–bisulfate equilibrium

$$HSO_4^- \overset{K_A}{\rightleftharpoons} SO_4^{2-} + H^+ \quad (8)$$

must be also considered. Equations 1, 3, 4, and 8 yield

$$C_M^0 = [Fe^{3+}]\left(1 + \frac{K_1}{[H^+]} + K_{ML}[SO_4^{2-}] + \frac{K_{MHL}[H^+][SO_4^{2-}]}{K_A}\right) \quad (9)$$

and

$$C_L^0 = [SO_4^{2-}]\left(1 + \frac{[H^+]}{K_A} + K_{ML}[Fe^{3+}] + \frac{K_{MHL}[Fe^{3+}][H^+]}{K_A}\right) \quad (10)$$

By subtracting the absorbance of a ferric solution prepared in the absence of sulfate (A_i) from the measured absorbance of the same ferric solution in the presence of a known concentration of sulfate ion (A_T), the absorbance (ΔA) due to the presence of $FeSO_4^+$ and $FeHSO_4^{2+}$ was taken as

$$\Delta A = A_T - A_i = \epsilon_{FeSO_4^+}[FeSO_4^+] + \epsilon_{FeHSO_4^{2+}}[FeHSO_4^{2+}] \quad (11)$$

It is recognized that the value of A_i is not strictly equal to the sum of the absorbances from Fe^{3+} and $FeOH^{2+}$ in the presence of sulfate ions. However, at the low pH values used in these experiments A_i is negligible in comparison to A_T and, consequently, eq 11 yields correct formation constants for the ferric sulfate complexes.

Since Fe^{3+} is in excess over SO_4^{2-}, eq 11 can be approximated as

$$\Delta A = \epsilon_{FeSO_4^+}K_{ML}C_M^0[SO_4^{2-}] + \frac{\epsilon_{FeHSO_4^{2+}}K_{ML}C_M^0[H^+][SO_4^{2-}]}{K_A} \quad (12)$$

which, in combination with eq 10, gives

$$\Delta A = \frac{C_M^0 C_L^0}{\left(1 + \frac{[H^+]}{K_A} + K_{ML}C_M^0 + \frac{K_{MHL}C_M^0[H^+]}{K_A}\right)} \times \left(\epsilon_{FeSO_4^+}K_{ML} + \frac{\epsilon_{FeHSO_4^{2+}}K_{MHL}[H^+]}{K_A}\right) \quad (13)$$

This rearranges to

$$\frac{C_M^0}{\Delta A} = \frac{C_M^0\left(K_{MHL}\frac{[H^+]}{K_A} + K_{ML}\right)}{C_L^0 D} + \frac{\left(1 + \frac{[H^+]}{K_A}\right)}{C_L^0 D} \quad (14)$$

where

$$D = \epsilon_{FeSO_4^+}K_{ML} + \epsilon_{FeHSO_4^{2+}}K_{MHL}([H^+]/K_A) \quad (15)$$

Plots of $C_M^0/\Delta A$ vs. C_M^0/C_L^0 at fixed $[H^+]$ and C_L^0 should yield straight lines if the assumptions described by eq 12 are valid.

The four independent parameters K_{ML}, K_{MHL}, $\epsilon_{FeSO_4^+}$, and $\epsilon_{FeHSO_4^{2+}}$ were evaluated by a multiparametric curve-fitting procedure. A general program for effecting nonlinear regression[19] was combined with a subroutine that solved eq 13 to yield the value of ΔA at each experimental point for any set of values of the parameters furnished by the main body of the program, and also with the coordinates of the experimental points (ΔA, C_M^0, C_L^0, and $[H^+]$). Execution began with crude estimates of the parameters. The squares of the differences between the values of ΔA computed from these estimates and the measured values were summed, and the estimates were adjusted by the main portion of the program in ways that minimized the sum. The computations were made with a Digital Equipment Corp. PDP8/I minicomputer.[19] In most of the work reported here, preference has been given to the computerized data analysis as opposed to the less reliable graphical treatment.

2. *Potentiometric Titrations.* Hedström's graphical procedures for determining the equilibrium constants K_1, K_2, and K_{22} as defined by eq 1 and

$$Fe^{3+} \overset{K_2}{\rightleftharpoons} Fe(OH)_2^+ + 2H^+ \quad (16)$$

$$2Fe^{3+} \overset{K_{22}}{\rightleftharpoons} Fe_2(OH)_2^{4+} + 2H^+ \quad (17)$$

were not at all satisfactory when applied to the potentiometric data obtained at 55 and 80 °C. A curve-fitting procedure, using the previously mentioned CFT4 computer program[19] proved to be applicable to the analysis of these systems.

The relationship between the measured redox potentials ($E_{red.}$) and formal potentials (E_0') is given by the Nernst expression

$$E_{red.} = E_0' - \frac{RT}{F}\ln([Fe^{2+}]/[Fe^{3+}]) \quad (18)$$

where RT/F is the Nernst coefficient, and $[Fe^{3+}]$ and $[Fe^{2+}]$ are equilibrium free iron(III) and iron(II) ion concentrations. E_0' is dependent on $[H^+]$ since it includes the liquid junction potential.

Calculation of the free ferric ion concentration was accomplished by substitution of the previously defined

hydrolysis equilibrium expressions (eq 1, 16, and 17) into the mass balance expression for total $[Fe^{3+}]$:

$$[Fe^{3+}]_{tot} = [Fe^{3+}] + [FeOH^{2+}] + [Fe(OH)_2^{+}] + 2[Fe_2(OH)_2^{4+}] \quad (19)$$

and solving the resulting quadratic expression

$$[Fe^{3+}]^2 + [Fe^{3+}]\left(\frac{1}{2K_{22}}\right)([H^+]K_1 + K_2 + [H^+]_2) - \frac{[Fe^{3+}]_{tot}[H^+]^2}{2K_{22}} = 0 \quad (20)$$

A three-parameter fit in which E_0', K_2, and K_{22} were adjustable parameters and K_1 was provided as a fixed quantity (values determined by the spectrophotometric procedure) was used to evaluate the experimental data. The measured redox potentials and equilibrium $[H^+]$ values were supplied as input data.

3. *Temperature Jump Stopped-Flow.* The proton transfer reaction described by eq 1 is of central importance in a quantitative analysis of the hydrolytic equilibria of iron(III). At the same time, a static, thermodynamic determination of equilibrium parameters for reaction 1 is always subject to interference from competing equilibria leading to the formation of polynuclear iron(III) species. This complication is minimized when the iron(III) solution concentrations are rather low,[17] but this necessarily leads to a decrease in the experimentally observable quantity (i.e., the absorbance change). An alternate and accurate method was sought to independently check the reliability of the spectrophotometric data. The relaxation time for reaction 1 under our experimental conditions is in the submicrosecond range,[20] and is separated from that for the dimerization reaction by more than three orders of magnitude. Analysis of the temperature jump relaxation amplitude corresponding to reaction 1 alone allows, in principle, the determination of both K_1 and $\Delta H°$. From eq 1 and the mass balance condition for iron(III), it can be shown that a small change in absorbance, δA, resulting from a temperature perturbation of 4.0 °C is given by

$$\delta A = (\epsilon_{FeOH^{2+}} - \epsilon_{Fe^{3+}})\left(\frac{\partial[FeOH^{2+}]}{\partial \ln K_1}\right)_{T,P} \partial \ln K_1 = \Gamma(\epsilon_{FeOH^{2+}} - \epsilon_{Fe^{3+}})\,\partial \ln K_1 \quad (21)$$

where

$$\Gamma = \left(\frac{1}{[Fe^{3+}]} + \frac{1}{[FeOH^{2+}]} + \frac{1}{[H^+]}\right)^{-1} \quad (22)$$

Multiplying the numerator and denominator of the right-hand side of eq 22 by $[Fe(OH)^{2+}][H^+]$, simplifying, and combining with eq 21 gives a more useful form:

$$\delta A = \frac{[FeOH^{2+}][H^+]}{[FeOH^{2+}] + [H^+] + K_1}(\epsilon_{FeOH^{2+}} - \epsilon_{Fe^{3+}})\frac{\Delta H^0}{RT}\frac{\Delta T}{T} \quad (23)$$

where $\Delta H°$ is the thermodynamic enthalpy change for reaction 1, ΔT = 4.0 °C, and all other constants have been previously defined. Equation 23 describes a linear ($\Delta H°$) and a nonlinear (Γ) dependence of equilibrium parameters on the changes in absorbance, δA. Both $\Delta H°$ and K_1 can be simultaneously evaluated with a high degree of accuracy, since relative changes in absorbance as low as 10^{-4} can be measured with the present instrument.[16] In eq 23 the effects of temperature on the molar absorptivities and the density of the solution are neglected because they are negligible in the studied systems.[16] The extinction coefficient for Fe^{3+}, $\epsilon_{Fe^{3+}}$, was assigned a value of 5.

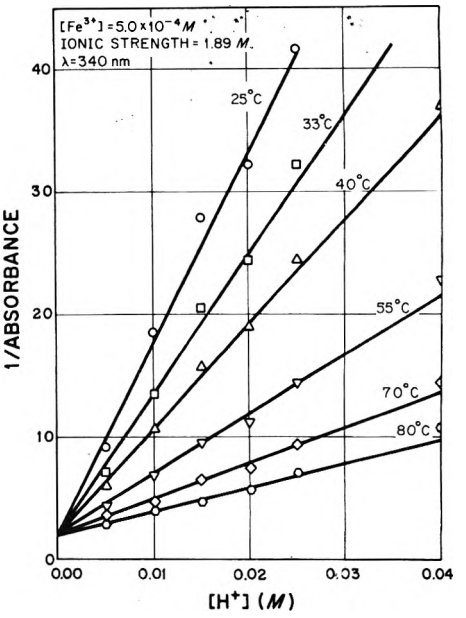

Figure 2. Plots of reciprocal absorbance (λ 340 nm) vs. total added acid concentration used to determine K_1 and $\epsilon_{FeOH^{2+}}$ at various temperatures. The ionic strength was 1.89 M and $[Fe^{3+}]_{tot} = 5.0 \times 10^{-4}$ M.

In practice, acidic iron(III) solutions were neutralized in the flow apparatus, and a temperature jump of 4.0 °C applied 50 ms after complete mixing. This approach eliminated problems due to the slow formation of hydrolytic iron(III) polymers, since the resulting change in absorbance was recorded within 25 μs.

Results

1. *$FeOH^{2+}$.* The equilibrium constants for the formation of $FeOH^{2+}$ were determined from absorbancies at 340 nm for temperatures of 25, 33, 40, 55, 70, and 80 °C over a range of ionic strengths and $[H^+]$ values while $[Fe^{3+}]_{tot}$ was kept constant at 5×10^{-4} M.

Excellent linear plots of $1/A$ vs. $[H^+]$, as expected from eq 2, were obtained for all of the ionic strengths (μ) investigated. A typical plot at μ = 1.89 M is presented in Figure 2. It is readily apparent that the relative error in the measurements decreased as the temperature increased, which is, of course, due to the higher absorbances at higher temperatures. At a particular ionic strength all $1/A$ vs. $[H^+]$ plots for various temperatures extrapolate to the same intercept indicating that the extinction coefficient for $FeOH^{2+}$ ($\epsilon_{FeOH^{2+}}$) shows little variation with temperature at fixed ionic strength over the range investigated.

The reversibility of the hydrolysis was checked at several ionic strengths by gradually cooling the samples from 80 to 25 °C over a period of approximately 1 h. The redetermined absorbance values were found to be virtually identical with the values measured for the unheated solutions; the differences never exceeded ±0.003 absorbance units, indicating that equilibrium conditions prevailed in the studied solutions.

Table I presents a compilation of the equilibrium constants for $FeOH^{2+}$, obtained at various temperatures and ionic strengths. The error in the K_1 values is estimated at no more than ±10%.

A Van't Hoff plot of $\ln K_1$ vs. $1/T$ (K^{-1}) gave a value of $\Delta H°$ = 7.7 ± 0.3 kcal/mol for the first hydrolysis of Fe^{3+} (μ = 2.67 M).

TABLE I: Equilibrium Constants for $FeOH^{2+}$

μ, M	T, °C	10^3K_1	μ, M	T, °C	10^3K_1
2.67	25	1.16	1.00	25	1.47
	33	1.54		33	1.93
	40	2.15		40	2.66
	55	3.6		55	4.7
	70	6.2		70	8.6
	80	8.8		80	11.9
2.25	25	1.23	0.50	25	1.75
	33	1.63		33	2.38
	40	2.21		40	3.3
	55	3.9		55	6.3
	70	6.7		70	11.1
	80	9.5		80	16.0
1.89	25	1.24	0.10	25	2.46
	33	1.68		33	3.5
	40	2.26		40	4.9
	55	4.1		55	8.9
	70	7.0		70	15.3
	80	10.5		80	23.2

The extinction coefficient of $FeOH^{2+}$ was independently determined in the flow temperature jump apparatus by neutralizing a dilute Fe(III) solution to a pH of ~7, and recording the corresponding absorbance within 5 ms after complete mixing. The value of 922 cm^2 mol^{-1} obtained in this manner is in excellent agreement with the value of 917 cm^2 mol^{-1} at 340 nm determined by the static spectrophotometric method.

For an independent evaluation of both K_1 and $\Delta H°$, experiments over a broad range of acidities are essential (eq 23). Due to experimental difficulties at lower $[H^+]$ concentrations, only solutions with relatively high acid concentrations could be studied. Using the δA, $\epsilon_{FeOH^{2+}}$, and $\epsilon_{Fe^{3+}}$ values from the stopped-flow temperature jump measurements, as well as the spectrophotometrically determined K_1, a value of 8.1 ± 0.8 kcal/mol was obtained for $\Delta H°$, at an ionic strength of 2.67 M, which is in very good agreement with the enthalpy given above.

2. *$Fe(OH)_2^+$ and $Fe_2(OH)_2^{4+}$.* Potentiometric titration measurements were used to determine the formation constants K_2 and K_{22} for the hydrolysis complexes $Fe(OH)_2^+$ and $Fe_2(OH)_2^{4+}$, respectively. At each temperature (25, 55, and 80 °C) six titrations were carried out at a constant ionic strength of 2.67 M. Reproducible and stable potential readings were obtained with titrated solutions containing different ratios of Fe^{3+} to Fe^{2+} molar concentrations.

Table II gives the average values for K_2 and K_{22}. The apparently large error is in part due to computational problems related to the form of the expressions used in the curve fitting of the data. The consistency of the experiments themselves in a series of titrations at a particular temperature is illustrated by the excellent agreement between the experimental and calculated values of the formal potential E_0'.

3. *$FeSO_4^+$ and $FeHSO_4^{2+}$.* To determine the equilibrium constants for $FeSO_4^+$ and $FeHSO_4^{2+}$ according to the method described earlier, absorbances were measured at 340, 335, 330, and 325 nm at 25, 55, and 80 °C for several series of solutions in which the $[Fe^{3+}]$:$[SO_4^{2-}]$ ratios were varied. Each set of solutions was of different overall total acid concentrations (0.25, 0.5, 0.8, 1.0, and 1.2 M at 25 and 55 °C and 0.5, 0.8, 1.0, and 1.2 M at 80 °C). Ionic strength was adjusted to 2.67 M with $NaClO_4$ in all samples.

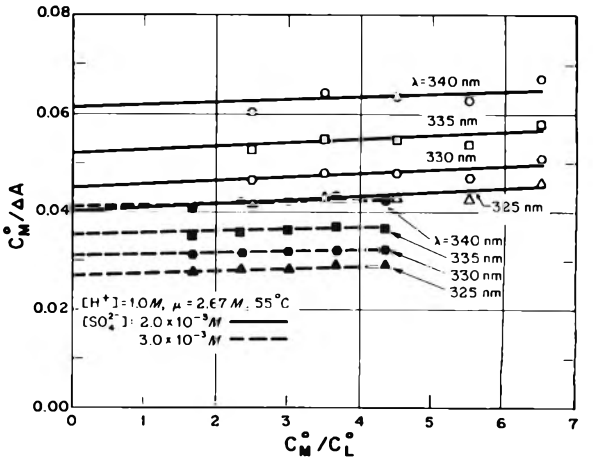

Figure 3. Plots of $C_M^0/\Delta A$ vs. C_M^0/C_L^0 used in the analysis of absorbance data obtained from ferric solutions in the presence of sulfate ions. These plots provide experimental verification that the assumptions made in deriving eq 12 were valid. $[H^+]_{tot}$ = 1.0 M, μ = 2.67 M, T = 55 °C, $[SO_4^{2-}]_{tot}$ = 0.002 or 0.003 M, and λ 340, 335, 330, or 325 nm.

The graphical plots gave linear relationships (Figure 3) as predicted by eq 14, indicating that the approximations made in deriving eq 12 were valid.

The absorbances were determined for five different total concentrations of Fe^{3+} ions at three $[Fe^{3+}]$:$[SO_4^{2-}]$ ratios for each and at five $[H^+]$ (4 at 80 °C), at four wavelengths at each of the three temperatures investigated for a total of 840 measurements.

The four parameter curve-fitting procedure was used to evaluate both the extinction coefficients and the equilibrium constants for $FeSO_4^+$ and $FeHSO_4^{2+}$. Table III gives the data for $FeSO_4^+$ which are subject to approximately 10% relative error. This is probably due primarily to the fact that the formation of $NaSO_4^-$ ion pairs could not be taken into consideration.

The calculation of the formation constant for the $FeHSO_4^{2+}$ complex from the spectrophotometric data necessitated the knowledge of bisulfate ion dissociation constant (eq 8) which in turn required information on the $NaSO_4^-$ ion pair formation constant. Table IV gives the latter at 25, 55, and 80 °C for two different ionic strengths. The error is mainly due to the problems encountered with the ion selective electrode. For comparison purpose, some relevant literature values are also included in this same table.

A considerable number of studies deal with the acid dissociation constant of HSO_4^- ion for a range of ionic strengths and temperatures.[21,22] The reasons for carrying out additional measurements in this work are (a) the great discrepancy in published data by different authors, and (b) the lack of information for the conditions used in the

TABLE II: Equilibrium Constants for the Formation of $Fe(OH)_2^+$ and $Fe_2(OH)_2^{4+}$ at an Ionic Strength of 2.67 M

T, °C	K_1[a]	E_0'(initial)	K_2	K_{22}	E_0'(final)
25	0.0012	564.4 ± 2.3	2.0×10^{-6} $\pm 1.3 \times 10^{-6}$	6.0×10^{-4} $\pm 1.7 \times 10^{-4}$	563.6 ± 1.8
55	0.0036	620.7 ± 1.4	2.9×10^{-5} $\pm 1.4 \times 10^{-5}$	1.8×10^{-3} $\pm 1.3 \times 10^{-3}$	621.9 ± 1.0
80	0.0088	667.4 ± 1.1	6.3×10^{-4} $\pm 2.1 \times 10^{-4}$	3.5×10^{-3} $\pm 1.3 \times 10^{-3}$	672.6 ± 2.0

[a] From spectrophotometric determinations.

TABLE III: Extinction Coefficients and Equilibrium Constants for $FeSO_4^+$ at an Ionic Strength of 2.67 M

T, °C	Wavelength, nm	$\epsilon_{FeSO_4^+}$	$K_{FeSO_4^+}$ (K_{ML})
25	340	990 ± 120	84 ± 7
	335	1110 ± 100	
	330	1280 ± 60	
	325	1450 ± 130	
55	340	1090 ± 170	245 ± 20
	335	1210 ± 100	
	330	1300 ± 100	
	325	1450 ± 150	
80	340	1240 ± 60	1020 ± 110
	335	1310 ± 50	
	330	1440 ± 60	
	325	1500 ± 120	

TABLE IV: $NaSO_4^-$ Ion Pair Formation Constants

T, °C	μ, M	$K_{NaSO_4^-}$	Ref
25	2.67	2.7 ± 0.5	This work
25	1.89	2.5 ± 0.5	This work
55	2.67	3.5 ± 0.5	This work
55	1.89	3.3 ± 0.5	This work
80	2.67	4.3 ± 0.5	This work
80	1.89	4.0 ± 0.5	This work
25	0.69	2.02	23
25	0	4.47-5.25	24, 25, 26

TABLE V: HSO_4^- Dissociation Constants

T, °C	Ionic strength, M	K_A
25	2.67	0.073 ± 0.011
	1.89	0.069 ± 0.008
	1.50	0.062 ± 0.006
	1.00	0.060 ± 0.007
	0.50	0.049 ± 0.005
55	2.67	0.024 ± 0.004
	1.89	0.022 ± 0.003
	1.50	0.022 ± 0.001
	1.00	0.021 ± 0.003
	0.50	0.019 ± 0.002
80	2.67	0.0082 ± 0.0012
	1.89	0.0080 ± 0.0010
	1.50	0.0079 ± 0.0002
	1.00	0.0077 ± 0.0008
	0.50	0.0070 ± 0.0002

precipitation work described in the Introduction. For example, the majority of reported values at high temperatures are for ionic strengths extrapolated to zero. Table V gives the dissociation constants for the bisulfate anion at different temperatures for five different ionic strengths.

With the aid of the appropriate values for $K_{NaSO_4^-}$ and K_A, as well as the spectrophotometric data on the Fe^{3+}–SO_4^{2-} system, the formation constant of $FeHSO_4^{2+}$ was calculated to be $K_{MHL} = 4 \pm 1$ ($\mu = 2.67$ M) at 25, 55, and 80 °C. This is in reasonable agreement with the value of 6 ± 1 (at 25 °C and $\mu = 1.2$ M) as determined by Lister and Rivington.[18] The relative errors are large, which is in part due to the magnitude of the constants and in part to the complexity of the system.

Species Distribution Diagram

Experimentally determined values of the equilibrium constants $K_1(FeOH^{2+})$, $K_2(Fe(OH)_2^+)$, $K_{22}(Fe_2(OH)_2^{4+})$, $K_{ML}(FeSO_4^+)$, and $K_{MHL}(FeHSO_4^{2+})$ were used to calculate the distributions of different ferric solutes as a function of pH at 25, 55, and 80 °C. In some instances the formation of $Fe(SO_4)_2^-$ was also considered as estimated from

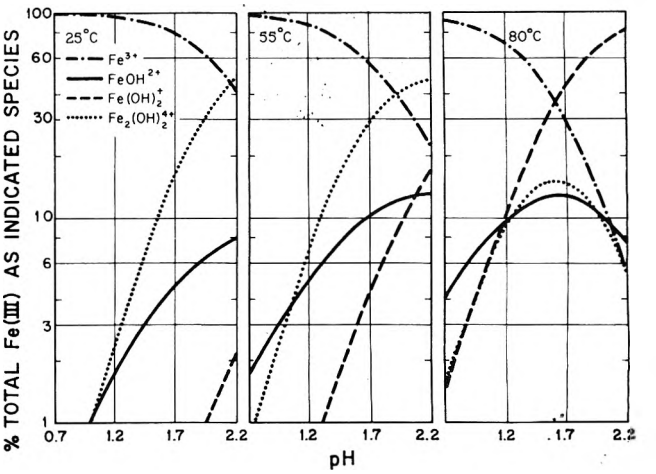

Figure 4. Species distribution diagrams as a function of pH at 25, 55, and 80 °C for ferric hydroxo complexes. $[Fe^{3+}]_{tot} = 0.18$ M and $\mu = 2.67$ M in all cases.

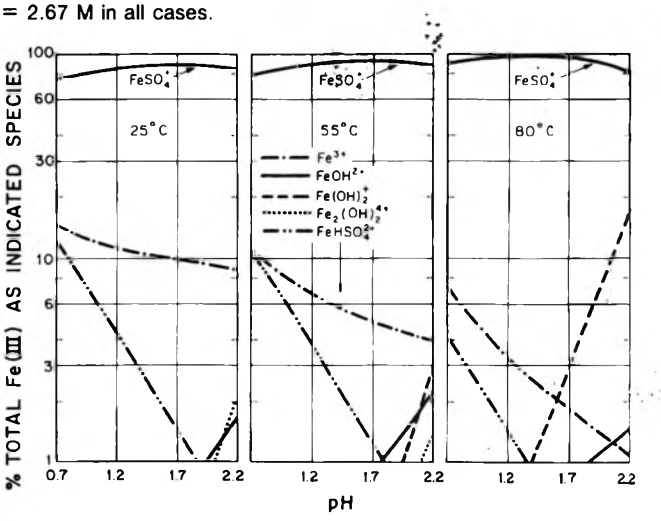

Figure 5. Species distribution diagrams as a function of pH at 25, 55, and 80 °C for ferric hydroxo and sulfato complexes. $[Fe^{3+}]_{tot} = 0.18$ M, $[SO_4^{2-}]_{tot} = 0.53$ M, and $\mu = 2.67$ M in all cases.

the literature data,[27] but it was consistently found that the concentration of this complex was negligible and, therefore, it was not included in the final diagrams. Species distributions calculated both in the absence and in the presence of sulfate ion are given in Figures 4 and 5, respectively.

Discussion

The determinations of equilibrium constants reported in this work were carried out in order to establish the composition of salt solutions which were used in the preparation of monodispersed basic ferric sulfate particles. Thermodynamic data for the ferric complexes available in the literature for conditions similar as used in the present study are summarized in Table VI and compared with the values obtained here. Some marked differences are observed, particularly in the case of the dimer, $Fe_2(OH)_2^{4+}$, which reflect the inherent difficulties encountered in the quantitative evaluation of ferric hydrolysis processes by different techniques. The situation is further aggravated when the studies are extended to higher temperatures.

The fact that excellent agreement was found for the extinction coefficients and the enthalpies of formation for the $FeOH^{2+}$ species as obtained independently by spectrophotometry and by the temperature jump amplitude determinations indicates the reliability of the data reported in Table I.

TABLE VI: Comparison of the Equilibrium Constants for Ferric Hydroxo and Sulfato Complexes

$FeOH^{2+}$

T, °C	μ, M	10^3K_1	$\epsilon_{FeOH^{2+}}$ (λ 340 nm)	ΔH° kcal/mol	Ref
25	0.1	2.89	925		28
25	0.1	2.46	917	8.5	This work
25	0.5	1.58	890		29
25	0.5	1.75	917	8.5	This work
25	0.53	1.74			30
25	1.0	1.47	917	8.2	This work
25	1.0	1.64		10.2	31
25	2.67	1.16	917	7.7	This work
25	3.0	0.90			14, 32
25	3.0	1.28	925		28
25	3.0	1.00		10.2	33
45	2.67	2.58	917	7.7	This work
45	3.0	3.00		10.2	33

$Fe(OH)_2^+$

T, °C	μ, M	10^7K_2	Ref
25	2.67	20.0	This work
25	3.0	4.9	14, 32

$Fe_2(OH)_2^{4+}$

T, °C	μ, M	10^3K_{22}	Ref
25	2.67	0.6	This work
25	3.0	1.22	14
25	3.0	1.10	32
25	3.0	4.4	33
45	3.0	9.3	33
51	3.0	25.1	12
55	2.67	1.8	This work

$FeSO_4^+$

T, °C	μ, M	K_{ML}	$\epsilon_{FeSO_4^+}$	Ref
25	0.5	205		34
35	0.5	280		34
28	1.0	107		35
25	1.2	165	690 (λ 340 nm) 810 (λ 335 nm) 970 (λ 330 nm)	18
25	1.2	132		36
25	1.53	117		27
25	2.0	110		36
25	2.67	84	990 (λ 340 nm) 1110 (λ 335 nm) 1280 (λ 330 nm) 1450 (λ 325 nm)	This work
25	3.0	105		27

The equilibrium constants for $FeSO_4^+$ were also determined spectrophotometrically and the error analysis shows comparable precision as with the values obtained for $FeOH^{2+}$.

Spectrophotometric procedures become very cumbersome, if not impossible, in determining the equilibrium constants of $Fe(OH)_2^+$, $Fe_2(OH)_2^{4+}$, and higher polymeric species. Therefore, the potentiometric titrations were employed. The results indicate that precision of the data obtained from electrochemical work is much lower than from optical determinations. Thus, it would seem preferable to employ spectrophotometry in ferric solution complex chemistry whenever possible.

Fortunately, $FeOH^{2+}$ and $FeSO_4^+$ complexes seem to play the dominant role in the formation of basic ferric sulfate. The availability of good thermodynamic data for these two species is essential for the determination of the equilibria responsible for the precipitation of the monodispersed colloidal particles in acidic solutions containing ferric and sulfate ions. To prepare such sols, the solutions of appropriate concentrations are aged either for several hours at higher temperatures or for several weeks or months at room temperature. Typical conditions used in these experiments are: $[Fe^{3+}] = 0.18$ M, $[SO_4^{2-}] = 0.27$–0.53 M, and pH 1.6–1.7. When aging at 25 °C, a slightly higher pH is required (1.8–1.9).

TABLE VII: Molar Concentrations of Various Complexes Present at Different Temperatures in a Solution Initially 0.18 M in $Fe(NO_3)_3$ and 0.53 M in Na_2SO_4 (Total Concentrations) at pH 1.7

Species	Temperature 25 °C	55 °C	80 °C
Fe^{3+}	1.78×10^{-2}	8.89×10^{-3}	3.30×10^{-3}
$FeOH^{2+}$	1.07×10^{-3}	1.60×10^{-3}	1.46×10^{-3}
$Fe(OH)_2^+$	8.9×10^{-3}	6.4×10^{-4}	5.23×10^{-3}
$Fe_2(OH)_2^{4+}$	4.8×10^{-4}	4.0×10^{-4}	1.1×10^{-4}
$FeSO_4^+$	1.58×10^{-1}	1.66×10^{-1}	1.69×10^{-1}
$FeHSO_4^{2+}$	2.57×10^{-3}	2.25×10^{-3}	8.0×10^{-4}
SO_4^{2-}	1.06×10^{-1}	7.60×10^{-2}	5.00×10^{-2}
HSO_4^-	2.91×10^{-2}	6.32×10^{-2}	1.22×10^{-1}
$NaSO_4^-$	2.35×10^{-1}	2.23×10^{-1}	1.87×10^{-1}

It is important that at room temperature only alunite type colloidal particles of hexagonal crystal symmetry form having a chemical composition $Fe_3(SO_4)_2(OH)_5 \cdot 2H_2O$. At higher temperatures, monodispersed colloidal monoclinic particles of the composition $Fe_4(SO_4)(OH)_{10}$ may also precipitate, in addition to the hexagonal microcrystals.

The similarities between the precipitation conditions and the final products suggest that essentially the same chemical reactions are responsible for solid phase formation at both 25 and 80 °C. Evidently, it is the concentration of one or more of the simple solute species which influences the marked differences which are observed in the rates of precipitation.

With the thermodynamic data obtained in this work, it is possible to compute the composition of the solutions in which ferric sulfate particles are formed. One such case is illustrated in Table VII.

It is evident that $FeSO_4^+$ is the dominating species at all temperatures. $FeOH^{2+}$ is the most abundant hydrolyzed product at lower temperatures. However, with increasing temperature, the relative concentration of $Fe(OH)_2^+$ rises and at 80 °C this species exceeds in content the primary hydrolysis product, $FeOH^{2+}$.

Experimental support for the species distribution was obtained from temperature jump measurements on solutions in which basic ferric sulfate particles were formed. Typical results are shown in Figure 6. Only two major relaxation effects are observed, one fast process within the rise time of the instrument ($\tau << 7$ μs), and a much slower process with a relaxation time of ~7 ms. This can be understood in terms of fast protolytic equilibria coupled with ferric sulfate complexation steps.[20,36] The absence of additional relaxation processes, as well as the complete reversibility of the spectra of the ferric solutions with respect to heating, indicate that the concentration of polynuclear ferric species is negligible.

The compositional analysis suggests that the hexagonal $Fe_3(SO_4)_2(OH)_5 \cdot 2H_2O$ solid is formed via an overall reaction of the type:

$$FeOH^{2+} + 2FeSO_4^+ + 6H_2O \rightarrow Fe_3(SO_4)_2(OH)_5 \cdot 2H_2O + 4H^+ \quad (24)$$

Obviously, similar stoichiometry would apply if the dimer, $Fe_2(OH)_2^{4+}$, participated in the particle nucleation and growth processes.

At higher temperatures only, the increasing amount of the $Fe(OH)_2^+$ complex would explain the simultaneous appearance of the monoclinic species, as a result of the

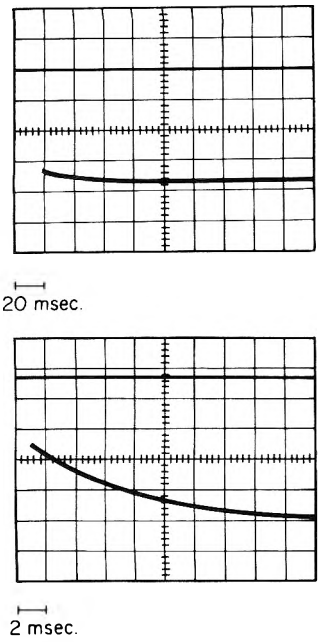

Figure 6. Temperature jump experiments on solutions in which basic ferric sulfate particles are formed. $[Fe^{3+}]_{tot}$ = 0.18 M, $[SO_4^{2-}]_{tot}$ = 0.53 M, pH 1.7; temperature, 25 °C; wavelength λ, 454 nm. Horizontal scale (top trace) 20 ms/major division; (bottom trace) 2 ms/major division. Vertical scale in decreasing absorbance in arbitrary units.

following summary reaction:

$$3Fe(OH)_2^+ + FeSO_4^+ + 4H_2O \rightarrow Fe_4(SO_4)(OH)_{10} + 4H^+ \quad (25)$$

The proposed overall processes differ somewhat from the ones suggested earlier[2] when the necessary equilibrium constants were unknown.

An extensive kinetic study is in progress, using the temperature jump stopped-flow technique, which should further define the reaction mechanisms involved in the formation of basic ferric sulfate precipitates.

Acknowledgment. We are greatly indebted to Professor Louis Meites for his advice in various aspects of this work and particularly in the analysis of data. We also acknowledge technical assistance of Mr. R. Wilhelmy with the temperature jump measurements. Ramesh C. Patel thanks the Research Corporation and the Petroleum Research Fund, administered by the American Chemical Society, for grants in support of instrumentation.

References and Notes

(1) Supported by the American Iron and Steel Institute Project No. 63-269.
(2) Part I: E. Matijević, R. S. Sapieszko, and J. B. Melville, *J. Colloid Interface Sci.*, **50**, 567 (1975).
(3) Part of a Ph.D. Thesis by R. S. Sapieszko.
(4) H. R. Copson, *Proc. ASTM*, **45**, 554 (1945).
(5) W. H. J. Vernon, *Trans. Faraday Soc.*, **31**, 1668 (1935).
(6) G. Schikorr, *Werkst. Korros.*, **15**, 457 (1964).
(7) U. R. Evans and C. A. J. Taylor, *Corr. Sci.*, **12**, 227 (1972).
(8) R. A. Oriani and L. Zwell, private communication.
(9) K. A. Chandler and J. F. Stanners, *Proc. Int. Congr. Met. Corros., 2nd*, 55–56 (1963).
(10) J. D. Dana and E. S. Dana, "The System of Mineralogy", 7th ed, Vol. 2, Wiley, New York, N.Y., 1951, pp 555–567.
(11) J. D. H. Donnay and H. M. Ondik, "Crystal Data-Determinative Tables", 3rd ed, Vol. 2, U.S. Dept. of Commerce, Washington, D.C., 1973, pp H 238–H 241.
(12) L. N. Mulay and P. W. Selwood, *J. Am. Chem. Soc.*, **77**, 2693 (1955).
(13) P. H. Hsu, *Soil Sci. Soc. Am. Proc.*, **31**, 353 (1967).
(14) B. O. A. Hedström, *Ark. Kem.*, **6**, 1 (1953).
(15) R. C. Patel and G. Atkinson, paper presented at 160th National Meeting of the American Chemical Society, Chicago, Ill., Sept 1970.
(16) R. C. Patel, *Chem. Instrum.* **7**, 83 (1976).
(17) T. H. Siddall and W. C. Vosburgh, *J. Am. Chem. Soc.*, **73**, 4270 (1951).
(18) M. W. Lister and D. E. Rivington, *Can. J. Chem.*, **33**, 1591 (1955).
(19) L. Meites, "The General Multi-parametric Curve Fitting Program CFT4". Hard-copy listings of the basic program and a number of modifications of it that serve a variety of different but related purposes, together with a 220-page manual of instructions, explanation, and documentation may be obtained by remitting $45.00 to the Computing Laboratory of the Department of Chemistry, Clarkson College of Technology, Potsdam, N.Y. 13676.
(20) P. Hemmes, L. D. Rich, D. L. Cole, and E. M. Eyring, *J. Phys. Chem.*, **75**, 929 (1971).
(21) D. D. Perrin, *Pure Appl. Chem.*, **20**, 133 (1969).
(22) L. G. Sillen and A. E. Martell, *Chem. Soc., Spec. Publ.*, **No. 17** (1964).
(23) R. M. Pytkowicz and D. R. Kester, *Am. J. Sci.*, **267**, 217 (1969).
(24) R. M. Izatt, D. Eatough, J. J. Christensen, and C. H. Bartholomew, *J. Chem. Soc. A*, 45 (1969).
(25) I. L. Jenkins and C. B. Monk, *J. Am. Chem. Soc.*, **72**, 2695 (1950).
(26) R. A. Robinson and R. H. Stokes, "Electrolyte Solutions", Butterworths, London, 1955, Chapter 14.
(27) B. N. Mattoo, *Z. Phys. Chem.*, **19**, 156 (1959).
(28) R. M. Milburn and W. C. Vosburgh, *J. Am. Chem. Soc.*, **77**, 1352 (1955).
(29) A. R. Wilson and H. Taube, *J. Am. Chem. Soc.*, **74**, 3509 (1952).
(30) C. Brosset, *Sven. Kem. Tidskr.*, **53**, 434 (1941).
(31) R. M. Milburn, *J. Am. Chem. Soc.*, **79**, 537 (1957).
(32) K. Schlyter, *Trans. R. Inst. Technol., Stockholm*, **No. 196** (1962).
(33) O. E. Zvyagintsev and S. B. Lyakhmanov, *Russ. J. Inorg. Chem.*, **13**, 643 (1968).
(34) G. G. Davis and W. M. Smith, *Can. J. Chem.*, **40**, 1836 (1962).
(35) R. A. Whiteker and N. Davidson, *J. Am. Chem. Soc.*, **75**, 3081 (1953).
(36) F. P. Cavasino, *J. Phys. Chem.*, **72**, 1378 (1968).

Standard State Entropies of the Aqueous Rare Earth Ions

Frank H. Spedding,* Joseph A. Rard, and Anton Habenschuss

Ames Laboratory—ERDA and Department of Chemistry, Iowa State University, Ames, Iowa 50011 *(Received January 25, 1977) Publication costs assisted by the Ames Laboratory—USERDA*

Recently data have become available for the activity coefficients of 14 rare earth chlorides, and for the heats of dilution of 13 rare earths chlorides, from dilute solution to saturation at 25 °C. In addition, new heats of solution data have been reported for the hydrated crystals of 13 of the rare earth chlorides. These data have been used here, together with crystal entropy data, to calculate standard state ionic entropies for the rare earth ions in aqueous solution. The standard state ionic entropies form two series when plotted against the inverse square of the ionic radius of the rare earth ion. The S shape of this series curve was found to be consistent with a decrease in the rare earth ion's inner-sphere hydration number between Nd and Tb, and with an increase in total ionic hydration from La to Lu.

Introduction

Bertha and Choppin[1] have reported values for the standard state ionic entropies of the rare earth ions, based on thermodynamic data for the rare earth iodates. These ionic entropies form an S-shaped curve when plotted against the ionic radius (or atomic number) of the rare earth ion. Bertha and Choppin have interpreted this S shape in terms of a change in the overall hydration of the cation across the rare earth series. Hinchey and Cobble[2] noted that Bertha and Choppin had to estimate the entropies of the rare earth iodate crystals, and they concluded that the S shape of Bertha and Choppin's entropy series curve was an artifact of the method of data treatment. Hinchey and Cobble[2] also calculated a set of standard state ionic entropies based on data for the rare earth chlorides, for which more nearly complete thermodynamic data were available. Hinchey and Cobble felt that their entropy values were a linear function of the inverse square of the ionic radius (Powell–Latimer correlation[3]), within the scatter of the data.

Hinchey and Cobble[2] found it necessary to estimate free energies of solution for the hydrated crystals of 7 of the rare earth chlorides, from data for 7 of the other rare earths. Activity coefficient data are now available for 14 of the rare earth chlorides[4] up to saturation. Hinchey and Cobble's estimates of the free energies of solution agree moderately well with the experimental values except for $YbCl_3 \cdot 6H_2O$ and $LuCl_3 \cdot 6H_2O$ (they gave no estimate for Tm). New measurements have since become available for the heats of solution of the hydrated crystals of 13 of the rare earth chlorides,[5] and some of the earlier measurements for these salts appear to be somewhat in error. Also, when Hinchey and Cobble did their calculations, crystal heat capacities were available only to 224–262 K, so they found it necessary to extrapolate these data to 298 K. New heat capacity data have been measured for several of the hydrated rare earth chloride crystals[6] up to 300 K. Data are therefore now available that can be used to calculate much more accurate standard state ionic entropies for the aqueous rare earth ions than have previously been available. The data are now sufficiently accurate to determine whether the standard state ionic entropies are a linear function of the inverse square of the ionic radius, as found by Hinchey and Cobble,[2] or S shaped as found by Bertha and Choppin.[1] Therefore, standard state ionic entropies have been calculated for the aqueous rare earth ions. Examination of this property as a function of the ionic radius of the rare earth ion should yield important information about ion–solvent interactions in these solutions.

Calculations and Results

Spedding et al.[4] have measured the water activities and activity coefficients of 14 rare earth chlorides from dilute solution to saturation at 25 °C. These measurements were performed by the isopiestic method, with KCl and $CaCl_2$ solutions as isopiestic reference solutions. More accurate osmotic coefficients have since become available for the $CaCl_2$ reference solutions.[7] Consequently, the rare earth chloride isopiestic data of Spedding et al.[4] were recalculated to conform to the new $CaCl_2$ reference values and then fitted to equations of the type

$$\phi = 1 - (A/3)m^{1/2} + \sum_i A_i m^{r_i} \tag{1}$$

where $A = (0.51082)(3)(\sqrt{6})(2.302585) = 8.6430$, and ϕ and m are the osmotic coefficient and molality of the solution, respectively. The r_i were fixed at the values of Spedding et al.[4] These values of r_i and the least-squares A_i are given in Table I, along with the standard deviation of the fit, SD, for each salt. In most cases, these standard deviations are smaller than those obtained by Spedding et al., due to the improved reliability of the $CaCl_2$ standard data. The free energies of solution were changed only 0.15% or less by this recalculation, but the data were recalculated in order to obtain more accurate entropies of solution.

The water activity, a_1, of a solution is given by

$$\ln a_1 = -\nu m M_1 \phi / 1000 \tag{2}$$

where $\nu = 4$ is the number of ions formed by the complete dissociation of one molecule of rare earth chloride, and $M_1 = 18.0154$ g mol^{-1} is the molecular weight of water. The mean molal activity coefficient of the salt in this solution, $\gamma_\pm$, is obtained by substituting eq 1 into the Gibbs–Duhem relation and integrating to obtain

$$\ln \gamma_\pm = -A m^{1/2} + \sum_i ((r_i + 1)/r_i) A_i m^{r_i} \tag{3}$$

This equation is just the Debye–Hückel limiting law with a series of terms in powers of the molality added.

The solution of crystals of rare earth chloride hydrate in water can be represented by the equation

$$RECl_3 \cdot nH_2O(c) = RE^{3+}(aq) + 3Cl^-(aq) + nH_2O(l) \tag{4}$$

From data for a saturated solution in equilibrium with hydrated crystals, the standard Gibbs free energy of solution is given by

$$\Delta \bar{G}_s^\circ = -RT \ln (27 m_s^4 \gamma_{\pm s}^4 a_{1s}^n) \tag{5}$$

where $RT = 592.48$ cal mol^{-1} at 298.15 K, m_s is the molality of the saturated solution, and $\gamma_{\pm s}$ and a_{1s} are the activity

TABLE I: Coefficients and Powers for Osmotic Coefficient Polynomials

i	r_i	A_i	r_i	A_i
		$LaCl_3$		$PrCl_3$
1	0.75	−8.363812	0.75	−9.789942
2	0.875	50.822366	0.875	56.472725
3	1	−65.948766	1	−73.865134
4	1.125	26.573326	1.125	30.654999
5	3	−0.0540019	1.5	−0.4041491
6	4	3.58981×10^{-3}	3	-3.06288×10^{-2}
7	9	3.72456×10^{-7}	9	5.58410×10^{-7}
SD		0.0016		0.0016
		$NdCl_3$		$SmCl_3$
1	0.75	−13.517253	0.75	−14.178938
2	0.875	69.559821	0.875	73.502731
3	1	−88.695765	1	−95.646086
4	1.125	35.826688	1.125	39.733298
5	2.5	−0.1494141	2	−0.3586169
6	3	1.51161×10^{-2}	7	-1.64153×10^{-4}
7	9.5	1.37777×10^{-7}	7.5	7.83068×10^{-5}
SD		0.0013		0.0012
		$EuCl_3$		$GdCl_3$
1	0.75	−14.969349	0.75	−15.811253
2	0.875	75.967276	0.875	79.956895
3	1	−98.033903	1	−104.099388
4	1.125	40.430981	1.125	43.451566
5	2	−0.3245541	2	−0.4198653
6	3.5	-4.83493×10^{-3}	8	-3.59899×10^{-5}
7	12	1.11116×10^{-8}	8.5	1.79676×10^{-5}
SD		0.0010		0.0016
		$TbCl_3$		$DyCl_3$
1	0.75	−14.019302	0.75	−10.492606
2	0.875	74.359808	0.875	62.354017
3	1	−98.298388	1	−86.102964
4	1.125	41.463732	1.125	38.701423
5	2	−0.4162668	1.5	−1.3624282
6	7.5	-1.07496×10^{-5}	5	-5.59297×10^{-3}
7	11.5	4.33870×10^{-8}	5.5	2.32340×10^{-3}
SD		0.0018		0.0015
		$HoCl_3$		$ErCl_3$
1	0.75	−3.003857	0.75	−11.523597
2	0.875	28.799617	0.875	64.183495
3	1	−35.132119	1	−84.413459
4	1.125	12.005130	1.125	35.117187
5	2	0.5546639	2	−0.2613983
6	3	-1.33706×10^{-1}	4	-2.77474×10^{-3}
7	4	1.03159×10^{-2}	10	1.82992×10^{-7}
SD		0.0020		0.0020
		$TmCl_3$		$YbCl_3$
1	0.75	−5.237336	0.75	−8.687038
2	0.875	37.927936	0.875	51.328464
3	1	−48.469568	1	−65.650989
4	1.125	18.822774	1.125	26.126851
5	2.5	0.0826491	3.5	−0.0167532
6	4	-3.91392×10^{-2}	8.5	5.51363×10^{-6}
7	4.5	1.36348×10^{-2}	12	-1.68351×10^{-8}
SD		0.0015		0.0013
		$LuCl_3$		YCl_3
1	0.75	−9.110257	0.75	−8.300105
2	0.875	53.179841	0.875	53.009614
3	1	−68.121464	1	−72.896197
4	1.125	27.170052	1.125	32.331370
5	3.5	−0.0185506	1.5	−1.0375494
6	7.5	2.76843×10^{-5}	5.5	-1.36931×10^{-3}
7	10	-3.12089×10^{-7}	6.5	2.52539×10^{-4}
SD		0.0016		0.0022

coefficient and water activity of the solution at saturation. Values of m_s, $\gamma_{\pm s}$, a_{1s}, and $\Delta\bar{G}_s°$ are given in Table II, along with the hydrate compositions. The standard state for the solvent in a solution is the pure solvent while that of the solute, for free energy calculations, is a hypothetical solution with a mean molality of one and a mean molal activity coefficient of one, with both components at 25 °C and 1 atm pressure.

The heats of solution of the hydrated rare earth chloride crystals, $\Delta\bar{H}_s°$, have been reported by Spedding and Miller,[8] Spedding and Flynn,[9] Spedding, Naumann, and Eberts,[10] Csejka and Spedding,[11] Spedding et al.,[5] and Hinchey and Cobble.[2] These values are listed in Table III and have been reextrapolated, where sufficient data have been reported, to infinite dilution using recent values for the heats of dilution of these salts.[5] The extrapolations

TABLE II: Standard Free Energy of Solution Data

Hydrate	m_s, mol kg^{-1}	$\gamma_{\pm s}$	a_{1s}	$\Delta\bar{G}_s^\circ$, cal mol^{-1}
$LaCl_3 \cdot 7H_2O$	3.8944	4.785	0.4744	−5792
$PrCl_3 \cdot 7H_2O$	3.8969	5.633	0.4597	−6050
$NdCl_3 \cdot 6H_2O$	3.9309	6.198	0.4470	−6658
$SmCl_3 \cdot 6H_2O$	3.6414	5.110	0.4874	−6327
$EuCl_3 \cdot 6H_2O$	3.5839	5.208	0.4922	−6369
$GdCl_3 \cdot 6H_2O$	3.5898	5.774	0.4849	−6564
$TbCl_3 \cdot 6H_2O$	3.5733	6.369	0.4816	−6761
$DyCl_3 \cdot 6H_2O$	3.6302	7.409	0.4666	−7045
$HoCl_3 \cdot 6H_2O$	3.6987	8.796	0.4492	−7361
$ErCl_3 \cdot 6H_2O$	3.7840	9.986	0.4302	−7562
$TmCl_3 \cdot 6H_2O$	3.8814	11.73	0.4095	−7828
$YbCl_3 \cdot 6H_2O$	4.0018	13.92	0.3873	−8108
$LuCl_3 \cdot 6H_2O$	4.1239	16.60	0.3659	−8395
$YCl_3 \cdot 6H_2O$	3.9478	12.45	0.4017	−7941

TABLE III: Standard Heats of Solution

Hydrate	$\Delta\bar{H}_s^\circ$, cal mol^{-1}	No. of determinations	Ref
$LaCl_3 \cdot 7H_2O$	−7357 ± 67[a]	3	9
	−6693 ± 5	4	5
	−6693[b]		
$CeCl_3 \cdot 7H_2O$	−6873 ± 35	2	8
	−6873[b]		
$PrCl_3 \cdot 7H_2O$	−7034 ± 20	2	9
	−7005 ± 4	4	5
	−7015[b]		
$PrCl_3 \cdot 6H_2O$	−9672 ± 12	3	9
	−9672[b]		
$NdCl_3 \cdot 6H_2O$	−9144 ± 84	2	8
	−9106 ± 21	12	10
	−9138 ± 18	3	5
	−9115[b]		
$SmCl_3 \cdot 6H_2O$	−9008 ± 193[a]	3	9
	−8613 ± 6	4	5
	−8613[b]		
$EuCl_3 \cdot 6H_2O$	−8770 ± 30	4	2
	−8714 ± 6	2	5
	−8751[b]		
$GdCl_3 \cdot 6H_2O$	−8412 ± 81[a]	2	9
	−9119 ± 7	4	5
	−9119[b]		
$TbCl_3 \cdot 6H_2O$	−9554 ± 27	10	5
	−9554[b]		
$DyCl_3 \cdot 6H_2O$	−10049 ± 16	9	11
	−9973 ± 9	4	5
	−10026[b]		
$HoCl_3 \cdot 6H_2O$	−10416 ± 15	8	5
	−10416[b]		
$ErCl_3 \cdot 6H_2O$	−11409 ± 32[a]	2	9
	−10743	1	5
	−10743[b]		
$TmCl_3 \cdot 6H_2O$	−11122	1	5
	−11122[b]		
$YbCl_3 \cdot 6H_2O$	−10774 ± 39[a]	2	9
	−11515 ± 11	3	5
	−11515[b]		
$LuCl_3 \cdot 6H_2O$	−11910 ± 20	5	2
	−11860 ± 11	3	5
	−11891[b]		
$YCl_3 \cdot 6H_2O$	−11147 ± 19	3	9
	−11147[b]		

[a] This value not used in computing the recommended value. [b] Recommended value.

of the heat of solution data for Ce were made using the averages of the heats of dilution for lanthanum and praseodymium chloride, and the averages of the erbium and thulium chloride data were used for Y. The recommended best values for these heats of solution were obtained by averaging data sets proportional to the number of determinations of that heat quantity from the various

TABLE IV: Entropy Data for Rare Earth Chloride Hydrates and Rare Earth Ions

Hydrate	$\bar{S}_c^\circ$,[a] gibbs mol^{-1}	$\Delta\bar{S}_s^\circ$,[b] gibbs mol^{-1}	$\bar{S}_{RE}^\circ$,[c] gibbs mol^{-1}	S_e°,[d] gibbs mol^{-1}	$\bar{S}_{adj}^\circ$,[e] gibbs mol^{-1}
$LaCl_3 \cdot 7H_2O$	110.6	−3.02	−49.9	0.0	−49.9
$PrCl_3 \cdot 7H_2O$	111.2[f]	−3.24	−49.5	4.4	−53.9
$NdCl_3 \cdot 6H_2O$	99.7	−8.24	−49.3	4.6	−53.9
$SmCl_3 \cdot 6H_2O$	99	−7.67	$-49._4$	3.6	$-53._0$
$EuCl_3 \cdot 6H_2O$	97.3	−7.99	−51.5	2.2	−53.7
$GdCl_3 \cdot 6H_2O$	97.1[g]	−8.57	−52.3	4.1	−56.4
$TbCl_3 \cdot 6H_2O$	96.5[g]	−9.37	−53.6	5.1	−58.7
$DyCl_3 \cdot 6H_2O$	96.0	−10.00	−54.8	5.5	−60.3
$HoCl_3 \cdot 6H_2O$	96.4[g]	−10.25	−54.6	5.6	−60.2
$ErCl_3 \cdot 6H_2O$	95.3	−10.67	−56.1	5.5	−61.6
$TmCl_3 \cdot 6H_2O$	95.5	−11.05	−56.3	5.1	−61.4
$YbCl_3 \cdot 6H_2O$	94.6	−11.43	−57.6	4.1	−61.7
$LuCl_3 \cdot 6H_2O$	89.5[g]	−11.73	−63.0	0.0	−63.0
$YCl_3 \cdot 6H_2O$	92	−10.75	$-59._5$	0.0	$-59._5$

[a] Entropy of hydrated rare earth chloride crystal. [b] Standard entropy of solution of hydrated crystal. [c] Standard state entropy of rare earth ion. [d] "Electronic" contribution to the ionic entropy (free ion value). [e] Adjusted standard state ionic entropy. [f] Data from ref 2. [g] Data from ref 6 (also see note 18). All other $\bar{S}_c^\circ$ values from ref 15 and 16.

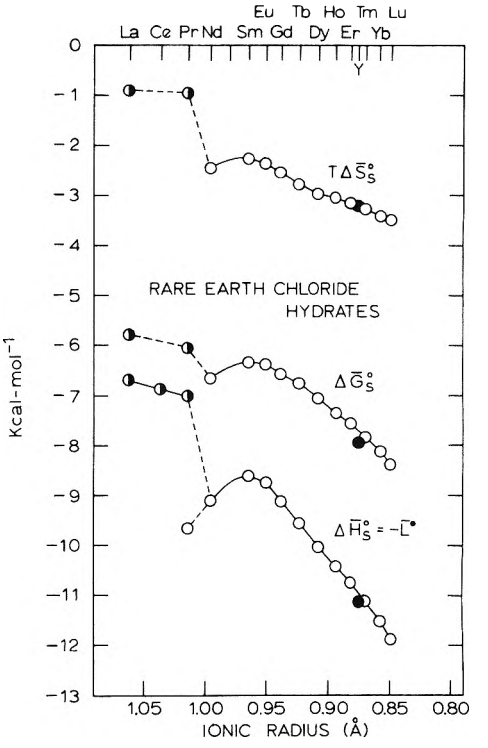

Figure 1. Standard enthalpies, free energies, and temperature entropy products for the solution of hydrated rare earth chloride crystals. Open and filled circles are for hexahydrates, half-filled circles for heptahydrates. Yttrium is indicated by a filled circle.

sources of data. Several of the heats of solution reported by Spedding and Flynn[9] appear to have systematic errors present when these data are compared to independent determinations. For this reason, these heats of solution were redetermined in this laboratory.[5] The new data were used in the calculations and some of Spedding and Flynn's data were given weights of zero. Standard entropies for the solution process can then be calculated from

$$\Delta\bar{G}_s^\circ = \Delta\bar{H}_s^\circ - T\Delta\bar{S}_s^\circ \quad (6)$$

and these $\Delta\bar{S}_s^\circ$ values are given in Table IV. These entropies of solution correspond to the entropy changes

that occur when 1 mol of the crystalline hydrate is dissolved in water to form a solution with each component in its standard state.

Figure 1 is a plot of $\Delta\bar{G}_s°$, $\Delta\bar{H}_s°$, and $T\Delta\bar{S}_s°$ of solution as a function of the ionic radius of the rare earth ion.[12,13] The heat of solution of $PrCl_3·6H_2O$ may not be completely reliable since chemical analysis of the hydrate indicated that it may have contained some heptahydrate[9] (this praseodymium chloride hexahydrate heat of solution is not used in obtaining the ionic entropies). Figure 1 indicates that the heptahydrates and hexahydrates exhibit different series trends in their thermodynamic properties of solution (the crystals of neodymium to lutetium chloride hexahydrate are known to be isostructural, as are the heptahydrates). The scatter in these data appear to be fairly small, about 0.1–0.2 gibbs mol^{-1} (gibbs = cal deg^{-1}) for $\Delta\bar{S}_s°$ at least for Sm through Lu where there are enough salts to clearly establish the series trends.

If the standard entropy of solution, $\Delta\bar{S}_s°$, is added to the entropy of the hydrated rare earth chloride crystal, $\bar{S}_c°$, the resulting value is the absolute entropy of 1 mol of aqueous rare earth chloride and n mol of water, each in its standard state. If the entropy of n mol of liquid water and 3 mol of chloride ions are subtracted from the above sum, the result is the standard state ionic entropy of the rare earth ion. Using 16.71 gibbs mol^{-1} for the entropy of liquid water[14] and 13.5 gibbs mol^{-1} for the chloride ion,[14] we have

$$\bar{S}_{RE}° = \bar{S}_c° + \Delta\bar{S}_s° - n(16.71) - 3(13.5) \quad (7)$$

for the standard state ionic entropies of the rare earth ions. Values of $\bar{S}_c°$ for most of the rare earth chloride hydrates were taken from the NBS tabulations,[15,16] and are based mainly on the heat capacity data of Pfeffer et al.[17] The crystal entropies of $GdCl_3·6H_2O$, $TbCl_3·6H_2O$, $HoCl_3·6H_2O$, and $LuCl_3·6H_2O$ were taken from Spedding et al.,[6,18] and are based on heat capacity measurements up to 300 K. In this latter study,[6] care was taken to remove occluded solution from the crystals. The measurements of Pfeffer et al.[17] were for crystals containing some occluded solution,[6] and require 36 to 74 K extrapolations of the heat capacity data to 298 K. The crystal entropies reported by the NBS were obtained by subtracting the magnetic "bumps" from the original heat capacity data of Pfeffer et al.,[17] followed by numerical integration of the resulting data to obtain the lattice entropies, and then adding on the free ion "electronic" entropies as given in the next paragraph.[19] No value was given for the entropy of $PrCl_3·7H_2O$ in the NBS tabulations so this value was taken from Hinchey and Cobble's extrapolation of lower temperature heat capacity data.[2] The crystal entropies, entropies of solution, and standard state ionic entropies are given in Table IV. These ionic entropies are based on the convention of assigning a value of zero for the standard state entropy of the hydrogen ion, and these values are absolute entropies except for the somewhat arbitrary assignment of the entropy of the hydrogen ion. The standard state ionic entropies of the aqueous rare earth ions are plotted as a function of the inverse square of the ionic radii in Figure 2.

The standard state ionic entropies of the rare earth ions contain an "electronic" entropy contribution of approximately

$$S_e° = R \ln (2J + 1) \quad (8)$$

where J is the quantum number for the total electronic angular momentum of the ground state. This value is correct if the degeneracy of the ground state of the rare earth ion is not lifted a sufficient amount to have some of the states not fully populated in aqueous solution at 298 K, due to ligand field effects. For some purposes this equation may not be an adequate approximation (this will be discussed in more detail below). The values of $S_e°$ are listed in Table IV. The "electronic" entropy values for Eu^{3+} and Sm^{3+} contain contributions from thermally populated higher electronic states with different J values. This "electronic" entropy contribution is superimposed on trends due to solvation of the rare earth ion, and it effectively masks the solvation trends of the ionic entropy since the "electronic" entropy varies significantly with rare earth. If this "electronic" entropy is subtracted from the ionic standard state entropy to obtain the adjusted standard state ionic entropy, $\bar{S}°_{adj}$, for each rare earth, then the resulting adjusted entropies might be expected to show direct correlations with solvation trends in aqueous solution. Values of $\bar{S}°_{adj}$ are given in Table IV and are illustrated in Figure 2.

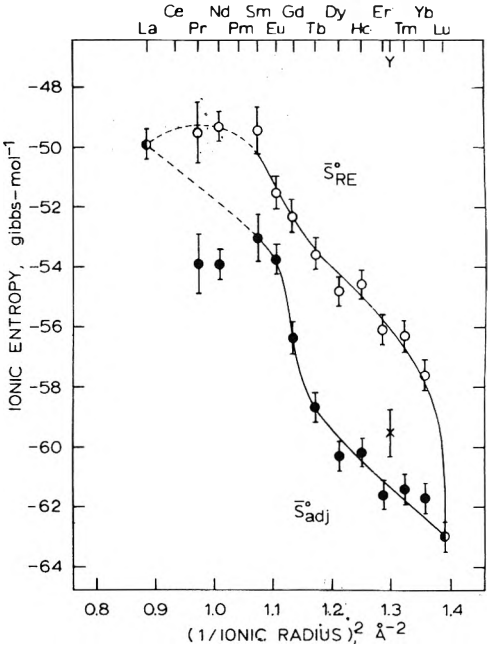

Figure 2. Open circles indicate conventional standard state ionic entropies; closed circles indicate ionic entropies adjusted to remove "electronic" entropies; half-filled circles indicate rare earths for which $S_e° = 0$; the cross indicates yttrium.

As seen from Figure 2, the adjusted standard state ionic entropies of the heavy rare earths (Tb to Lu) are more negative than those for the lighter rare earths, which indicates that a more ordered condition exists in solutions of the heavy rare earths. The adjusted standard state entropy of the Y^{3+} ion falls about 1.5 gibbs mol^{-1} from the position expected from its ionic radius. This difference may occur since Y^{3+} has one less completed electron shell than the lanthanides, and its position in the rare earth series frequently changes with the property being studied. Also, the crystal entropy of $YCl_3·6H_2O$ was estimated by an indirect method from decomposition pressure data[19] rather than calculated from experimental heat capacity data. Therefore, the reason for the higher adjusted standard state ionic entropy of Y^{3+} could also be experimental error.

There exist sufficient data for $Gd(NO_3)_3·6H_2O$ to calculate another value of the standard state ionic entropy of the Gd^{3+} ion. Using the heat of solution[20] of 3032 cal mol^{-1}, and isopiestic data[21] of $m_s = 4.3701$ mol kg^{-1}, $\gamma_{\pm s} = 0.7854$, and $a_{1s} = 0.5705$, then $\Delta\bar{S}_s° = 19.83$ gibbs mol^{-1}. Thus, $\bar{S}_{RE}° = 133.2 + 19.83 - 6(16.71) - 3(35.0) = -52.2$

gibbs mol^{-1} and $\bar{S}°_{adj}$ = −56.3 gibbs mol^{-1}. The crystal entropy and the nitrate ion entropy were taken from the NBS tabulations,[14,16] and the crystal entropy is based on an extrapolation of heat capacity data[17] from 220 to 298 K. These standard state ionic entropies are in excellent agreement (0.1 gibbs mol^{-1}) with values obtained from the $GdCl_3·6H_2O$ data.

The adjusted standard state ionic entropies from Tb to Lu appear to be a linear function of the inverse square of the ionic radius, to within the scatter of the entropy data (approximately ±0.5 gibbs mol^{-1}). If a line is drawn through the adjusted standard state ionic entropies of Tb through Lu, then the entropies of all of the other rare earths (La to Gd) fall above this line on the graph. This indicates that the adjusted standard state ionic entropies do not follow the Powell–Latimer correlation across the entire rare earth series, although they may follow it for the heavy rare earths. Similarly, the (unadjusted) standard state ionic entropies do not follow the Powell–Latimer correlation.

The adjusted standard state ionic entropies decrease rapidly with atomic number (become more negative) from Sm to Tb and then decrease more slowly from Tb to Lu. The adjusted standard state ionic entropies from La to Sm show a less clearly defined trend, but they are definitely higher (less negative) than for the heavy rare earths. In Figure 2 a smooth curve was tentatively drawn from La to Sm, and this curve bypasses the Pr and Nd entropies. The slopes for the adjusted standard state ionic entropies are nearly equal for La to Sm and for Tb to Lu, if the La and Sm data are more reliable than the Pr and Nd data. This similarity of slopes for the series behavior of the light and heavy rare earths is frequently found for the thermodynamic and transport properties of rare earth chloride and perchlorate solutions,[4,5,22,23] and this was also assumed to be the case for the adjusted standard state ionic entropies.

If the La^{3+} and Sm^{3+} adjusted standard state ionic entropies are nearly correct, then the implication is that the adjusted standard state ionic entropies of Pr^{3+} and Nd^{3+} are low by about 2–3 gibbs mol^{-1}. Among the factors that might account for this are the following:

(1) Pfeffer et al.[17] did not report the hydrate of $PrCl_3$ for which the heat capacities were measured. Since their samples could conceivably have contained a mixture of hexa- and heptahydrate, the value of $\bar{S}_c°$ may be low and this would cause $\bar{S}_{RE}°$ and $\bar{S}°_{adj}$ to be low for Pr^{3+}. Because of this uncertainty in the $PrCl_3$ hydrate composition, the NBS did not report a value of $\bar{S}_c°$ for this salt.[19]

(2) The NBS procedure to obtain $\bar{S}_c°$ involved adding $R \ln (2J + 1)$ to the lattice entropy. In the calculation of $\bar{S}°_{adj}$ we subtract out this same "electronic" entropy value. The ligand field splittings in the hydrated rare earth chloride crystals and in the aqueous solutions are not very different (both cases have low symmetry), so some cancellation of errors occurs in the calculation of $\bar{S}°_{adj}$. For $PrCl_3·7H_2O$ the NBS did not report a value of $\bar{S}_c°$ so we used Hinchey and Cobble's value,[2] based on direct integration of the original heat capacity data. The true value of the "electronic" entropy for this salt is probably less than the theoretical $R \ln (2J + 1)$ value, so subtraction of $R \ln (2J + 1)$ from $\bar{S}_{RE}°$ for Pr^{3+} may overcorrect for this effect and make $\bar{S}°_{adj}$ too low for this ion.

(3) The approximate cancellation of errors for $\bar{S}°_{adj}$ when NBS $\bar{S}_c°$ values are used should be more nearly exact if the symmetry of the rare earth ion in the crystal is similar to that of the corresponding aquo ion. There is reason to believe that the inner-sphere coordination number of the Nd^{3+} ion may be higher by one in the aqueous solution (see below) than in the hydrated chloride crystal. A similar condition occurs for Pm^{3+}–Gd^{3+}, but the differences between the coordination numbers of the rare earth ions in the hydrated crystals and their average coordination numbers in aqueous solution decrease to zero by Tb^{3+}. It is not known whether this would cause $\bar{S}°_{adj}$ to move in the proper direction for these rare earths.

(4) Another possibility is that the Pr^{3+} and Nd^{3+} data are reasonable but the La^{3+} data are in error, or that all three values are reliable. We do not think that this is the case, but we cannot entirely eliminate these possibilities.

The error bars for Figure 2 were estimated assuming uncertainties of ±0.2 gibbs mol^{-1} for $\Delta\bar{S}_s°$, and ±0.3 gibbs mol^{-1} for $\bar{S}_c°$ except for Pr, Sm, and Y. The crystal hydrate entropies for Sm and Y were reported to only two significant figures,[15,16] so their $\bar{S}_c°$ values were assigned an uncertainty of ±0.6 gibbs mol^{-1}. An uncertainty of 0.8 gibbs mol^{-1} was assumed for $\bar{S}_c°$ of Pr, but the actual error may be larger as discussed above. There may be systematic errors present in $\bar{S}_c°$ and $S_e°$ for the various rare earths, and these errors are difficult to estimate without measuring additional data. The crystal entropies of Spedding et al.[6] for the rare earth chloride hexahydrates of Gd, Tb, Ho, and Lu are within 0.1–0.6 gibbs mol^{-1} of the NBS values, obtained from extrapolation of Pfeffer et al.[17] heat capacity data to 298 K. No estimates were made of the standard state entropies of Ce^{3+} and Pm^{3+} since there is some uncertainty in the behavior of the light rare earths. We do feel that a redetermination of the heat capacities of the hydrated chlorides of La, Pr, and Nd, and a determination of the heat capacities of the hydrated chloride of Ce, are essential in order to clarify the behavior of the standard state ionic entropies of the rare earth ions as a function of the ionic radius. For these redeterminations, attention should be paid to the composition of the hydrates, and the presence of occluded solution in the crystals should be avoided. Direct experimental heat capacity data for $YCl_3·6H_2O$ would also be desirable.

Bertha and Choppin,[1] Krestov,[24] and others have calculated the standard state absolute entropies of the gaseous trivalent rare earth ions at 25 °C from the Sackur–Tetrode equation (Krestov neglected the contribution of higher electronic states for Sm and Eu). The gas phase absolute entropies do not vary in an S-shaped fashion with atomic number, but exhibit minima at La, Eu, and Lu, and maxima at Nd and Ho. This variation is due, of course, to the variation in the "electronic" entropy contribution. The nonelectronic portion of the gas phase ionic entropies increases by only 0.68 gibbs mol^{-1}, in a monotone fashion, from La to Lu. If each gas phase standard state ionic entropy is subtracted from the (unadjusted) standard state ionic entropy for the corresponding aqueous rare earth, the resulting difference is equal to the standard entropy of hydration of the rare earth ion. These entropies of hydration exhibit a shape similar to the adjusted standard state ionic entropies, since the "electronic" entropy terms nearly cancel.[25] This suggests that all, or nearly all, of the variation of $\bar{S}°_{adj}$ with ionic radius is due to the rare earth–water interaction.[26]

In the absence of crystal entropy data for most of the rare earth iodates, entropy of solution data for these salts cannot yield completely reliable standard state entropies for the rare earth ions. Except for a slight skewing of their entropy values, the basic trend found by Bertha and Choppin[1] is correct, and so is their discussion of hydration trends across the rare earth series. Hinchey and Cobble's entropies[2] also exhibit the basic trend found above, but

because of the need to approximate some thermodynamic data and also because of errors in some of the then available heat of solution data, the true shape of their standard state entropy series curve was obscured by scatter.

The radii of the rare earth ions decrease from La to Lu (lanthanide contraction). As a consequence, the surface charge density on the rare earth ion increases from La to Lu, and this should give rise to an increase in the extent of the ion–dipole interactions between the rare earth ion and the water molecules around the rare earth ion. The result from this radius decrease is that the total amount of ionic hydration increases from La to Nd and Tb to Lu, giving rise to a decrease in entropy (increase in order) with decreasing ionic radius. Spedding et al.[27] have proposed that the inner-sphere hydration numbers of the ions of the heavy rare earths (Tb–Lu) are smaller by one than for the light rare earths (La–Nd), and that Pm through Gd exist as intermediate forms in aqueous solution. When this inner-sphere hydration number change occurs, one possibility is that the outer layers of water can move in closer to the rare earth ion, and more water outside the first hydration sphere is affected in going from one rare earth to the next, between Nd and Tb, than when the inner-sphere hydration number remains constant. Consequently, the adjusted standard state ionic entropy decreases more rapidly with decreasing ionic radius, between Nd and Tb, than it does for La to Nd and Tb to Lu.

Our data do not provide a detailed description of the nature of the species with intermediate coordination in Pm–Gd solutions. The possibility was suggested previously[27] that the Pm–Gd ions exist in solution with two different inner-sphere coordination numbers. These two different species were assumed to exist in equilibrium mixtures, and extensive changes also occur in the outer coordination spheres as a result of differences in the inner sphere. Mioduski and Siekierski[28] have noted that another possibility exists; namely, that fractional coordination can occur for Pm to Gd, with all ions of a given rare earth having the same inner-sphere fractional coordination. Presumably, in this model, one water is gradually displaced from the inner coordination sphere of the rare earth ion between Nd and Tb, and the water being displaced can be considered as belonging partially to the inner hydration sphere and partially to the outer coordination sphere (the water bound to the cation does exchange rapidly with the bulk solvent, so this statement should apply to the average species). By Tb, all of this "extra" water would be in the outer sphere. This possibility could explain the spectral results of Geier and Karlen[29] and Reuben and Fiat,[30] which have been interpreted as giving no evidence for the equilibrium between different hydration forms. Both of the above possibilities are consistent with the variation of the adjusted standard state ionic entropies with the ionic radii.

Acknowledgment. This work was performed for the U.S. Energy Research and Development Administration, Division of Physical Research, under Contract No. W-7405-eng-82. The authors thank R. H. Schumm for furnishing details and references related to the NBS values for the crystal entropies for the various salts.

References and Notes

(1) S. L. Bertha and G. R. Choppin, *Inorg. Chem.*, **8**, 613 (1969).
(2) R. J. Hinchey and J. W. Cobble, *Inorg. Chem.*, **9**, 917 (1970).
(3) R. E. Powell and W. M. Latimer, *J. Chem. Phys.*, **19**, 1139 (1951).
(4) F. H. Spedding, H. O. Weber, V. W. Saeger, H. H. Petheram, J. A. Rard, and A. Habenschuss, *J. Chem. Eng. Data*, **21**, 341 (1976).
(5) F. H. Spedding, C. W. DeKock, G. W. Pepple, and A. Habenschuss, *J. Chem. Eng. Data*, **22**, 58 (1977).
(6) F. H. Spedding, D. C. Rulf, and B. C. Gerstein, *J. Chem. Phys.*, **56**, 1498 (1972).
(7) J. A. Rard, A. Habenschuss, and F. H. Spedding, *J. Chem. Eng. Data*, **22**, 180 (1977).
(8) F. H. Spedding and C. F. Miller, *J. Am. Chem. Soc.*, **74**, 4195 (1952).
(9) F. H. Spedding and J. P. Flynn, *J. Am. Chem. Soc.*, **76**, 1474 (1954).
(10) F. H. Spedding, A. W. Naumann, and R. E. Eberts, *J. Am. Chem. Soc.*, **81**, 23 (1959).
(11) D. A. Csejka and F. H. Spedding, IS-338, unclassified USAEC report, Ames Laboratory, Ames, Iowa, 1960.
(12) D. H. Templeton and C. H. Dauben, *J. Am. Chem. Soc.*, **76**, 5237 (1954).
(13) W. H. Zachariasen in "The Actinide Elements", G. T. Seaborg and J. J. Katz, Ed., McGraw-Hill, New York, N.Y., 1954.
(14) D. D. Wagman, W. H. Evans, V. B. Parker, I. Halow, S. M. Bailey, and R. H. Schumm, *Natl. Bur. Stand. U.S., Tech. Note*, **No. 270-3** (1968).
(15) D. D. Wagman, W. H. Evans, V. B. Parker, I. Halow, S. M. Bailey, and R. H. Schumm, *Natl. Bur. Stand. U.S, Tech. Note*, **No. 270-5** (1971).
(16) R. H. Schumm, D. D. Wagman, S. M. Bailey, W. H. Evans, and V. B. Parker, *Natl. Bur. Stand. U.S., Tech. Note*, **No. 270-7** (1973).
(17) W. Pfeffer, et al., *Z. Phys.*, **154**, 301 (1959); **162**, 358, 413 (1961); **164**, 295 (1961); **168**, 305, 474 (1962).
(18) The crystal entropy of $GdCl_3 \cdot 6H_2O$ in ref 6 is based on heat capacity measurements only above 14 K, and the reported value at 298 K contained an error in the extrapolation of the heat capacity data below this temperature. The correct crystal entropy of 97.1 gibbs mol^{-1} was used in our calculations, B. C. Gerstein, private communication. The standard state solute entropies in ref 6 are in error due to the neglect of the presence of six waters as a product of the solution process.
(19) R. H. Schumm, private communications.
(20) F. H. Spedding, J. L. Derer, M. A. Mohs, and J. A. Rard, *J. Chem. Eng. Data*, **21**, 474 (1976).
(21) J. A. Rard, L. E. Shiers, D. J. Heiser, and F. H. Spedding, *J. Chem. Eng. Data*, accepted for publication.
(22) F. H. Spedding, L. E. Shiers, M. A. Brown, J. L. Derer, D. L. Swanson, and A. Habenschuss, *J. Chem. Eng. Data*, **20**, 81 (1975).
(23) F. H. Spedding, L. E. Shiers, and J. A. Rard, *J. Chem. Eng. Data*, **20**, 66 (1975).
(24) G. A. Krestov, *Sov. Radiochem.*, **5**, 229 (1963).
(25) The ligand field splittings of the ground state are known to change slightly in going from one type of crystal to another, in going from a crystal to a molten salt solution, from molten salt to aqueous solution, etc. Unfortunately, the ligand field splittings of the ground state are not known in detail for all of the rare earth aquo ions.
(26) G. R. Choppin, *Pure Appl. Chem.*, **27**, 23 (1971).
(27) F. H. Spedding, M. J. Pikal, and B. O. Ayers, *J. Phys. Chem.*, **70**, 2440 (1966).
(28) T. Mioduski and S. Siekierski, *J. Inorg. Nucl. Chem.*, **37**, 1647 (1975).
(29) G. Geier and U. Karlen, *Helv. Chim. Acta*, **54**, 135 (1971).
(30) J. Reuben and D. Fiat, *J. Chem. Phys.*, **31**, 4909 (1969).

The Size, Shape, and Hydration of Nonionic Surfactant Micelles. Triton X-100

Robert J. Robson and Edward A. Dennis*

Department of Chemistry, University of California at San Diego, La Jolla, California 92093 *(Received December 15, 1976)*

Publication costs assisted by the National Science Foundation

Calculations of the size, shape, and hydration of micelles composed of the nonionic surfactant Triton X-100 were performed based on molecular weight and intrinsic viscosity data. Geometrical considerations show that if the hydrophobic core as well as the whole micelle is spherical, then its structure cannot contain the distinct polar and apolar regions that are classically assumed for micelles. On the other hand, ellipsoids of revolution would be consistent with a classical micellar structure and an oblate rather than a prolate ellipsoid would be most consistent with intrinsic viscosity measurements and volume calculations.

Triton X-100 is a commercial, polydisperse preparation of *p*-(1,1,3,3-tetramethylbutyl)phenoxypolyoxyethylene glycols, containing an average of 9.5 oxyethylene units per molecule. Knowledge of the size, shape, and hydration of micelles of this surfactant is important in interpreting previous ^1H and ^{13}C NMR studies on the structure of Triton X-100 micelles.[1-3] The molecular weight of Triton X-100 micelles in aqueous solution was first determined in 1954 by Kushner and Hubbard[4] using light scattering techniques, and has since been measured many times. A summary of the reported values for the molecular weight of Triton X-100 is given in Table I.

While a number of calculations have been made, the size, shape, and hydration of Triton X-100 micelles remains unresolved. For example, the correlation of micellar molecular weight measurements with hydrodynamic measurements such as intrinsic viscosity can provide an estimate of the limits of shape and hydration. However, shape and hydration cannot be separated easily. The Triton X-100 micelle is considered by many[4,11,13] to be spherical and with sufficient bound water to fit the intrinsic viscosity measurements (summarized in Table II). Wright[14] has recently suggested, using transient electric birefringence techniques, that the Triton X-100 micelle may not be spherical. Unfortunately, supporting data are lacking.[14]

This note will attempt to show on the basis of purely geometrical considerations that, if the micelle is indeed spherical, then several oxyethylene groups must be imbedded in the hydrophobic core, and if this does not occur then the hydrophobic core as well as the whole Triton X-100 micelle cannot be spherical. If the micelle is not spherical, then an ellipsoid of revolution is a likely candidate for the micelle shape, with an oblate micelle being a better choice than a prolate micelle.

Hydrophobic Region

Let us consider first the hydrophobic region. If the average micellar molecular weight is 90 000, and the average molecular weight per monomer is 628, the aggregation number is 143. Tanford[15] has discussed the fact that the radius of the hydrophobic core of a spherical micelle may not exceed the maximum length of the hydrocarbon chain, and indeed may even be shorter. We will consider the hydrophobic region to consist of the entire octylphenyl group, which should have a density of approximately 0.87 g/cm^3 based on densities of similar molecules and assuming that the hydrophobic interior resembles a droplet of liquid hydrocarbon. From this, one can calculate the volume of the hydrophobic group to be 363 Å^3. The total volume of the hydrophobic region is then 143 monomers x 363 Å^3/monomer = 51 900 Å^3. This would correspond to a sphere of radius 23 Å. Clearly this is too large, since, from Corey–Pauling–Koltung models, the length of the octylphenyl group is less than 10 Å. Assuming a length of 10 Å, volume calculations can be made for prolate and oblate ellipsoids.

For a prolate ellipsoid, the radius of a sphere of equal volume is $(ab^2)^{1/3}$ where a is the semiaxis of the long dimension and b is the semiaxis of the short dimension. Therefore, in assuming b = 10 Å, one can calculate a to be 123 Å. Similarly, for an oblate ellipsoid, the radius of a sphere of equal volume is $(a^2b)^{1/3}$. Here, with b assumed to be 10 Å, a would be 35 Å. These two models for the hydrophobic core are shown in Figure 1.

Hydrophilic Region

Now let us consider the effect of the oxyethylene chain on the micelle size and shape. The conformation of the oxyethylene chain in Triton X-100 micelles is not known. At the extremes, the chain might be fully extended, sometimes called the zig-zag conformation,[16,17] which would add about 34 Å for 9.5 oxyethylene units, or it might form a random coil[18] (adding about 16 Å).[19] A third conformation which has been suggested for the oxyethylene chain is the meander conformation.[16] This would add about 17 Å for 9.5 oxyethylene units.[25]

For simplicity, we will use a value of 17 Å for the average length of the oxyethylene chain. Micelle sizes and shapes can be calculated using the dimensions of the prolate and oblate hydrophobic regions. For example, the semiaxis b of the prolate micelle will be 10 Å for the hydrophobic region plus 17 Å for the oxyethylene chain, giving 27 Å. Similarily, the semiaxis a will be 123 Å plus 17 Å giving 140 Å. The calculations for both the prolate and oblate models are summarized in Table III, along with the axial ratios and volumes assuming a solid ellipsoid. Figure 2 shows the two micelle models schematically.

From the axial ratios of the prolate and oblate ellipsoids, the viscosity factors of Simha[26] can be calculated. For the prolate ellipsoid model, ν = 6.1, and for the oblate ellipsoid model, ν = 2.8. An average value of about 5.3 cm^3/g for the intrinsic viscosity $[\eta]$ has been calculated from hydrodynamic measurements (Table II). The difference between the measured intrinsic viscosity $[\eta]$ and Simha's viscosity factor ν can be attributed to hydration of the ellipsoids by the following equation:

$$[\eta] = \nu(\bar{v} + \delta v_0)$$

where $\bar{v}_0$ is the partial specific volume of the solvent (1.0), $\bar{v}$ is the partial specific volume of Triton X-100 (0.91),[11,27] and δ = H_2O/surfactant (g/g). For the oblate ellipsoid,

TABLE I: Molecular Weight of Triton X-100 Micelles

Technique	Temp, °C	Additives	Mol wt	Aggr no.	Ref
Light scattering	Room temp		90 000	140	4
		40 mM NaCl	90 000	140	4
		120 mM NaCl	90 000	140	4
Light scattering	25		66 700	111	5
Light scattering	25		81 300	135	6
Ultracentrifugation	25		63 100	100	7
Light scattering	30		105 000		8
		500 mM NaCl	150 000		8
		500 mM $CaCl_2$	153 000		8
Light scattering	25		73 500		9
Ultracentrifugation	20	50 mM Tris, pH 8	97 300		10
Ultracentrifugation	20	100 mM NaOAc, pH 5	86 000	134	11
Ultracentrifugation	25	10 mM $NaHPO_4$, pH 7	81 250		12
Light scattering	20		93 000		13
	25		98 000		13
	30		113 000		13

TABLE II: Intrinsic Viscosity of Triton X-100 Micelles

Temp, °C	$[\eta]$, cm^3/g	Ref
Room temp	5.5	4
20	5.5	11
20	4.7	13
30	5.2	13

TABLE III: Physical Parameters for Prolate and Oblate Micelle Models

Property	Micelle model: Prolate	Micelle model: Oblate
Semiaxes, Å a	140	52
b	27	27
a/b	5.2	1.9
V, $Å^3$	428 000	306 000
H_2O/surfactant (g/g) calcd for $[\eta] = 5.3$	−0.1	1.0
H_2O/surfactant (g/g) calcd for V ($Å^3$) above	1.9	1.1

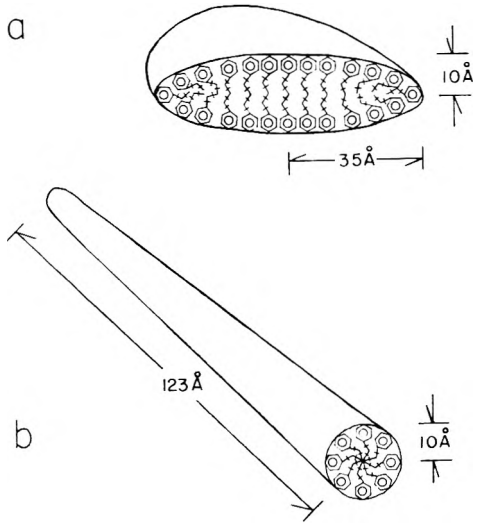

Figure 1. Cutaway views of the hydrophobic core of the (a) oblate and (b) prolate micelle model showing one-half of the core.

δ is 1.0 g/g (H_2O/surfactant), and δ for the prolate ellipsoid is −0.1 g/g (H_2O/surfactant)—clearly an impossible value.

The amount of entrapped water can also be calculated from volume considerations. The difference in the volume of the oblate ellipsoid (if it were solid) and the volume occupied by the detergent per micelle gives a volume that theoretically could be filled with water. The volume occupied by the 143 detergent monomers is 143 000 $Å^3$, thus leaving a 163 000 $Å^3$ excess. From the macroscopic density of water one can calculate that this volume could

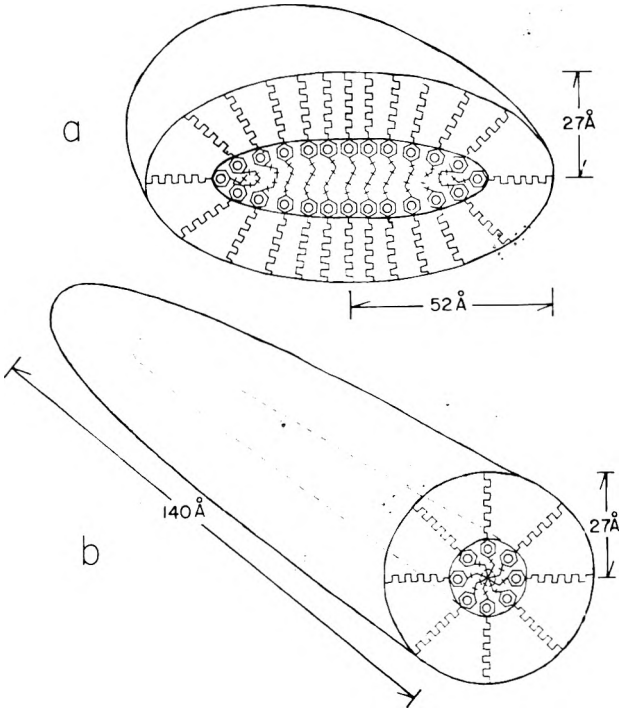

Figure 2. Cutaway views of the (a) oblate and (b) prolate micelle model showing one-half of the micelle.

contain 5400 water molecules, or 1.1 g/g (H_2O/surfactant). In the same manner, for the prolate micelle, volume considerations show an "excess" volume in the micelle sufficient to accommodate 1.9 g/g (H_2O/surfactant).

Comparison of Oblate and Prolate Ellipsoid

Table III summarizes the values of entrapped water calculated from the volume differences and from the intrinsic viscosity measurements. For an oblate ellipsoid, both calculations suggest that about 1 g of H_2O is entrapped per gram of surfactant, whereas the calculations for a prolate ellipsoid give widely divergent results.

The use of 16 or 34 Å for the length of the oxyethylene chains does not qualitatively change our results. Using 16 Å, the prolate micelle needs −0.1 g/g (H_2O/surfactant) to fit the measured $[\eta]$, compared with 1.7 g/g (H_2O/surfactant) to fit volume calculations; for the oblate model the numbers are 1.0 and 0.9 g/g, respectively. Using 34 Å, the prolate model requires 0.3 g/g (H_2O/surfactant) to fit $[\eta]$ and 7.5 g/g (H_2O/surfactant) to fit volume calculations; for the oblate model, the micelle requires 1.1 and 4.9 g/g, respectively. Thus the calculation of g/g (H_2O/surfactant) to fit the volume for the oblate ellipsoid be-

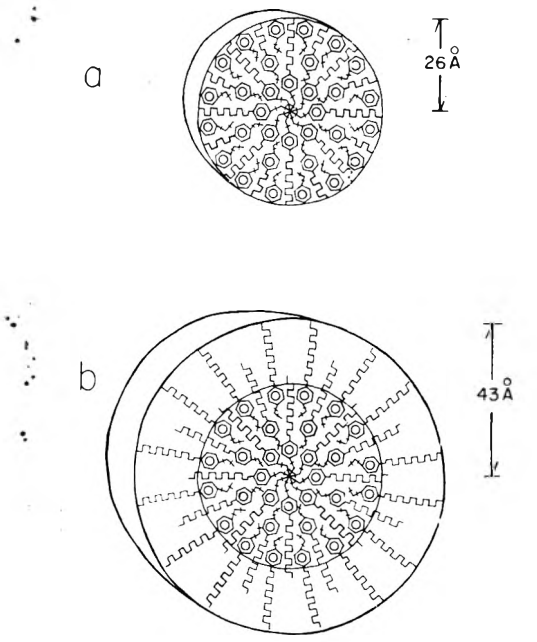

Figure 3. A schematic diagram of one-half of the (a) hydrophobic core and (b) whole micelle for the spherical micelle model for Triton X-100 is shown. It is not possible to precisely calculate the arrangement of groups in this model because one does not have the limits imposed by a distinct hydrophobic/hydrophilic boundary. For the purpose of this diagram, however, it is assumed that the center of the core consists of that number of octylphenyl groups which would fill a sphere of radius 10 Å based on volume/density calculations, plus additional octylphenyl groups arranged radially from this sphere. This model necessitates that additional oxyethylene groups be present in the core region, contributing an additional volume to it, and extending its radius somewhat beyond 23 Å. This picture therefore shows 12 Triton monomers in the center of the hydrophobic core, with their oxyethylene groups extending outward through the core, and the remainder of the Triton molecules having less of their oxyethylene chains imbedded in the core. It is assumed for this diagram that the average length of the oxyethylene chains is 17 Å as in the preceding models; if a fully extended model is assumed, fewer oxyethylene units would be present in the hydrophobic core. For the whole micelle, it is assumed that the hydrophilic region extends one oxyethylene chain length (17 Å) beyond the hydrophobic core making the radius of the whole micelle about 43 Å; this size for a spherical micelle is consistent with the intrinsic viscosity data and volume calculations if 1.2 g/g (H_2O/surfactant) is added.

comes quite large at large chain extensions, but not as unreasonably large as the same calculation for the prolate micelle.

In summary, if the hydrophobic region is restricted to a short dimension of the core equal to the length of the hydrophobic group, one finds that the hydrophobic core and probably the entire Triton X-100 micelle cannot be spherical. The main difficulty in interpreting intrinsic viscosity measurements is the inseparability of shape and hydration. However, using the geometrical considerations described here for the hydrophobic region and a reasonable, although necessarily arbitrary, length for the oxyethylene chains, one finds the oblate micelle a much more reasonable shape than the prolate micelle for two reasons: (1) The oblate micelle is sufficiently symmetric so that some H_2O can be added to fit measured $[\eta]$, and some hydration of the oxyethylene chain is expected, and (2) volume calculations show that the physical space around the oxyethylene chains correlates well with the water needed to fit $[\eta]$. It should be noted that Tanford[15] has also come to the conclusion that oblate ellipsoids are preferred over prolate ellipsoids for several other surfactants. While these calculations suggest that an oblate ellipsoid would be the most reasonable model for both the hydrophobic core and the total micelle, it should be noted that the polydispersity of the oxyethylene chains could result in a nonuniform distribution of oxyethylene groups around the micelle, allowing the overall shape to be closer to spherical than the average calculations suggest.

Spherical Micelle Model

The possibility must also be considered that a sharp boundary does not exist between the hydrophobic interior and the oxyethylene chains, in contradiction to the classical picture of micelles.[15] If the first few oxyethylene groups at the octylphenyl end of some Triton X-100 molecules were contained in the hydrophobic core, it would be possible to accommodate a spherical model for the hydrophobic region as well as the total micelle. The core would have to have a radius of about 23 Å to accommodate the volume of the octylphenyl moieties, plus an added radius to allow for the volume contributed by the added oxyethylene units (a few angstroms), making a rather large hydrophobic core. A schematic diagram of one possible arrangement according to this model is shown in Figure 3. Thus, a spherical micelle would be possible only if several oxyethylene chains were imbedded in the hydrophobic core, and any proposals for a spherical micelle for Triton X-100 must explicitly state that the micelle does not have the classically distinct regions composed of only polar or apolar groups.

Acknowledgment. We wish to thank Professors Charles Tanford and Karol Mysels for critically reading this manuscript, and Professor Aksel Bothner-By for pointing out the reasonableness of the nonclassical micelle model. This work was supported by Grants BMS 75-03560 and PCM 76-21552 from the National Science Foundation.

References and Notes

(1) A. A. Ribeiro and E. A. Dennis, *Biochemistry*, **14**, 3746 (1975).
(2) A. A. Ribeiro and E. A. Dennis, *J. Phys. Chem.*, **80**, 1746 (1976).
(3) E. A. Dennis and A. A. Ribeiro, *ACS Symp. Ser.*, **No. 34**, 453 (1976).
(4) L. M. Kushner and W. D. Hubbard, *J. Phys. Chem.*, **58**, 1163 (1954).
(5) A. M. Mankowich, *J. Phys. Chem.*, **58**, 1027 (1954).
(6) A. M. Mankowich, *Ind. Eng. Chem.*, **47**, 2175 (1955).
(7) C. J. Dwiggins, Jr., R. J. Bolen, and H. N. Dunning, *J. Phys. Chem.*, **64**, 1175 (1960).
(8) K. Kuriyama, *Kolloid. Z.*, **181**, 144 (1962).
(9) A. M. Mankowich, *J. Am. Oil Chem. Soc.*, **41**, 449 (1964).
(10) J. S. Kahn and I. C. Chang, *Photochem. Photobiol.*, **4**, 733 (1965).
(11) S. Yedgar, Y. Barenholz, and V. G. Cooper, *Biochem. Biophys. Acta*, **363**, 98 (1974).
(12) C. J. Biaselle and D. B. Millar, *Biophys. Chem.*, **3**, 355 (1975).
(13) M. Corti and V. Degiorgio, *Opt. Commun.*, **14**, 358 (1975).
(14) A. K. Wright, *J. Colloid Interface Sci.*, **55**, 109 (1976).
(15) C. Tanford, "The Hydrophobic Effect: Formation of Micelles and Biological Membranes", Wiley, New York, N.Y., 1973, pp 74–78; *J. Phys. Chem.*, **78**, 2469 (1974).
(16) M. Rosch in "Nonionic Surfactants, Surfactant Science Series", Vol. 1, M. J. Schick, Ed., Marcel Dekker, New York, N.Y., 1967, pp 753–792.
(17) The length of the zig-zag (fully extended) chain was calculated by multiplying the oxyethylene number (9.5) by the length of one oxyethylene unit, 3.6 Å, obtained from CPK models.
(18) P. J. Flory, "Principles of Polymer Chemistry", Cornell University Press, Ithaca, N.Y., 1953, pp 399–430.
(19) The length of the random coil was taken as $2R_G$ where R_G is the radius of gyration defined by

$$R_G^2 = h_{av}^2/6$$

where h_{av} is the root-mean-square end-to-end distance for polyoxyethylene chains. Values for h_{av} were obtained from the Flory–Fox[20] equation

$$[\eta] = \Phi(h_{av})^{3/2}/M$$

using measured values of the intrinsic viscosity for short chain polyoxyethylenes, $\Phi = 2.1 \times 10^{21}$, and M as the molecular weight of an oxyethylene chain of 9.5 units. An average value of $[\eta]$ (0.0360 dL/g) from three laboratories was used.[21-23] h_{av} was calculated to be 19.3 Å, and $2R_G$ to be 16 Å. It should be noted that for low molecular weight oxyethylene chains, the assumptions in the Flory–Fox theory should not apply[24] since the ratio of h_{av} to the degree of

polymerization has not yet attained its asympotic value. Bailey and Koleske[24] note that the short chain cannot be considered as an impermeable coil, and since the chain is not very large compared to the solvent molecules, one cannot regard the solvent as a structureless continuum. Therefore the random coil calculation must be regarded as highly approximate.
(20) P. J. Flory and T. G. Fox, Jr., *J. Am. Chem. Soc.*, **73**, 1904 (1951).
(21) C. Sadron and P. Rempp, *J. Polym. Sci.*, **29**, 127 (1958).
(22) J. A. Faucher and R. W. Callard, unpublished studies cited by F. E. Bailey, Jr., and J. V. Koleske in "Nonionic Surfactants, Surfactant Science Series", Vol. 1, M. J. Schick, Ed., Marcel Dekker, New York, N.Y., 1967, pp 794–822.
(23) C. Rossi and C. Cuniberti, *Polym. Lett.*, **2**, 681 (1964).
(24) F. E. Bailey, Jr., and J. V. Koleske, "Poly(ethylene oxide)", Academic Press, New York, N.Y., 1976, pp 29–86.
(25) The length of the meander chain was calculated by multiplying the oxyethylene number by the length of one oxyethylene unit, 1.8 Å.
(26) R. Simha, *J. Phys. Chem.*, **44**, 25 (1940).
(27) C. Tanford, Y. Nozaki, J. A. Reynolds, and S. Makino, *Biochemistry*, **3**, 2369 (1974).

Heats and Entropies of Adsorption of Sulfur Dioxide at Low Surface Coverages on Chrysotile Asbestos at 323 K

William J. Murphy and Robert A. Ross*

Department of Chemistry, Lakehead University, Thunder Bay, Ontario, Canada P7B 5E1 *(Received October 19, 1976)*

The adsorption of sulfur dioxide at 323 K has been studied on chrysotile asbestos by measurement of adsorption/desorption isotherms and calorimetric heats of adsorption. The effects of heat treatment at 150, 300, 500 and 700 °C were determined on two series of chrysotile samples. One series was chosen to evaluate the effect of the presence of brucite, $Mg(OH)_2$, on the adsorption characteristics, Quebec chrysotiles, in contrast with the behavior of samples in the absence of brucite, Californian chrysotiles. The overall range of heats of adsorption values varied from ~100 to 11.5 kcal mol^{-1}. In the absence of brucite, two distinctive surfaces seem to form on activation, one between 150 and 300 °C and the other from 500 to 700 °C. Surfaces formed in the lower temperature range probably retain sulfur dioxide through hydrogen bond formation within and without the hollow fiber centers of the dissociated fiber conglomerates. On 700 °C surfaces adsorbate/adsorbent interaction between surface oxygen bridge bonds and sulfur dioxide facilitates chemisorption perhaps through surface sulfite formation. The presence of brucite has a substantial effect on the adsorption parameters and this has been related to the perturbation influences of this material on the chrysotile crystal structure. Entropy coverage curves, θ = 0.03 to 0.5, have been calculated to assess and contrast the mobilities of the adsorbed molecular layers in the two series of chrysotiles.

Introduction

Studies on the adsorption of sulfur-containing gases on porous materials are not only of intrinsic interest but also have direct value in the development of surface chemical processes concerned with the removal of known gaseous air pollutants. Through recent publications we have reported values of both heats and entropies of adsorption for sulfur dioxide on a wide range of materials including γ-Al_2O_3[1] and activated charcoal.[2]

The present study has extended the work to an examination of the sorption of sulfur dioxide at 323 K on chrysotile asbestos minerals which had been activated at 150, 300, 500, and 700 °C. These minerals, as particulate matter, are also associated with environmental health hazards.[2]

Two types of naturally occurring chrysotile minerals, of differing physical and chemical properties, were chosen for the study. The presence of brucite ($Mg(OH)_2$) in a series of samples was regarded as a particularly important feature since it has a profound effect on the structural changes of chrysotile[3] on heating and would be expected to influence the adsorptive properties of these materials. Further, since synergetic phenomena have been reported to exist between tobacco smoke and asbestos in health studies,[4,5] the present study may have some value in the assessment of possible synergetic relationships between sulfur dioxide and asbestos—probably the two best documented atmospheric pollutants.

Experimental Section

Materials. Chrysotile samples were supplied by (a) Lake Asbestos, Black Lake, Quebec (sample 7T/5, Quebec chrysotile) and (b) Union Carbide Corp. (Calidria asbestos sample HPO, Californian chrysotile). The major impurities were brucite ($Mg(OH)_2$), 10% in sample a and magnetite (Fe_3O_4), 3.75% in sample a; 0.75% in sample b.

The sulfur dioxide (Matheson of Canada, anhydrous grade, >99.98% pure) was drawn directly from the cylinder after line flushing to a trap attached to the apparatus. It was then outgassed at 10^{-4} Torr and vacuum distilled over trays of phosphorus pentoxide. This purification procedure was repeated at least six times. Middle portions only were used and GLC analyses showed these to be greater than 99.999% pure.

Activation conditions for all samples treated at 150, 300, 500, and 700 °C were 24 h in air. Surface areas of all samples were determined from nitrogen adsorption/desorption isotherms at 77 K.[6]

Apparatus and Procedure. Calorimetric heats of adsorption were determined in a vessel similar to that described by Robinson and Ross.[7] The calorimeter was operated in the adiabatic mode and the heat measurement conditions were adapted from those used by Smith and Ford[8] as recently reported.[3] Entropies of adsorption were calculated from classical thermodynamic equations.[9,10]

Results

The adsorption/desorption isotherms of sulfur dioxide at 323 K on both chrysotile samples which had been activated at 150, 300, 500, and 700 °C are shown in Figures 1 and 2, which show that, in general, Californian chrysotile activated at a given temperature exhibited larger adsorption capacities than Quebec chrysotile activated at the same temperature. Further, Figures 1 and 2 show that

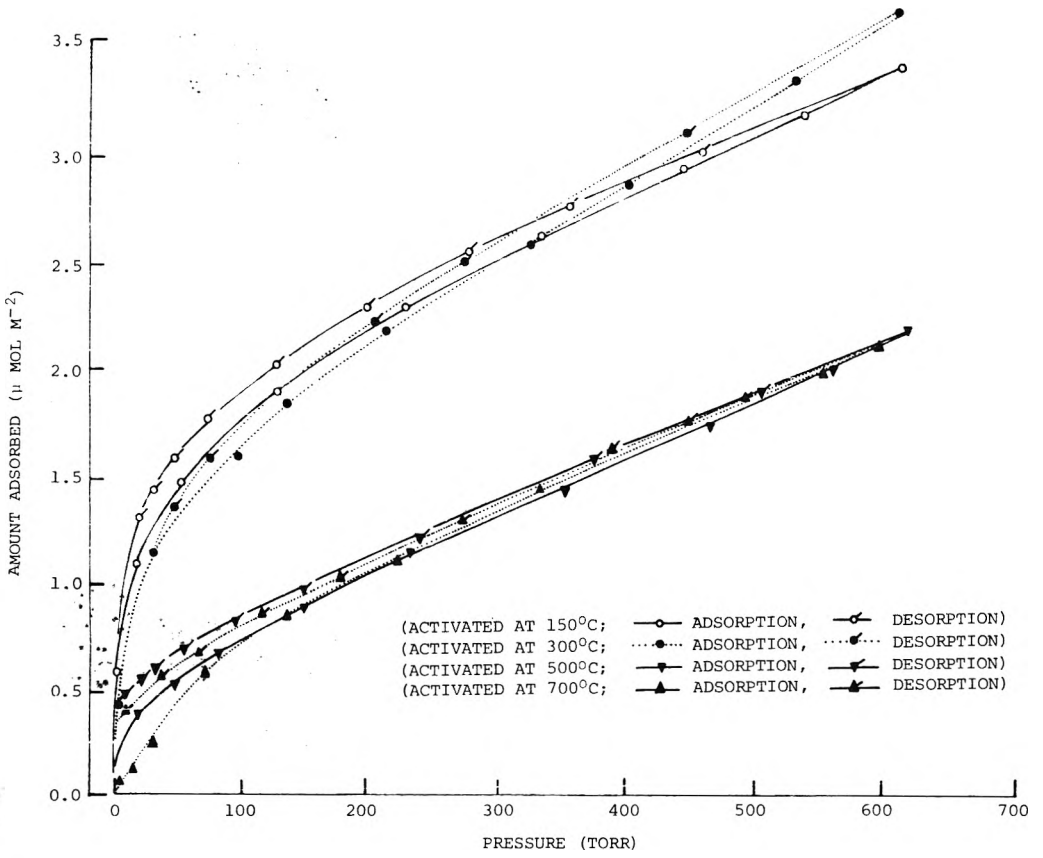

Figure 1. Adsorption/desorption isotherms for sulfur dioxide on activated Californian chrysotile at 323 K.

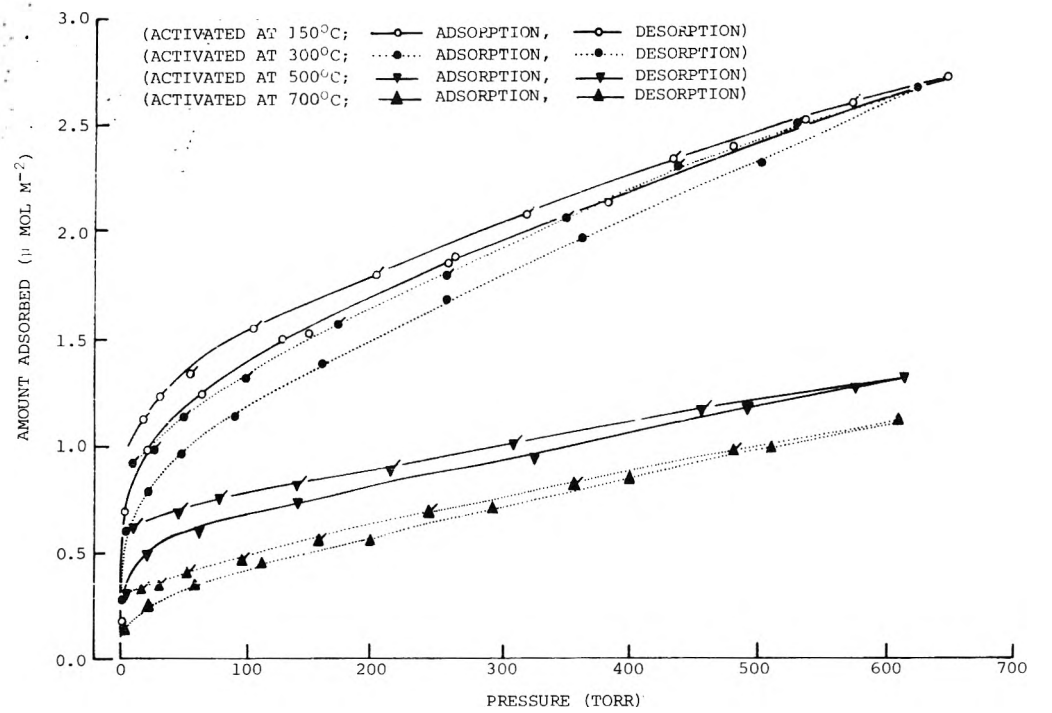

Figure 2. Adsorption/desorption isotherms for sulfur dioxide on activated Quebec chrysotile at 323 K.

Californian chrysotile exhibited less hysteresis than Quebec chrysotile at the various temperatures. Figure 1 also indicates that on heating Californian samples from 150 to 300 °C, the extent of adsorption at lower pressures of sulfur dioxide (<350 Torr) decreased, whereas the adsorption capacity at 600 Torr increased. Further increase in activation temperature from 300 to 500 °C resulted in an overall decrease in the amount of sulfur dioxide adsorbed over the total pressure range while the extension of heat treatment to 700 °C produced no further change in the amount adsorbed. The adsorption/desorption isotherms, for sulfur dioxide on the Quebec chrysotile series, Figure 2, show that increasing the activation temperature from 150 to 300 °C resulted in a decrease in the extent of adsorption at lower pressures (<250 Torr). A further increase in activation temperature to 700 °C produced an overall decrease in the extent of adsorption over the complete pressure range.

The heats of adsorption of sulfur dioxide at 323 K on both chrysotile samples, activated at 150, 300, 500, and 700

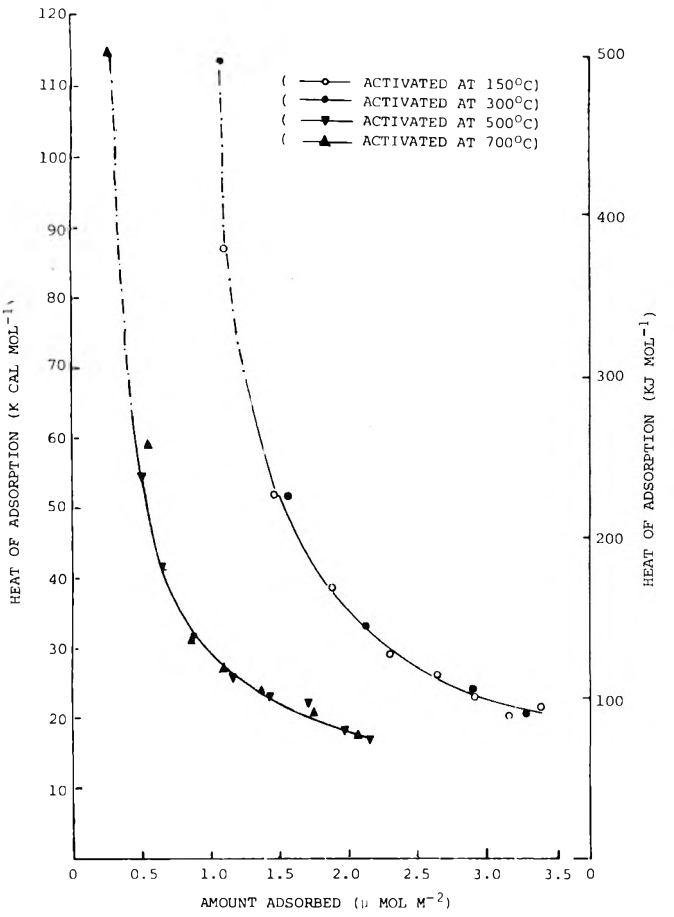

Figure 3. Variation of the heats of adsorption of sulfur dioxide with amount adsorbed on Californian chrysotile at 323 K.

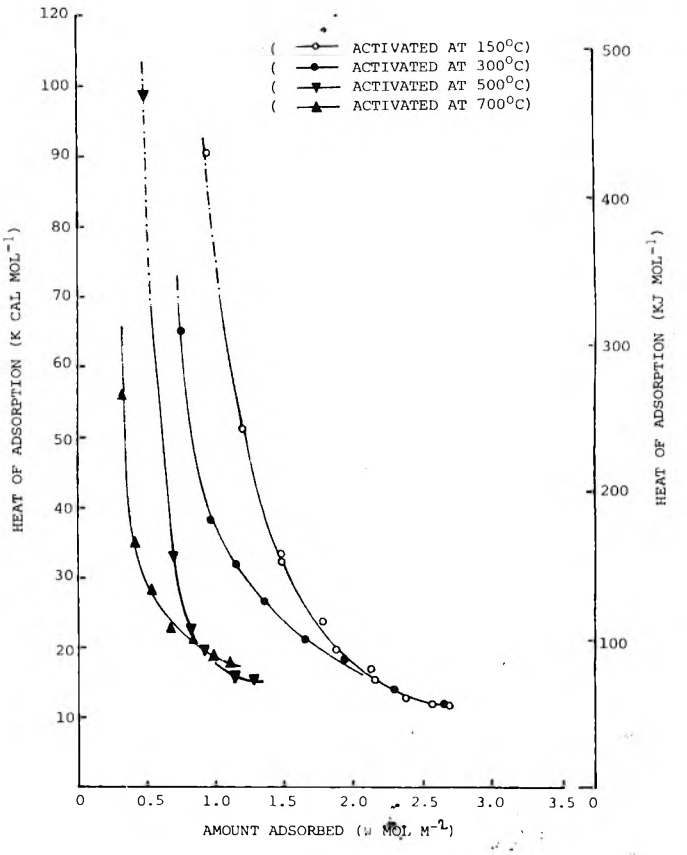

Figure 4. Variation of the heats of adsorption of sulfur dioxide with amount adsorbed on Quebec chrysotile at 323 K.

°C, are shown in Figures 3 and 4. All adsorbents exhibited very high heats of adsorption at low coverages which fell sharply with increasing coverage to a "limiting value". The initial heats of adsorption were of the same order for all adsorbents whereas the "limiting values" were found to differ considerably depending both on chrysotile type and activation temperature.

Figure 3 shows that, on activating Californian chrysotile from 150 to 700 °C, two distinct heats of adsorption vs. coverage profiles result in "high" (500–700 °C) and "low" (150–300 °C) activation temperature regions.

Progressive activation of Quebec chrysotile from 150 to 700 °C resulted in an overall increase in the limiting value of the heats of adsorption from 11.5 (150 and 300 °C) to ~18.0 kcal mol^{-1} (700 °C), Figure 4. Increasing the temperature of activation also had the effect of increasing the rate at which the heats of adsorption of sulfur dioxide on Quebec chrysotile decreased with increase in coverage.

Figure 5 shows the plots of the experimental differential molar entropies vs. coverage for the Californian samples together with the theoretical entropy for an immobile film. Entropy data obtained for the Quebec samples were slightly more sensitive to activation temperature as might be anticipated from Figure 4, otherwise similar trends were apparent. The entropies of adsorption for sulfur dioxide on all the adsorbents increased from values very much below the configuration entropy to a limiting value on or slightly above that of an immobile layer.

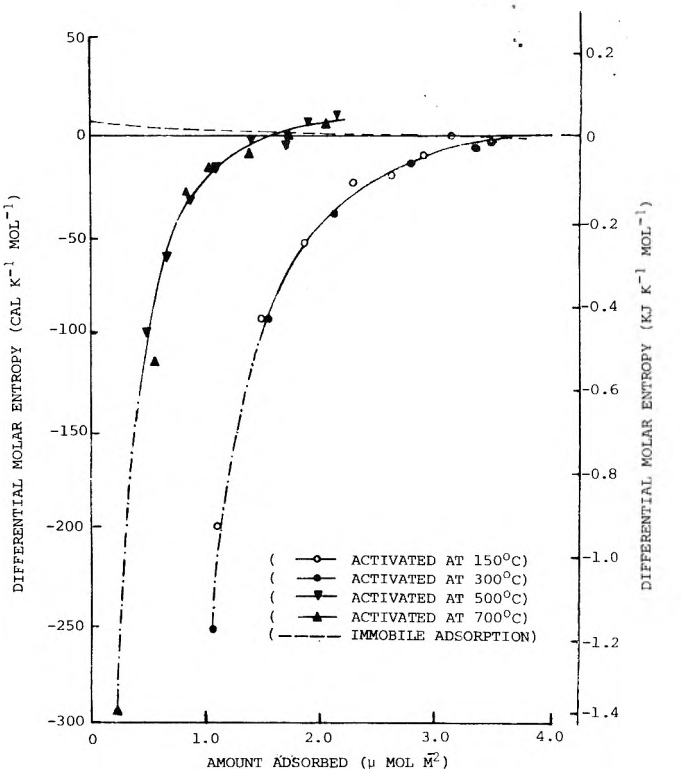

Figure 5. Differential molar entropies of adsorption for sulfur dioxide on Californian chrysotile at 323 K.

Discussion

Californian Chrysotile. The amounts of sulfur dioxide adsorbed on Californian chrysotile increased with activation between 150 and 300 °C and then decreased with the extension of heat treatment to 700 °C, Figure 1. Further, Figure 3 indicates that two distinctive surfaces were produced on activation, one at lower temperatures (150–300 °C) and the other at higher temperatures (500–700 °C).

Current literature on the thermal degradation of chrysotile in general[11,12] and of Californian chrysotile in

particular[6] indicates that, as the activation temperature is increased, there is a decrease in the total water content of 1% w/w from 150 to 300 °C and 12% w/w from 300 to 700 °C. The main dehydration (~500 to 600 °C) has been associated with the disruption of the external layer of chrysotile[11] and the elimination of six hydroxyl groups, see eq 1, while the remaining water loss, both above and

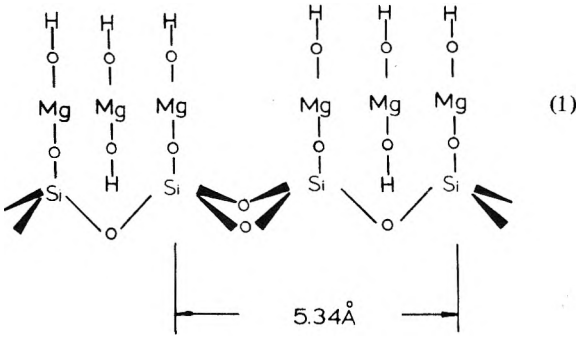

(1)

below the main dehydration temperature range, has been linked to the removal of the remaining hydroxyl groups from the subsurface layers.

These results suggest that the amount of sulfur dioxide adsorbed on Californian chrysotile is dependent on the surface hydroxyl group content and that perhaps hydrogen bonds may be formed between the adsorbate and adsorbent.

However, the slight but significant increase in the adsorption capacity at 610 Torr, from 3.40 to 3.65 μmol m^{-2}, for the 150 and 300 °C surfaces, respectively (Figure 1), may indicate that perhaps more than one effect has occurred. Recently, we showed that increasing the temperature of activation from 150 to 300 °C produces (a) a dissociation of fiber conglomerates into more discrete fibers resulting in the exposure of more hydroxyl groups to the adsorbate per unit area of surface and (b) an increase in the percentage of smaller pores (<25 Å radius) which may be related to the removal of water plugs from, for example, the hollow fiber centers. A combination of both effects could explain the observed phenomena, namely, a slight increase in the extent of adsorption at pressures above 350 Torr and a decrease in adsorption below this datum.

The desorption isotherms for sulfur dioxide on the various Californian samples show that the adsorption was reversible on 150 and 300 °C surfaces whereas some irreversible behavior indicative of chemisorption was detected on the surfaces activated at higher temperatures.

The magnitudes of the heats of adsorption at low surface coverages on all the Californian chrysotiles, Figure 3, also indicates that chemical forces are involved in the adsorbate–adsorbent interactions. At the same time the limiting values of the heats of adsorption on both "low" and "high" temperature surfaces, 22 and 16 kcal mol^{-1}, respectively, are very high for purely physical interactions since the heat of liquefaction of sulfur dioxide at 323 K is ~4.75 kcal mol^{-1}.[6]

Previously, it has been shown that the heat of formation of one hydrogen bond is of the order of 3–6 kcal mol^{-1} [13] and this, together with the extent of adsorption reversibility, would indicate that as many as three or four hydrogen bonds per adsorbate molecule may be formed. The formation of multiple bonds between sulfur dioxide and suitably spaced surface hydroxyl groups would be favorable since the O–O distance in the sulfur dioxide molecule is of the order of 2.5 Å[14] which compares favorably with the cell parameters for chrysotile (eq 1).

The decrease in the limiting value of the heats of adsorption, Figure 3, with increase in activation temperature would be consistent with a decrease in the number of available adsorption sites, that is, hydroxyl groups, and hence a decrease in the probability of multiple bond formation. However, Figure 1 shows that, as the activation temperature was increased to 500 and 700 °C, the adsorption of sulfur dioxide was more irreversible at low pressures indicating that the removal of hydroxyls from the surface facilitates stronger interaction, to the extent of chemisorption, between adsorbate and adsorbent. An explanation of this irreversibility could be found in the creation of oxygen bridge bonds on dehydration followed by surface sulfite formation, thus:

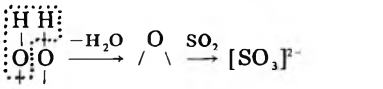

(2)

Tests to confirm the presence of microquantities of sulfite, in both chrysotile series, proved to be inconclusive although sulfite formation under similar experimental conditions in the magnesium oxide–sulfur dioxide system has been reported.[15]

Figure 5 shows that the experimental differential entropy increased with surface coverage from a value much below the level expected for immobile adsorption (i.e., adsorption in which only one degree of freedom is left to the adsorbed molecule[9]) to a value which coincided with the model for immobile adsorption for the low activation temperature surfaces and which was slightly greater than the immobile adsorption model for the 500 and 700 °C surfaces. These observations are consistent with (a) chemisorption interactions at low coverages ($\theta < 0.1$) for all activation ranges and (b) multipoint adsorption which would have the effect of reducing the mobility of the adsorbate.

Quebec Chrysotile. The adsorption isotherms for sulfur dioxide on Quebec chrysotile, in general, were similar to those for Californian samples, Figure 2. However, irreversibility was more pronounced and hysteresis more evident.

The variations of the heats of adsorption with surface coverage, Figure 4, were quite different to those observed with Californian samples. Thus, in particular, the heat curves for the Quebec samples differed with the surface activation temperature.

It has been noted recently[6] that the presence of brucite, $Mg(OH)_2$, in the Quebec material stabilizes the chrysotile structure to thermal degradation. Brucite is destabilized in the process. Magnesium oxide is formed and it may be postulated that it causes a perturbation of the donor–acceptor region equilibrium in the Taylor–Ball or Brindley–Hayami mechanisms[16–18] for chrysotile dehydration by acting as a sink for migratory protons and upsetting the balance of cation migration between the donor–acceptor regions, eq 3. Both of these regions are

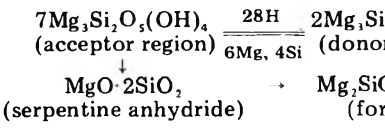

(3)

necessary for dehydration.

The result of brucite dehydration may be exemplified in Figure 4 as the decrease in the heats of adsorption of sulfur dioxide on Quebec chrysotile at low coverages are believed to be due to a decrease in the numbers of labile hydroxyl group sites associated with brucite. The heat curve for Quebec chrysotile activated at 300 °C, Figure 4, merges with that for the 150 °C sample at higher coverages, indicating that the same sites are responsible for adsorption at higher coverages for both these adsorbents,

consistent with the observation that the chrysotile surface matrix was unchanged from 150 to 300 °C.

The heats of adsorption at a given coverage decreased further with the 500 °C surface indicating a continued decrease in the availability of surface hydroxyl groups, Figure 4. This figure also shows that, as the activation temperature was increased to 500 and then to 700 °C, the limiting heat of adsorption rose to 15 and ~18 kcal mol^{-1}, respectively, consistent with a decrease in the stabilizing effect of magnesium oxide on the chrysotile surface hydroxyl groups.

The behavior of the 500 and 700 °C Quebec chrysotile surfaces can be related to the results of structural studies earlier[6] which showed that this material on activation at 500 °C retained a large degree of the chrysotile crystal structure whereas Californian chrysotile activated at this temperature had entered an "x-ray amorphous phase"[18] where dehydration to serpentine anhydride took place. At 700 °C both Californian and Quebec chrysotiles dehydrated to forsterite.

We conclude that sulfur dioxide is both chemically and physically adsorbed on chrysotile asbestos samples which have been activated up to 700 °C, whether brucite is present or not. The very high adsorption heats and low entropy values indicate that sulfur dioxide could compete favorably for surface adsorption sites on these asbestos materials with, for example, water which has been shown to be adsorbed reversibly.[19]

References and Notes

(1) R. W. Glass and R. A. Ross, *Can. J. Chem.*, **50**, 2451 (1972).
(2) J. R. Kramer, O. Mudroch, and S. Tihor, "Asbestos in the Environment", Report to Environment Canada, May 1974.
(3) W. J. Murphy, R. A. Ross, and R. W. Glass, *Ind. Eng. Chem., Prod. Res. Develop.*, **16**, 69 (1977).
(4) E. C. Hammond and I. J. Selikoff in "Biological Effects of Asbestos", Proceedings of Working Conference at the I.A.R.C., Lyon, France, 1973, p 312.
(5) I. J. Selikoff, E. C. Hammond, and J. Cheng, *J. Am. Med. Assoc.*, **204** (2), 104 (1968).
(6) W. J. Murphy and R. A. Ross, *Clays Clay Miner.*, in press.
(7) E. Robinson and R. A. Ross, *J. Chem. Soc. A*, 2521 (1969).
(8) W. R. Smith and D. G. Ford, *J. Phys. Chem.*, **69**, 3587 (1965).
(9) C. Kemball, *Adv. Catal.*, **2**, 233 (1950).
(10) R. W. Glass and R. A. Ross, *J. Phys. Chem.*, **77**, 2571 (1973).
(11) A. A. Hodgson, "Fibrous Silicates", Royal Institute of Chemistry, Lecture Ser. No. 4, 1965.
(12) B. S. Girgis, *Trans. J. Br. Ceram. Soc.*, **74** (4), 135 (1975).
(13) A. V. Kiselev and V. I. Lygin, "Infrared Spectra of Adsorbed Species", L. H. Little, Ed., Academic Press, New York, N.Y., 1966.
(14) R. W. Glass and R. A. Ross, *Can. J. Chem.*, **49**, 2832 (1971).
(15) R. W. Glass and R. A. Ross, *Can. J. Chem.*, **50**, 2817 (1972).
(16) M. C. Ball and H. F. W. Taylor, *Mineral. Mag.*, **32**, 754 (1961).
(17) M. C. Ball and H. F. W. Taylor, *Mineral. Mag.*, **33**, 467 (1963).
(18) G. W. Brindley and R. Hayami, *Mineral. Mag.*, **35**, 189 (1965).
(19) G. J. Young and F. H. Healey, *J. Phys. Chem.*, **58**, 881 (1954).

Temperature Dependence of the Phosphorescence Lifetimes of Benzene–Chloroform Complexes

William Moehle[†] and Martin Vala*

Department of Chemistry, University of Florida, Gainesville, Florida 32611

(Received November 22, 1976)

The temperature dependence (10–90 K) of the phosphorescence lifetime of benzene complexed with chloroform and deuterated chloroform in 3-methylpentane has been studied. Nonexponential decays are observed at all temperatures and attributed to emission from 1:1 and 2:1 chloroform:benzene complexes. The temperature dependence of the two deconvoluted lifetimes have been fit to two Arrhenius-type rate expressions and the Arrhenius parameters interpreted in terms of the thermal production of a chloroform- or solvent-substituted hexatriene from the benzene triplet state. It is proposed that the precursor to the substituted hexatriene is an exterplex, an excited state complex formed between chloroform, triplet benzene, and the solvent. The comprehensive experiments of Simons and co-workers are shown to be consistent with this suggestion. It is further proposed that the known solvent and temperature dependence of (uncomplexed) benzene phosphorescence in hydrocarbon matrices arises from solvent-substituted hexatriene formation via a precursor benzene–solvent exciplex. Closed- and open-shell INDO molecular orbital calculations on the triplet and ground state benzene–H_2 model system are supportive of benzene–solvent exciplex formation. The possible existence of benzene exciplexes in other phases is discussed. In liquid alkanes, where benzene is known to be a radiation shield under γ irradiation, protection of the solvent from CH bond rupture via energy transfer in a benzene–solvent exciplex is suggested.

I. Introduction

The temperature dependence of the phosphorescence lifetime of benzene in condensed media has been the subject of a number of investigations.[1-4] A remarkable dependence on both temperature and solvent has been demonstrated. For a given solvent, temperature independent lifetimes have been observed below 50–60 K while above this temperature a rapid decrease in lifetime has been noted. An Arrhenius-type relation for observed phosphorescence decay rate has been shown[1] to adequately describe most of the experimental results. Interestingly, the Arrhenius parameters have been found to vary greatly from solvent to solvent. The preexponential factors lie between 10^3 and 10^9, and the activation energies (ΔE) between 500 and 2000 cm^{-1}. Various explanations for these large solvent effects have been proposed. Since the ΔE values are of the same order of magnitude as vibrational energies, energy redistribution into vibrations of either benzene[1,3] or of the solvent[3] have been suggested. Different isomeric forms of benzene (which revert to ordinary benzene in the ground state) have been found[5,6] after

[†] Present address: Department of Chemistry, University of Rochester, Rochester, N.Y. 14627.

electronic excitation at high temperatures, and the formation of these species has been proposed as a possible cause of the strong temperature dependence.

Two theoretical explanations for the experimental observations have been advanced. Fischer[7] has attributed the strong temperature dependence to the pseudorotational motion of benzene in its lowered D_{2h} symmetry of the first triplet state. However, this approach has been criticized[8,9] on several grounds. The temperature dependence predicted by the pseudorotation model does not give a good fit to the experimental results throughout the entire temperature range investigated,[8] and more importantly, pseudorotational and temperature-dependent lifetimes do not always occur in the same temperature region.[9,10] In a different approach, Lin[11] has derived a formula which is similar to an Arrhenius-type expression, but his estimates of the intramolecular radiationless decay rates (preexponential factors) are orders of magnitude too small. Thus, despite much discussion, there appears to be no generally accepted explanation for the strong temperature and solvent dependence of benzene's phosphorescence lifetime.

In this paper we propose that the solvent plays an integral role in the phosphorescence decay of benzene in condensed media. It has been previously observed that benzene does undergo a photochemical reaction in certain solvents. Gibson, Blake, and Kalm[12] discovered that when benzene was irradiated in either an isopentane–methylcyclohexane mixture or in an ether–isopentane–ethanol mixture a photoproduct was produced whose spectrum was similar to that of hexatriene. Subsequent work by Leach and Migirdicyan[13-18] and by Anderson, Chilton, and Porter[19] showed that the photoproduct was a solvent-substituted hexatriene. The former authors proposed[13,15,18] that a biradical mechanism was involved while the latter ones suggested[19] a four-center concerted mechanism. Subsequent ESR work[20] failed to detect the presence of the hexatriene biradical, thereby lending indirect support to the four-center proposal. Photoproduct formation was found[21] to depend linearly on exciting light intensity. Of the two possible precursor states (i.e., the first excited singlet and triplet states), the longer lifetime of the triplet is thought to make it the more likely precursor.

Of central importance to the investigation reported here are a series of comprehensive spectroscopic and photochemical studies on benzene by Simons and co-workers.[22-25] Simons, Perrins, and Smith[22] discovered that there was a substantial change in the appearance of the phosphorescence spectrum of benzene in glassy 3-methylpentane (3MP) upon addition of chloroform. This change was attributed to the complexation of $CHCl_3$ with benzene, a phenomenon which has long been known to occur.[26] It was further noted that compounds with at least one CH bond such as $CHCl_2CCl_3$ had a similar effect, but others such as CCl_4 had none, and that with $CHCl_3$ present the photoproduct changed from a solvent-substituted hexatriene to a chloroform-substituted one. Substitution of $CDCl_3$ for $CHCl_3$ as the complexing agent produced no spectral changes but did result in the photolytic production of solvent-substituted hexatriene, although at a slower rate than in its absence. From phosphorescence lifetime work at 77 K, Simons and Smith[24] established that changes in the decay rate accompanied this change in photoproduct formation. They also noted a puzzling nonexponential decay from the benzene–$CHCl_3$ complex while the benzene–$CDCl_3$ complex decayed exponentially.

Later work on hexatriene formation from benzene derivatives (up to hexaethylbenzene) led Simons and co-workers[25] to conclude that certain steric factors were important in the hexatriene formation process. It was proposed that the chloroform sat atop the benzene ring with its CH bond along the benzene sixfold axis and that the initial step in hexatriene formation involved a tilt away from this axis. Similar work on benzene in C_2H_5OH, C_2H_5OD, and C_2D_5OD glasses also led[26] these workers to propose that an intermolecular vibronic coupling was operative in these systems and was, in fact, instrumental in the radiationless decay of the benzene triplet state.

The major aim of the present work was to obtain an understanding of the strong temperature and solvent dependence of the benzene phosphorescence lifetime in condensed media. It appeared conceivable to us that the wide variation in the previously observed Arrhenius parameters for benzene in various solvents was connected with the photolytic formation of solvent-substituted hexatrienes. We reasoned that a connection might be made if an investigation of the temperature dependence of the phosphorescence lifetimes were made on a benzene–solvent system known to form hexatrienes. As detailed above, Simons' work has shown conclusively that solvent- or chloroform-substituted hexatrienes are formed upon irradiation of benzene in 3MP glasses with $CDCl_3$ or $CHCl_3$, respectively. In this investigation, the temperature dependence of the phosphorescence lifetimes was measured using the same benzene–chloroform–3MP system. We have fit our results to two Arrhenius-type rate equations and from our data propose the formation of an *exterplex*, formed from excited triplet benzene, chloroform, and solvent, as a precursor to hexatriene formation. It will be seen that this model provides a framework for understanding a wide variety of photophysical and photochemical phenomena involving benzene in different phases.

II. Experimental Procedures

The apparatus used to obtain the benzene phosphorescence lifetimes and spectra has been described previously.[27] In the present work the excitation source was a low-pressure 12-W Hg arc (Hanovia). Solvent components which were either spectrograde ($CHCl_3$, Malinckrodt), 99.8 atom % ($CDCl_3$, Aldrich) or 99+% (3MP, Aldrich) were tested for impurity emission at 338–340 nm (the 0–0 region of the triplet–singlet transition of the benzene–chloroform complex), upon irradiation at 254 nm. None was observed under normal operating conditions. This spectral region is of special importance to this study since uncomplexed benzene has essentially no (0,0) emission and cannot interfere with either the spectral or lifetime observations of the complex in this region. An emission bandpass of 0.3 nm was used to record spectra and of 1.8 to 2.4 nm to record lifetimes. Decay curves were routinely recorded for a period greater than four half-lives (of the slower component, if nonexponential) on a 1024 channel digital signal averager (Tracor Northern-NS-570) and the final averaged decay curve read out on a Wang programmable calculator (Model 700 C). Deconvolution procedures for nonexponential decays have been described elsewhere.[27]

A sample cell utilizing an O-ring-sealed suprasil quartz window was constructed for placement on the cold finger of a closed cycle liquid helium dewar (Air Products Displex). A front surface excitation and 90° emission optical arrangement was employed. Prior to cooldown, dry nitrogen was bubbled through the solutions to remove oxygen which is frequently[28] a triplet quencher, although not usually so for benzene.[4,29] The sample cell was filled in a nitrogen atmosphere. Solutions of 0.394 mM benzene and 0.399 M $CXCl_3$ (X = H or D) in 3MP were used.

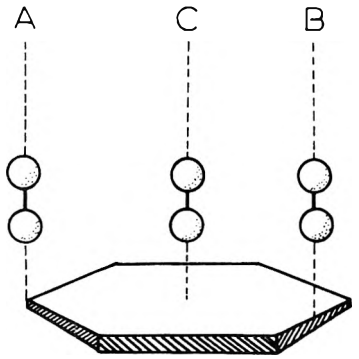

Figure 1. Three different modes of approach of hydrogen molecule and benzene used in INDO calculations. (A) Hydrogen approaches from above a benzene carbon atom. (B) Hydrogen approaches from above the midpoint of a benzene carbon–carbon bond. (C) Hydrogen approaches along the benzene sixfold axis.

Solutions with one tenth the above chloroform concentration were also prepared in order to study the effect of concentration on the spectrum.

Samples were cooled directly from room temperature to the operating temperature (10–90 K) on the Displex. No significant effect was noted if the cooling process was halted at the freezing point of the glass for 30 min. Two hours were allowed for thermal equilibrium to be attained in the glass. Temperature changes during the experiment were kept to less than 10 K and a period of 30 min allowed for reestablishment of thermal equilibrium. It is important to remark here that although our sample cooling procedure corresponds to a relatively slow cooling process (3 K/min) there is evidence (vide infra) that a nonequilibrium ratio of uncomplexed benzene to 1:1 to 2:1 (chloroform:benzene) complex is formed.

III. Calculational Procedures

To determine the theoretical feasibility of complex formation between benzene and a chloroform or an alkane solvent molecule, we chose to investigate a simplified model: benzene with the hydrogen molecule. The capacity of hydrogen to form a bound species with triplet or ground state benzene is expected to parallel that of a CH bond of an alkane or chloroform but without the computational complications introduced by orientational and steric factors from other "inert" parts of the interacting partner. Although this is certainly a gross assumption, we feel it is justified since we are only interested in qualitative behavior.

INDO molecular orbital calculations were carried out using QCPE program 141 originally written by Dobosh[30] and later modified by Pople and Beveridge.[31] Open shell INDO calculations for ground state H_2 and triplet state benzene were performed as a function of intermolecular distance for three different H_2–benzene orientations. In each, the H_2 was allowed to approach the plane of the benzene ring from above since this would optimize its interaction with the π electron cloud and is consistent with the probable geometry of the benzene–chloroform complex as determined by Simons.[22,24] The H–H bond was kept perpendicular to the benzene ring plane since steric considerations in alkanes and chloroform would probably prohibit any other type of approach. The three different approaches employed are sketched in Figure 1. The first (A) has the H_2 directly above a carbon atom, the second (B) above the midpoint of a carbon–carbon bond, and the third (C) along the benzene C_6 axis above the middle of the ring. A similar calculation for ground state H_2 interacting with ground state benzene was also performed for the above approach pathways using a closed shell INDO scheme. In all calculations the H_2 equilibrium bond length of 0.7461 Å was kept constant.

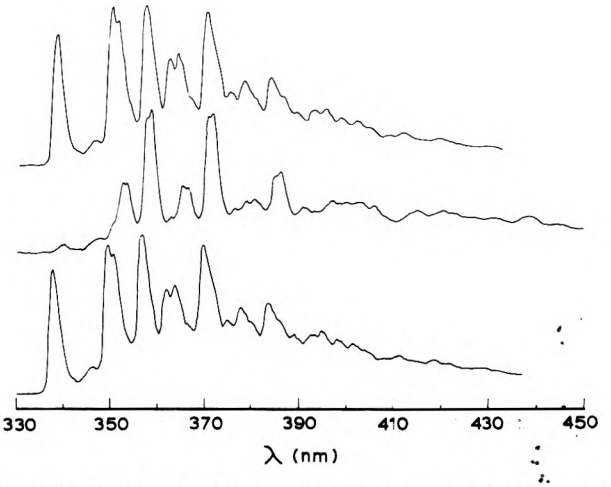

Figure 2. Phosphorescence spectra of benzene and its chloroform complexes at 15 K in 3-methylpentane: (top) benzene and $CHCl_3$; (middle) benzene alone; (bottom) benzene and $CDCl_3$.

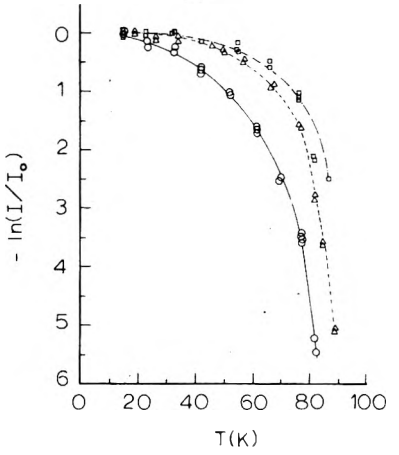

Figure 3. Phosphorescence intensity vs. temperature ($-\ln I/I_0$ vs. T(K) where I_0 is the intensity at 15 K) for complexed and uncomplexed benzene: (squares) benzene alone; (triangles) benzene and $CDCl_3$; (circles) benzene and $CHCl_3$.

IV. Experimental Results

The phosphorescence spectra of benzene and its complexes with $CHCl_3$ and $CDCl_3$ at ~15 K in 3MP are shown in Figure 2. Spectra were also recorded at 77 K and were found to essentially agree with previously reported results.[22,32] Upon further cooling to 15 K there is some change in the spectra with some peaks now showing a more resolved doublet structure. The uncomplexed benzene spectrum shows almost no emission in the 338–340-nm region where its 0–0 band is located, but does show 992-cm^{-1} ring breathing mode progressions built on vibronic origins corresponding to one quantum of the ν_8 (1596 cm^{-1}, e_g) mode and of the ν_9 (1178 cm^{-1}, e_g) mode. Similar progressions are also observed in the complexed benzene spectra, with an additional 992-cm^{-1} progression built on the now intense 0–0 bond.

A plot of ln (phosphorescence intensity) vs. temperature is shown in Figure 3. The plot shows the results for the 0–0 band of the benzene complexes and the ν_8 vibronic origin for uncomplexed benzene; the strong dependence of phosphorescence intensity on temperature is apparent. The effect of slow and normal cooling rates (vide supra) is shown in Figure 4. Phosphorescence decay curves for the benzene complexes were obtained by monitoring the

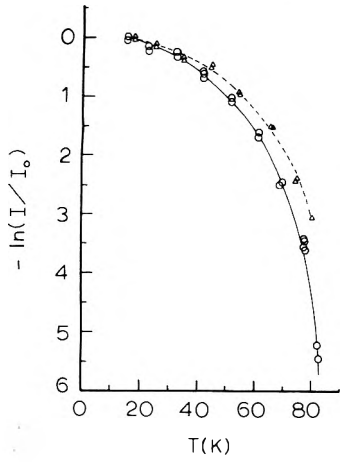

Figure 4. Effect of "slow" and "normal" cooling on phosphorescence intensity of benzene complexed with $CHCl_3$ in 3-methylpentane: (circles) "normal" cooling (see text); (triangles) "slow" cooling (see text).

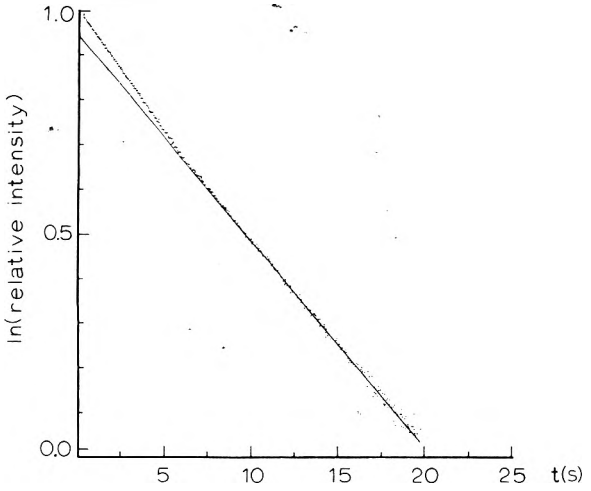

Figure 5. Typical phosphorescence decay curve: ln (intensity) vs. time for benzene–$CHCl_3$ complex.

emission solely in the 338–340-nm region. From plots of ln (intensity) vs. time, a typical example of which is shown in Figure 5, it is easily seen that the observed lifetimes are nonexponential. The component lifetimes, obtained by deconvolution procedures previously described,[27] are shown as a function of temperature (13–90 K) in Figures 6 and 7. Above 80–90 K, the intensity of the 0–0 band is too weak to allow the measurement of the lifetimes on our apparatus.

V. Decay Rate Expressions

We have fit our lifetime results to two different decay rate expressions, both of which originate under the same set of assumptions. We briefly review their derivations and assumptions here. Consider a system with a ground state singlet (S_0) and two excited triplet states T_1 and T_2. (T_1 and T_2 do not necessarily denote two different electronic states of the molecule, but merely two energetically different species of the total system under consideration. Vide infra.) Assuming the intersystem crossing rate constants from the excited singlet to T_1 and T_2 are fast (i.e., not rate determining) the rate equations for decay from them to the ground state are

$$-[T_2] = +(k_{21} + k_{20})[T_2] - k_{12}[T_1] \quad (1)$$

$$-[T_1] = -k_{21}[T_2] + (k_{10} + k_{12})[T_1] \quad (2)$$

where the rate constants, k_{ij}, describe the radiative and/or radiationless decay between the ith initial and the jth final

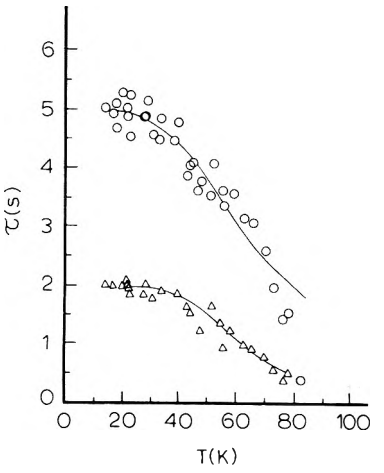

Figure 6. Phosphorescence lifetime (τ) as a function of temperature for the benzene–$CHCl_3$ complex: (circles) long-lived component; (triangles) short-lived component.

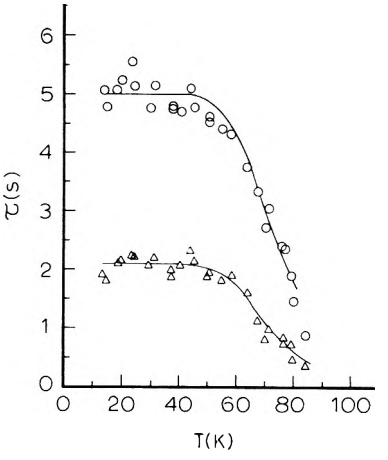

Figure 7. Phosphorescence lifetime (τ) as a function of temperature for the benzene–$CDCl_3$ complex. See Figure 6 caption for symbols.

state. Assuming that $k_{12}, k_{21} >> k_{20}, k_{10}$ the solutions of these coupled differential equations are[33]

$$[T_1] = \frac{\{[T_1]_0 + [T_2]_0\}}{K+1}e^{-kt} + \frac{\{K[T_1]_0 - [T_2]_0\}}{K+1}e^{-mt} \quad (3)$$

$$[T_2] = \frac{K\{[T_1]_0 + [T_2]_0\}}{K+1}e^{-kt} + \frac{\{[T_2]_0 - K[T_1]_0\}}{K+1}e^{-mt} \quad (4)$$

where $k = (k_{10} + Kk_{20})/(K+1)$, $m = k_{21}(K+1)$, and $K = k_{12}/k_{21}$ and $[T_1]_0$ and $[T_2]_0$ refer to the initial concentration of molecules in T_1 and T_2, respectively (i.e., just before decay).

If thermal equilibrium is immediately established between T_1 and T_2, then

$$[T_2]_0/[T_1]_0 = k_{12}/k_{21} = e^{-\Delta E_{21}/kT} \quad (5)$$

where ΔE_{21} is the energy difference between T_2 and T_1. The general solutions, (3) and (4), reduce to

$$[T_1] = k_{21}([T_1]_0 + [T_2]_0)e^{-kt}/(k_{12} + k_{21}) \quad (6)$$

$$[T_2] = k_{12}([T_1]_0 + [T_2]_0)e^{-kt}/(k_{12} + k_{21}) \quad (7)$$

TABLE I: Parameters Determined from Observed Phosphorescence Decay Rates for Benzene Complexes in 3MP

Complex	Expression[a]	Slow decay rate			Fast decay rate		
		k_{10}, s^{-1}	k_{20}, s^{-1}	ΔE_{21}, cm^{-1}	k_{10}, s^{-1}	k_{20}, s^{-1}	ΔE_{21}, cm^{-1}
C_6H_6-$CHCl_3$	I	0.205 ± 0.005	5.4 ± 2.6	160 ± 20	0.52 ± 0.02	130 ± 70	240 ± 30
	II	0.205 ± 0.005	6.4 ± 3.0	160 ± 20	0.52 ± 0.02	130 ± 70	240 ± 30
	III	0.201	4.2 ± 1.6	150 ± 20	0.501	90 ± 40	220 ± 20
	IV	0.201	5.0 ± 1.8	150 ± 20	0.501	100 ± 50	220 ± 20
C_6H_6-$CDCl_3$	I	0.203 ± 0.004	660 ± 650	420 ± 50	0.48 ± 0.01	2200 ± 3000	420 ± 70
	II	0.203 ± 0.004	660 ± 650	420 ± 50	0.48 ± 0.01	2200 ± 3000	420 ± 70
	III	0.200	450 ± 400	400 ± 50	0.474	1600 ± 1900	400 ± 60
	IV	0.200	450 ± 400	400 ± 50	0.474	1600 ± 1900	400 ± 60

[a] Expression I: $k = k_{10} + k_{20}e^{-\Delta E_{21}/kT}$. Expression II: $k = (k_{10} + k_{20}e^{-\Delta E_{21}/kT})/(1 + e^{-\Delta_{21}/kT})$. Expression III: similar to I, except that k_{10} is constant during fit of k_{20} and ΔE_{21} (see text). Expression IV: similar to II, except that k_{10} is constant during fit of k_{20} and ΔE_{21} (see text).

where the overall decay rate constant, k, is now

$$k = \frac{k_{10} + k_{20}e^{-\Delta E_{21}/kT}}{1 + e^{-\Delta E_{21}/kT}} \quad (8)$$

If $\Delta E_{21}/kT >> 1$, this decay rate constant (k) becomes

$$k = k_{10} + k_{20}e^{-\Delta E_{21}/kT} \quad (9)$$

and (6) and (7) reduce to

$$[T_1] = [T_1]_0 e^{-kt} \quad (10)$$

$$[T_2] = [T_2]_0 e^{-kt} \quad (11)$$

It is apparent that (9) is the Arrhenius rate expression with k_{10} equivalent to the temperature-independent rate, and k_{20}, the preexponential factor. It is this expression which was used by Nieman[1] and others[2-4] to describe the temperature dependence of the benzene phosphorescence decay times. We have used both this expression (eq 9, hereafter called I) and its predecessor (eq 8, hereafter called II). Two further modifications of these forms (III and IV) were also used; in these the low temperature decay rate k_{10} was first found by averaging the temperature independent portion of the curves in Figures 6 and 7 and then treating it as a constant in the subsequent determination of k_{20} and ΔE_{21}. These latter modifications were explored because expressions I and II invariably showed a tendency to fit the onset region poorly when all parameters were allowed to vary. This tendency has been noted previously[1] and usually gives somewhat high values for k_{10} and correspondingly low values for k_{20} and ΔE_{21}. This general mismatch is not as pronounced here as in previous work because of the relatively large errors in the decay rates caused by the necessary nonexponential deconvolution procedures. A weighted least-squares program (SUPER)[34] was used to fit the results. The solid lines in Figures 6 and 7 represent the best calculated fit to the data using expression IV; the resulting best parameters are given in Table I.

VI. Discussion

A. *Spectral Results.* There appears to be a discrepancy between our phosphorescence spectral results for complexed benzene, given in Figure 2, and those of Simons.[22] Our spectra show several bands at higher energies than Simons'. Simons has attributed[22] several shoulders on the blue edge of his origin band to a 2:1 complex. As previously mentioned, our experimental cooling conditions probably cause a nonequilibrium ratio of 2:1 vs. 1:1 chloroform–benzene complex pairs. We therefore believe that our higher energy peaks are due to emission from 2:1 complexes. With a slower cooling procedure it is expected that more complete relaxation can occur in the matrix and a different proportion of 1:1 and 2:1 benzene–chloroform complexes form. The slightly different temperature dependences for the benzene–chloroform complex phosphorescence intensities noted in Figure 4 for the different cooling rates are no doubt caused by this effect.

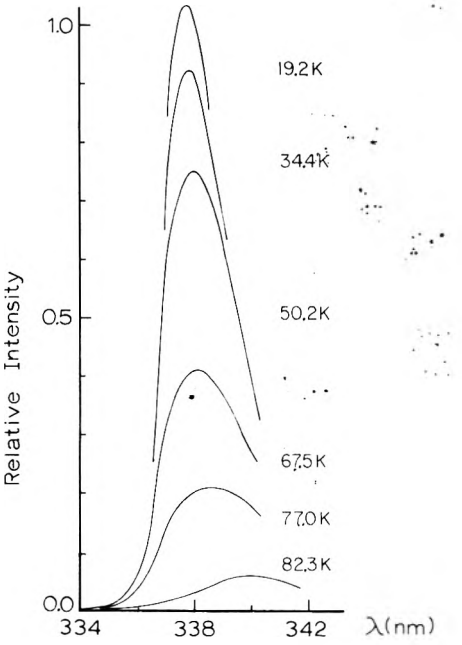

Figure 8. Phosphorescence intensity of the 0–0 band of the benzene–$CHCl_3$ complex as a function of wavelength and temperature. For the upper three spectra only their peaks are shown for clarity.

Support for the existence of two emitting species comes from the blue shift of the 0–0 band of the benzene–chloroform complex with decreasing temperature (cf. Figure 8). The shift and intensification can best be understood in terms of different intensity contributions from the two different complexes (1:1 and 2:1) at different temperatures. Reduction of the chloroform concentration by a factor of 10 also appeared to cause some shift in the location of the 0,0 band, but this result is complicated by the reduction of the band intensity and the appearance of new peaks that indicate the presence of uncomplexed benzene.

B. *Lifetime Results.* The observation of nonexponential phosphorescence decays in all the benzene–chloroform complexes is not unexpected in view of the fact that more than one emitting species is present. Indeed, what is surprising is the observation by Simons and co-workers[24] of an *exponential* decay in the benzene–$CDCl_3$ system. Although Simons has identified two emitting species from his absorption and phosphorescence work in both isotopic complexes he curiously ignores them as possible causes of the nonexponentiality observed in the benzene–$CHCl_3$

system. Instead, the nonexponentiality was attributed[24] to different intermolecular vibronic interactions and different orientations and fluctuations of the assemblage of complexes in the solvent cage.

We offer another interpretation which is consistent with both Simon's and our findings. Although $CHCl_3$ and $CDCl_3$ show the same complexing strength toward benzene,[23] the emission intensity from the benzene–$CDCl_3$ complex is two-to-three times stronger than that from the benzene–$CHCl_3$ system.[24] If it is assumed (1) that the intensity enhancement in the benzene–$CDCl_3$ system is due exclusively to an increase in the emission from 1:1 complexes and (2) that the nonexponentiality results from the overlapping decays from the 2:1 and 1:1 complexes, Simons' result can be understood. An exponential decay from the benzene–$CDCl_3$ complex is observed because emission from the 1:1 complex predominates over the now more weakly emitting 2:1 complex. On the other hand, in the benzene–$CHCl_3$ system (in which the emission intensities of the 2:1 and 1:1 complexes are more nearly the same) decay contributions from each species leads to an observed nonexponential decay. The fact that our cooling procedure produces both complexes about equally and that our observed decays are nonexponential for both isotopic chloroform complexes is consistent with this interpretation.

The identification of our two lifetime components with either the 1:1 or the 2:1 complex is aided by Simons' previous work[24] on the lifetime of the benzene–$CDCl_3$ system in 3MP at 77 K. His measured lifetime of 1.7 s is in reasonably good agreement with our long-lived component of 2.2 s for the same system. The difference can most likely be ascribed to a small temperature difference in the two experiments for, as Figure 7 shows, at ~77 K both components of our phosphorescence decay are very sensitive to temperature. Because Simons was observing the decay of the 1:1 complex, we can with reasonable confidence infer that our long-lived component originates from the 1:1 complex and the short-lived component originates from the 2:1 complex.

C. *Exterplex Formation.* From a comparison of the average lifetimes and phosphorescence efficiencies for the two isotopic complexes, Simons has concluded[24] that the difference in lifetimes at 77 K results from the difference in nonradiative decay rates for the two complexes. Intermolecular vibronic coupling differences between the CH(D) fragment of $CHCl_3(CDCl_3)$ and the benzene ring were proposed as the cause of the different nonradiative rates. With our results (cf. Table I), it is possible to explore further the reasons for the nonradiative rate difference. The low temperature decay rate (k_{10}) is seen to be the same, within experimental error, for both isotopic complexes. Thus, the combined radiative and nonradiative decay rate from the lowest triplet (T_1) to the ground state is unaffected by the complexing partner, $CHCl_3$ or $CDCl_3$. Large differences are observed for ΔE_{21} and k_{20} for the two isotopic complexes, however. To account for these differences, we propose a model in which triplet benzene forms an excited complex with a chloroform and a solvent molecule. Such an excited termolecular complex (referred to in section V as species T_1) has been termed an *exterplex*.[35,36] Chloroform is, of course, already complexed to benzene in the ground state, so that the attraction of a solvent molecule in the complex triplet state is reminiscent of simple exciplex formation. In this case, however, the exciplex formation is between a previously formed complex and a solvent molecule. Within the lifetime of the exterplex there is an exchange or transfer of benzene triplet electronic energy to the CH(D) bonds of one of the complexing partners. The efficiency of this transfer is governed by the magnitude of the Franck–Condon overlap factor of the energy-accepting CH(D) vibrational modes. With sufficient thermal activation the potential barrier to hexatriene formation is surmounted. Thermal equilibrium exists between the exterplex and the thermally activated (and nonemissive) reactive intermediate (in section V, species T_2). Thus, in terms of the previously outlined kinetic model, thermal activation through an energy gap ΔE_{21} will lead to photoproduct formation and to the introduction of an additional pathway for radiationless energy decay. This pathway will be strongly dependent on both solvent and temperature.

The increase observed in ΔE_{21} for both lifetime components upon replacement of $CDCl_3$ for $CHCl_3$ in the complex (cf. Table I) is consistent with the contention that the CH(D) fragment is the important energy acceptor. Upon deuteration the triplet zero point energy of the complex is expected to decrease and the ΔE_{21} increase correspondingly. Simons and co-workers have also noted[24] that the phosphorescence intensity of the benzene–$CDCl_3$ complex is two to three times more intense than the benzene–$CHCl_3$ one. Because the ΔE_{21} is larger in the benzene–$CDCl_3$ complex, triplet energy dissipation via the nonradiative pathway is reduced and the radiative pathway correspondingly enhanced.

The present model for intermolecular energy decay is not incompatible with Simons', but simply views the process in a slightly different manner. The *inter*molecular vibronic coupling described by Simons as the mechanism for energy transfer is, in our model, envisaged as occurring *intra*-exterplex. We prefer the exterplex viewpoint in the condensed phase since its simpler bimolecular analogue, the exciplex, has recently been recognized as an intermediate in a number of photochemical reactions.[37,38]

Emission from termolecular excited state complexes has already been observed,[39] although it has also been recognized[38,40] that the formation of products from such an excited state complex may be so rapid that no emission is observable.

Although it has been implied above that only one potential barrier to substituted hexatriene formation exists, there are several pieces of data which indicate that more than one is present. The first is Simons' observation of chloroform-substituted vs. solvent-substituted hexatriene formation upon irradiation of $CHCl_3$– and $CDCl_3$–benzene complexes, respectively. That two different types of photoproducts can be formed implies that the complex is more properly viewed as a 1:1:1 chloroform–benzene–solvent complex, i.e., an exterplex. Thermal activation of this exterplex will preferentially result in the chloroform-substituted hexatriene because of a larger Franck–Condon overlap between the benzene and the chloroform CH fragment than between the benzene and a solvent CH fragment. Deuterating the chloroform causes the process leading to chloroform-substituted hexatriene to be less probable because of the smaller Franck–Condon overlap in the CD vs. the CH fragment. The Franck–Condon overlap with the solvent CH fragment is now larger and energy transfer into that bond occurs preferentially. Each exterplex should thus possess at least two barriers corresponding to the triplet benzene reaction with either of its partners. The higher energy associated with complex formation in $CDCl_3$ vs. $CHCl_3$ (cf. Table I) is seen to reflect not only a reduction of the zero point energy of the complex upon deuteration but also the larger barrier to solvent- vs. chloroform-substituted hexatrienes. The larger barrier is thought to arise from differences in the CH bond

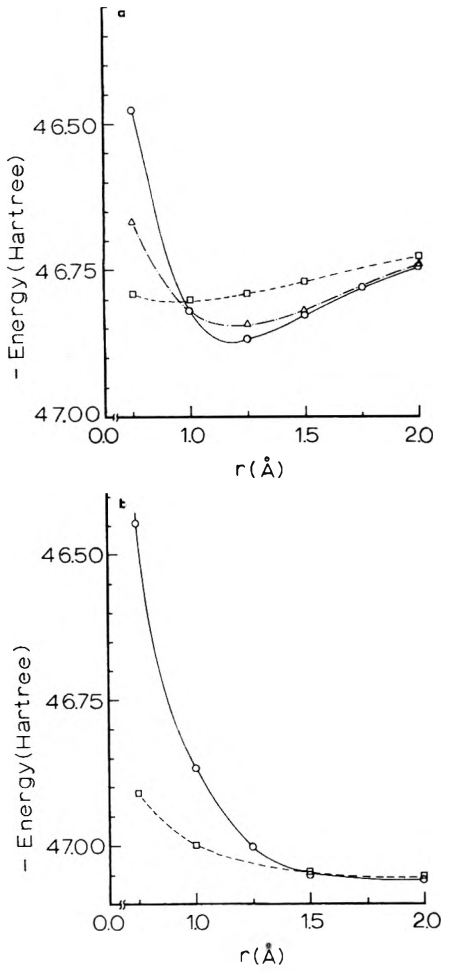

Figure 9. (a) Calculated total energy for the triplet state benzene–hydrogen molecule pair as a function of intermolecular distance for three different modes of approach (cf. Figure 1 for three approaches). The intermolecular distance is measured from the benzene plane to the nearest atom of the hydrogen molecule: (circles) approach A; (triangles) approach B; (squares) approach C. (b) Calculated total energy for the ground state benzene–hydrogen molecule pair as a function of intermolecular distance for two different modes of approach. See Figure 9a caption for further information.

strengths of the complexing partners and the steric barriers which must be overcome prior to hexatriene formation.

The second piece of evidence for several intermolecular radiationless processes comes from the temperature dependence of the phosphorescence lifetimes of the benzene–$CHCl_3$ complex. The experimental data for the long-lived component (1:1 complex) are not fit well for temperatures above ~70 K (cf. Figure 6). The decay values between 70 and 80 K are substantially shorter than the best-fit prediction indicating the need for a second Arrhenius-type term (i.e., $k_{31}\exp(-\Delta E_{31}/kT)$). Unfortunately, the lifetimes could not be followed to sufficiently high temperatures to allow determination of these additional parameters. The physical significance of such an additional term lies in the additional nonradiative channel possible with both chloroform and solvent-partners in the exterplex. That the need for such a term is greatest in the 1:1 benzene–$CHCl_3$ complex (cf. Figure 6) is understandable since in this case the energy transfer to the CH fragment of either the solvent or the chloroform may occur with more nearly equal probability than in the benzene–$CDCl_3$ system.

VII. Theoretical Calculations

Figure 9a gives a plot of the total energy of the H_2–triplet benzene system as a function of intermolecular distance

TABLE II: Results of Open Shell INDO Calculations on the H_2-C_6H_6(T) System as a Function of Intermolecular Separation

Approach[a]	r, Å	Total energy,[b] hartrees	Valence electron density H(1)[c]	H(2)	C (nearest)
A	0.75	−46.474	0.88	1.14	3.91
	1.00	−46.821	0.94	1.13	3.87
	1.25	−46.869	1.03	1.11	3.84
	1.50	−46.827	1.14	1.08	3.84
	1.75	−46.780	1.13	1.06	3.90
	2.00	−46.745	1.08	1.03	3.96
B	0.75	−46.668	0.84	1.13	3.84
	1.00	−46.821	0.96	1.11	3.83
	1.25	−46.844	1.15	1.09	3.84
	1.50	−46.817	1.17	1.07	3.88
	2.00	−46.745	1.09	1.03	3.94
C	0.75	−46.790	1.12	1.07	3.94
	1.00	−46.802	1.12	1.05	3.94
	1.25	−46.791	1.11	1.04	3.95
	1.50	−46.768	1.08	1.03	3.96
	2.00	−46.726	1.03	1.01	3.97

[a] Cf. Figure 1. [b] C_6H_6 energy triplet = −45.290 hartrees; H_2 energy = 1.475 hartrees; total energy system = −46.765 hartrees. [c] H(1) is the farther of the two hydrogens from the benzene plane.

of the three pathways of approach and Figure 9b plots similar results for the H_2–ground state benzene system. It is readily apparent that a stabilization occurs between triplet benzene and H_2, but not between ground state benzene and H_2, indicating the true exciplex character of the interaction. The strongest exciplex is formed with H_2 approaching over a carbon atom rather than along the C_6 axis or over a carbon–carbon bond. The changes in valence electron density at each of the three important atomic centers (the two hydrogens in H_2 and the closest carbon in benzene) upon approach of the two interacting partners is informative. As shown in Table II, the electron density at the carbon decreases while at the nearest hydrogen, H(2), it increases, indicating that the benzene acts as an electron donor and transfers electron density to the H_2. Since the H_2 must accept this extra electron density in an antibonding orbital, the H–H bond will be weakened. This is an important result in explaining the photochemical activity of the benzene triplet manifold in alkane solvents since it is the CH bond of the solvent which must be broken in order to form the solvent-substituted hexatriene.

One last set of calculations were performed in an attempt to more closely describe the most favorable conformation for the benzene–H_2 exciplex as a precursor to hexatriene formation. The most stable benzene–H_2 exciplex conformation (A) was chosen as a starting point and the distant hydrogen moved to a position such that the hydrogen molecule was parallel to the aromatic ring. This hydrogen was then rotated about the first to determine whether there were even more stable conformations than the initial perpendicular approach (A). The existence of such positions of increased stability in the potential energy surface could act as the driving force to bring the H_2 (or CH for an alkane) into a more favorable position from which concerted solvent-substituted hexatriene formation might occur. Figure 10 gives the results of this calculation for different angles of H_2 rotation for an intermolecular separation of 1.25 Å. It can be seen that a more stable conformation does exist in which the hydrogen molecule lies above and at a slight angle to a benzene C–C bond. It is significant that a conformation of this sort is the most stable of all those investigated since the geometry of the precursor transition state would intuitively be expected

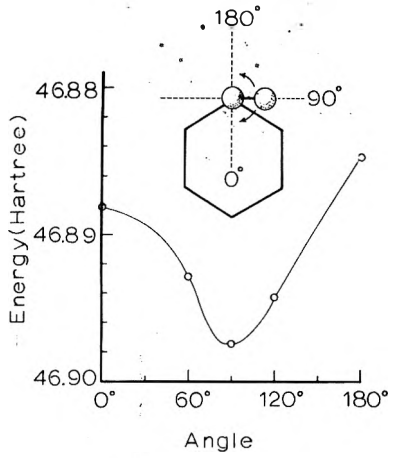

Figure 10. Calculated total energy for the triplet state benzene–hydrogen molecule pair at a fixed intermolecular distance (1.25 Å) as a function of relative intermolecular orientation.

to be similar to this for a concerted mechanism leading to substituted hexatriene. We identify this transition state with our previously discussed complex potential barrier. It is no doubt true that such a transition state in a benzene–alkane exciplex (or benzene–chloroform complex) will be destabilized by steric factors. This could then explain the observed differences in ΔE_{21} found for benzene phosphorescence in different solvents.[1-4]

VIII. Comments on Possible Exciplex Formation in Other Phases

Benzene reactions similar to those that occur in low temperature matrices apparently also occur in the gas phase. Semeluk and Unger have shown[41-43] that triplet state benzene is responsible for the photochemical rupture of the C–H bond in gas phase chloroform. The rupture of the energetically stronger C–H bond instead of the weaker and more numerous C–Cl bonds is consistent with the involvement of an exciplex. The structure of this exciplex may be readily envisioned as similar to the low temperature benzene–chloroform discussed above.

In the liquid phase, benzene is known as a radiation shield for a number of materials. The introduction of benzene into liquid hydrocarbons[44,45] and alcohols[46] shields the C–H bonds of the solvents from rupturing upon exposure to γ irradiation with no concommitant degradation of the benzene. The shielding mechanism probably involves energy transfer to the benzene followed by radiationless deactivation of benzene via collisions in the solution. Such an energy transfer could be efficiently effected with exciplex formation between the solvent and benzene. In low temperatures matrices the energy exchange (from benzene to CH-bearing solvent) leads to substituted hexatriene formation because of the constraints on molecular motion by the rigid lattice. In liquids, on the other hand, the energy exchange in the exciplex simply leads to energy degradation because of the more highly efficient collisional deactivation pathways available in this phase.

While benzene is not known to phosphoresce in liquid solutions, other materials that can accept benzene triplet energy can be used to monitor the amount of triplet benzene present. The isomerization of *cis*-butene-2 has been used[47] to show that the yield of triplet benzene in cyclohexane depends on a process with an activation energy of 785 cm^{-1} and preexponential factor of 3.4×10^8 s^{-1}. Both these values are in the same range as those determined from previous lifetime studies of benzene in various low temperature alkane matrices. While the butene isomerization results have been interpreted in terms of an activation energy for intersystem crossing of benzene, the data are also consistent with exciplex formation between cyclohexane and benzene, as discussed in this paper.

Acknowledgment. One of us (W. M.) acknowledges the NSF for a traineeship for the period 1969–1973 and the Graduate School, University of Florida, for a Graduate Research Fellowship (1973–1974). The Computing Center at the University of Florida is acknowledged for use of its facilities. This research has been supported by the National Science Foundation (GP 12740 and MSP 74-06926).

References and Notes

(1) G. F. Hatch, M. D. Erlitz, and G. C. Nieman, "Molecular Luminescence", E. C. Lim, Ed., W. A. Benjamin, New York, N.Y., 1969, pp 21–38.
(2) I. H. Leubner and J. E. Hodgkins, *J. Phys. Chem.*, **73**, 2545 (1969).
(3) I. H. Leubner, *J. Phys. Chem.*, **74**, 77 (1970).
(4) N. G. Kilmer and J. D. Spangler, *J. Chem. Phys.*, **54**, 604 (1971).
(5) D. Bryce-Smith and H. C. Longuet-Higgins, *Chem. Commun.*, 593 (1966).
(6) K. E. Wilzbach, A. L. Harkness, and L. Kaplan, *J. Am. Chem. Soc.*, **90**, 1116 (1968).
(7) S. Fischer, *Chem. Phys. Lett.*, **10**, 397 (1971).
(8) D. Haaland, Ph.D. Dissertation, University of Rochester, 1973, pp 104–112.
(9) G. F. Hatch, M. D. Erlitz, and G. C. Nieman, *J. Chem. Phys.*, **49**, 3723 (1968).
(10) M. S. de Groot, I. A. M. Hesselman, and J. H. van der Waals, *Mol. Phys.*, **10**, 91 (1965).
(11) S. H. Lin, *J. Chem. Phys.*, **44**, 3759 (1966).
(12) G. E. Gibson, N. Blake, and M. Kalm, *J. Chem. Phys.*, **21**, 1000 (1953).
(13) S. Leach and E. Migirdicyan, *J. Chim. Phys.*, **54**, 643 (1957).
(14) S. Leach and E. Migirdicyan, *J. Chim. Phys.*, **58**, 409 (1961).
(15) S. Leach and E. Migirdicyan, *J. Chim. Phys.*, **58**, 416 (1961).
(16) S. Leach and E. Migirdicyan, *J. Chim. Phys.*, **58**, 762 (1961).
(17) E. Migirdicyan, *J. Chim. Phys.*, **63**, 520 (1966).
(18) E. Migirdicyan, *J. Chim. Phys.*, **63**, 535 (1966).
(19) E. Anderson, H. T. J. Chilton, and G. Porter, *Proc. Chem. Soc.*, 352 (1960).
(20) E. Migirdicyan, *J. Chim. Phys.*, **63**, 543 (1966).
(21) S. Leach and E. Migirdicyan, *J. Chim. Phys.*, **56**, 749 (1959).
(22) N. C. Perrins, J. P. Simons, and A. L. Smith, *Trans. Faraday Soc.*, **67**, 3415 (1971).
(23) N. C. Perrins and J. P. Simons, *Trans. Faraday Soc.*, **65**, 390 (1969).
(24) J. P. Simons and A. L. Smith, *Chem. Phys. Lett.*, **16**, 536 (1972).
(25) J. P. Simons and A. L. Smith, *J. Chem. Soc., Faraday Trans. 2*, **70**, 53 (1974).
(26) C. J. Creswell and A. L. Allred, *J. Phys. Chem.*, **66**, 1469 (1962).
(27) W. Moehle, D. Mahoney, J. Wrobel, and M. Vala, *Mol. Phys.*, accepted for publication.
(28) S. P. McGlynn, T. Azumi, and M. Kinoshita, "Molecular Spectroscopy of the Triplet States", Prentice-Hall, Englewood Cliffs, N.J., 1969.
(29) D. M. Haaland and G. C. Nieman, *J. Chem. Phys.*, **59**, 1010 (1973).
(30) P. Dobosh, Program CNINDO, No. 141 from the Quantum Chemistry Program Exchange, Chemistry Department, Room 204, Indiana University, Bloomington, Ind. 47401.
(31) J. A. Pople and D. L. Beveridge, "Approximate Molecular Orbital Theory", McGraw-Hill, New York, N.Y., 1970.
(32) P. G. Russell and A. C. Albrecht, *J. Chem. Phys.*, **41**, 2536 (1964).
(33) B. DiBartolo, "Optical Interactions in Solids", Wiley, New York, N.Y., 1968.
(34) J. Baiardo, unpublished results.
(35) D. Creed and R. Caldwell, *J. Am. Chem. Soc.*, **96**, 7369 (1974).
(36) We utilize the Birks[37] definition of exciplex (and, by analogy, of exterplex): an excited state complex including all entities which interact, either collisionally or by electron exchange, without implying that the excited state complex has a finite binding energy.
(37) J. B. Birks, "Photophysics of Aromatic Molecules", Wiley-Interscience, New York, N.Y., 1970.
(38) See, e.g., J. Saltiel, D. E. Townsend, B. D. Watson, and P. Shannon, *J. Am. Chem. Soc.*, **97**, 5688 (1975), and references therein.
(39) H. Beens and A. Weller, *Chem. Phys. Lett.*, **2**, 140 (1968).
(40) M. V. Hershberger and R. W. Lumry, *Photochem. Photobiol.*, **23**, 391 (1976).
(41) G. P. Semeluk and I. Unger, *Nature (London)*, **198**, 853 (1963).
(42) I. Unger and G. P. Semeluk, *Can. J. Chem.*, **44**, 1427 (1966).
(43) S. H. Ng, G. P. Semeluk, and I. Unger, *Can. J. Chem.*, **46**, 2459 (1968).
(44) J. A. Stone and P. T. Dyne, *Radiat. Res.*, **17**, 353 (1962).
(45) J. K. Thomas and I. Mani, *J. Chem. Phys.*, **51**, 1334 (1969).
(46) W. V. Sherman, *Adv. Free Radical Chem.*, **3**, 1–82 (1969).
(47) R. B. Cundall and D. A. Robinson, *Chem. Phys. Lett.*, **14**, 438 (1972).

Luminescence and Triplet Absorption of *o*-, *m*-, and *p*-Methylbenzoic Acids

A. U. Acuña,* A. Ceballos, and M. J. Molera

Instituto de Química Física "Rocasolano", C.S.I.C., Serrano 119, Madrid-6, Spain *(Received December 28, 1976)*

Publication costs assisted by Consejo Superior de Investigaciones Científicas, Spain

The transient absorption spectra of flashed *o*-, *m*-, and *p*-methylbenzoic acids (o-MBOH, *m*-MBOH, and *p*-MBOH) in the 290–340-nm region are recorded and the transient is identified as the emitting lowest π,π^* triplet state. The absorption and emission spectra of the three acids at room temperature and 77 K have been investigated and drastic solvent dependence of fluorescence and phosphorescence quantum yields has been found. These changes are attributed to different photophysic properties of monomeric and dimeric species. Glassy matrices containing either monomer or dimer MBOH were obtained by controlling solvent polarity and cooling rate. Thus the quantum yields and lifetimes of each species could be determined. The quenching of fluorescence in the monomer is interpreted in terms of strong coupling among n,π^* and π,π^* excited states, increasing the ISC process $S_1 \rightsquigarrow T$. In the dimer, hydrogen bonding raises the energy of n,π^* states and weakens the coupling allowing fluorescence to appear. Steric effects present in o-MBOH are also discussed.

Introduction

It is not unusual to find in heterocyclic molecules very close-lying electronically excited states that, in general, have different orbital nature. The photophysics of these compounds becomes, then, strongly dependent on small changes in the relative situation of the lower excited states. It seems that in carboxyl aromatic compounds a similar situation may arise. Thus, in benzoic acid (BOH) important changes in the emissive yields result after ground state dimerization by hydrogen bonding. These changes have been the subject of previous research in our laboratories[1-3] and in others.[4] In this paper, the luminescent properties of monomers and ground state dimers of the three methyl benzoic acids (o-MBOH, *m*-MBOH, and *p*-MBOH, respectively) are studied using a method already described.[2] Briefly, it is based on the use of two solvents: one of medium polarity (ether/isopentane) as a glassy matrix where the acid is in its monomeric slightly solvated form, and the other, a nonpolar solvent (methylcyclohexane/isopentane) where if rapidly cooled to 77 K, the acid is almost completely dimerized. It seems that this method has applicability even for the ortho-substituted acid, where the low solubility and association constant may result in incomplete dimerization. In addition, for this compound, we consider other effects due to steric hindrance between –COOH and $-CH_3$ groups, and to the solvent. The increase in radiationless transition rates following the loss of coplanarity is particularly evident in these experiments.

A qualitative picture is developed to explain the photophysics of these three compounds, based on the excited states distribution previously proposed[2,4] for the parent molecule, benzoic acid. The energy of the n,π^* excited states is thought to be the main factor in channeling the luminescence, either as fluorescence or as phosphorescence.

Experimental Section

Materials. The three methylbenzoic acids were commercial (BDH Ltd) products purified by vacuum sublimation and zone melting.[5] Quinine sulfate (Aldrich) and 9,10-diphenylanthracene (Aldrich) were recrystallized. Isopentane, methylcyclohexane, and diethyl ether were purified by a procedure described elsewhere,[1] similar to that of Potts.[6] Ethanol (Merck "fluorimetric grade") was used without further purification. All the solvents were nonemissive under our experimental conditions. Glass-forming mixtures were 5:1 v/v isopentane:methylcyclohexane (P_5M), 1:1 v/v diethyl ether:isopentane (EP), and 5:5:2 v/v diethyl ether:isopentane:ethanol (EPA). Sample solutions were degassed by freeze–pump–thaw cycles to a residual pressure of 2×10^{-5} Torr.

Methods. Absorption measurements at 77 K were effected with a Varian 635 spectrophotometer fitted with a quartz cryostat built in these laboratories.

Emission spectra were recorded on a Perkin-Elmer MPF-3 fluorescence spectrometer fitted with a phosphorescence accessory. The excitation lamp and monochromator were calibrated using Rhodamine B as a photon counter.[7] The emission setup was calibrated using xenon and standard filament lamps. Emission quantum yields at room temperature were measured by comparison with the fluorescence yield of quinine sulfate in 0.1 N H_2SO_4. Fluorescence and phosphorescence quantum yields at low temperatures are based on the proposed value of 1.0 for the fluorescence yield of 9,10-diphenylanthracene in EPA at 77 K.[8] Phosphorescence lifetimes were measured oscilloscopically. Decay data were tested for double exponential mixing with a numerical analysis procedure[9] using a desk computer. Quantum yields are believed to have a combined error of ≈10%, although precision was better than 5%.

The experimental arrangement for low temperature flash photolysis used in this work has been already described.[1]

Results and Discussion

T–T Spectra. The transient absorption spectra of flashed o-MBOH, *m*-MBOH, and *p*-MBOH in P_5M at 77 K are represented in Figure 1. They correspond to the dimeric species in all three cases, and were obtained with a time delay of a few milliseconds after the photolytic flash. No other bands that could be ascribed to T–T absorption were observed. Lack of transparency of EP glass in the UV precludes the observation of T–T monomer spectra. Owing to differences in solubility among the three acids in P_5M, variable concentrations of the order 10^{-3} to 10^{-4} have been used to record the spectra in Figure 1. As was expected from the results obtained with benzoic acid,[1] the mean lifetime values obtained for the transients are the same as those resulting from phosphorescence measurements, which shows the π,π^* triplet character of the transient detected by flash photolysis.

In spite of the low energy of the light pulse (ca. 200 J), a new diffuse band appeared after a number of flashes on BOH, thus showing that some irreversible photolysis took

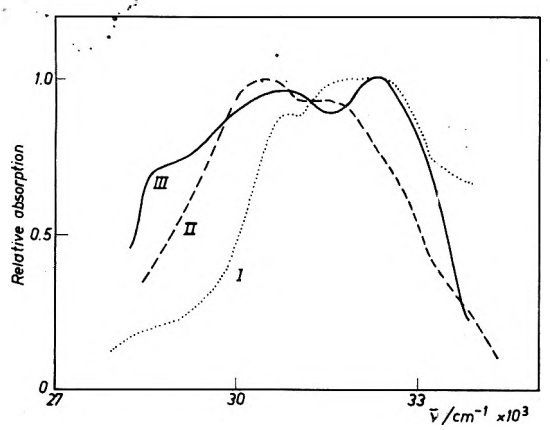

Figure 1. T–T absorption spectra at 77 K of the dimeric species of *m*-, *p*-, and *o*-methylbenzoic acids on curves I, II, and III, respectively. The solvent was P_5M.

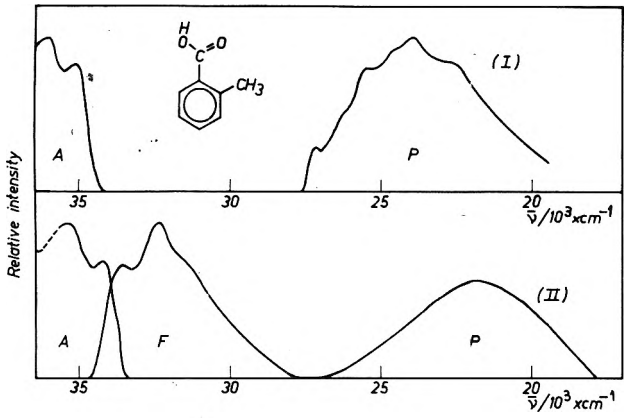

Figure 2. Absorption and luminescence spectra of *o*-MBOH at 77 K: (I) monomeric species in EP; (II) dimeric species in P_5M.

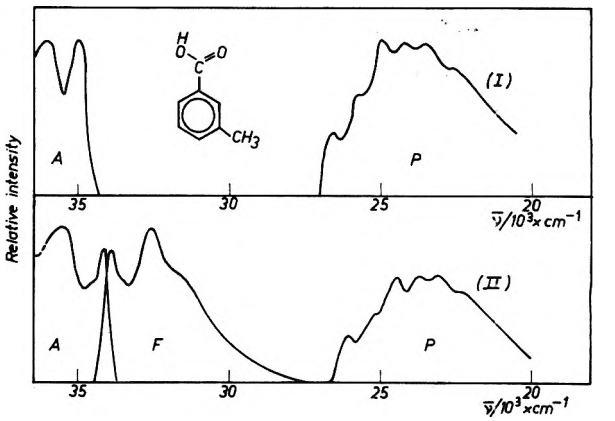

Figure 3. Absorption and luminescence spectra of *m*-MBOH at 77 K: (I) monomeric species in EP; (II) dimeric species in P_5M.

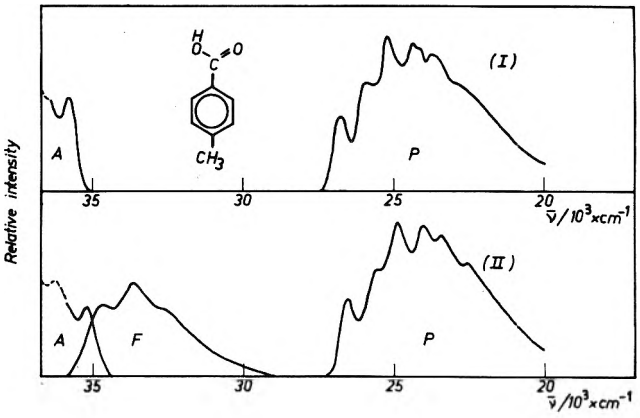

Figure 4. Absorption and luminescence spectra of *p*-MBOH at 77 K: (I) monomeric species in EP; (II) dimeric species in P_5M.

place.[1] Taking into account the high values of the intersystem crossing quantum yield (vide infra) and of the mean lifetime of the first triplet, it is likely that the photochemistry of benzoic and toluic acids is a multiphotonic process.

A common characteristic of all three T–T spectra is their lack of structure. This might result from the dissociative character of the higher excited triplets.

In *p*-MBOH the higher frequency maximum is clearly red-shifted if compared with the corresponding maxima of o-MBOH and *m*-MBOH. This may be indicative of a long axis polarization in this transition, because similar shifts of the ^1L_a band in the singlet manifold of para-disubstituted benzenes have been ascribed by Stevenson[10] to polarization of the transition moment in the para direction.

Finally, since the energies and shape of the triplet absorption spectra of the three toluic acids are very similar to those of the benzoic acid,[1] we may conclude that methyl substitution does not modify the triplet excited states distribution, as expected from the lack of gross perturbation displayed on the singlet manifold.[1]

Emission Spectra and Quantum Yields. The emission spectra of the three toluic acids were studied with ≈ 10^{-4}–10^{-5} M solutions at room temperature and at 77 K. No differences in the emission spectra at both temperatures were observed by varying the exciting wavelength over the range 255–270 nm.

No fluorescence from either acid in the comparatively polar solvent EP was detected ($\phi_F < 0.001$) at either 298 or 77 K. It may be safely assumed, by analogy with the results obtained with BOH,[2,3] that only the solvated monomer of each acid is present in the corresponding EP solution. On the other hand, fluorescence is produced from each acid in P_5M at 298 K, where the equilibrium concentration of dimers is finite. The absorption and emission spectra of *o*-, *m*-, and *p*-MBOH in EP and P_5M at 77 K are shown in Figures 2, 3, and 4, respectively. These spectra also show that, at low temperatures, fluorescence is only produced from dimer molecules but not from the monomers contained in the glass. In Table I are shown the values of transition energies and quantum yields derived from the above described spectra. No true fluorescence quantum yields have been determined at 298

TABLE I: Transition Energies (cm^{-1}), Quantum Yields, and Phosphorescence Lifetimes (s) for *o*-, *m*-, and *p*-Methylbenzoic Acids in 5:1 Isopentane:Methylcyclohexane (P_5M) and 1:1 Diethyl Ether:Isopentane (EP)

	o-MBOH		*m*-MBOH		*p*-MBOH	
Solvent	EP	P_5M	EP	P_5M	EP	P_5M
$S_1 \xleftarrow{298K} S_0$	35100		34980		35700	
$S_1 \xleftarrow{77K} S_0$	35100	34250	34980	34100	35700	35200
$S_1 \xrightarrow{77K} S_0$		33600		33900		34750
$T_1 \xrightarrow{77K} S_0$	27100		26580	26100	26880	26500
η_F[a](298 K)	0	0.011	0	0.014	0	0.009
ϕ_F (77 K)	0	0.17	0	0.35	0	0.30
ϕ_P (77 K)	0.79	0.19	0.70	0.39	0.90	0.65
τ_P	1.30	1.16	2.64	3.85	2.41	3.45

[a] Apparent quantum yield (see text).

K; η_F is the ratio between the number of photons emitted by dimer fluorescence and the total number of photons absorbed by both monomer and dimer contained in the mixture.

Fluorescence radiative lifetimes were calculated from the Strickler and Berg formula;[12] the values for the three toluic acids are of the same order (25–30 ns) as the value previously computed[1] for BOH. Assuming that k_{ic} (internal conversion) is negligible at 77 K, approximate values of k_{isc} (intersystem crossing) may be calculated from the fluorescence quantum yields at 77 K (Table I), yielding a value of $k_{isc} \approx 1$ to 2×10^8 s^{-1} for the three toluic acids.

The solvent-dependent emissive behavior of toluic acids is much the same as that of BOH. In all cases (Figures 2, 3, and 4), fluorescence is completely quenched in the monomer and if, for each dimer, quantum yields of fluorescence and phosphorescence (Table I) are added, a value is obtained which is practically equal to the corresponding monomer phosphorescence quantum yield. This suggests that dimerization changes only the ISC probability, without gross alteration of the initial probability of populating the first singlet by light absorption. The deviation of *o*-MBOH from this behavior should be attributed to the expected steric effect (vide infra).

Dependence of ISC on Dimerization. Let us consider first which excited states are to be expected when a methyl group is substituted for a hydrogen atom at the meta and para positions of benzoic acid. The peculiarities of the ortho acid will be dealt with in a later paragraph. As mentioned above, the small inductive and hyperconjugative effect of methyl substitution is unable to modify largely the π aromatic system of these molecules. As a matter of fact, we effected the perturbation approach of Petruska[11,13] for the first singlet transition (^1L_b state) substituting our experimental frequency shifts at 77 K, somewhat different from those utilized by that author, and obtained a better agreement between theoretical prediction and experiment.

There is no significant absorption that could be assigned to the n,π^* transition. Introduction of a methyl group into the ortho, meta, and para positions of benzaldehyde left the n,π^* transition substantially unchanged.[14] Accordingly, it is presumed that in methylbenzoic acids such transition is immersed under the first singlet absorption as in benzoic acid.[15] The energy and intensity of the charge transfer (CT) transitions are not independent of the nature and position of the substituent in these compounds[16] although such effects are small. Thus, the largest bathochromic shift of the first transition with a CT component at ≈230 nm (which corresponds to the para acid) is less than 1500 cm^{-1}. Moreover, the frequency of the exciting light in the luminescence experiments reported here was kept low enough to excite the $S_1 \leftarrow S_0$ transition only. Thus, it appears that the ISC mechanism advanced before[2,4] to describe the solvent dependence of the luminescence of benzoic acid could be generalized to include the similar effects found in the toluic acids. The n,π^* singlet state, resulting from the excitation of a nonbonding electron of the –CO group, is probably almost degenerated with the first π,π^*, or even a little lower in energy (<1000 cm^{-1}) for monomeric molecules, i.e., in EP solutions. This results in a high ISC rate quenching the fluorescence. Whether this high $S_1 \rightsquigarrow T$ crossing efficiency implies a first-order or a second-order coupling mechanism[15] cannot be specified in light of the experiments described here. Ground state dimerization through hydrogen bonding, i.e., in P_5M solutions, raises the energy of the n,π^* states, leading to an important perturbation of the coupling mechanism to such an extent that now the compound becomes fluorescent. The low fluorescence recorded at room temperature originates on the dimeric population present in its finite equilibrium concentration.

Steric Effects on Quantum Yields. There is an hypsochromic and hypochromic shift of the first possible CT band in the room temperature absorption spectrum of o-MBOH. It has been explained[16] taking into account the steric hindrance to coplanarity of the –COOH group and the benzene ring due to methyl substitution. The other transitions remain virtually unchanged.

Conformational differences between ground and excited states of the monomeric species at 77 K must be low because the phosphorescence emission of o-MBOH is not substantially different from that of the meta and para isomers (Figure 2, Table I). We observe only a slight loss of structure and a clear increase in the decay rate. However, in the dimeric species, the phosphorescence becomes a broad, red-shifted, diffuse band, with a considerable quenching of phosphorescence yield, and an increased decay rate.

These facts suggest significant differences in the nuclear geometries of ground (S_0) and excited (T_1) states. In the crystal the dimer is known to be planar. The interplanar angle, θ, between the carboxyl group and benzene ring, determined by x-ray analyses,[17] is 1.6°. Assuming that the conformation in the glassy matrix is not very different, a twisted ($\theta \neq 0$) emitting triplet would be responsible for the diffuse phosphorescence. This conformation may result from different equilibrium values of θ in S_0 and T_1. Alternatively, the θ equilibrium angle might be the same in both states but it would be possible to find a nonrelaxed population of conformers in T_1.[18] Along its way from S_1 to T_1 the molecule would accumulate excitation energy in the interplanar torsional vibration. If it radiates before reaching the equilibrium conformation in the highly viscous matrix, a diffuse spectrum would result. Although there is no straightforward evidence to substantiate the first possibility, i.e., a T_1 with different equilibrium angle than S_0, we think that the red shift on the maximum of the diffuse band would favor it.

The lower ϕ_P of the ortho dimer might reflect a less efficient $S_1 \rightsquigarrow T$ crossing followed by an enhanced radiationless internal conversion $S_1 \rightsquigarrow S_0$. However, this seems unlikely remembering that the excited states distribution has not changed very much, and the faster IC would have to compete with the ISC, but without quenching all the fluorescence. Instead, it is felt that the distorted T_1 enhances the nonradiative $T_1 \rightsquigarrow S_0$ pathway. This has been shown to occur in a number of compounds.[19] The faster phosphorescence lifetime of the ortho isomer compared with the meta and para (Table I) is in agreement with this suggestion.

On the other hand, it is interesting to note that radiative phosphorescence lifetimes show that little has changed in the pure radiative mechanism: τ_{RP} = 5.1 s (ortho), 6.4 s (meta), and 3.7 s (para).

Therefore, it appears that the photophysics of the ortho acid may also fit in the general mechanism described before to explain the luminescence of benzoic acid, and *m*- and *p*-methylbenzoic acids.

Acknowledgment. This work has been carried out under Contracts No. 2.1.22 and 1192 with the III Plan de Desarrollo and the Comision Asesora (1976–1979), respectively.

References and Notes

(1) A. U. Acuña, A. Ceballos, J. A. García Domínguez, and M. J. Molera, *An. Quim.*, **71**, 22 (1975).

(2) A. U. Acuña, A. Ceballos, and M. J. Molera, *J. Chem. Soc., Faraday Trans. 2*, **72**, 1469 (1976).
(3) A. U. Acuña, A. Ceballos, and M. J. Molera, *An. Quim.*, in press.
(4) H. Baba and M. Kitamura, *J. Mol. Spectrosc.*, **41**, 302 (1972).
(5) Kindly provided by Professor M. Colomina.
(6) J. W. Potts, *J. Chem. Phys.*, **20**, 809 (1952).
(7) J. Yguerabide, *Rev. Sci. Instrum.*, **39**, 1048 (1968).
(8) G. Heinrich, S. Schoof, and H. Guston, *J. Photochem.*, **3**, 315 (1974–1975).
(9) J. Menéndez and A. U. Acuña, *J. Chem. Educ.*, **53**, 98 (1976).
(10) P. E. Stevenson, "The Effects of Strongly Perturbing Substituents on Benzene" in "Systematics of the Electronic Spectra of Conjugated Molecules", Wiley, New York, N.Y., 1964.
(11) J. Petruska, *J. Chem. Phys.*, **34**, 1120 (1961).
(12) S. J. Strickler and R. A. Berg, *J. Chem. Phys.*, **37**, 814 (1962).
(13) J. Petruska, *J. Chem. Phys.*, **34**, 1111 (1961).
(14) E. A. Braude and F. Sondheimer, *J. Chem. Soc.*, 3754 (1955).
(15) C. Seliskar, O. Khalil, and S. P. McGlynn in "Excited States", Vol. I, E. Lim, Ed., Academic Press, New York, N.Y., 1974.
(16) H. Suzuki, "Electronic Absorption Spectra and Geometry of Organic Molecules", Academic Press, New York, N.Y., 1967, p 475.
(17) C. Katayama, private communication.
(18) For a detailed discussion on this point in the case of fluorescence emission in carboxylanthracene compounds, see T. C. Warner, T. Matthews, and B. Soller, *J. Phys. Chem.*, **80**, 533 (1976).
(19) For a comprehensive discussion see C. T. Lin and J. A. Stikeleader, *Chem. Phys. Lett.*, **38**, 561 (1976).

Confirmation of O^- Formation in γ-Irradiated 10 M NaOH/$H_2{}^{17}O$ Alkaline Ice Glass by Electron Paramagnetic Resonance Studies

S. Schlick* and Larry Kevan

Department of Chemistry, Wayne State University, Detroit, Michigan 48202 *(Received February 7, 1977)*

The EPR identification of $^{17}O^-$ in γ-irradiated 10 M NaOH glassy ice containing 34 atom % oxygen-17 is confirmed at both X and Q band. The ion is characterized by $g_\perp = 2.070$, $g_\parallel = 2.002$, and $A_\parallel = 99 \pm 3$ G. The spin density is largely localized in a 2p orbital on O^- (~0.69), but a significant fraction seems delocalized onto the surrounding matrix.

Introduction

The major species detected by electron paramagnetic resonance (EPR) in γ-irradiated $NaOH/H_2O$ glassy ices at 77 K are the trapped electron, O^-, and a small yield of hydrogen atoms.[1] Identification of the O^- radical ion is based upon comparison of the experimental g values of $g_\parallel = 2.002$ and $g_\perp = 2.070$ with those predicted theoretically, e.g., $g_\perp > g_\parallel \simeq g_e$ for the case of tetragonal symmetry.[2] O^- has been observed in a variety of surroundings such as in alkali halide single crystals[3] and adsorbed on various metal oxide surfaces.[4]

In this study we have analyzed the hyperfine structure of O^- in an oxygen-17 doped alkaline ice glass as well as the g anisotropy to provide confirmation of the O^- identification and a more detailed picture of the electronic structure and trapping site of O^- in this matrix.

Experimental Section

Water containing 40 atom % oxygen-17 from the Weizman Institute in Israel was used to make up 10 M NaOH solutions. The deuterium content in the ^{17}O enriched water was 90 atom % as measured by high-resolution nuclear magnetic resonance. In the 10 M NaOH solution the deuterium content was 80% and the ^{17}O content was 34%. Samples were prepared in 4.0-mm o.d. spectrosil quartz tubes.

Irradiations were carried out at 77 K in a ^{60}Co γ source at a dose rate of 0.2 Mrad/h to a typical total dose of 2.4 Mrad. EPR measurements were made at ~9 GHz on a Varian E-4 spectrometer and at ~35 GHz on a Varian E-9 spectrometer using 100-kHz field modulation. Typical microwave powers were 10–20 mW to enhance the O^- signal, which is not easily saturable, relative to the easily saturable trapped electron signal. Spectra at lower power have been studied previously.[5] All measurements were made at 77 ± 3 K either in liquid nitrogen or in a cold flow gas system.

Results

Figure 1a shows the X-band EPR spectrum of γ-irradiated 10 M NaOH ice made from water with 40 atom % ^{17}O at 10 mW microwave power. The $g_\perp$ and $g_\parallel$ lines for O^- as well as the splitting due to $A_\parallel$ of ^{17}O ($I = 5/2$) are indicated. Lines denoted by D are derived from the high (90%) deuterium content of the ^{17}O enriched water. Lines denoted by H are superpositions of H atom lines from the sample and from the quartz sample tube; they are unambiguously identified by their 507-G splitting.[1] The trapped electron is superimposed on $g_\parallel$ of O^-, but it is highly saturated at 10 mW microwave power and so does not show clearly.

Figure 2 shows saturation curves for lines $A_\parallel(1)$, $A_\parallel(2)$, $g_\perp$, and $g_\parallel$ and D(3). Line D(3) is easily saturated and can therefore be assigned to trapped deuterium atoms.[1] From the known deuterium atom splitting of 78 G the positions of the other two deuterium atom lines can be ascertained as shown. It is clearly seen that lines $A_\parallel(1)$, $A_\parallel(2)$ accompany lines $g_\perp$ and $g_\parallel$ since these four lines show little saturation. The intensity of the signal denoted by $g_\parallel$ is not exactly linear with $(\text{power})^{1/2}$ because in this region $g_\parallel$ from the O^- signal overlaps with the signal from the trapped electron. Therefore $A_\parallel(1)$, $A_\parallel(2)$ can be assigned to $^{17}O^-$ and the six $A_\parallel$ components of O^- can be picked out to completely account for all the lines in the spectrum of Figure 1. The larger intensity of the two low-field lines of the oxygen-17 sextet has also been observed for O^- adsorbed on a magnesium oxide surface and can be successfully reproduced by computer simulation.[6] The observed splitting of ^{17}O in the parallel direction is 98 ± 2 G and is similar to that reported previously for O^- on MoO (103 G[4]) and on MgO (96 G[6]).

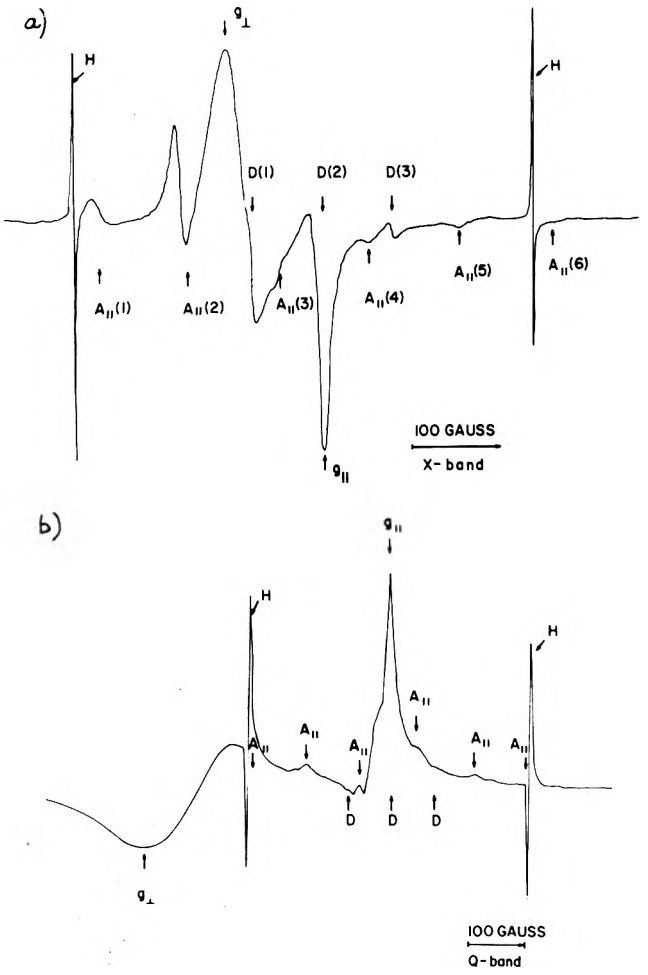

Figure 1. X-band (a) and Q-band (b) EPR spectrum of γ-irradiated (2.4 Mrad) 10 M NaOH/$H_2{}^{17}O$ at 77 K at 10 mW microwave power (>10 mW for the Q band). The lines due to H and D atoms are marked. The $g_\perp$ and $g_{||}$ components of O^- are marked along with the $A_{||}$ components of $^{17}O^-$.

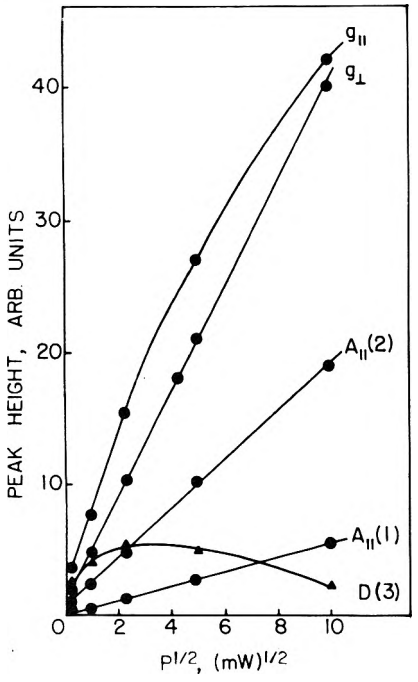

Figure 2. Microwave power saturation curves for five of the lines denoted in the EPR spectrum of Figure 1a.

The incompatibility of the **g** tensor with other all-oxygen molecules such as O_3^- and O_2^- as well as the observation of a large hyperfine splitting in the parallel direction confirms the previous assignment of O^-.

Figure 1b shows a Q-band spectrum at high microwave power, (>10 mW) at 77 K. Four of the expected six $A_{||}$ lines of $^{17}O^-$ are observed; the other two overlap the H atom lines. The measured splitting is 100 ± 1 G which agrees with the X-band results. As in X-band no additional splitting from the perpendicular direction is observed. It is important to note that the width of the $g_\perp$ signal does not change from normal (^{16}O) water to ^{17}O enriched water. Moreover, comparison of Figures 1a and 1b shows that the width of the perpendicular component of O^- is about 4 times bigger at Q band (~150 G) than at X band (~40 G). These observations suggest that there is an inhomogeneity in the O^- sites which is reflected in the $g_\perp$ value and that the experimental $g_\perp$ signal is an envelope of differing sites. The $A_\perp$ component for $^{17}O^-$ is expected to be small[2-4] (≲20 G) and therefore not observable for line widths of 40 to 150 G.

Discussion

The observed $A_{||}$ hyperfine splitting confirms the identification of the axially symmetric spectrum in γ-irradiated 10 M NaOH glassy ice as O^-. We now discuss the electronic structure of O^- in this matrix based on its **g** tensor and hyperfine tensor.

*O^- **g** Tensor.* Following previous work on O^- in crystals[3] we depict the electronic configuration as $2p_x{}^2 2p_y{}^2 2p_z{}^1$. For axial symmetry the $2p_x$ and $2p_y$ levels are degenerate and lie below $2p_z$ by energy ΔE. This configuration corresponds to a hole in the 2p levels which is equivalent to an electron in the inverted level system (i.e., $2p_z{}^1 2p_x{}^0 2p_y{}^0$). It is convenient to use the hole formalism to calculate the **g** tensor but we must remember that in this case ΔE is formally negative.[7] We calculate the **g** tensor to first order in $\lambda/\Delta E$ where λ is the spin–orbit coupling constant and obtain the following relations where $g_e = 2.0023$ is the g factor for a free electron:

$$g_{||} = g_{zz} = g_e$$

$$g_\perp = g_{xx} = g_{yy} = g_e - 2\lambda/\Delta E$$

The spin–orbit coupling constant for O^- is not known experimentally, but it has been estimated as $\lambda = 0.014$ eV from the atomic energies of the isoelectronic sequence of F, Ne^+, Na^{2+}, etc.[8] Since ΔE is negative due to our hole formalism $g_\perp > g_e$ and $g_{||} \sim g_e$ as found experimentally. From $g_\perp = 2.070$ and $\lambda = 0.014$ eV we find $\Delta E = 0.40$ eV.

No optical absorption from O^- in glassy NaOH/H_2O ices has been reported. However, an absorption spectrum attributed to O^- with a peak at 240 nm (5.17 eV) has been reported from pulse radiolysis studies of alkaline aqueous solutions containing N_2O and H_2O_2.[9] If this optical absorption is correctly assigned to O^- it is apparent that the electronic transition does not correspond to the $2p_{x,y} \rightarrow 2p_z$ transition in O^-.

The $g_\perp$ values for O^- in alkali halide crystals average 2.27 + 0.03[3] and on metal oxide surfaces average 2.03 ± 0.01.[2] O^- occupying an F^- site in a X-irradiated $3[Ca_3(PO_4)_2]\cdot CaF_2$ single crystal has also been reported with $g_\perp = 2.052$.[10] The results for O^- in NaOH/H_2O ice lie closest to this latter value, but it is clear that the magnitude of the axial field splitting can vary widely with the matrix.

^{17}O Hyperfine Splitting. The average of X- and Q-band data gives $|A_{||}| = 99 \pm 3$ G. $A_\perp$ could not be observed, perhaps because of a dominant contribution to the line width in the perpendicular direction from $g_\perp$ inhomogeneity.

In the absence of data for the full ^{17}O hyperfine tensor in O^-, it is impossible to obtain directly the isotropic

splitting and the anisotropic dipolar tensor. Nevertheless, the total splitting with the field along the axis of the 2p orbital can be separated into isotropic and dipolar contributions by the following approach.[11] For the dipolar contribution, values of 2β range form 103 to 120 G,[12] with the former value usually perferred.[13]

The isotropic splitting is due most probably to spin polarization and can be estimated from the relationship $a_0 = -41\rho_{2p}$, which has been shown to hold rather well for π radicals.[14] Thus we can write $A_{\parallel} = -(103 + 41)\rho_{2p} = -144\rho_{2p}$. Applying this to the observed $A_{\parallel} = 99$ G, we obtain $\rho_{2p} = 0.69$. The isotropic splitting thus calculated is −28 G. This value is close to the value of −24 G, obtained from data of ref 4, with the following choice of signs: $A_{\parallel} = -103$ G, $A_{\perp} = +15$ G.

Since the total spin density on O^- is less than 1 (0.69), the implication is that a considerable amount of spin is delocalized onto the surrounding matrix of O^- in alkaline ice glass.

Acknowledgment. This research was partially supported by the U.S. Energy Research and Development Administration under Contract No. E(11-1)-2086.

References and Notes

(1) L. Kevan in "Actions Chimiques et Biologiques des Radiations", Vol. 13, M. Haissinksy, Ed., Masson, Paris, 1969, pp 57–84; L. Kevan in "Radiation Chemistry of Aqueous Systems", G. Stein, Ed., Wiley-Interscience, New York, N.Y., 1968, pp 21–71
(2) J. H. Lunsford, *Catal. Rev.*, **8**, 135 (1973).
(3) J. R. Brailsford and J. R. Morton, *J. Chem. Phys.*, **51**, 4794 (1969); J. R. Brailsford, J. R. Morton, and L. E. Vannotti, *J. Chem. Phys.*, **49**, 2237 (1968).
(4) Y. Ben Taarit and J. H. Lunsford, *Chem. Phys. Lett.*, **19**, 348 (1973), and references therein.
(5) S. Schlick, P. A. Narayana, and L. Kevan, *J. Chem. Phys.*, **64**, 3153 (1976).
(6) N.-B. Wong and J. H. Lunsford, *J. Chem. Phys.*, **55**, 3007 (1971).
(7) A. Carrington and A. D. McLachlan, "Introduction to Magnetic Resonance", Harper and Row, New York, N.Y., 1967, pp 132–138.
(8) P. H. Kasai, *J. Chem. Phys.*, **43**, 3322 (1965).
(9) J. Rabani, *Adv. Chem. Ser.*, **No. 81**, 131 (1968).
(10) B. Segall, G. W. Ludwig, H. H. Woodbury, and P. D. Johnson, *Phys. Rev.*, **128**, 76 (1962).
(11) E. Melamud, S. Schlick, and B. L. Silver, *J. Magn. Reson.*, **14**, 104 (1974).
(12) P. B. Ayscough, "Electron Spin Resonance in Chemistry", Methuen, London, 1967, Appendix III.
(13) S. Schlick, *J. Chem. Phys.*, **56**, 654 (1972).
(14) E. Melamud and B. L. Silver, *J. Phys. Chem.*, **77**, 1896 (1973).

Photoinduced Isomerization of Ion Radicals. The Conversion from 1,3-Cyclohexadiene to 1,3,5-Hexatriene Cation Radicals

Tadamasa Shida,* Tatsuhisa Kato, and Yoshio Nosaka

Department of Chemistry, Faculty of Science, Kyoto University, Kyoto 606, Japan *(Received January 13, 1977)*

The cation radical of 1,3-cyclohexadiene isomerizes to the cation radical of *all-trans*-1,3,5-hexatriene upon photoexcitation with visible light. The conversion involves three intermediate cations of hexatriene having the conformations of cis–cis–cis, cis–trans–cis, and trans–cis–trans. All the cations of the triene exhibit similar but distinguishable electronic absorption spectra in the visible and the near-IR regions. The conformation of the cations as well as the photoconversion among them are consistently accounted for by INDO and CNDO/S calculations for the cations. Some kinetic analysis is made for two conformers in the photostationary state.

Introduction

Although the photochemical ring opening of 1,3-cyclohexadiene to 1,3,5-hexatriene is a familiar electrocyclic process with abundant documentations,[1] nothing is known about the behavior of the respective cation radicals under photoexcitation. In this work the cation radicals were newly produced in rigid matrices at low temperatures and the photoinduced conversion was studied by optical absorption spectroscopy. The absorption bands of the cation radicals appear in a convenient spectral region from the near-infrared through near-UV, which permits detailed studies on the wavelength dependence of the photoinduced conversion.

As a consequence of the present study the cation radical of 1,3-cyclohexadiene is found to convert ultimately to the cation radical of *all-trans*-1,3,5-hexatriene upon illumination with light of λ 400–500 nm:

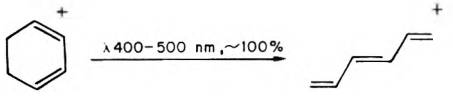

The above conversion, however, is not a single reaction, but involves three intermediate cationic species as shown in Scheme I. The intermediates B, C, and D are very sensitive to light and change as the arrows indicate. The electronic spectra of the four conformers B, C, D, and E are similar but are distinct enough to permit optical studies on the individual steps in the scheme. The potential surfaces calculated by the method of INDO and CNDO/S are consistent with the proposed scheme and account for

Scheme I

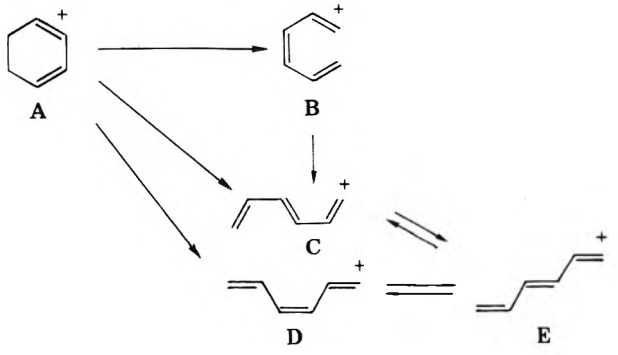

TABLE I: Excited States of Cation Radicals of Cyclohexadiene and Hexatriene

Molecule	State	Transition energy, eV	Oscillator strength	Major configurations
1,3-Cyclohexadiene[a] (A)	1^2B_2	2.04 (2.72)[b]	0.0304 (0.0208)	0.832 (0.850) $(\pi_1^1\pi_2^2)$ + 0.503 (0.492) $(\pi_1^2\pi_3^1)$
	2^2B_2	4.04 (3.53)	0.4452 (0.1318)	0.513 (0.518) $(\pi_1^1\pi_2^2)$ + 0.837 (−0.804) $(\pi_1^2\pi_3^1)$
1,3,5-Hexatriene (t-t-t) (E)	1^2B_g	1.70 (2.30)	0.0845 (0.0301)	0.852 (0.784) $(\pi_1^2\pi_2^1\pi_3^2)$ − 0.427 (0.518) $(\pi_1^2\pi_2^2\pi_4^1)$
	2^2B_g	2.87 (3.99)	0.7433 (0.6900)	0.438 (0.566) $(\pi_1^2\pi_2^1\pi_3^2)$ + 0.785 (0.772) $(\pi_1^2\pi_2^2\pi_4^1)$
1,3,5-Hexatriene (t-c-t) (D)	1^2A_2	1.70 (2.19)	0.0446 (0.0129)	0.859 (0.812) $(\pi_1^2\pi_2^1\pi_3^2)$ + 0.415 (0.481) $(\pi_1^2\pi_2^2\pi_4^1)$
	1^2B_2 (cis band)	2.98 (3.87)	0.0259 (0.0182)	0.807 (0.687) $(\pi_1^1\pi_2^2\pi_3^2)$ + 0.343 (−0.570) $(\pi_1^2\pi_2^2\pi_5^1)$ + 0.276 (−0.413) $(\pi_1^2\pi_2^1\pi_3^1\pi_4^1)$
	2^2A_2	2.92 (3.89)	0.6163 (0.5420)	0.425 (−0.528) $(\pi_1^2\pi_2^1\pi_3^2)$ + 0.803 (0.802) $(\pi_1^2\pi_2^2\pi_4^1)$
1,3,5-Hexatriene (c-t-c) (C)	1^2B_g	1.68 (2.16)	0.0799 (0.0149)	0.856 (−0.729) $(\pi_1^2\pi_2^1\pi_3^2)$ − 0.424 (0.597) $(\pi_1^2\pi_2^2\pi_4^1)$
	2^2B_g	2.86 (3.62)	0.4993 (0.4270)	0.435 (0.632) $(\pi_1^2\pi_2^1\pi_3^2)$ + 0.801 (0.740) $(\pi_1^2\pi_2^2\pi_4^1)$

[a] The structure of the cation radical of 1,3-cyclohexadiene was assumed to be the same as that of neutral molecule determined by Oberhammer and Bauer.[11] The geometrical parameters for all hexatrienes were assumed as C–C 1.46 Å, C=C 1.35 Å, C–H 1.10 Å, <C–C–C 120°. π represents molecular orbitals for π electron. [b] The values with and without parentheses correspond to the results obtained by CNDO/S[13] and Longuet-Higgins-Pople type calculations.[2] The observed order of transition energies which increases as C < D < E (cf. Figure 8) is reproduced by CNDO calculation, e.g., C (3.62 eV) < D (3.89 eV) < E (3.99 eV), although the absolute agreement with the experiment is slightly better with the LHP type calculation than with CNDO.

the photodynamic processes of the system.

Recapitulation of the Method of Rigid Matrix

Since all the cation radicals in Scheme I are reactive under normal conditions, the formation of the cations and their spectroscopic measurement were carried out in a glassy matrix frozen at 77 K.[2] In this section a general brief explanation of the method of matrix isolation will be made.

A matrix consisting of equivolumes of CCl_3F and CF_2BrCF_2Br is chosen in the present study for the following reasons:[2,3] (1) When the freon mixture, abbreviated as FM, is γ irradiated at 77 K, the electron ejected upon ionization of FM is scavenged by reaction 2. The

$$FM + \gamma \rightarrow FM^+ + e^- \quad (1)$$

$$e^- + CF_2BrCF_2Br \rightarrow CF_2BrCF_2 + Br^- \quad (2)$$

counterpart positive charge migrates by resonant charge transfer among the freon molecules until it encounters a solute molecule of 1,3-cyclohexadiene or 1,3,5-hexatriene[4]

$$FM^+ + S \rightarrow FM + S^+ \quad (3)$$

Reaction 3 is exothermic by the amount of energy approximately equal to the difference of ionization potentials between FM and the solute. The relatively high ionization potential of freons[5] ensures irreversible charge localization at the solute molecule. Since the yield of ionization in FM per unit radiation energy absorbed can be determined (cf. Experimental Section), the yield of S^+ is also obtained by scavenging all the positive charge in reaction 1 and measuring the absorbed energy by dosimetry.[20] For complete scavenging of the migrating charge concentrations of solute of the order of 20 mM were found to be sufficient. Because of the relatively low concentration of the solute the radiation energy is absorbed almost entirely by the major component of FM to result in its ionization as a main event. (2) Since there is no C–H bond in both constituents of the freon mixture, the matrix does not absorb appreciably in the spectral region from 270 to 2700 nm allowing optical measurement of solute cations over a wide spectral range. (3) It is known that a perhalogenated solvent such as FM exerts little solute–solvent interaction.[6] Therefore, the vibronic structure of the solute cations is not obliterated allowing easy identification of the absorption spectrum.

In particular, the following features should be noted. The solute molecule is oxidized to its cation radical without any oxidizing agent, thus the system remains relatively clean. The ions produced are immobilized in the frozen medium, thus preventing any reactions with other components in the system. By-products other than the ions S^+ and Br^- are neutral species absorbing only in the UV region, thus absorptions appearing in the longer wavelength region can be solely attributed to the solute cation.

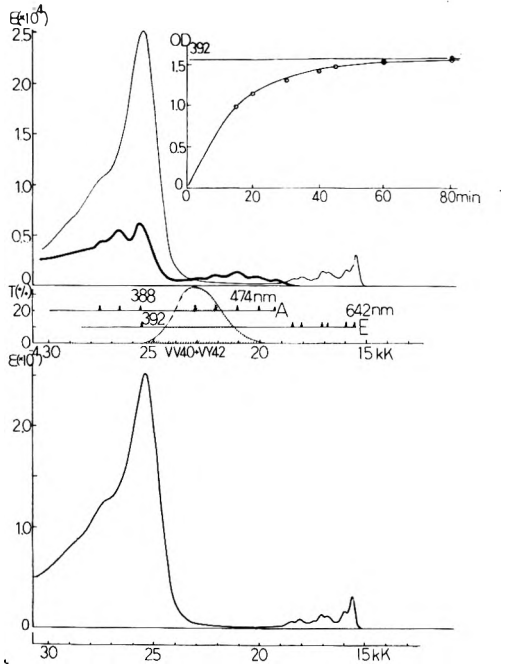

Figure 1. (a. Upper). The bold curve shows the absorption spectrum of the cation radical of 1,3-cyclohexadiene (A). The fine curve is the same as above after prolonged illumination with a 100-W tungsten lamp and glass filters VV40 + VY42 whose transmission efficiency $T(\%)$ is given by the shaded area. The main absorption maxima of both spectra are indicated by the stick spectra which are the schematic representation of spectra in Figure 8. The inset shows the increase of optical density at 392 nm with time of illumination through the filters mentioned. (b. lower). Absorption spectrum of the cation radical of *all-trans*-1,3,5-hexatriene (E). The abscissas for both Figure 1a and 1b are in units of 10^3 cm^{-1} and are in common.

Experimental Results

1. *Conversion of 1,3-Cyclohexadiene to 1,3,5-Hexatriene Cations.* The absorption spectra of γ-irradiated frozen solutions of 20 mM 1,3-cyclohexadiene and *all-trans*-1,3,5-hexatriene in FM appear as the bold curves of Figure 1a and 1b, respectively. All spectra in this and the following figures were obtained by subtracting the background absorption prior to irradiation from the spectra obtained after irradiation. According to the general consideration on the formation of solute cation (cf. Re-

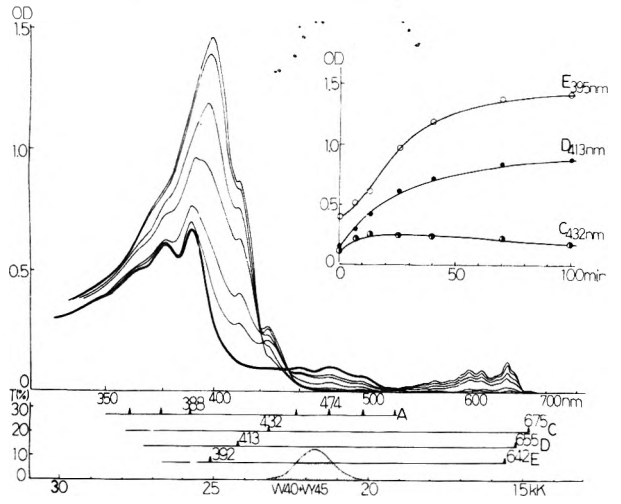

Figure 2. Spectral changes of A (bold curve) with illumination through filters VV40 + VY45. See the caption for Figure 1.

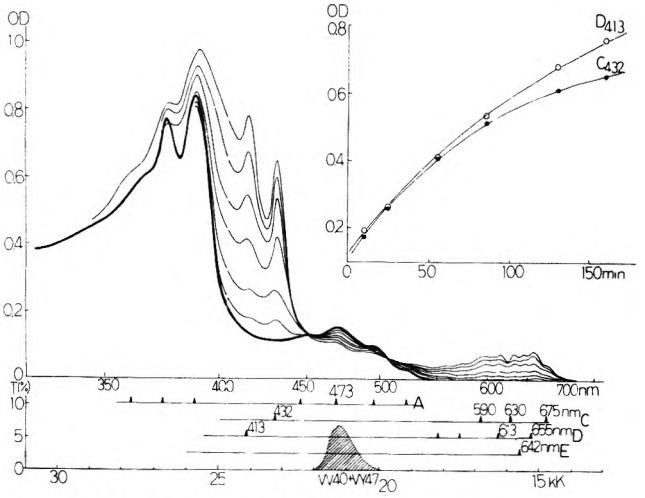

Figure 3. Spectral changes of A (bold curve) with illumination through filters VV40 + VY47. See the caption for Figure 1. The ordinate of the inset is the increment of optical densities of C and D obtained by subtraction of the remaining background absorption of A.

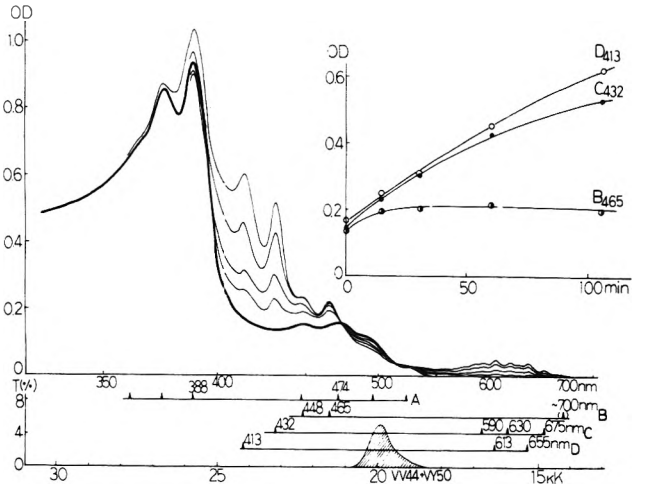

Figure 4. Spectral changes of A (bold curve) with illumination through filters VV44 + VY50. See the caption for Figure 1.

capitulation) they are assigned to the cation radicals of the diene and triene. It is obvious that the absorption at 420–550 nm and at λ <420 nm of the diene and the absorption at 520–650 nm and at λ <420 nm of the triene are due to lower π electronic transitions as a semiempirical Longuet-Higgins–Pople type calculation tabulated in Table I indicates. In Figure 1 (and in the following figures) the stick spectra denote the absorption maximum in units of nm. The redundant representation is intended to assist the identification of closely absorbing species.

When the sample yielding the bold curve in Figure 1a was bleached with tungsten light through glass filters VV40 + VY42 whose transmission efficiency is shown by the shaded area (λ 390–500 nm), the spectrum changed to that shown by the fine curve which is almost identical with the spectrum in Figure 1b. The inset of Figure 1a demonstrates the growth of the absorption at 392 nm as a function of illumination time. The optical density at the leveling-off point agrees with that measured for a hexatriene solution irradiated in the same cell and with the same radiation dose. The agreement of the photoinduced spectrum with the spectrum in Figure 1b indicates that all the cation radicals of 1,3-cyclohexadiene, denoted A, have been converted to the cation radicals of *all-trans*-1,3,5-hexatriene, denoted E, under illumination with λ 390–500 nm.

The wavelength of the exciting light obtained with the above filters is relatively broad. Use of a sharper band width (VV40 + VY45, λ 430–500 nm) gave a different absorption spectrum exhibiting two new absorption maxima at 432 and 413 nm as Figure 2 illustrates. The details of the vibrational structure at λ >550 nm are slightly different from those in Figure 1. The dependence of the absorptions on the illumination time and the reference to the result in the following figures indicate that the spectra in Figure 2 comprise two new species designated for convenience C (432 nm) and D (413 nm). Both accompany small absorption peaks at λ >550 nm as indicated by the stick spectra. The overlap of the absorption due to A, C, D, and E prevents a precise determination of the constituents, but the inset gives a rough interrelation among the components where C and D are measured by the increment of OD_{432} and OD_{413}, respectively, and E by OD_{392} after a correction for the overlapping absorption of A.

The significant difference between the effect of the broader (VV40 + VY42) and the narrower (VV40 + VY45) bandpass filters led us to test the effect of attenuating the band width of the exciting light. Illumination with filters VV40 + VY47 (λ 445–500 nm) gave the result shown in Figure 3. Although the spectral features are similar to those of early stages in Figure 2, the accumulation of C and D is larger and the growth of E is slower. Further attenuation of light by using filters VV44 + VY50 (λ 470–550 nm) revealed new absorption maxima at 465 and 448 nm as Figure 4 shows. Referring to the result discussed in connection with Figures 5 and 6 (see below), they are ascribed to species B. Although not apparent in Figure 4, the absorptions at 465 and 448 nm seem to be associated with a very weak and structureless absorption at 550–750 nm (cf. Figure 8).

All the above filters transmit wavelengths corresponding to the first absorption band of A. To see the effect of excitation on the second excited state of A, filters VV40 + UVD1A (λ 320–400 nm) were used to obtain the result shown in Figure 5. The accumulation of B, C, and D is similar to the result in Figure 4.

2. *Photochemical Behavior of the Intermediates.* Species B, C, and D are intermediates in the sense that they all turn, ultimately, to E upon illumination with light corresponding to their absorption bands. Figure 6 summarizes the rather complicated behavior of the intermediates upon selective photoexcitation.

When a sample exhibiting the absorption of A, B, C, D, and E (cf. Figure 4 or 5) was bleached with filters VR65

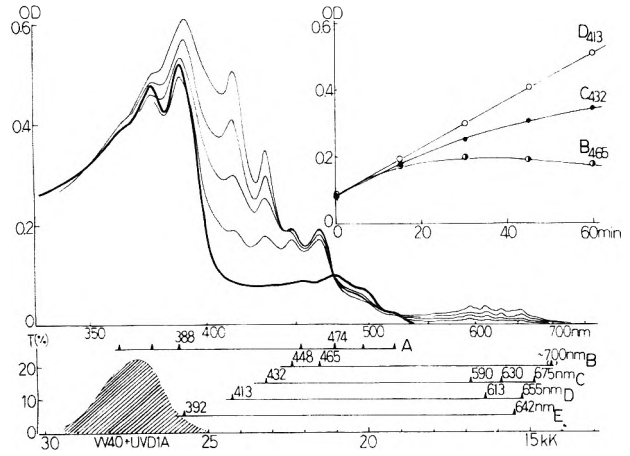

Figure 5. Spectral changes of A (bold curve) with illumination through filters VV40 + UVD1A. See the caption for Figure 1.

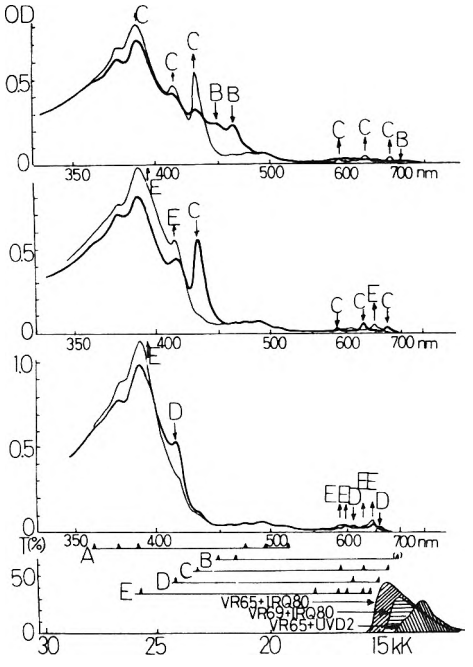

Figure 6. (a, top) Spectral changes induced by illumination of samples exhibiting the absorptions A, B, C, and D (bold curve) with tungsten light through filters VR65 + UVD2. Intermediate curves such as those in Figures 2–5 have been omitted. (b, middle) Effect of illumination of the sample corresponding to the fine curve of Figure 6a with light through filters VR69 + IRQ80. (c, bottom) Effect of illumination of the sample corresponding to the fine curve of Figure 6b with light through filters VR65 + IRQ80. The upward and downward arrows indicate the increase and decrease of the peaks which are identified as denoted by the symbols (cf. Figure 8). The wavelengths in nm for the absorption maxima in the stick spectrum have been omitted (cf. Figures 1–5). The transmission efficiency curves of the filters used are shown collectively at the bottom.

+ UVD2 (λ 680–1000 nm), the spectrum changed from that of the bold to the fine curve in Figure 6a. This result indicates that the disappearing species B absorbs at wavelengths as long as λ >680 nm and that B transforms to C upon illumination. Successive bleaching of the above sample with filters VR69 + IRQ80 (λ 660–850 nm) caused the spectrum to change from that of the bold curve to fine curves in Figure 6b. As will be shown in Figure 8 which is a collection of the resolved spectra of each species, wavelengths of λ >660 nm are absorbed effectively only by C. Therefore the change in Figure 6b is attributed to a photoinduced transformation from C to E. The apparent constancy of the absorption at 413 nm, ascribed to D, may be due to the fact that the exciting light does not correspond to the absorption band of D (cf. Figure 8). When the sample corresponding to the last stage in Figure 6b was bleached with slightly shorter wavelengths using filters VR65 + IRQ80 (λ 620–850 nm), species D faded quickly but soon attained a constant level of absorption (cf. Figure 6c).

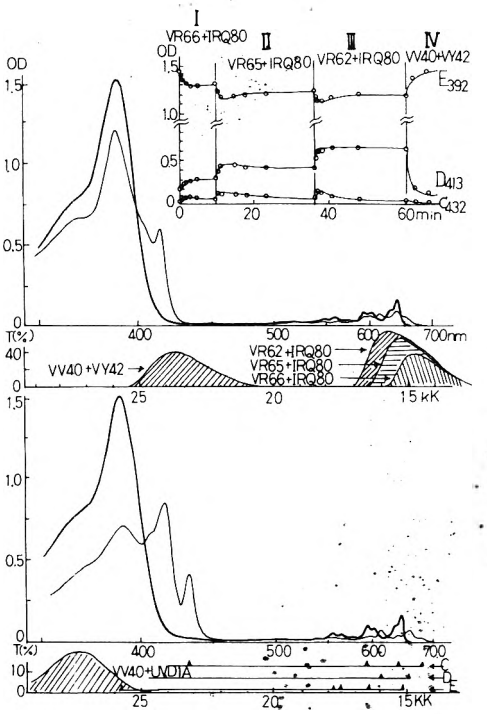

Figure 7. (a) Spectral changes of E (bold curve) with the illumination through filters VR66 + IRQ80, VR65 + IRQ80, VR62 + IRQ80, and VV40 + VY42. To avoid complexity only an intermediate curve corresponding to the last of the series of illumination with VR62 + IRQ80 is shown in the fine curve. (b) Spectral changes of E (bold curve) with illumination through filters VV40 + UVD1A. Since light through the filters is not effectively absorbed by C and D, the spectrum after illumination shown in the fine curve comprises mainly C and D.

Samples corresponding to the bold curve in Figure 6a were also bleached with filters VV40 + VY47 (λ 440–500 nm) to observe the effects of excitation of the absorption bands of B at 448 and 465 nm (cf. Figure 8). Quick disappearance of B accompanied a concomitant increase in C similarly to the result in Figure 6a. After the complete disappearance of B continued illumination caused a slow decrease in A and an increase in C and D which is essentially the repetition of the run described in connection with Figure 3. Excitation of C and D by their second absorption bands at 432 nm for C and at 413 nm for D using filters VV40 + VY44 (λ 420–500 nm) or VV40 + VY42 (λ 390–500 nm) resulted in the disappearance of both C and D to increase E. Prolonged illumination after the disappearance of C and D eliminated the underlying A also to enhance the absorption of E which is the same experiment as that described in Figure 1.

3. *Photochemical Behavior of the Hexatriene Cation.* Figure 7 demonstrates the effect of illumination of E with wavelengths corresponding to its first absorption band. Filters VR66 + IRQ80 (λ 630–850 nm) transmit light which is barely absorbed by E at the long wavelength edge of the first absorption band. The effect of illumination is shown in Figure 7 and in section I of the inset. It is seen that a photostationary state between C, D, and E is attained. With slightly shorter wavelengths (VR65 + IRQ80, λ 620–850 nm) a new stationary state was brought about as section II of the inset demonstrates. Still shorter wavelengths (VR62 + IRQ80, λ 590–850 nm) stepped up the yield of D measured by OD_{413} and depressed that of C

measured by OD_{432}. The different behavior of C and D will be explained in the Discussion. As soon as the wavelength became short enough to excite C and D by their second absorption band, a drastic change in the absorption took place as shown in section IV in the inset of Figure 7a.

Photoexcitation of E by its second absorption band using filters VV40 + UVD1A (λ 320–400 nm) yielded the result shown in Figure 7b. In contrast to the excitation with longer wavelengths described above an appreciable amount of C as well as D persisted under steady illumination.

Discussion

1. *Experimental Attempts for Assignment of the Intermediates.* Since all the intermediate species B, C, and D are photoconverted to the t–t–t conformer cation,[21] synonymously called E, and since they are derived from the cation radical of cyclohexadiene, they are reasonably assumed to be light sensitive geometrical conformers of the hexatriene cation radical. The recovery of C and D from E by optical excitation of the latter also adds to the credibility of this assumption. Since the band width of light through the filters is relatively broad, doubt might arise that other light sensitive absorbers might have been bleached out during the illumination. However, the self-consistency of the result described below seems to ensure that the species involved are A to E in all cases.

The possibility that the photoexcitation of the cation radical of cyclohexadiene leads to the formation of cation radicals of bicyclohexenes may be ruled out on the grounds that the latter cations, being ethylenic in nature, would not absorb in the visible region contrary to our observations.

There are six possible planar conformers for the cation radical of hexatriene, that is, symmetrical c–c–c, c–t–c, t–c–t, and t–t–t as well as asymmetrical t–c–c and t–t–c. If one could prepare each conformer separately and oxidize it by reaction 3 to its cation radical, the identification of the intermediates would be straightforward. However, the only conformers that can be isolated are t–t–t and t–c–t[7] and the latter isomerizes gradually to the former at room temperature. Other conformers are probably so unstable that they are not obtainable under ordinary conditions.

Since t–c–t and t–t–t conformers can be isolated by gas chromatography (cf. Experimental Section), parallel experiments for the production of their cation radicals were carried out. The result, however, turned out to be an apparent enigma: the t–c–t conformer in the FM matrix gave the same spectrum as that of the t–t–t conformer shown in Figures 1b and 7 (it was checked, of course, that the former conformer had not isomerized to the latter during sample preparation). The result, however, may be accounted for consistently by the consideration of the exothermicity of positive charge transfer from freon to hexatriene molecules (reaction 3); as is stated in the Recapitulation section, the exothermicity is roughly equal to the difference of the ionization potentials between both molecules. A survey of standard tables for the ionization potential reveals values of 11.77 ± 0.02 eV for CCl_3F, ~11.0 ± 0.5 eV for CF_2BrCF_2Br, and 8.4 ± 0.2 eV for hexatriene. Thus, the solute cation at the moment of charge transfer may contain an energy of a few electron volts.[5,8] The energetic cation of t–c–t conformer may surmount the potential barrier separating the two conformations to assume the more stable t–t–t conformation (cf. subsection 3 below).

The final assignment of the intermediates will be made by having recourse to the analysis in terms of molecular orbital calculations in subsections 3 and 4. Before proceeding to the analysis the procedure for resolution of superposing spectra will be mentioned.

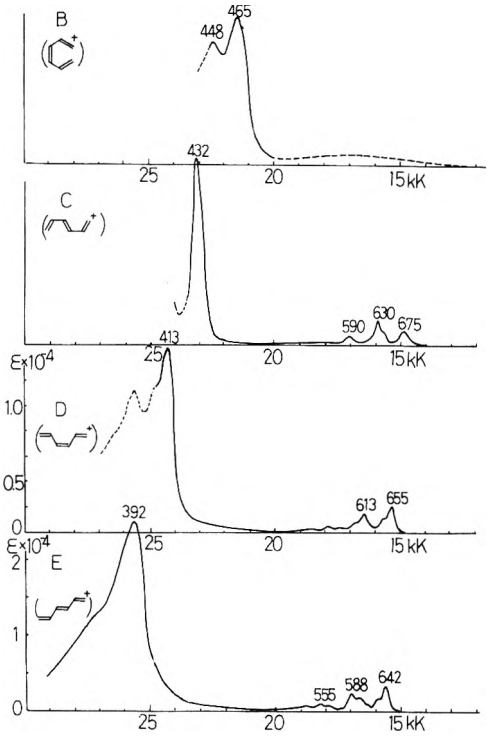

Figure 8. Collection of the resolved spectra of B, C, D, and E which are concluded to be the hexatriene conformers as shown in the parentheses.

2. *Resolution of Spectra and Reaction Scheme.* The concomitant change of absorption of more than two species as demonstrated in the insets of Figures 2–5 indicates that the attenuated light is absorbed simultaneously by several species which absorb at the wavelengths of the filtered light.

The spectrum at the final stage of section III in Figure 7a was assumed to comprise D and E. Referring to the spectrum of E in Figure 1b, the spectrum of D was extracted with the aid of a computer in combination with a graphic display unit. Likewise, spectra containing the constituents A, C, D, and E (Figures 3, 6b, and 6c) and those containing C, D, and E (Figure 7) were computer processed to deduce the spectrum of C. The remaining component B was obtained from an analysis of Figures 4, 5, and 6a. Because of the overlap of the spectrum the complete determination of each component was not feasible and the broken curve in Figure 8 implies the uncertainty inherent in the determination. In Figure 8 the extinction coefficients of A and E have been determined on the basis of the ionization G value of the FM matrix (cf. Recapitulation and Experimental Section). The counterbalance relation between the increasing and decreasing species gives a rough estimation of the extinction coefficients of the other components also. The extinction coefficients of D in Figure 8 were determined referring to the results in Figures 2–6. It is noted that the spectral feature of B is markedly different from those of the other components C, D, and E. The extremely broad and weak first absorption band indicates that the equilibrium nuclear configuration in the first excited state is significantly different from that in the ground state.

Scheme I in the Introduction is constructed by referring to the following features of experiment.

(1) The nonzero initial slope for the formation of B, C, and D as shown in the inset of Figures 2–5 indicates that the three are produced simultaneously from A. If con-

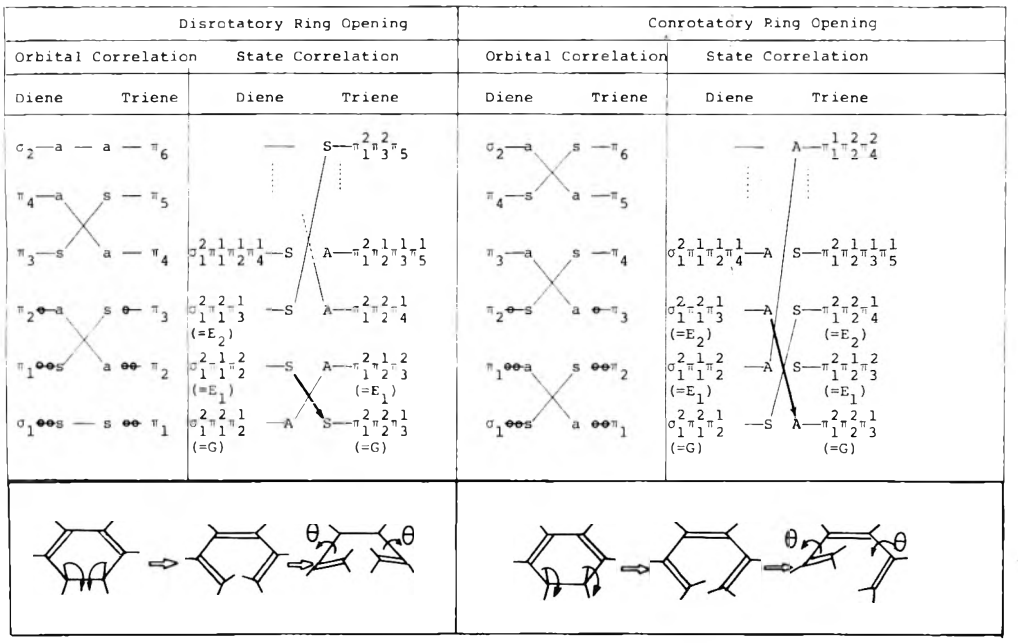

Figure 9. Correlation diagram between the cation radicals of 1,3-cyclohexadiene and 1,3,5-hexatriene. σ and π denote the respective molecular orbitals. The arrows indicate that the first (E_1) and second (E_2) excited states of the diene produce the triene in the ground state (G) by disrotatory and conrotatory bond scission, respectively.

secutive processes such as A → B → C and A → B → D were major reactions for the formation of C and D, the dependence of the formation on the illumination time would be such that the decline of B accompanied a rapid increase of C and D.

(2) However, part of C is produced also by way of B → C as indicated by the transformation in Figure 6a. The elusiveness of B may be attributed to the efficient transformation from B to C under illumination with $\lambda \simeq 400$–800 nm.

(3) C and D convert independently to E upon the excitation with wavelengths of their absorption (Figure 6b and 6c), and the path from C to D seems prohibited.

(4) The pair of C and E and that of D and E attain equilibrium under illumination (Figure 7).

3. *Ring Opening Process and INDO Calculation.* Consideration of conservation of orbital symmetry,[9] or equivalently the analysis in terms of a HOMO–LUMO interaction,[10] leads to the correlation of the cation radicals of 1,3-cyclohexadiene and 1,3,5-hexatriene as shown in Figure 9. The electronic ground, the first excited, and the second excited states of both cations may be described approximately by the configurations denoted by G, E_1, and E_2 in Figure 9. The bold connecting lines indicate that the cation of cyclohexadiene in the first and the second excited states is destined for the ground state of the hexatriene cation by disrotatory and conrotatory ring opening, respectively.

At the instance of bond scission of A, whether it is disrotatory or conrotatory, the triene cation will be in a c–c–c like conformation.[11]

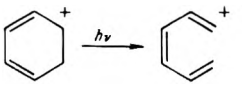

(4)

Starting from the c–c–c conformer the six planar conformers mentioned earlier may be defined by giving the dihedral angle ϕ around the central double bond and two rotational angles θ around the carbon–carbon single bonds. The three sets of coordinate shown in Figure 10 may be self-explanatory; the coordinate in Figure 10a is for the conformational change involving only one rotation around the single bond while those in Figure 10b and 10c are for

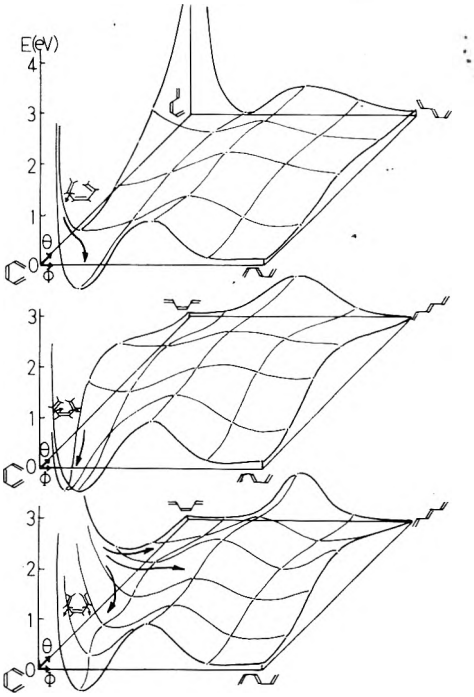

Figure 10. (a, top) The potential energy surface for the cation radical of hexatriene in the ground state as calculated by the INDO OPEN program with the assumption that only one of the two carbon–carbon single bonds undergoes rotation by θ. The surface was drawn by smoothly connecting the dots which represent the calculated energies. The arrow on the surface indicates qualitatively a possible reaction route initiated by reaction 4 in the text. The corners correspond to four planar conformers. (b, middle) Same as above except for the assumption that the two rotational angles θ rotate in the same direction. (c, bottom) Same as above except that the two angles θ rotate in the opposite sense. The three arrows indicate the routes to reach three products B, C, and D in the text.

the simultaneous rotations. There are two possibilities: that the two angles rotate in the same sense and in the opposite sense. The ordinate represents the total energy, the sum of the electronic and nuclear repulsion energies, of the ground state of the hexatriene cations. It was calculated by the INDO OPEN program of Pople and Beveridge,[12] the nuclear repulsion energy being approx-

imated by the point charge model. All bond angles were assumed to be 120° and the bond lengths were fixed as C–C 1.46 Å, C=C 1.35 Å, and C–H 1.10 Å. Fixing the bond angle and length may be unrealistic for the deforming hexatriene cation radicals, however, we consider that the calculation will provide a general grasp of the relative stability of the cations.

Since A in the photoexcited state produces B, C, and D simultaneously as emphasized in subsection 2, there should be three paths for the "nascent" hexatriene cation produced by reaction 4 in its electronic ground state which terminate at three potential minima. Only the diagram in Figure 10c seems to meet the requirement. The analysis of the MO calculation indicates that most of the instability of the t–c–c conformer in Figure 10a comes from the nuclear repulsion between the hydrogen atoms on C_2 and C_6. In this context it is pointed out that the conformation of t–c–c does not occur usually in related polyenic compounds such as retinals and carotenoid systems. The disrotatory bond scission predicted for the first excited state of A would entail the rotation of the two angles θ in the opposite sense to mitigate severe nuclear repulsion between the oncoming hydrogen atoms on the terminal carbon atoms (cf. the scheme in Figure 9). By the same token the conrotatory scission predicted for the second excited state of A would favor rotation in the same direction in which case only one product of a c–c–c like conformation should be expected (Figure 10b). The fact that the excitation of A to its second excited state produces C and D (cf. Figure 5) indicates that the scission in the second excited state is preceded by rapid internal conversion of A from the second excited state to the first. Thus, the fate of photoexcited A, whether in the first or in the second excited state, seems to be characterized by the potential surface in Figure 10c.

Now that there are three potential minima and three intermediates to be compared, there remains the one-to-one correspondence between them. This was performed by calculations for electronic excited states of hexatriene cations which will be described in the following.

4. *CNDO/S Calculation.* Figure 11 illustrates the potential surfaces of hexatriene cations as calculated by the CNDO/S OPEN-SHELL program by Jaffé and his coworkers.[13] Not only the surface for the ground state but also those for the two low-lying excited states are shown. (A few other excited states of forbidden character have been omitted in Figure 11.) It is noted that the total energies in the vicinity of $\phi = \theta = 0$ become unrealistically small which suggests the failure of the CNDO approximation owing to the closeness of the nuclei. The nuclear repulsion energy was assumed to be proportional to the electron–electron repulsion energy. The point charge approximation and the Dewar formula for the nuclear repulsion were also tested but the results were even worse than above. Except for the corner of $\phi = \theta = 0$ the general feature of the potential surface for the ground state is similar between the INDO and CNDO calculations. The fact that the uppermost surface resembles the surface for the ground state is a natural consequence of the even alternant π electronic system (cf. Table I for the character of the second excited state).

If one ignores the irrational corner, the rest of the surface provides a consistent background for the reaction scheme assumed; according to Figure 11 the illumination of E with λ 630–850 nm (VR66 + IRQ80) will bring the cation onto the surface of the first excited state where the cation will take the route toward potential minima nearby. The attainable minima will be at $\phi \simeq 45°$ and $\theta \simeq 180°$ and

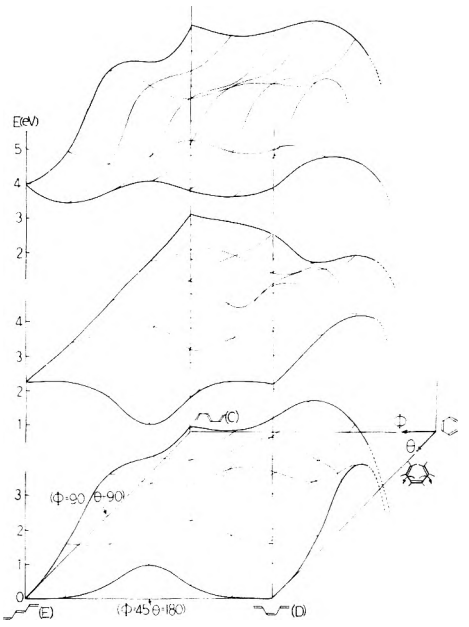

Figure 11. The potential energy surfaces for the cation radicals of hexatriene in the ground (G), the first excited (E_1), and the second excited states (E_2) as calculated by CNDO/S program with the assumption that the two rotational angles θ rotate in the opposite sense. Note that the ordinates for the three surfaces are successively shifted to avoid overlap.

at $\phi \simeq 90°$ and $\theta \simeq 90°$. Deactivation at these points will produce t–c–t and t–t–t conformers for the former and c–t–c and t–t–t for the latter. This is comparable with the experimental result shown in Figure 7a where two species C and D appear upon illumination of E. The illuminating red light of λ 630–850 nm was also absorbed by the newly produced C and D so that the three conformers soon attained a photostationary state (cf. inset of Figure 7). Such an attainment of the stationary state can be explained by the potential surfaces for the ground and the first excited states in Figure 11.

The gradual decrease in the absorption of C and D in sections II and III of Figure 7a might be accounted for as follows. Some of the photoexcited C, D, and E may be deactivated without suffering a conformational change on the surface of the first excited state. Such a vertical deactivation would produce an electronic ground state with thermal activation. The "hot" cation thus formed may surmount the potential barrier for the ground state. In view of the slight instability of C and D relative to E (cf. Figure 11) thermally activated C and D may convert to E in the ground state. This is remniscent of the failure of the formation of the t–c–t cation by the amply exothermic reaction 3 (cf. subsection 1 of Discussion).

The remaining intermediate B corresponds to the potential minimum near the c–c–c corner in Figure 10c. The similarity of its spectrum to that of the cation of cyclooctatriene shown in Figure 8 supports this assignment.

For the final allocation of C and D to the two conformations t–c–t and c–t–c one has to rely on the general consideration on the results of experiment and calculation; the prediction of instability of c–t–c relative to t–c–t (cf. Figure 10) and the elusiveness of C in comparison with D suggest that C and D correspond to c–t–c and t–c–t, respectively. Moreover, the CNDO/S calculation for t–t–t, t–c–t, and c–t–c cations indicates that the strong near-UV absorption band shifts toward red in this order. (cf. Table I. Note, however, another calculation with the PPP approximation gives a different order.) According to Figure 11 both c–t–c and t–c–t in the first excited state do not appear to be convertible which is consistent with the

TABLE II: Vibration Frequencies in cm^{-1} of the Excited 1,3,5-Hexatriene (t-t-t) Molecule and the Cation Radical

Fundamental frequency[a]	Neutral molecule (1^1B_u)[7]	Cation radical ($1B_g$ of E)[b]
ν_1	1626	1636
ν_2	1232	1090
ν_3	350	345

[a] ν_1, ν_2, and ν_3 are assigned[7] as totally symmetric double bond stretching, single bond stretching, and in-plane bending, respectively. [b] The values for the cation radical are not corrected for the overlap of bands.[7]

experimental finding that C and D are not related in their formation. The appearance of C and D from E upon the excitation to the second excited state with λ 320–400 nm (VV40 + UVD1A) as shown in Figure 7b is explicable in terms of the internal conversion of E from its second excited to the first excited state (cf. potential surfaces for E_1 and E_2 in Figure 11).

Figure 12 demonstrates relevant spectra concerning the cation radical of hexatriene. It is interesting to note that the vibrational structure of the first absorption band of E is very similar to that of the first excited singlet state ($1B_u$) of the neutral hexatriene molecule in the t–t–t conformation recently observed by Gavin and Rice.[7] The two spectra of Figure 12a and 12b and the frequencies in Table II suggest that the fundamental vibrational modes are little affected by the π electronic charge on the cation. Figure 12c and 12d show the photoelectron[14] and photodissociation spectra[15] observed for the gaseous cation radical of hexatriene. They bear general resemblance to the spectrum in Figure 12b obtained for the condensed phase. The solvent shift is fairly small as mentioned in the Recapitulation in connection with a perhalogenated solvent. An even more pertinent spectrum was reported recently by Allan and Maier.[19] They observed the emission spectrum of the cation radical of t–t–t hexatriene in the gas phase. The mirror image relation holds good between the emission and absorption spectra. The present work together with that of Dunbar and Allan-Maier indicate that the first excited state of the hexatriene cation has three fates: photoisomerization, photodecomposition, and photoemission. The fraction undergoing isomerization will be estimated in the following subsection.

5. *Kinetic Consideration.* The photostationary state corresponding to section III of Figure 7a yields two species D and E with a slight amount of C. If C is ignored, the following kinetic equations can be derived:

$$\begin{aligned} d[E]/dt &\simeq -10^3\alpha_{ED}I_0r^{-1}(1 \\ &- e^{-2.303(\epsilon_E[E]+\epsilon_D[D])r})\epsilon_E[E](\epsilon_E[E] \\ &+ \epsilon_D[D])^{-1} + 10^3\alpha_{DE}I_0r^{-1}(1 \\ &- e^{-2.303(\epsilon_E[E]+\epsilon_D[D])r})\epsilon_D[D](\epsilon_E[E] \\ &+ \epsilon_D[D])^{-1} \end{aligned} \quad (5)$$

$$d[D]/dt = -d[E]/dt \quad (6)$$

where [E] and [D] are the molar concentrations of species E and D, respectively; t is the illumination time in seconds; α_{ED} and α_{DE} are the quantum efficiencies when photoexcited E and D become D and E via the potential surface for the first excited state; I_0, is the intensity of the incident beams in units of einstein cm^{-2} s^{-1} which are transmitted through the filters VR62 + IRQ80 to be absorbed by D and E; r is the optical path length in cm;

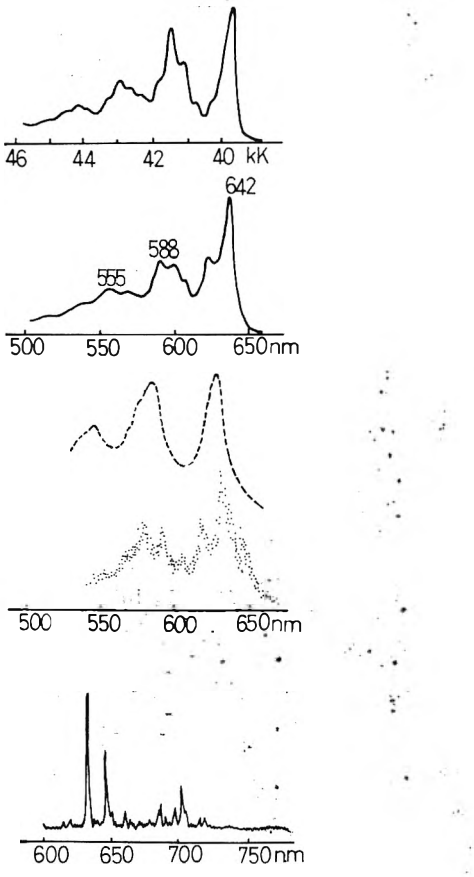

Figure 12. Pertinent spectra concerning the molecule and the cation radical of 1,3,5-hexatriene. (a) The first absorption band of neutral all trans hexatriene reproduced from ref 7. (b) Magnification of the first absorption band of the spectrum of E at the bottom of Figure 8. (c) Photoelectron spectrum of hexatriene reproduced from ref 14. (d) Photodissociation spectrum of the hexatriene cation radical in the gas phase.[14] (e) Emission spectrum of the cation radical of t–t–t hexatriene.[19]

and ε is the molar extinction coefficient per cm. The range of the effective wavelength is determined by the filters and the absorption spectrum of D and E.

Since at infinite illumination time both $d[E]/dt$ and $d[D]/dt$ tend to zero as shown in section III of Figure 7a, the following equation is obtained where the products $\epsilon_D[D]r$ and $\epsilon_E[E]r$ have been replaced with the respective optical densities:

$$\alpha_{ED}(\lambda)/\alpha_{DE}(\lambda) = (OD_D(\lambda)/OD_E(\lambda))_{t=\infty} \quad (7)$$

It is emphasized that the ratio varies with the effective wavelength λ which, for the filters VR62 + IRQ80, ranges from 590 to 670 nm. Because of the overlap of the absorptions of D and E the ratio in eq 7 is difficult to determine for the wavelength range mentioned. However, one may estimate the ratio, with reference to Figure 8, by measuring the more discernible peak at 413 nm due to D and the one at 392 nm due mainly to E. The ratio thus determined for the filters used turned out to be $\alpha_{ED}/\alpha_{DE} \simeq 0.5$.

For longer wavelengths the ratio tends to become smaller (cf. sections I and II vs. III in the inset of Figure 7a). This may be attributed to the depression of α_{ED} because the insufficient energy of longer wavelengths may prevent the excited E from undergoing isomerization to D on the surface of the first excited state.

During the initial of illumination eq 6 is simplified as follows:

$$d[D]/dt \simeq 10^3\alpha_{ED}I_0r^{-1}(1 - e^{-2.303\epsilon_E[E]r}) \quad (8)$$

Hence, the increment of D as measured by the optical

density at 413 nm can be expressed as

$$\Delta OD_{D,413} \simeq 10^3 \alpha_{ED} I_0 \epsilon_{D,413}(1 - e^{-2.303\epsilon_E[E]r})\Delta t \quad (9)$$

In eq 9 the product $I_0(\lambda)(1 - e^{-2.303OD_E(\lambda)})$ should be summed up over the effective wavelengths λ 590 nm (determined by the cutoff filters) to 670 nm (determined by the end of the absorption), however, an average value (= I_0 in eq 8 and 9) was used whose sum over the wavelengths spanned by the filters VR62 + IRQ80 is equal to the total intensity $I_0^t = 1.10 \times 10^{-7}$ (einstein cm^{-2} s^{-1}) (cf. Experimental Section). Accordingly an average for $\overline{OD_E(\lambda)}$ was substituted to $\epsilon_E[E]r$ in eq 9. $\Delta OD_{D,413}$, Δt, and $\overline{OD_E(\lambda)}$ from Figure 7a and $\epsilon_{D,413}$ from Figure 8, together with the total intensity I_0^t, yields the quantum efficiency as $\alpha_{ED} \simeq 0.089$ which, in turn, yields $\alpha_{DE} \simeq 0.2$.

Experimental Section

1. *Materials.* 1,3-Cyclohexadiene from Tokyo Kasei was distilled under vacuum to remove stabilizers and polymeric impurities. The distillate showed a single peak on VPC analysis using a 90-cm column packed with β,β′-oxydipropionitrile.[16] 1,3,5-Hexatriene from K & K Laboratory was also trap-to-trap distilled. It contained about 60% t–t–t and 40% t–c–t conformers which could be separated by the chromatographic column described above.[16]

The components of the freon mixture, CCl_3F and CF_2BrCF_2Br, were obtained from Daikin, Inc., and were used without purification because a preliminary test showed that distillation modified from that described by the previous workers[3] did not affect the result of the experiment significantly.

Tetramethyl-*p*-phenylenediamine free base was obtained from a commercial dihydrochloride and was purified by sublimation. Potassium Reineckate used for actinometry was synthesized according to the literature.[17]

2. *Optical Measurements.* Purified 1,3-cyclohexadiene and 1,3,5-hexatriene were dissolved in FM to a concentration of 20 mM and were degassed by freeze–thaw cycles in a Suprasil optical cell having an optical path length of 1–2 mm. The path length was calibrated by employing a suitable colored solution. The deaerated solution was frozen to a transparent glassy solid at 77 K and its absorption was measured using a Cary 14 RI and a Hitachi EPS-3T spectrophotometer before and after irradiation with ^{60}Co γ rays.

The irradiated sample was subsequently photobleached using various Toshiba glass filters in combination with a 100-W tungsten lamp. Heat rays were absorbed by a water filter and stray light was reduced by constructing a suitable filter mount.

3. *Actinometry.* The popular ferric trioxalate actinometer[18] is not suitable for the present system because the wavelengths transmitted through the filters VR62 + IRQ80 are beyond the reach of the above actinometer. Although the Reineckate actinometer[17] covers longer wavelengths, it is also incapable to measure the near-infrared light. Therefore, the intensity of the incident beam in eq 5–9 was determined in the following way. Reineckate solutions placed in the same position as in the bleach experiment were photoreduced using the same lamp and the filters VV40 + VY45 (λ 430–500 nm). Reference to the emission spectrum of a 100-W tungsten lamp[18] and the transmission efficiency curves of filters VV40 + VY45 and VR62 + IRQ80 gives the ratio of the total flux I_0^t transmitted through the two sets of filter which turned out to be 1:45.5. Since I_0^t for the former set was determined as 2.42×10^{-9} einstein cm^{-2} s^{-1} by Reineckate actinometry, the total flux through the filters VR62 + IRQ80 was found to be 1.10×10^{-7} einstein cm^{-2} s^{-1}.

4. *Determination of ε for the Cation Radicals.* As described in the Recapitulation section all cation radicals were produced in the frozen freon mixture by eq 3. Knowing the yield of the ionization in eq 1 per unit absorbed radiation energy, that is, the *G* value in units of ions/100 eV, the amount of solute cation produced by eq 3 can be calculated by measuring the absorbed energy. The ionization *G* value in FM was determined by using tetramethyl-*p*-phenylenediamine free base as a standard positive charge scavenger.[4] The value obtained was *G*(ionization) = 2.09. The radiation dosimetry was carried out using a Fricke solution taking proper account of an abnormally high density of the freon mixture at 77 K.

Acknowledgment. 1,3,5-Hexatriene was a gift from Dr. Mark Seats of the University of Chicago. The CNDO/S program was offered by Professor Hans H. Jaffé of the University of Cincinnati. Dr. Masashi Imamura of the Institute of Physical and Chemical Research permitted us to use the facilities of the institute. Several comments of Professor Hiroshi Kato of Nagoya University were most valuable. We are greatly indebted to the people mentioned. This work was supported by grants from the Kurata Foundation and the Nishina Memorial Foundation.

References and Notes

(1) (a) R. Srinivasan, *J. Am. Chem. Soc.*, **82**, 5063 (1960); **83**, 2806 (1961); **84**, 3982 (1962); (b) P. Datta, T. D. Goldfarb, and R. S. Boikess, *ibid.*, **93**, 5189 (1971); (c) J. E. Baldwin and S. M. Krueger, *ibid.*, **91**, 6444 (1969).
(2) T. Shida and S. Iwata, *J. Am. Chem. Soc.*, **95**, 3473 (1973).
(3) A. Grimison and G. A. Simpson, *J. Phys. Chem.*, **72**, 1776 (1968).
(4) T. Shida and W. H. Hamill, *J. Chem. Phys.*, **44**, 2369, 4372 (1966).
(5) K. Watanabe, T. Nakayama, and J. Mottl, *J. Quant. Spectrosc. Radiat. Transfer*, **2**, 369 (1962).
(6) C. W. Lawson, F. Hirayama, and S. Lipsky, *J. Chem. Phys.*, **51**, 1590 (1969).
(7) R. M. Gavin, Jr., S. Risemberg, and S. A. Rice, *J. Chem. Phys.*, **58**, 3160 (1973).
(8) R. P. Blaunstein and L. G. Christophorou, *Radiat. Res. Rev.*, **3**, 69 (1971).
(9) R. Hoffmann and R. B. Woodward, *Acc. Chem. Res.*, **1**, 17 (1968).
(10) K. Fukui, "Theory of Orientation and Stereoselection", Springer, Berlin, 1975.
(11) H. Oberhammer and S. H. Bauer, *J. Am. Chem. Soc.*, **91**, 10 (1969).
(12) J. A. Pople and D. L. Beveridge, "Approximate Molecular Orbital Theory", McGraw-Hill, New York, N.Y., 1970.
(13) H. M. Chang, H. H. Jaffé, and C. A. Masmanidis, *J. Phys. Chem.*, **79**, 1118 (1975).
(14) R. C. Dunbar, *J. Am. Chem. Soc.*, **98**, 4671 (1976).
(15) M. Beez, G. Bieri, H. Bock, and E. Heilbronner, *Helv. Chim. Acta*, **56**, 1028 (1973).
(16) J. C. Hwa, P. L. Benneville, and H. J. Sims, *J. Am. Chem. Soc.*, **82**, 2537 (1960).
(17) E. E. Wegner and A. W. Adamson, *J. Am. Chem. Soc.*, **88**, 394 (1966).
(18) C. A. Parker, "Photoluminescence of Solutions", Elsevier, Amsterdam, 1968.
(19) M. Allan and J. P. Maier, *Chem. Phys. Lett.*, **43**, 94 (1976).
(20) The technique for the measurement of solute ions is established in radiation chemistry. See, e.g., *J. Phys. Chem.*, **73**, 4311 (1969).
(21) The notation t–t–t implies that four successive carbon atoms in hexatriene are in the trans–trans–trans conformation.

Investigation of Physical Triplet Quenching by Electron Donors

Ulrich Steiner,* Gerhard Winter, and Horst E. A. Kramer

Institut für Physikalische Chemie der Universität Stuttgart, Pfaffenwaldring 55, D-7000 Stuttgart 80, West Germany *(Received July 26, 1976; Revised Manuscript Received December 2, 1976)*

Absolute radical yields, as determined by flash spectroscopy, are reported for the reaction of the thionine triplet $^3TH^+$ and its protonated form $^3TH_2^{2+}$ with a variety of electron donors in methanolic solution. The yields are extrapolated to infinite donor concentrations. Two methods of obtaining absolute yields are described. The different yields with different donors are due to partial physical quenching of the triplets in the electron transfer reaction. The results are discussed in terms of different models, capable of explaining bimolecular intersystem crossing processes. A triplet exciplex as an intermediate in the electron transfer reaction is favored.

Introduction

For the study of fast electron transfer processes the use of electronically excited species is most convenient, as they can be rapidly produced by short excitation pulses and are more reactive than the ground state molecules, the electron affinity, or ionization potential respectively, being more favorable for the electron transfer reaction by the amount of the excitation energy.

Since the first experimental proof by Leonhardt and Weller[1] of radical formation in the fluorescence quenching of perylene by amines in polar solvents, electron transfer reactions with excited singlet states have been extensively studied.[2] In general the quantum yield of radical formation is quite low even under conditions of complete fluorescence quenching and does not exceed absolute values of 0.5.[3] This is mainly due to the possibility of the originating radical pair to undergo fast recombination to the energetically lower ground state competing with the formation of free radicals by diffusive separation.

Besides radical formation and deactivation to the ground state fast bimolecular triplet formation constitutes a third channel of electronic deactivation in the quenching of excited singlet states by electron donors or acceptors.[4]

For electron transfer reactions of excited triplet states much less experimental information about the mechanism is available than in the singlet case. This is because, due to their lower energy, triplet states are less reactive than the corresponding excited singlet states and in the case of long singlet lifetimes, the triplet reaction cannot be separated from the singlet reaction.

In the case of triplets reacting with electron donors or acceptors in polar solvents there are two reaction channels: electron transfer, giving the radicals, or bimolecular physical quenching giving the ground state molecules. The physical quenching is an intersystem crossing process and from this point of view corresponds to the fast triplet formation in the case of singlet reactions, rather than to the spin conserving ground state deactivation. In a radical pair originating from an overall triplet encounter complex the unpaired electron spins are still in a triplet alignment. Hence a fast geminate recombination to the ground state molecules is spin forbidden and one should expect higher yields of free radicals than in the case of singlet reactions.[5] In this paper we report the absolute quantum yields of radical formation and physical quenching of the thionine triplet $^3TH^+$ and its protonated form $^3TH_2^{2+}$ in their reactions with a variety of electron donors in methanolic solution, as determined by flash spectroscopy.

We expect that systematic investigations of this kind will improve understanding of the mechanisms of both bimolecular intersystem crossing and electron transfer.

The intermediates of thionine photoreductions have been extensively studied.[6-9] A list of the intermediates relevant to the present work is given in Table I. Unless the concentrations of the electron donors are very high, the thionine triplet is the primary reacting state. As the lifetime of the first excited singlet state is very short (2.4×10^{-10} s[6,37]) almost complete triplet quenching can be achieved with many electron donors before singlet quenching is observed.

Acids of different strengths are required to protonate thionine and its photochemical intermediates. Strong acids are needed to protonate the thionine ground state TH^+ (pK in water is -0.3[9]) but the corresponding equilibrium in the triplet state

$$^3TH^+ + H^+ \rightleftharpoons {}^3TH_2^{2+}$$

has a pK^* of 7.0 in methanol.[10] By the acceptance of an electron the triplet forms are converted to the corresponding forms of semireduced thionine. The equilibrium between the semireduced thionine TH· (basic semithionine) and its protonated form TH_2^+· (acid semithionine) corresponds to a pK^* of 10.4 in methanol.[10] The rate constants for electron transfer reactions with the thionine triplets $^3TH^+$ and $^3TH_2^{2+}$, in the following denoted as "basic" and "acid" triplet, are found to be correlated with the free enthalpy of these reactions[11] analogously to singlet quenching by electron donors as reported by Rehm and Weller.[12] As the acid triplet has a higher redox potential than the basic form one can understand its higher reactivity, which is observed especially with donors, which react fairly slowly with the basic triplet.[10,13]

For the study of the quantum yields of radical formation and physical quenching the comparison of the triplet forms $^3TH^+$ and $^3TH_2^{2+}$ appear to be interesting cases of variation of the electron accepting component, as these excited species can be transformed into each other by an adiabatic reaction.

Experimental Section

The flash apparatus was the same as described by Kramer.[14] A Kodak Wratten filter No. 15 was inserted between the flash lamp and the photolysis cell to absorb light of wavelengths shorter than 500 nm. The solutions investigated were deaerated by passing N_2 (oxygen content lower than 5 ppm) through them for 0.5 h.

Chemicals. Methanol (Merck p.A.) was used as solvent throughout. Thionine was purified according to Endriss.[15] The purity of the donor compounds was of the highest commercial grade; additional purification is given in parentheses: 9,10-dimethylanthracene (DMA, EGA, recrystallized twice from ethanol), diazabicyclo[2.2.2]octane

TABLE I: List of Symbols for Thionine and Its Intermediates

TH^+	Thionine	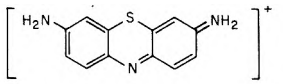	
$^3TH^+$	Basic triplet	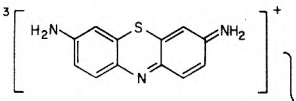	$pK_a^* = 7.0$ (methanol)[a]
$^3TH_2^{2+}$	Acid triplet	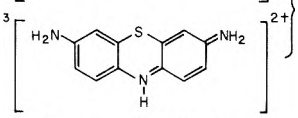	
$TH\cdot$	Basic semithionine	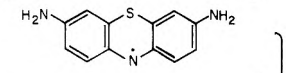	$pK_a^* = 10.5$ (methanol)[a]
$TH_2^{+}\cdot$	Acid semithionine	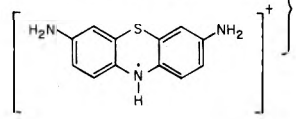	

[a] The asterisk is used to indicate pH and pK values in methanol.[17,18]

(DABCO, EGA), 1,3-diphenylisobenzofurane (EGA), azulene (Fluka), *p*-bromoaniline (Merck), bromobenzene (Merck, distilled in vacuo), allylthiourea (Merck, twice recrystallized from water), selenourea (Merck, recrystallized from water under an N_2 atmosphere), hydroquinone (Merck, recrystallized twice from water under an N_2 atmosphere). *p*-Methoxydimethylaniline was synthesized in our laboratory according to the procedures in ref 16 and purified by sublimation. The phosphoric acid was 96% (Merck p.A.). Buffer solutions of pH* 8.6 in methanol (for definition, see ref 17) were prepared according to Broser and Fleischhauer.[18] The resulting solutions were 0.015 M in phenylacetic acid and 0.005 M in sodium methylate.

Methods. The donor substances were chosen to fulfill the following conditions: Complex formation between donor–acceptor molecules in the ground state should be excluded. This was ensured by checking the additivity of the absorption spectra. With donor concentrations at which reaction with the thionine triplet occurs almost quantitatively, no appreciable singlet quenching should be observed. This was examined by measuring the thionine fluorescence. No donors, whose rate constants with the basic thionine triplet were less than 8×10^6 M^{-1} s^{-1}, were investigated in compliance with the latter condition.

For the determination of the yields of the electron transfer reaction

$$^3TH^+ + R \rightarrow TH\cdot + R^{+}\cdot \quad (1)$$

or

$$^3TH_2^{2+} + R \rightarrow TH_2^{+}\cdot + R^{+}\cdot \quad (2)$$

measurements of radical concentrations are preferable to those of concentrations of the reacting molecules, since the percentage changes of the latter are small. The quantity of semithionine produced proved to be a suitable measure for yields with different donors. Due to its strong absorption and the long wavelength position of its absorption band (see Figure 1) the acid form of semithionine $TH_2^{+}\cdot$ is more suitable than the basic form $TH\cdot$, since the absorption maxima of the cation radicals of the donors are at shorter wavelengths.

As was shown in an earlier paper,[19] in unbuffered methanolic solutions electron transfer reactions with the basic thionine triplet $^3TH^+$ yield the basic semithionine $TH\cdot$. The difference in pK^* between triplet and semithionine makes it possible, however, to find a pH* at which the basic semithionine is quantitatively protonated, while the basic triplet is not protonated.[10] Therefore the reactions of the basic triplet were investigated in methanolic solutions, buffered at pH* 8.6 (the buffer concentration was 0.02 M). As the protonation is very fast, it is still the reaction of $^3TH^+$ with the donor R which determines the rate of formation and the yield of the detected radicals $TH_2^{+}\cdot$:

$$^3TH^+ + R \rightarrow \left[TH\cdot + R^{+}\cdot \xrightarrow[H^+]{\text{fast}} \right] TH_2^{+}\cdot + R^{+}\cdot \quad (3)$$

To produce the acid triplet we used 0.1 M phosphoric acid in methanol. Under this condition protonation occurs in the triplet state, not in the ground state. Again the protonation is very fast and the reaction of $^3TH_2^{2+}$ with the donor is rate determining:

$$\left[^3TH^+ + R \xrightarrow[H^+]{\text{fast}} \right] {}^3TH_2^{2+} + R \rightarrow TH_2^{+}\cdot + R^{+}\cdot \quad (4)$$

The lifetime of the two triplet forms in the presence of the corresponding buffer or acid concentrations, given above, was determined to be 12 μs in the absence of any quencher. The lifetime of the semithionine radicals (initial slope of the decay curve, converted into a first-order rate constant—the order of the decay is not uniform) was in all cases longer than 1 ms, so that the yield of semithionine could be measured conveniently after complete triplet reaction.

The molar extinction coefficients of the basic triplet $^3TH^+$ and the acid semithionine $TH_2^{+}\cdot$, respectively, were determined by simultaneously measuring the optical density changes at 780 and 600 nm (maximum of ground state absorption). For this purpose the monitoring light beam was split behind the photolysis cell in order to measure the intensity by two monochromator photomultiplier assemblies. Solutions of thionine (2.5 to 4×10^{-6} M) were used. Semithionine was produced by adding 5×10^{-4} M 9,10-dimethylanthracene to the solution, buffered at pH* 8.6. (The absorption of the DMA cation at 780 nm amounts to less than 3% of the semithionine absorption, as can be seen if a basic solution containing 5×10^{-5} M sodium methylate is used. In this case only the basic form of the semithionine $TH\cdot$ is formed, which does not absorb at 780 nm.[7] Hence the absorption observed is due to the DMA cation radical only. From its absorption at 780 nm it can be concluded that, according to the optical density spectrum given in ref 20, the absorption at 600 nm is also negligible relative to the thionine ground state absorption.)

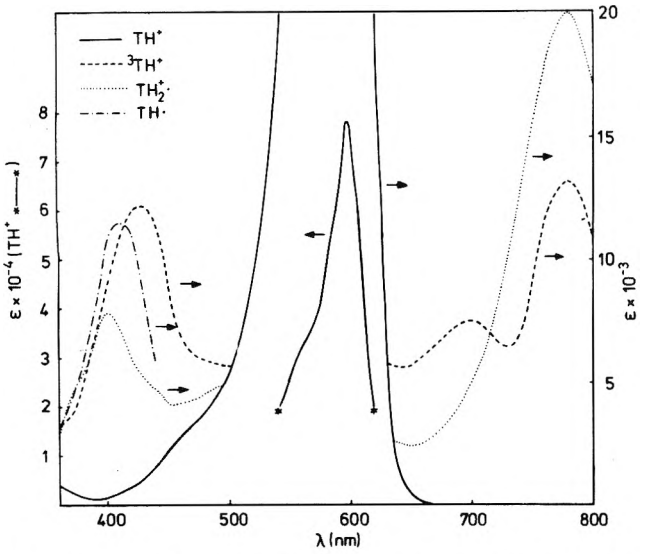

Figure 1. Absorption spectra of thionine ground state TH^+, basic triplet $^3TH^+$, basic semithionine TH·, and acid semithionine TH_2^+· in methanol. The spectra were taken with dye concentrations of 2×10^{-5}, 6×10^{-6}, 4×10^{-6}, and 5×10^{-6} M. respectively. The two forms of semithionine were produced by DABCO (2×10^{-3} M), for TH· the methanol was unbuffered, for TH_2^+· the buffer had a pH* of 8.6 (see Experimental Section). The spectra of the intermediates were taken in oxygen free solutions, they are corrected for ground state absorption.

The concentrations of the intermediates were calculated, assuming that the optical density change at 600 nm is entirely due to the disappearance of thionine ground state. This yields a lower bound of the concentration of the intermediates and hence an upper bound of their extinction coefficients ($\epsilon_{780}(^3TH^+) = 13200$, $\epsilon_{780}(TH_2^+\cdot) = 20000$). The spectra of the intermediates (Figure 1) were measured with higher concentrations of thionine. Therefore accurate measurements in the region of the 600-nm peak of the ground state absorption were not possible. In the spectral region, however, where the absorption of the ground state is comparable to that of the intermediates, the spectra of the intermediates could be obtained by correcting the measured change in optical density for the calculated change in the ground state absorption. If the extinction coefficients used for the intermediates were too high, the corrected spectra should be curved downward in the region of the sharp rise of the ground state absorption. This is not the case (see Figure 1). So we can assume that the extinction coefficients obtained by the procedure described above are fairly accurate.

Evaluation of the Quantum Yield. The concentration of radicals produced by constant flash intensity is proportional to the quantum yield of radical formation only if the concentration of the absorbing ground state does not change appreciably during the flash duration. (In the case of appreciable bleaching during the flash, triplet molecules deactivated to the ground state might become excited again. Such an effect would increase the apparent radical yield of substrates exhibiting strong physical quenching compared to substances with a better radical forming ability.) Flash intensity therefore was kept small, so that not more than 10% of the thionine molecules were excited by a single flash.

Extrapolation to Infinite Donor Concentration. When evaluating the yield of semithionine produced, one has to take into account that even without adding any electron donor, a certain amount of semithionine is formed. This is presumably due to a partially occurring dismutation reaction of dye triplets with the ground state dye (the so-called DD process[21]). At constant concentration of the ground state this process may be considered to be quasi-monomolecular.

Scheme I

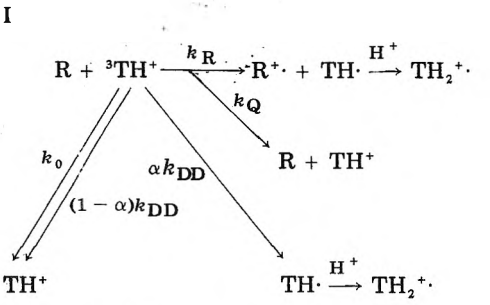

To calculate the radical yield for the basic triplet we made use of kinetic Scheme I. For the reactions of the acid triplet, according to eq 4, the protonation of the basic triplet is the first step. The acid triplet $^3TH_2^{2+}$, thus produced, is then subject to the same reactions as the basic triplet in Scheme I. The schemes differ only in that the protonation occurs at the semithionine stage in the first case and at the triplet stage in the second case.

The rate constants in Scheme I refer to the following processes: k_0, monomolecular triplet decay to the ground state; k_{DD}, quasi-monomolecular quenching by reaction of the triplet with ground state molecules (DD process); α, fraction of radical formation in the DD process; k_R, radical formation by the reaction with the donor; k_Q, physical quenching by the donor. (It should be noted that it is kinetically equivalent whether the last two processes are treated as independent or as proceeding via a common intermediate.)

The hypothetical triplet concentration present after the flash if the triplet had infinite lifetime will be denoted $[^3TH^+]_0$. One obtains for $[TH_2^+\cdot]$, the acid semithionine concentration after the completed triplet reaction:

$$[TH_2^+\cdot] = \frac{\alpha k_{DD} + k_R[R]}{k_0 + k_{DD} + (k_R + k_Q)[R]}[^3TH^+]_0 \qquad (5)$$

Writing

$$x = [TH_2^+\cdot]/[^3TH^+]_0$$

$$x_0 = \alpha k_{DD}/(k_0 + k_{DD})$$

$$a = k_R/(k_0 + k_{DD})$$

$$b = (k_R + k_Q)/(k_0 + k_{DD}) \qquad (6)$$

one obtains

$$x = (x_0 + a[R])/(1 + b[R]) \qquad (7)$$

or

$$1/(x - x_0) = b/(a - bx_0) + 1/((a - bx_0)[R]) \qquad (8)$$

$1/(x - x_0)$ plotted against $1/[R]$ must give a straight line. Denoting the semithionine absorption produced with a donor by E, and the corresponding quantity for donor free solutions by E_0, this linear relationship must hold also for $1/(E - E_0)$ vs. $1/[R]$, because E and E_0 are proportional to x and x_0, respectively. Thus it is possible to extrapolate to E_∞, i.e., E for $[R] \to \infty$. The half-quenching concentration of the donor $[R]_{1/2}$ can be obtained according to Figure 2. It is related to the triplet lifetime τ_0 in quencher free solution by the equation:

$$[R]_{1/2}(k_R + k_Q) = k_0 + k_{DD} = 1/\tau_0 \qquad (9)$$

From the measured value of the lifetime τ_0 and the half-quenching concentration the sum of the quenching rate constants $(k_R + k_Q)$ can be calculated. This extrapolation procedure was applied to most of the sub-

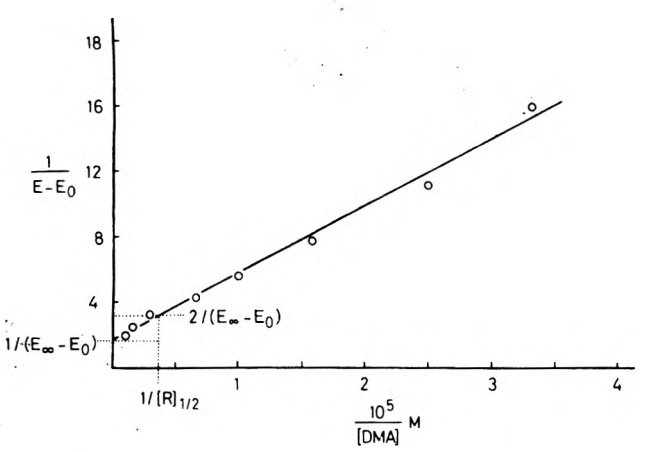

Figure 2. Illustration of the extrapolation procedure for obtaining the semithionine absorption produced in the limiting case of infinite donor concentration. The determination of the half-quenching concentration from this plot is also shown. (Quencher DMA, $[TH^+] = 2 \times 10^{-5}$ M.)

stances. In the case of donors with radical yields of less than 30% this procedure could no longer be employed, since the measured changes of the quantity of semithionine produced varied too little. The sum of the quenching rate constants was then obtained directly from measurements of the triplet lifetime dependence on the donor concentration in nonbuffered solutions. With the known value of the quenching rate constant, determined by the latter method, donor concentrations could be chosen at which the limiting case of a quantitative reaction between triplet and donor was almost realized and the singlet reaction was still negligible. The acid semithionine absorption E obtained in buffered solutions is related to E_∞, the corresponding absorption for $[R] \to \infty$, by

$$E_\infty = E + (E - E_0)\frac{1/\tau_0}{(k_R + k_Q)[R]} \tag{10}$$

Absolute Values of the Quantum Yields. The absolute quantum yield of radical formation from the triplet state when the donor concentration approaches infinity is given by

$$\eta_R = \frac{k_R}{k_R + k_Q} = \frac{[TH_2^{+}\cdot]_\infty}{[^3TH^+]_0} = \frac{\epsilon'}{\epsilon}\frac{E_\infty}{E_0'} \tag{11}$$

$[TH_2^{+}\cdot]_\infty$ is the concentration of acid semithionine produced with donor concentrations extrapolated to infinity. E_0' is the hypothetically obtainable triplet absorbance in the absence of any quenching process, and ϵ and ϵ' are the molar extinction coefficients of semithionine and triplet, respectively. It was found convenient to carry out the determination of the absolute value of the limiting quantum yield $k_R/(k_Q + k_R)$ for one standard substance with the basic triplet form and to compare the extrapolated values of the other donors with this standard. The standard substance chosen was DMA, because of its high radical yield and the stability of its solutions. E_0' was determined using solutions without quencher. The procedure is illustrated in Figure 3. The change of the optical density E' at 780 nm in quencher free solutions and with low flash intensity (negligible depletion of the ground state) is described by the differential equations:

$$dE_T/dt = c_1 I(t) - c_2 E_T \tag{12}$$

$$dE_S/dt = c_3 E_T \tag{13}$$

and

$$E' = E_T + E_S \tag{14}$$

where $I(t)$ is the flash intensity, given in arbitrary units

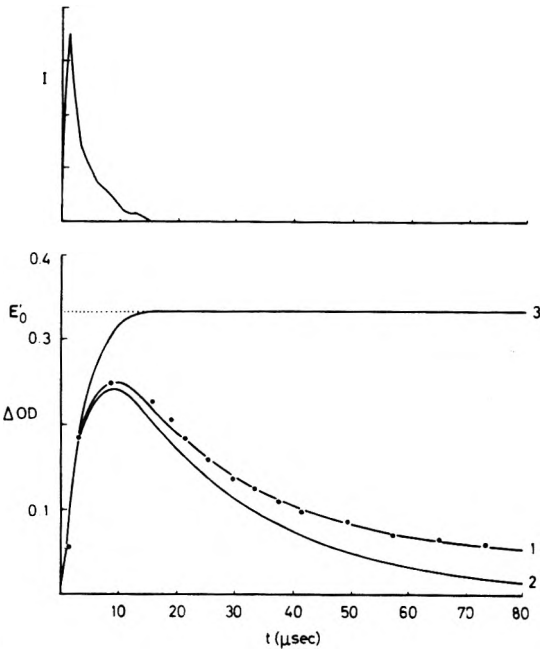

Figure 3. Determination of total concentration of triplets produced by a flash. ΔOD at 780 nm is plotted vs. time for a solution without quencher. (●) Experimental, $[TH^+] = 4 \times 10^{-5}$ M; computer simulation: curve 1, ΔOD due to triplet $^3TH^+$ plus semithionine $TH_2^{+}\cdot$; curve 2, ΔOD due to the triplet alone; curve 3, ΔOD due to the triplet alone, if infinite lifetime is assumed. The upper part of the figure shows the time dependence of the flash intensity.

and obtained by recording the flash stray light. E_T and E_S are the optical densities due to the triplet or the semithionine, respectively. c_1 is a constant comprising the calibration factor of the arbitrary flash intensity as well as the extinction of the ground state and the geometry of the cuvette. c_2 and c_3 are constants which are related to the rate constants of Scheme I ($k_0 + k_{DD}$), αk_{DD}, and to the extinction coefficients of the species involved. By a proper choice of these constants the numerically calculated curve $E'(t)$ can be fitted to the experimental one. E_0' is then obtain as the result of integrating eq 12 and setting $c_2 = 0$.

Second Method of Determination of Absolute Quantum Yields. The use of the extinction coefficients which are uncertain by an experimental error of ±10% can be avoided if the disappearance of thionine from its ground state is observed directly and solutions with and without donor are compared. Since for such measurements the ground state has to be depopulated to a considerable extent, the condition of constant optical density for the absorption of the exciting flash light is no longer valid and hence the change in optical density no longer represents a linear measure of the quantum yield.

The best conditions for evaluating the quantum yield are given now in the limiting case of a small initial dye concentration, where there are only small optical densities for the absorption of the flash light. The pumping rate is then given by

$$-d[TH^+]/dt = jI(t)[TH^+] \tag{15}$$

incorporating a proportionality constant j to be determined. The following two coupled differential equations result from Scheme I:

$$d[^3TH^+]/dt = jI(t)[TH^+] - (k_0 + (k_Q + k_R)[R])[^3TH^+] \tag{16}$$

$$d[TH^+]/dt = -jI(t)[TH^+] + (k_0 + k_Q[R])[^3TH^+] \tag{17}$$

TABLE II: Total Quenching Constants ($k_Q + k_R$) and Radical Yields ($\Phi_R = k_R/(k_Q + k_R)$) of Different Electron Donors in Their Reactions with Basic and Acid Thionine Triplet $^3TH^+$ and $^3TH_2^{2+}$

Donors	Reaction with $^3TH^+$		Reaction with $^3TH_2^{2+}$	
	$(k_Q + k_R)^a$	Φ_R	$(k_Q + k_R)^a$	Φ_R
9,10-Dimethylanthracene	3.5×10^9	0.80 ± 0.08	4.0×10^9	0.80 ± 0.08
Azulene	2.0×10^9	0.75 ± 0.08	4.0×10^9	0.85 ± 0.09
1,3-Diphenylisobenzofuran	4.5×10^9	0.80 ± 0.08	4.0×10^9	0.85 ± 0.09
4-Methoxydimethylaniline	5.0×10^9	0.80 ± 0.1		
Hydroquinone	$2.5 \times 10^{9\,b}$	0.85 ± 0.09[b]	2.5×10^9	0.80 ± 0.08
Diazabicyclo[2.2.2]octane	8.0×10^8	0.85 ± 0.09		
4-Bromoaniline	3.0×10^9	0.40 ± 0.05	4.0×10^9	0.45 ± 0.05
Bromobenzene	$<4 \times 10^4$		$<4 \times 10^4$	
Thiourea	7.5×10^6	0.20 ± 0.03	8.0×10^8	0.16 ± 0.02
N-Allylthiourea	8.0×10^6	0.31 ± 0.03	7.0×10^8	0.30 ± 0.03
Selenourea	4.5×10^9	0.04 ± 0.01	3.5×10^9	0.10 ± 0.02

[a] Units: M^{-1} s^{-1}. [b] Presumably hydrogen transfer.

(k_{DD} is negligible at thionine concentrations as low as 10^{-6} M) the numerical solutions of which can be fitted, by a suitable choice of the rate constant k_R, to the experimentally obtained curve. (The rate constants k_0 and ($k_R + k_Q$) can be obtained independently, from lifetime measurements and the half-quenching concentrations of the donors.) The constant j is determined by a corresponding experiment without donor addition. The limiting yield of radical formation with infinite donor concentration is then given by $k_R/(k_R + k_Q)$.

For values of $1/((k_Q + k_R)[R])$, short compared to the half-width of the flash, the evaluation may be simplified further. In this case the concentration of the triplet is well approximated by the quasi-stationary value

$$[^3TH^+] = \frac{jI(t)[TH^+]}{(k_Q + k_R)[R]} \tag{18}$$

This leaves one differential equation

$$-d[TH^+]/dt = \eta_R jI(t)[TH^+] \tag{19}$$

yielding

$$\eta_R = \frac{\ln([TH^+]_{t=0}/[TH^+]_{t=\infty})}{j\int_0^\infty I(t)\,dt} = \text{constant} \times \ln\frac{E(600)_{t=0}}{E(600)_{t=\infty}} \tag{20}$$

Under these special conditions the quantity $\ln (E(600)_{t=0}/E(600)_{t=\infty})$ represents a linear measure of the quantum yield required. ($t = \infty$ means a long time as compared to the half duration of the flash, but a short time on the time scale of the semithionine decay. So in our case we had $t \approx 25$ μs.) The advantage of this second method is that it works independently of the pH of the solution, as long as the ground state is not protonated or deprotonated. By means of this second method the same absolute value of radical formation from the triplet state was obtained as using the first method, DMA being the donor in both cases. In the case of donors giving low semithionine yields, this method clearly demonstrates, that the reduced yield of radicals is due to the bimolecular repopulation of the thionine ground state (Figure 4).

Special Properties of Some of the Donors. There were some problems due to the basic strength of some of the donors. *p*-Bromoaniline is a rather weak base which is not protonated by the methanolic buffer of pH* 8.6. In the presence of 0.1 M methanolic phosphoric acid the extent of protonation is near 50% at a *p*-bromoaniline concentration of 10^{-2} M so that measurements of the reactivity and the quantum yield with the acid triplet were still possible. The effective concentration of unprotonated *p*-bromoaniline in each experiment was determined

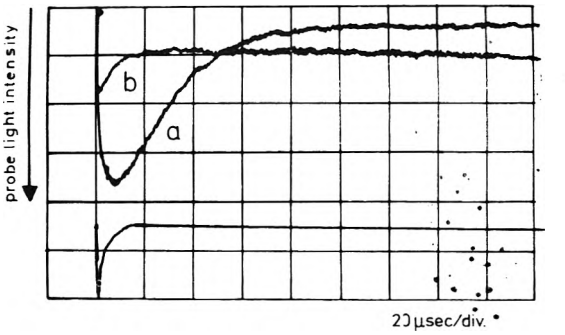

Figure 4. Demonstration of physical quenching of the thionine triplet $^3TH^+$ by thiourea: (a) change in transparency at 600 nm (maximum of ground state absorption) due to repopulation of the ground state from the triplet state without thiourea; (b) the same measurement in the presence of 6.5×10^{-2} M thiourea. Flash intensity and thionine concentration (10^{-6} M) were the same for a and b. The solvent was oxygen free methanol.

spectroscopically. The protonated form of *p*-bromoaniline shows no quenching of the thionine triplet $^3TH_2^{2+}$, as could be shown by experiments with the completely protonated *p*-bromoaniline in the presence of HCl.

The pK_a* value of the singly protonated form of DABCO in methanol was determined by potentiometric titration with methanolic HCl to be 8.4. The buffer of pH* 8.6 may be used in this case, too, if the degree of protonation is taken into account. The reaction with the acid triplet, however, can no longer be measured. Also for *p*-methoxydimethylaniline only the reaction with the basic triplet could be studied, but the buffer of pH* 8.6 could not be used with this substance. The radical yield was determined by the second method. (The molar extinction coefficient of the donor radical amounts to less than 2000 at 600 nm[22].)

Results and Discussion

The results for the triplet quenching constants (physical quenching plus radical formation) as well as the radical yields under conditions of complete triplet quenching are given in Table II. In general the quenching constants are of an order of magnitude expected for electron transfer reactions according to the results of Vogelmann et al.[11] for similar systems. The rate constant of hydroquinone with the basic triplet is high, however, as compared to the methylated compound *p*-dimethoxybenzene (10^7 M^{-1} s^{-1}),[11] though the one-electron oxidation potential of hydroquinone certainly is not lower than that of *p*-dimethoxybenzene. A possible explanation might be that in the reaction of the basic triplet with hydroquinone a hydrogen transfer takes place, the free enthalpy of this reaction being more favorable than that for electron transfer.[23] In fact

Scheme II

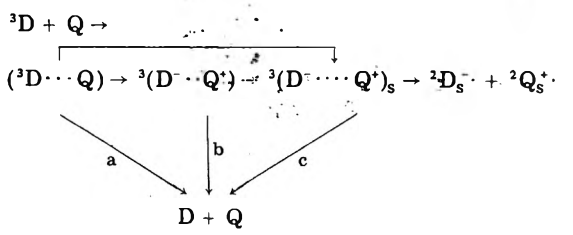

in nonbuffered methanol direct formation of acid semithionine TH_2^+· can be observed.

The results demonstrate that for many of the electron donors, whose reactions with the thionine triplets have been studied, the radical yields are quite high. There are, however, compounds showing considerable or even dominant physical quenching. As the measured lifetime of the semireduced thionine is much longer than the flash duration, a recombination of free radicals during the first 20 μs after flash triggering can be ruled out as a possible cause of the decrease of radical yields. On the other hand, the experiments, excluding complex formation of the ground state molecules and quenching of the singlet excited thionine; confirm that electron transfer and physical quenching are dynamical processes of the thionine triplets. The question arises, whether both processes are independent or whether they are coupled in that they pass through a common intermediate.

The various possibilities are illustrated in Scheme II, analogous to the one used by Mataga.[3b] Here ^3D is the triplet excited dye molecule, Q the quencher, $(^3D\cdots Q)$ is an encounter complex, $^3(D^-\cdots Q^+)$ is a triplet exciplex, $^3(D^-\cdots Q^+)_s$ the solvated radical pair, still in an overall triplet state, and $^2D^-$· and $^2Q^+$· are free radicals. The channel, denoted "reaction" in Mataga's scheme, is not important in our case, at least for the dye component, there is no fast chemical reaction other than radical formation.

Assuming first that the physical quenching is independent of electron transfer (reaction a), we have to consider triplet–triplet energy transfer and the external heavy atom effect as possible mechanisms.

Triplet–triplet energy transfer can be excluded as a substantial cause of triplet deactivation; when using azulene (triplet energy 38.6 kcal/mol[24]), the donor which probably has the lowest triplet energy and a short triplet lifetime, the radical yield is high. There may, however, be a small influence of triplet–triplet energy transfer: The conditions are more favorable in the case of the basic triplet form (triplet energy 39 ± 1.5 kcal/mol[14]) than for the acid triplet form (triplet energy 30 ± 2.5 kcal/mol[14]). In fact a slightly higher radical yield is found with the latter.

From Table II it can be seen that all donor compounds, exhibiting high physical quenching efficiency, contain heavy atoms or, in the case of the thioureas, at least atoms with moderate spin–orbit coupling constants. As is well known, intersystem crossing processes may be enhanced by external heavy atom perturbation.[25] As was shown in fluorescence quenching experiments, the quenching efficiency of heavy atom quenchers decreases with increasing energy gap between the two coupling levels of different multiplicity in the fluorescing molecule.[26] If this gap is larger than 30 kcal much higher concentrations of the quencher are necessary than those involved in our experiments.

As may be learned from the comparison of *p*-bromoaniline with bromobenzene, the quenching efficiency of the former cannot be explained merely by the presence of the bromine atom. (There is no quenching of the thionine triplets with bromobenzene up to concentrations of 1 M.) Stronger evidence for an interrelation between electron transfer and the physical quenching reaction is given by the reactivity of thiourea and allylthiourea toward the different triplet forms of thionine. For these donors the radical yields with both triplet forms are the same, though the reaction with the acid triplet form is about 100 times faster than with the basic form. This means that the rate constants of both radical formation and physical quenching are increased by a factor of 100, which strongly suggests that the physical quenching follows the electron transfer step, the latter being rate determining. In order to explain the physical quenching one should therefore discuss an intersystem crossing process in the primarily formed electron transfer product, which competes with the formation of free radicals (b or c, Scheme II).[27]

Triplet exciplexes, if formed in electron transfer reactions, are not expected to be detectable by their phosphorescence in fluid solutions. Spectroscopic evidence has been given for triplet exciplexes in nonpolar solvents,[28] in polar solvents, however, their absorption spectra are not likely to be very different from the radical ion spectra.[29] From this point of view it would be of value to obtain some other means of probing triplet exciplexes in electron transfer reactions in polar solvents.

Intersystem crossing processes in the exciplex are often faster than in the excited single component.[30] This may in part be due to the fact that symmetry conditions are less restrictive for the intermolecular spin–orbit coupling matrix elements. Enhanced spin–orbit coupling should be expected when heavy atoms are introduced. This was verified by Gronkiewicz et al.[30] in the case of phosphorescing CT complexes. An exciplex model for the electron transfer reaction in our systems could explain the smaller radical yield with *p*-bromoaniline as compared to the other aromatics and of selenourea as compared to the thioureas.

Exciplexes can dissociate to form pairs of individually solvated radical ions. The electronic interaction of the geminate radicals decreases exponentially with their distance.[31] This may be seen, e.g., by the singlet–triplet splitting of the radical pair.[32] However, though the lowest electronic singlet and triplet state of the radical pair may become completely degenerate, the multiplicity of the reaction complex is retained in the resulting radical pair for a period of time which may be determined by various mechanisms. Spin–lattice relaxation is usually too slow to become important during the geminate phase of the radical pair in solutions of normal viscosity.[33] As was shown by Kaptein[34] for radical pairs with orbitally nondegenerate ground states the influence of spin–orbit coupling can also be neglected. Thus the heavy atom effect we observed favors the exciplex as the electron transfer intermediate, where the intersystem crossing takes place, rather than the radical pair.

Very recently it has been demonstrated by the magnetic field dependence of fast triplet formation from geminate radical pairs, produced by electron transfer from aromatic amines to singlet excited pyrene, that intersystem crossing in radical pairs can be due to the hyperfine coupling between electronic and nuclear spins.[35,36] The same mechanism might be operative in the intersystem crossing of radical pairs, originally formed in the electronic triplet state, making a recombination to singlet ground state products possible.

High rate constants would be expected for the recombination of the semithionine with the oxidized donor radicals (yielding the ground state molecules) due to the negative free enthalpy of these reactions. The long lifetime

observed for the semithionine radicals is not consistent with such a high recombination rate constant of counterradicals, however, unless it is assumed that the concentration of the oxidized counterradicals is diminished by some other process (e.g., involving the solvent). Such a process might be fast enough to prevent the recombination of freely diffusing radicals, but slow enough not to interfere with the geminate recombination phase of the radicals.

The reported yields of geminate recombination products due to hyperfine induced intersystem crossing are about 10%.[35] They are comparable to the small physical quenching yields of the donors in the upper half of Table I. It is doubtful, however, whether the hyperfine mechanism can account for the large intersystem crossing yields, which we have observed with some donors. The radicals of the thioureas and selenourea are expected to contribute less to the hyperfine coupling than the aromatic donor cations, as the radical electron is localized at atoms (S or Se) having nuclear spin zero for the major part of their natural isotopes. Furthermore in the radical pairs of our systems the diffusive separation of the radicals is not hindered by Coulomb attraction.

In order to obtain more conclusive information, experiments are in progress to test the magnetic field dependence of the radical yield in electron transfer reactions of triplet states.

Acknowledgment. We are indebted to Professor A. Weller and Dr. M. E. Michel-Beyerle for making preprints of their papers available to us. The help of D. Miller in translating the manuscript is gratefully acknowledged. We thank the Fonds der Chemischen Industrie and the Deutsche Forschungsgemeinschaft for their financial assistance.

References and Notes

(1) H. Leonhardt and A. Weller, *Z. Phys. Chem.* (*Frankfurt am Main*), **29**, 277 (1961); "Luminescence of Organic and Inorganic Materials", H. P. Kallmann and G. M. Spruch, Ed., Wiley, New York, N.Y., 1962, p 74.
(2) For references see ref 3a.
(3) (a) H. Masuhara, T. Hino, and N. Mataga, *J. Phys. Chem.*, **79**, 994 (1975); (b) T. Hino, H. Akazawa, H. Masuhara, and N. Mataga, *ibid.*, **80**, 33 (1976).
(4) N. Orbach and M. Ottolenghi in "The Exciplex", M. Gordon and W. R. Ware, Ed., Academic Press, New York, N.Y., 1975, p 75.
(5) K. H. Grellmann, A. R. Watkins, and A. Weller, *J. Lumin.*, **1,2**, 678 (1970).
(6) H. Fischer, *Z. Phys. Chem.* (*Frankfurt am Main*), **43**, 177 (1964).
(7) H. Fischer, H. E. A. Kramer, and A. Maute, *Z. Phys. Chem.* (*Frankfurt am Main*), **69**, 113 (1970).
(8) J. Faure, R. Bonneau, and J. Joussot-Dubien, *Photochem. Photobiol.*, **6**, 331 (1967); R. Bonneau and J. Jousset-Dubien, *ibid.*, **17**, 313 (1973).
(9) H. E. A. Kramer and A. Maute, *Photochem. Photobiol.*, **15**, 7 (1972).
(10) E. Vogelmann and H. E. A. Kramer, *Photochem. Photobiol.*, **23**, 383 (1976).
(11) E. Vogelmann, S. Schreiner, W. Rauscher, and H. E. A. Kramer, *Z. Phys. Chem.* (*Frankfurt am Main*), **101**, 321 (1976).
(12) D. Rehm and A. Weller, *Ber. Bunsenges. Phys. Chem.*, **73**, 834 (1969).
(13) E. Vogelmann, H. Schmidt, U. Steiner, and H. E. A. Kramer, *Z. Phys. Chem.* (*Frankfurt am Main*), **94**, 101 (1975).
(14) H. E. A. Kramer, *Z. Phys. Chem.* (*Frankfurt am Main*), **66**, 73 (1969).
(15) W. Endriss, Thesis, University of Stuttgart, 1961.
(16) D. G. Thomas, J. H. Billman, and C. E. Davis, *J. Am. Chem. Soc.*, **68**, 895 (1946).
(17) C. L. De Ligny, P. F. M. Luykx, M. Rehbach, and A. A. Wieneke, *Recl. Trav. Chim. Pays-Bas*, **79**, 699 (1960).
(18) W. Broser and H. Fleischhauer, *Z. Naturforsch. B*, **25**, 1389 (1970).
(19) U. Steiner, M. Hafner, S. Schreiner, and H. E. A. Kramer, *Photochem. Photobiol.*, **19**, 119 (1974).
(20) A. Kira, S. Arai, and M. Imamura, *J. Phys. Chem.*, **76**, 1119 (1972).
(21) (a) L. Lindqvist, *Ark. Kem.*, **16**, 79 (1960); (b) N. Kosui, K. Uchida, and M. Koizumi, *Bull. Chem. Soc. Jpn.*, **38**, 1958 (1965).
(22) W. Aichele, Diplomarbeit 1975, University of Stuttgart.
(23) D. Rehm and A. Weller, *Isr. J. Chem.*, **8**, 259 (1970).
(24) (a) P. Kröning, *Z. Phys. Chem.* (*Frankfurt am Main*), **86**, 225 (1973); (b) W. G. Herkstroeter, *J. Am. Chem. Soc.*, **97**, 4161 (1975).
(25) S. P. McGlynn, T. Azumi, and M. Kinoshita, "Molecular Spectroscopy of the Triplet State", Prentice-Hall, Englewood Cliffs, N.J., 1969.
(26) H. Dreeskamp and M. Zander, *Z. Naturforsch. A*, **28**, 1743 (1973); H. Dreeskamp, E. Koch, and M. Zander, *Chem. Phys. Lett.*, **31**, 251 (1975).
(27) After our manuscript had been written, we saw the recent paper of A. Treinin and E. Hayon, *J. Am. Chem. Soc.*, **98**, 3884 (1976), on the quenching of triplet states by inorganic ions. Their results, too, indicate that charge transfer has to occur to make the intersystem crossing process possible. In contrast to our results, however, with inorganic ions as quenchers no formation of radicals can be observed (except in one case), which these authors explain by the higher effectivity of the intersystem crossing process as compared to the dissociation of the CT complex.
(28) D. G. Whitten, J. K. Roy, and F. A. Carroll, in ref 4, p 247.
(29) N. Orbach and M. Ottolenghi, *Chem. Phys. Lett.*, **35**, 175 (1975).
(30) M. Gronkiewicz, B. Kozankiewicz, and J. Prochorow, *Chem. Phys. Lett.*, **38**, 325 (1976).
(31) F. Adrian, *J. Chem. Phys.*, **57**, 5107 (1972).
(32) K. Itoh, H. Hayashi, and S. Nagakura, *Mol. Phys.*, **17**, 561 (1969).
(33) B. Brocklehurst, *Nature* (*London*), **221**, 921 (1969).
(34) R. Kaptein, *J. Am. Chem. Soc.*, **94**, 6251 (1972).
(35) K. Schulten, H. Staerk, A. Weller, H.-J. Werner, and B. Nickel, *Z. Phys. Chem.* (*Frankfurt am Main*), **101**, 371 (1976).
(36) R. Haberkorn and M. E. Michel-Beyerle, *Z. Naturforsch. A*, **31**, 499 (1976); M. E. Michel-Beyerle, R. Haberkorn, W. Bube, E. Steffens, H. Schröder, H. J. Neusser, E. W. Schlag, and H. Seidlitz, *Chem. Phys.*, **17**, 139 (1976).
(37) Note Added in Proof: Meanwhile the lifetime of the first excited singlet state of thionine has been determined experimentally to be 3.6×10^{-10} s at a concentration of 2.5×10^{-4} M in methanol. (E. Vogelmann, M. Hauser, and G. Heidt, private communication.)

Electron Spin Resonance Line Shapes of Vanadyl Complexes in the Slow Tumbling Region

G. V. Bruno, J. K. Harrington, and M. P. Eastman*

Department of Chemistry, The University of Texas at El Paso, El Paso, Texas 79968 *(Received December 3, 1976)*

Publication costs assisted by The University of Texas at El Paso

ESR line shapes that are appropriate for vanadyl spin probes in the slow tumbling region have been calculated by the stochastic Liouville method. Spectral line shapes, which were computed with axially symmetric magnetic parameters, agreed well with experimental ESR spectra of vanadyl acetylacetonate in toluene for slow tumbling rotational correlation times $\tau \sim 8 \times 10^{-11}$–$7 \times 10^{-8}$ s/rad. Particularly good agreement was obtained for $\tau \sim 8 \times 10^{-11}$–$1 \times 10^{-9}$ s/rad. Values of τ may be determined for $\tau \sim 1 \times 10^{-9}$–$7 \times 10^{-8}$ s/rad even though only qualitative spectral agreement is obtained in this region. Significant nonsecular contributions to the line shapes arise from the large intramolecular magnetic interactions. The nonsecular terms are treated by a perturbation analysis that does not increase either the computation time or the storage space for the computer program. A simple expression for estimating τ is given for the range 9×10^{-10}–7×10^{-8} s/rad. Formulae for the motionally narrowed line widths, which are derived from the general slow tumbling equations, are in substantial agreement with previous motionally narrowed formulae. Slightly better agreement with experimental data does result from our general perturbation treatment of the nonsecular terms.

Introduction

Recently, paramagnetic spin probes have been employed in a wide variety of experiments to obtain structural and dynamical information.[1] In particular, nitroxide spin labels have been successfully used to study membranes,[2] micelles,[3] liquid crystals,[4] and proteins.[5] This technique utilizes a highly developed theory which relates ESR line shapes to well-defined magnetic and molecular parameters.[1,6-9]

Complexes containing the vanadyl ion VO^{2+} are being used increasingly as spin probes.[10-12] However, quantitative analysis of the experimental ESR line shapes for these probes has been limited to the motionally narrowed region and to the rigid limit region. The purpose of this paper is to apply the stochastic Liouville method[13] as developed by FBP[7] to calculate ESR line shapes in the slow tumbling region for vanadyl complexes.

The slow tumbling region refers to the region where the rotational motion is slow compared to the anisotropy of the intramolecular magnetic interactions. The resulting ESR line shape is no longer a superposition of Lorentzian lines. Because vanadyl complexes have a more orientation-dependent spin Hamiltonian than nitroxides, the slow tumbling region for vanadyl probes occurs at shorter rotational correlation times τ. For typical vanadyl complexes, slow tumbling occurs in the region $\tau \sim 10^{-10} \sim 10^{-7}$ s/rad. Longer τ yield essentially the rigid limit ESR spectrum.

Slow tumbling ESR spectra may be observed in experiments where the vanadyl spin probe is dissolved in a viscous medium[11b] or where the vanadyl ion is rigidly attached to a macromolecule[10] or a supramolecular structure (e.g., micelles[12]). Because vanadyl readily forms stable complexes with a wide variety of ligands,[14] the vanadyl ion may be used as a probe in binding to proteins.[10] In addition to the artificial incorporation of vanadyl ions, naturally occurring vanadium complexes have been found in living systems[15] and in petroleum.[16]

Because vanadyl acetylacetonate VOacac has such excellent ESR spectroscopic properties, Wilson and Kivelson[17] used this complex to verify the motionally narrowed theory for nondegenerate hyperfine lines.[8b] Since Wilson and Kivelson have done such a thorough study in the motionally narrowed region, VOacac was chosen as the model vanadyl ion complex for study in the slow tumbling region.

Experimental Section

Solutions of VOacac in toluene were prepared by standard vacuum line techniques. VOacac was purchased from Alfa Products and recrystallized from acetone.[19] Spectrograde toluene was stored under vacuum over sodium ribbon. Solutions were degassed by the repetitive freeze–thaw method. Vanadyl ion concentrations ($\lesssim 5 \times 10^{-4}$ M) were low enough that intermolecular effects were negligible.

The ESR spectra were taken at X band with a Varian (V-4502) spectrometer system. 100-kHz field modulation was used with low modulation amplitude so that no distortion in line shapes was observed. Microwave powers were low enough to preclude saturation effects. Temperature was controlled by a Varian E-257 variable temperature unit and measured with a copper–constantan thermocouple. Spectral calibrations were obtained from the hyperfine splittings of VOacac in toluene at 2 °C.[17]

Theory

The stochastic Liouville method has been developed as a general approach for the calculation of ESR line shapes in the slow tumbling region.[7] Here we apply this general theory to vanadyl ions in a manner that renders equations for the line shape which may be efficiently solved by computer.[19] Previous ESR studies of VOacac[17] have shown that (a) the only nuclear moment that the unpaired electron interacts to effect ESR spectra is the vanadium with spin $I = 7/2$; (b) the primary orientation-dependent contributions to the spin Hamiltonian are the **g** tensor and the electron–nuclear magnetic dipole **A** tensor interactions; (c) the principal axes for the **g** and **A** tensors coincide; and (d) the **g** and **A** tensors are very nearly axially symmetric. The motionally narrowed line widths calculated with

axially symmetric **g** and **A** tensor parameters differ by less than 0.5% from those that were calculated with completely asymmetric tensor values.[17]

The total spin Hamiltonian $H_s(\Omega)$ can be conveniently separated into an orientation independent component H_0, and orientation dependent part $H_1(\Omega)$, and a component $\epsilon(t)$ that represents the interaction of the electron spin with the oscillating microwave magnetic field so that[7]

$$H_s(\Omega) = H_0 + H_1(\Omega) + \epsilon(t) \tag{1}$$

For VOacac, H_0 and $H_1(\Omega)$ are given (in rad/s) by the formulae[8a]

$$H_0 = \frac{g_0\beta_e B_0}{\hbar}S_z + |\gamma_e|aI_zS_z + \frac{|\gamma_e|a}{2}(S_+I_- + S_-I_+) \tag{2a}$$

and

$$\begin{aligned} H_1(\Omega) = {} & (F - (8/3)^{1/2}DI_z)\mathbf{D}_{0,0}{}^2S_z + (\mathbf{D}_{0,1}{}^2I_+ \\ & - \mathbf{D}_{0,-1}{}^2I_-)DS_z + ((3/8)^{1/2}F - DI_z)(\mathbf{D}_{0,-1}{}^2S_- \\ & - \mathbf{D}_{0,1}{}^2S_+) + (D/\sqrt{6})\mathbf{D}_{0,0}{}^2(I_+S_- + I_-S_+) \\ & - D(\mathbf{D}_{0,-2}{}^2I_-S_- + \mathbf{D}_{0,2}{}^2I_+S_+) \end{aligned} \tag{2b}$$

Here β_e is the Bohr magneton, B_0 is the external magnetic field, $|\gamma_e|$ is the magnitude of the electron magnetogyric ratio, S and I are the appropriate electron and nuclear spin operators, and $\mathbf{D}_{0,m}{}^2$ represents the orientation dependent Wigner rotation matrices. The isotropic g value (g_0) is given by the formula

$$g_0 = {}^1/_3(g_\parallel + 2g_\perp) \tag{3}$$

and a, the isotropic splitting (in gauss), is given by the formula

$$a = {}^1/_3(A_\parallel + 2A_\perp) \tag{4}$$

The symbol F (in rad/s) is defined by the expression

$$F = {}^2/_3(g_\parallel - g_\perp)\frac{\beta_e B_0}{\hbar} \tag{5}$$

and D (in rad/s) is given by the formula

$$D = (|\gamma_e|/\sqrt{6})(A_\perp - A_\parallel) \tag{6}$$

Here $g_\parallel$, $g_\perp$ and $A_\parallel$, $A_\perp$ (in gauss) are the principal values of the **g** and **A** tensors, respectively. Nonsecular ($S_\pm$) terms have been included in eq 2 because the magnitude of the magnetic interactions is large for VOacac.[17] Spectral simulations at X band have justified the neglect of the nuclear Zeeman term in eq 2a. This approximation, which greatly reduces the number of equations to be solved, is commonly made for nitroxides[19,20] for which the term is more important.[21]

General equations whose solution yields unsaturated ESR line shapes for vanadyl ions are given in Appendices A and B. Equations that are presented in Appendix A have neglected the nonsecular portions of eq 2. A perturbation analysis is used in Appendix B to account for the nonsecular contributions to the line shape. This perturbation technique modifies eq A.1 in such a manner that the number of independent variables is not increased and the computational efficiency of the diagonalization method of solution[19,22] is retained.

The general eq A.1–A.4 and B.3, which are valid in the motionally narrowed region, may be compared to previous results which were derived from motionally narrowed theory. The motionally narrowed results may be obtained from eq A.1, A.2, A.4, and B.3 by considering only $L = 0$ and $L = 2$ terms.[7] When perturbation terms of the order $\sim a^4/\omega^2$, FDa^2/ω^2, etc. are neglected, the first derivative Lorentzian line widths (in gauss) may be expressed by the formula

$$\Delta H(m,\tau) = \alpha + \beta m + \gamma m^2 + \delta m^3 \tag{7}$$

where

$$\begin{aligned} \alpha = {} & \alpha'' + \frac{2\tau}{\sqrt{3}|\gamma_e|}\left\{\frac{F^2}{5}\left(1 + \frac{3}{4}u + \frac{3}{14}\frac{F}{\omega_x}\right)\right. \\ & + \frac{I(I+1)}{5}\left[D^2p + \frac{7}{3}D^2u - \frac{FD^2}{\omega_x}\left(\frac{20}{21} - \frac{5}{7}p\right)\right. \\ & \left.\left. + \sqrt{\frac{2}{3}}FDa(\omega^{-1} + \omega_x{}^{-1})\left(1 - \frac{3}{4}p\right)\right]\right\} \end{aligned} \tag{8a}$$

$$\begin{aligned} \beta = {} & \frac{2\tau}{\sqrt{3}|\gamma_e|}\left[-\frac{4}{5}\sqrt{\frac{2}{3}}FD\left(1 + \frac{3}{4}u + \frac{9}{28}\frac{F}{\omega_x}\right)\right. \\ & + \frac{I(I+1)D^2a}{5}(\omega^{-1} + \omega_x{}^{-1})\left(p - \frac{4}{3}\right) + \frac{8}{21}\sqrt{\frac{2}{3}}I(I \\ & \left. + 1)\frac{D^3}{\omega_x}\left(1 - \frac{3}{4}p\right) + \frac{1}{7}\sqrt{\frac{2}{3}}\frac{D^3}{\omega_x}p - \frac{D^2a}{5\omega}p\right] \end{aligned} \tag{8b}$$

$$\begin{aligned} \gamma = {} & \frac{2\tau}{\sqrt{3}|\gamma_e|}\left\{\frac{8D^2}{15}\left[1 - \frac{3}{8}p - \frac{u}{8} + \frac{F}{\omega_x}\left(1 - \frac{15}{56}p\right)\right]\right. \\ & \left. - \frac{1}{5}\sqrt{\frac{2}{3}}FDa(\omega^{-1} + \omega_x{}^{-1})\left(1 - \frac{3}{4}p\right)\right\} \end{aligned} \tag{8c}$$

and

$$\begin{aligned} \delta = {} & \frac{2\tau}{\sqrt{3}|\gamma_e|}\left[\frac{4}{15}D^2a(\omega^{-1} + \omega_x{}^{-1})\left(1 - \frac{3}{4}p\right)\right. \\ & \left. - \frac{64}{105}\sqrt{\frac{2}{3}}\frac{D^3}{\omega_x}\left(1 - \frac{15}{32}p\right)\right] \end{aligned} \tag{8d}$$

α'' is a residual line width (in gauss) that corresponds to the parameter $T_2{}^{-1}$ (i.e., $\alpha'' = (2/\sqrt{3}|\gamma_e|)T_2{}^{-1}$) that is used in eq A.1–A.3. α'' is usually attributed to a spin–rotation interaction at higher temperatures[23] and to intermolecular electron–nuclear dipolar interaction at the lower temperatures. τ is the rotational correlation time (in s/rad) and corresponds to τ_2 in eq A.1–A.3. ω_x is given by the equation

$$\omega_x{}^{-1} = \frac{\omega\tau^2}{(\omega\tau)^2 + 1} \tag{9a}$$

u, the nonsecular factor, is given by

$$u = [1 + \omega^2\tau^2]^{-1} \tag{9b}$$

and p, the pseudosecular factor, is given by

$$p = \left[1 + \frac{a^2\tau^2}{4}\right]^{-1} \tag{9c}$$

Note that $\omega_x{}^{-1} = \omega^{-1}(1 - u)$. All other terms in eq 8 have been previously defined.

Since ESR line widths are insensitive to rotational diffusion about the magnetic symmetry axis (the VO bond), eq 7 and 8 require only the single rotational correlation time for rotation about the axes perpendicular to the symmetry axis. For a spherical Brownian particle of radius r in a medium of viscosity η, the Debye theory of

rotational relaxation yields the familiar expression[24]

$$\tau = 4\pi r^3\eta/3kT \qquad (10)$$

Equations 7 and 8 relate τ to the measured line widths and the experimentally determined $g_{\parallel}$, $g_{\perp}$, $A_{\parallel}$, and $A_{\perp}$ values. In practice, τ is obtained from β and γ because of uncertainty in α and experimental error as well as theoretical imprecision for δ.[25]

Equations 7 and 8 agree in essence with the line width formulae of Wilson and Kivelson[17] that were obtained from motionally narrowed theory. Slight discrepancies occur because of differences in the perturbation treatment of nonsecular terms rather than differences between motionally narrowed theory and the general stochastic Liouville method. If the only perturbation terms in eq 8 to be considered are those that are proportional to (a/ω) and (a/ω_x), the cross-term contributions of Wilson and Kivelson[17] are obtained.

An appreciable downfield shift is obtained from eq A.1–A.4 and B.3 and is given (in gauss) by the formula

$$\Delta B(m) = -\frac{1}{|\gamma_e|}\left[\frac{3F^2}{20\omega_x} + \frac{7I(I+1)D^2}{15\omega_x} + \frac{I(I+1)a^2}{2\omega}\right] + \frac{m}{|\gamma_e|}\left[\frac{\sqrt{6}}{5}\frac{FD}{\omega_x}\right] + \frac{m^2}{|\gamma_e|}\left[\frac{D^2}{15\omega_x} + \frac{a^2}{2\omega}\right] \qquad (11)$$

Equation 11 agrees with the previously derived shifts for the motionally narrowed region.[26]

Results and Discussion

A. *Slow Tumbling ESR Line Shapes.* Experimental spectra for VOacac in toluene are shown at two different temperatures: −80 (Figure 1) and −99 °C (Figure 2). Simulated spectra calculated from eq A.1–A.4 and B.3 are presented as dashed lines in the respective figures. These two experimental spectra exhibit characteristics of two groups of slow tumbling line shapes. Figure 1 shows an experimental spectrum where the rotation of VOacac is fast enough to yield a line shape that has features characteristic of the motionally narrowed region but which is obviously in the slow tumbling region. The experimental spectrum in Figure 2, on the other hand, shows obvious rotational motion but exhibits characteristics of a rigid limit line shape.[17]

The slow tumbling region for VOacac refers to τ values between $\sim 8 \times 10^{-11}$ $\sim 7 \times 10^{-8}$ s/rad. The line width for the $m = 7/2$ hyperfine line begins to deviate significantly from the motionally narrowed result of eq 7 and 8 for τ longer than 8×10^{-11} s/rad. The ESR line shape becomes rather insensitive to rotation for τ longer than $\sim 7 \times 10^{-8}$ s/rad, although the use of completely asymmetric magnetic parameters may extend this limit slightly.

In Figure 1, the dashed line was calculated for Brownian rotational diffusion with $\tau = 4.3 \times 10^{-10}$ s/rad. The central region of the line shape is seen to have some similarity to the distinct symmetric hyperfine lines of the motionally narrowed region. The outside portions of the spectrum, however, show the asymmetry and shifting of the "hyperfine lines" that are characteristic of slow tumbling line shapes. The dashed simulated line shape is seen to be in very good agreement with the experimental spectrum and was fit by varying essentially only one parameter, τ. The magnetic parameters ($A_{\parallel} = -185.5g$, $A_{\perp} = -66.96g$, $g_{\parallel} = 1.9430$, and $g_{\perp} = 1.9820$) are the reported literature values for VOacac in toluene.[17] The simulated spectrum was relatively insensitive to the residual line width T_2^{-1} (α'') value. α'' was allowed to vary between 0.8 G, which

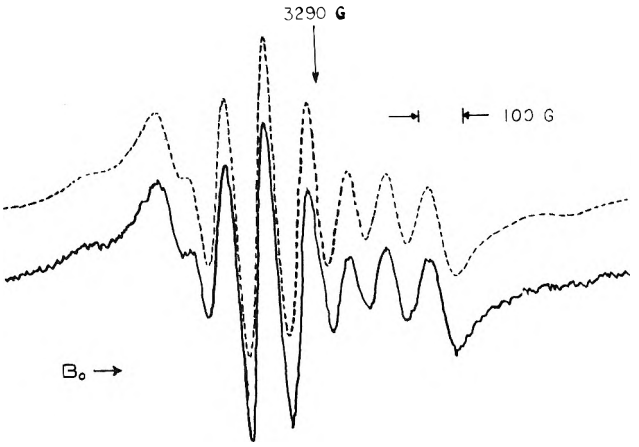

Figure 1. A comparison of simulated and experimental spectra for VOacac in toluene at −80 °C. — is the experimental spectrum. ------ is calculated for Brownian rotational diffusion with $\tau = 4.3 \times 10^{-10}$ s/rad and $\alpha'' = 2.0$ G.

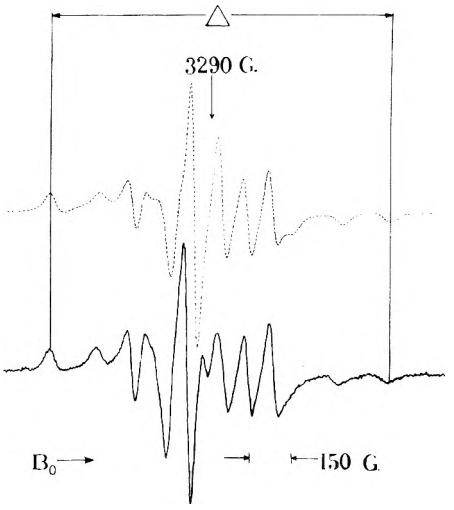

Figure 2. A comparison of simulated and experimental spectra for VOacac in supercooled toluene at −99 °C. — is the experimental spectrum. ------ is calculated for Brownian rotational diffusion with $\tau = 4.2 \times 10^{-9}$ s/rad and $\alpha'' = 7.5$ G. $A_{\parallel}$, $A_{\perp}$, $g_{\parallel}$, and $g_{\perp}$ are the same as those in Figure 1.

was obtained for −37 °C, and 7.5 G, which was estimated from the high and low field extrema lines of a spectrum taken at 77 K. Non-Brownian rotational reorientation (e.g., jump reorientation or "simple free" diffusion[20]) did not improve the overall spectral fit.

The computed spectrum in Figure 1 was in especially good agreement with the experimental spectrum for the outer spectral region. The most accurate measurement of τ would, therefore, fit these sections. Slight but systematic deviations were noted in comparing the interior regions. The resolved $m = -3/2$ "hyperfine line" has a slightly greater amplitude than the computed line while the $m = 1/2$ and $m = 3/2$ "hyperfine lines" have smaller amplitudes than the calculated lines.

In order to achieve the excellent agreement in Figure 1, nonsecular contributions for both "shift" and "line width" must be taken into account. Figure 3 is a comparison of such spectral line shapes where the nonsecular contributions are given by the perturbation analysis of Appendix B. The solid line is computed from eq A.1–A.4 that are modified by the complete expression B.3, while the dashed line is computed from the eq A.1–A.4 that are modified by only the diagonal terms of B.3, the "shift" terms. All other parameters are the same as those used

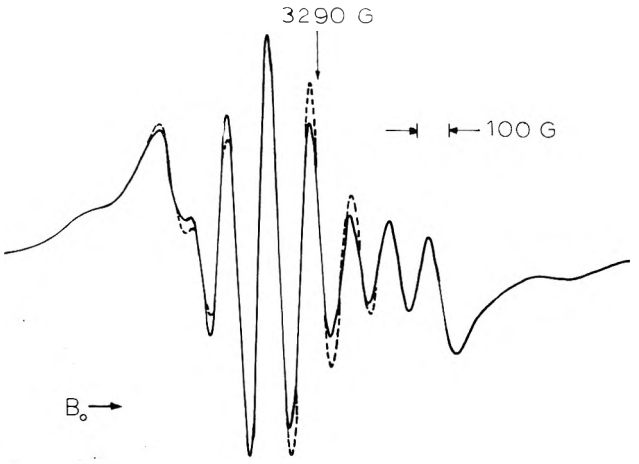

Figure 3. A comparison of calculated spectra for the importance of the perturbation "width" terms. — is calculated with both perturbation "width" and "shift" terms. This line shape is the same as the dashed line shape in Figure 1. ------ is calculated with only the perturbation "shift" term.

in Figure 1. The solid line spectrum in Figure 3 is the same line shape as the dashed line shape in Figure 1. The effect of including the nonsecular "width" terms is seen to be important especially in the interior portion of the spectrum. Figure 3 suggests that the slight deviations noted in Figure 1 may arise from residual nonsecular contributions that are not accounted for by the perturbation analysis in Appendix B.

In general for VOacac, the very good agreement between simulated and experimental spectra that is shown in Figure 1 is typical for the slow tumbling range of τ from 8×10^{-11} to 1×10^{-9} s/rad. For this range, the use of axially symmetric magnetic parameters and the perturbation treatment of the nonsecular spin Hamiltonian are good approximations. The accuracy in τ values (and the magnetic parameters) in this region is within 5%.

Figure 2 is representative of spectra in the slow tumbling region where the spectral line shapes have features similar to the rigid limit spectrum. The solid line is an experimental spectrum of VOacac in toluene at −99 °C which had been slowly cooled through the "freezing" point (−90 °C). The dashed line is a computer simulated spectrum with $\tau = 4.2 \times 10^{-9}$ s/rad and Brownian rotational diffusion. The experimental spectrum shows the distinctive low field "absorption" and high-field "emission" line shapes that characterize frozen spectral line shapes. Likewise, the highly asymmetric and overlapped central region is typical of spectra in the rigid limit. The simulated spectrum has been positioned so that the outside lines are aligned. The overall spectral line shapes are in good agreement. The outside lines are in very good agreement while the interior line shapes, except for a small range ~60 G up-field from the large central peak, are in reasonably good agreement. Since VOacac like nitroxide spin labels has $|A_z| >> |A_x| \approx |A_y|$,[27] the separation between the well-resolved outermost extrema peaks and their line shapes are insensitive to variation in $A_\perp$, $g_\parallel$, and $g_\perp$ values. These outside lines should be unaffected by the assumption of axially symmetric magnetic parameters.[28] The inner region of the computed spectrum, however, will have their "lines" slightly shifted relative to the respective experimental "lines" because axially symmetric magnetic parameters were used.[29] Nonsecular contributions, that are not adequately given by the perturbation analysis in Appendix B, may also result in deviations in the central portion of the spectra.

In general, for VOacac, Figure 2 is representative of the best fit of a simulated spectrum to an experimental spectrum for τ in the slow tumbling range 1×10^{-9} to 7×10^{-8} s/rad. Values of τ may be determined by varying τ until the separation between the two outermost extrema lines equals the respective experimental separation. The best value for τ is then determined by slight adjustments in parameters (e.g., α'', models of rotation, τ, etc.) that give the best overall agreement. The τ value in Figure 2 is judged to be accurate within 10%. Simulated spectra became insensitive to variation in τ for τ longer than $\sim 7 \times 10^{-8}$ s/rad.

B. *Estimation of* τ. A method for estimating τ in the range 9×10^{-10} to 7×10^{-8} s/rad is suggested by Figure 2. In analogy to previous studies made for nitroxides,[28,30] a useful parameter for vanadyl spin probes is defined by the formula

$$S = \Delta/7A_\parallel \qquad (12)$$

where Δ is the separation (in gauss) between the two outermost peaks (see Figure 2). S is a monotonically increasing function of τ and can be empirically fit to the expression[28]

$$\tau = a(1 - S)^b \qquad (13)$$

Although S is insensitive to reasonable variations in $A_\perp$, $g_\parallel$, and $g_\perp$ values, there is some dependency on the model of rotation and α''. For Brownian rotational diffusion, a least-squares analysis of eq 13 gave values of $a = 1.02 \times 10^{-11}$ s/rad, $b = -1.97$ for $\alpha'' = 1$ G and values $a = 1.38 \times 10^{-11}$ s/rad, $b = -1.84$ for $\alpha'' = 7.5$ G.

The above expressions are accurate to within ~5% over the range of τ from 9×10^{-10} to 7×10^{-8} s/rad for vanadyl spin probes with values of $A_\parallel$ between 150 and 200 G. However, the uncertainty in α'' and in the measurement of Δ (or $A_\parallel$) would, in practice, determine the accuracy with which τ may be estimated. Generally, the longer τ values will have larger inaccuracies for a given uncertainty in α'' or in the measurement of Δ. Thus, for an uncertainty of α'' between 1.0 and 7.5 G, the calculated uncertainty for τ would be ~1% for $\tau = 1 \times 10^{-9}$ s/rad, ~10% for $\tau = 5 \times 10^{-9}$ s/rad, and ~20% for $\tau = 3 \times 10^{-8}$ s/rad. Although accurate estimates of α'' may be difficult without the calculated spectral line shapes, the increased use of vanadyl probes would establish reasonable values. Likewise, for an uncertainty of ±5 G in the measurement of Δ relative to $7A_\parallel$, the calculated error in determining τ would be ~5% at 1×10^{-9} s/rad, ~15% at 5×10^{-9} s/rad, and ~40% at 3×10^{-8} rad/s. Experimentally, however, the measurement of Δ relative to $7A_\parallel$ should be more accurate for longer τ values.

C. *Motionally Narrowed Region.* Equations 7 and 8 yield slightly better fits to experimental line widths of VOacac in toluene than previously reported line width formulae.[17] For example, at −37 °C, $\tau = 7.6 \times 10^{-11}$ s/rad is found to fit best the experimental line width. For this value of τ, the above calculations yield $\alpha'' \sim 0.8$ G. This value of α'' is closer to the spin–rotational contribution to the VOacac line widths than the α'' values previously calculated at this temperature.[17,23] Likewise, δ is calculated to be −0.028 G which is closer to the experimental δ value −0.040 G than the δ value (~−0.016 G) previously obtained.[17] At 24 °C, where the imprecise theoretical δ value yields small contributions to the VOacac line widths, the τ values calculated from β and γ (2.17×10^{-11} and 2.20×10^{-11} s/rad, respectively) are in closer agreement than those based upon previous formule (1.78×10^{-11} and 2.01×10^{-11} s/rad, respectively).

Conclusion

The stochastic Liouville method has been appropriately applied to the calculation of ESR line shapes for vanadyl complexes in the slow tumbling region. Simulated spectral line shapes, which were calculated with axially symmetric magnetic parameters and whose nonsecular contributions were approximated by perturbation analysis, were in good agreement with experimental spectra of VOacac in toluene over the slow tumbling range of τ from $\sim 8 \times 10^{-11}$ to $\sim 7 \times 10^{-8}$ s/rad. If VOacac is considered a spherical Brownian particle of radius 3.28 Å,[17] the above range of τ is calculated from eq 10 to correspond to a viscosity range of 0.022 to 19.5 P at room temperature (25 °C). Likewise, this slow tumbling region would occur for a vanadyl ion that is rigidly attached to spherical Brownian particle with a radius range 4.9 to 47 Å that is dissolved in water at body temperature (37 °C).[31]

The many features of slow tumbling vanadyl spectra (see Figure 2) indicate that a plethora of simple empirical formulae could be developed to estimate accurate τ values without the computation of spectra. Equation 12 is an example that was briefly discussed in the previous section. The use of completely asymmetric magnetic parameters and a better approximation of the nonsecular contributions are needed for quantitative expressions that involve the positions or line widths of interior lines. An extensive and comprehensive account of such formulae will be given in a future publication.

The excellent agreement shown in Figure 1 indicates the potential use of VOacac as a spin probe for viscous liquid crystals.[11b] The nearly axially symmetric magnetic parameters of VOacac greatly simplifies calculations and interpretation. Nonsecular contributions to the line shape, which are seen in Figure 3 to be important in isotropic solvents, are even more important in liquid crystal solvents. Work in this laboratory is presently being conducted in this area.

Acknowledgment. We are grateful for the generous use of the computer facilities provided by the University of Texas at El Paso. Discussions with Professor J. H. Freed and Dr. C. F. Polnaszek are appreciated. This research was supported by the Robert A. Welch Foundation of Houston, Texas.

Appendix A

The form of the equations that are presented below is described in detail elsewhere.[17,19,20] The following general equations are derived from eq 2 but have neglected the nonsecular ($S_{\pm}$) portion. (See Appendix B for treatment of the nonsecular portion).

$$[(\omega - \omega_0 - ma) - i(T_2^{-1} + \tau_L^{-1})]C^L_{0,0}(2m + 2I + 2, 2m + 2I + 1) - (F - m\sqrt{\frac{8}{3}}D)\sum_{L'}N(L,L') \times \begin{bmatrix} L & 2 & L' \\ 0 & 0 & 0 \end{bmatrix}^2 C^{L'}_{0,0}(2m + 2I + 2; 2m + 2I + 1) + \frac{D}{\sqrt{2}}\sum_{L'}N(L,L')\begin{bmatrix} L & 2 & L \\ 0 & 0 & 0 \end{bmatrix}\begin{bmatrix} L & 2 & L' \\ 0 & -1 & 1 \end{bmatrix}[f(I,m) \times \bar{C}^{L'}_{0,1}(2m + 2I + 4, 2m + 2I + 1; 2m + 2I + 2, 2m + 2I + 3) + f(I,m-1)\bar{C}^{L'}_{0,1}(2m + 2I + 2, 2m + 2I - 1; 2m + 2I, 2m + 2I + 1)] = \delta_{L,0} \quad (A.1)$$

$$\{[\omega - \omega_0 - (m + {}^1/_2)a] - i(T_2^{-1} + \tau_L^{-1})\}\bar{C}^L_{0,1}(2m + 2I + 4, 2m + 2I + 1; 2m + 2I + 2, 2m + 2I + 3) + [F - (m + {}^1/_2)\sqrt{\frac{8}{3}}D]\sum_{L'}N(L,L')\begin{bmatrix} L & 2 & L' \\ 0 & 0 & 0 \end{bmatrix}\begin{bmatrix} L & 2 & L' \\ -1 & 0 & 1 \end{bmatrix}\bar{C}^{L'}_{0,1}(2m + 2I + 4, 2m + 2I + 1; 2m + 2I + 2, 2m + 2I + 3) + \frac{f(I,m)D}{\sqrt{2}}\sum_{L'}N(L,L')\begin{bmatrix} L & 2 & L' \\ 0 & 0 & 0 \end{bmatrix}\begin{bmatrix} L & 2 & L' \\ -1 & 1 & 0 \end{bmatrix} \times [C^{L'}_{0,0}(2m + 2I + 2, 2m + 2I + 1) + C^{L'}_{0,0}(2m + 2I + 4, 2m + 2I + 3)] - \frac{D}{2}\sum_{L'}N(L,L')\begin{bmatrix} L & 2 & L' \\ 0 & 0 & 0 \end{bmatrix}\begin{bmatrix} L & 2 & L' \\ -1 & -1 & 2 \end{bmatrix}[f(I,m + 1)\bar{C}^{L'}_{0,2}(2m + 2I + 6, 2m + 2I + 1; 2m + 2I + 2, 2m + 2I + 5) + f(I,m-1)\bar{C}^{L'}_{0,2}(2m + 2I + 4, 2m + 2I - 1; 2m + 2I, 2m + 2I + 3)] = 0 \quad (A.2)$$

$$\left\{\left[\omega - \omega_0 - \left(m + \frac{n}{2}\right)a\right] - i(T_2^{-1} + \tau_L^{-1})\right\}\bar{C}^L_{0,n}(2m + 2I + 2n + 2, 2m + 2I + 1; 2m + 2I + 2, 2m + 2I + 2n + 1) + (-1)^{n+1}\left[F - \left(m + \frac{n}{2}\right)\sqrt{\frac{8}{3}}D\right]\sum_{L'}N(L,L')\begin{bmatrix} L & 2 & L' \\ 0 & 0 & 0 \end{bmatrix}\begin{bmatrix} L & 2 & L' \\ -n & 0 & n \end{bmatrix}\bar{C}^{L'}_{0,n}(2m + 2I + 2n + 2, 2m + 2I + 1; 2m + 2I + 2, 2m + 2I + 2n + 1) + (-1)^{n+1}\frac{D}{2}\sum_{L'}N(L,L') \times \begin{bmatrix} L & 2 & L' \\ 0 & 0 & 0 \end{bmatrix}\begin{bmatrix} L & 2 & L' \\ -n & 1 & n-1 \end{bmatrix}[f(I,m)\bar{C}^{L'}_{0,n-1}(2m + 2I + 2n + 2, 2m + 2I + 3; 2m + 2I + 4, 2m + 2I + 2n + 1) + f(I,m + n - 1)\bar{C}^{L'}_{0,n-1}(2m + 2I + 2n, 2m + 2I + 1; 2m + 2I + 2, 2m + 2I + 2n - 1)] + (-1)^n\frac{D}{2}\sum_{L'}N(L,L')\begin{bmatrix} L & 2 & L' \\ 0 & 0 & 0 \end{bmatrix} \times \begin{bmatrix} L & 2 & L' \\ -n & -1 & n+1 \end{bmatrix}[f(I,m + n)\bar{C}^{L'}_{0,n+1}(2m + 2I + 2n + 4, 2m + 2I + 1; 2m + 2I + 2, 2m + 2I + 2n + 3) + f(I,m-1)\bar{C}^{L'}_{0,n+1}(2m + 2I + 2n + 2, 2m + 2I - 1; 2m + 2I, 2m + 2I + 2n + 1)] = 0 \quad (A.3)$$

$$Z'' = \mathrm{Im}\sum_{m=-I}^{I} C^0_{0,0}(2m + 2I + 2, 2m + 2I + 1) \quad (A.4)$$

I is the nuclear spin; Z'' is the absorption line shape; a, F, D are given by eq 5–7, respectively; ω is the microwave frequency; ω_0 is the external magnetic field in rad/s; T_2^{-1} is the orientation-independent half-width at half-height in rad/s ($\alpha'' = (2/\sqrt{3}|\gamma_e|)T_2^{-1}$);

$$N(L, L') = [(2L + 1)(2L' + 1)]^{1/2} \quad (A.5)$$

$$f(I, m) = [I(I + 1) - m(m + 1)]^{1/2} \quad (A.6)$$

τ_L^{-1} for Brownian rotational diffusion is given by the formula

$$\tau_L^{-1} = \frac{L(L + 1)}{6\tau} \quad (A.7)$$

where τ is the rotational correlation time ($\tau_2 = \tau$). τ_L^{-1} for other models of rotational reorientation is given explicitly elsewhere.[20] Equation A.1 is for $m = -I, -I + 1, \ldots, +I$; eq A.2 is for $m = -I, -I + 1, \ldots, I - 1$; eq A.3 is for $m = -I, -I + 1, \ldots, I - n$ and $n = 2, 3, \ldots, 2I$.

The spin states $|m_s, m_I\rangle$ are labeled as follows: $|1\rangle$ is $|^1/_2, -I\rangle$; $|2\rangle$ is $|^{-1}/_2, -I\rangle$; $|3\rangle$ is $|^1/_2, -I + 1\rangle$; $|4\rangle$ is $|^{-1}/_2, -I + 1\rangle$; etc. The coefficient $C^L_{0,n}(a,b)$ is $\langle a|C^L_{0,n}|b\rangle$ and refers to the transition a → b. Neglecting the nuclear Zeeman term in eq 2 reduces in half the number of coefficients for the "forbidden" transitions.[19,20] These coefficients are given by the combination

$$\bar{C}^L_{0,n}(a,b;c,d) = \frac{1}{\sqrt{2}}[C^L_{0,n}(a,b) \pm C^L_{0,-n}(c,d)] \qquad (A.8)$$

where the minus sign is for odd n values and the plus sign for even n values. $I = 7/2$ for the vanadyl ion. Coefficients $C^L_{0,n}$ that have $n > L$ are not permitted (do not couple to $C^0_{0,0}$). For maximum L values of 2 and 10, eq A.1–A.3 will generate 29 and 166 equations, respectively.

Equations A.1–A.3 with the modifications B.3 for nonsecular effects were solved numerically by the diagonalization method[19,22] on an IBM 360/65 computer. The simulated spectra in Figures 1 and 2 took 4 and 15 min, respectively, to compute.

Appendix B

In previous slow tumbling work, a perturbation treatment analogous to a Van Vleck transformation was used to obtain nonsecular frequency shifts that are appropriate for nitroxide free radicals.[22,32] Because vanadyl complexes have large intramolecular interactions that result in significant nonsecular contributions,[17] this perturbation treatment is generalized to account for both nonsecular "widths" and "shifts". The form of this perturbation theory that is appropriate for vanadyl probes has the term

$$-\sum_{kj}\sum_{L'n'}\frac{\langle L\ 0\ 0|H_1^x(\Omega)_{ij}H_1^x(\Omega)_{jk}|L'\ 0\ n'\rangle}{E_{jj}}C^{L'}_{0,n'}(k) \qquad (B.1)$$

added to $C^L_{0,0}(i)$ in eq A.1. The term (B.1) allows coupling between $C^L_{0,0}(i)$ and $C^{L'}_{0,n}(j)$ and results in a nonsecular "width" contribution.

When the term (B.1) is added to eq A.1, the coupling to $C^{L'}_{0,\pm1}(j)$ invalidates eq A.8 in a strict sense. Within the validity of this second-order perturbation theory, however, the coupling to $C^{L'}_{0,\pm1}(j)$ may be approximated by the expression

$$\frac{1}{\sqrt{2}}[\epsilon^{L'}_{0,1}(a,b) - \epsilon^{L'}_{0,-1}(c,d)]\bar{C}^{L'}_{0,1}(a,b;c,d) \qquad (B.2)$$

where $\epsilon^{L'}_{0,1}(a,b)$ and $\epsilon^{L'}_{0,-1}(c,d)$ are the nonsecular coupling from (B.1) between $C^L_{0,0}(i)$ and $C^{L'}_{0,1}(a,b)$, $C^{L'}_{0,-1}(c,d)$, respectively.

The only significant terms[32] given by the expressions B.1 and B.2 that should be added to the left-hand side of eq A.1 are given in B3.

The perturbation terms (B.3) do not create additional coefficients $C^L_{0,n}(j)$ to be solved for spectral line shape calculations. Also, terms (B.3) are not a function of ω_0. This treatment of the nonsecular terms, therefore, maintains the computational efficiency of the diagonalization method of solution[19] for eq A.1–A.4. An exact treatment of the nonsecular spin Hamiltonian would vastly

$$\begin{aligned}
&-\left[\frac{1}{\omega - i\tau_{L+2}^{-1}}\left\{\frac{3}{20}F^2 - \frac{\sqrt{6}}{5}FDm + \frac{D^2}{15}[7I(I+1) - m^2]\right\} + \frac{1}{\omega - i\tau_L^{-1}}\left\{\frac{a^2}{2}[I(I+1) - m^2]\right\}\right]C^L_{0,0}(2m+2I+2, 2m+2I+1)\\
&-\sum_{L'}\left[\frac{1}{\omega - i\tau_L^{-1}}\left\{-\frac{aD}{\sqrt{6}}[I(I+1) - m^2]\right\}\right.\\
&+\frac{1}{\omega - i\tau_{L'}^{-1}}\left\{\frac{3}{28}F^2 - \frac{\sqrt{6}}{7}FDm - \frac{2D^2}{21}[5I(I+1) - 8m^2] - \frac{aD}{\sqrt{6}}[I(I+1) - m^2]\right\}\Bigg]N(L,L')\\
&\times\begin{bmatrix}L & 2 & L'\\ 0 & 0 & 0\end{bmatrix}^2 C^{L'}_{0,0}(2m+2I+2, 2m+2I+1)\\
&+f(I,m)\sum_{L'}\left[\frac{1}{\omega - i\tau_L^{-1}}\left(\frac{\sqrt{3}}{8}aF - \frac{aD}{2\sqrt{2}} - \frac{aD}{2\sqrt{2}}m\right)\right.\\
&+\frac{1}{\omega - i\tau_{L'}^{-1}}\left\{\frac{5}{7\sqrt{8}}FD - \frac{5D^2}{14\sqrt{3}} + \frac{\sqrt{3}}{8}aF\right.\\
&\left.\left.-\frac{aD}{2\sqrt{2}}m - \frac{5D^2}{7\sqrt{3}}m\right\}\right]N(L,L')\begin{bmatrix}L & 2 & L'\\ 0 & 0 & 0\end{bmatrix}\\
&\times\begin{bmatrix}L & 2 & L'\\ 0 & -1 & 1\end{bmatrix}\bar{C}^{L'}_{0,1}(2m+2I+4, 2m+2I+1; 2m+2I+2, 2m+2I+3)\\
&+f(I,m-1)\sum_{L'}\left[\frac{1}{\omega - i\tau_L^{-1}}\left(\frac{\sqrt{3}}{8}aF + \frac{aD}{2\sqrt{2}} - \frac{aD}{2\sqrt{2}}m\right) + \frac{1}{\omega - i\tau_{L'}^{-1}}\left\{\frac{5FD}{7\sqrt{8}} + \frac{5D^2}{14\sqrt{3}}\right.\right.\\
&\left.\left.+\frac{\sqrt{3}}{8}aF - \frac{aD}{2\sqrt{2}}m - \frac{5D^2}{7\sqrt{3}}m\right\}\right]N(L,L')\\
&\times\begin{bmatrix}L & 2 & L'\\ 0 & 0 & 0\end{bmatrix}\begin{bmatrix}L & 2 & L'\\ 0 & -1 & 1\end{bmatrix}\bar{C}^{L'}_{0,1}(2m+2I+2, 2m+2I-1; 2m+2I, 2m+2I+1)
\end{aligned} \qquad (B.3)$$

increase the number of coefficients to be solved. Also, the form of the equations become similar to those that are obtained for saturated nitroxide line shapes, which used two diagonalizations.[19,34]

References and Notes

(1) "Spin Labelling: Theory and Application", L. Berliner, Ed., Academic Press, New York, N.Y., 1976.
(2) (a) W. L. Hubbell and H. M. McConnell, *J. Am. Chem. Soc.*, **93**, 314 (1971); (b) B. J. Gaffney and H. M. McConnell, *J. Magn. Reson.*, **16**, 1 (1974).
(3) A. S. Waggoner, O. H. Griffith, and C. R. Christensen, *Proc. Nat. Acad. Sci. U.S.A.*, **57**, 1198 (1967).
(4) (a) C. F. Polnaszek and J. H. Freed, *J. Phys. Chem.*, **79**, 2283 (1975); (b) G. R. Luckhurst and A. Swanson, *Mol. Phys.*, **24**, 1297 (1972); (c) H. Schindler and J. Seelig, *J. Chem. Phys.*, **59**, 1841 (1973).
(5) (a) D. D. Thomas, J. C. Seidel, J. S. Hyde, and J. Gergely, *Proc. Nat. Acad. Sci. U.S.A.*, **72**, 1729 (1975); (b) H. M. McConnell and B. G. McFarland, *Q. Rev. Biophys.*, **3**, 91 (1970).
(6) L. T. Muus and P. W. Atkins, Ed., "ESR Relaxation in Liquids", Plenum Press, New York, N.Y., 1972.
(7) J. H. Freed, G. V. Bruno, and C. F. Polnaszek, *J. Phys. Chem.*, **75**, 3385 (1971).
(8) (a) J. H. Freed and G. K. Fraenkel, *J. Chem. Phys.*, **39**, 326 (1963); (b) D. Kivelson, *ibid.*, **33**, 1094 (1960).
(9) C. F. Polnaszek, *Q. Rev. Biophys.*, in press.
(10) (a) N. D. Chasteen, R. J. DeKoch, B. Rodgers, and M. W. Hanna, *J. Am. Chem. Soc.*, **95**, 1301 (1973); (b) R. J. DeKoch, D. J. West, J. C. Cannon, and N. D. Chasteen, *Biochemistry*, **13**, 4347 (1974);

(c) N. D. Chasteen and J. J. Fitzgerald, *ibid.*, **13**, 4338 (1974).
(11) (a) G. R. Luckhurst, "ESR Relaxation in Liquids", L. T. Muus and P. W. Atkins, Ed., Plenum Press, New York, N.Y., 1972, Chapter XV; (b) G. C. Fryburg and E. Gelerinter, *J. Chem. Phys.*, **52**, 3378 (1970).
(12) R. F. Campbell and M. W. Hanna, *J. Phys. Chem.*, **80**, 1892 (1976).
(13) R. Kubo, "Stochastic Processes in Chemical Physics, Advances in Chemical Physics", Vol. XVI, K. E. Shaler, Ed., Wiley, New York, N.Y., 1969, p 101.
(14) J. Selbin, *Coord. Chem. Rev.*, **1**, 293 (1966).
(15) B. L. Vallee and W. E. C. Wacker, "The Proteins", Vol. 5, H. Neurath, Ed., Academic Press, New York, N.Y., 1970.
(16) T. F. Yen, "The Role of Trace Metals in Petroleum", T. F. Yen, Ed., Ann Arbor Science Publishers, Ann Arbor, Mich., 1975, Chapters I and X.
(17) R. Wilson and D. Kivelson, *J. Chem. Phys.*, **44**, 154 (1966).
(18) B. E. Bryant and W. C. Fernelius, *Inorg. Syn.*, **5**, 115 (1957).
(19) G. V. Bruno, Ph.D. Thesis, Cornell University, Ithaca, N.Y., 1973.
(20) S. A. Goldman, G. V. Bruno, C. F. Polnaszek, and J. H. Freed, *J. Chem. Phys.*, **59**, 3071 (1973).
(21) Varian Associates, NMR Table (Nuclear Magnetic Resonance), 4th ed.
(22) R. G. Gordon and T. Messenger, "ESR Relaxation in Liquids", L. T. Muus and P. W. Atkins, Ed., Plenum Press, New York, N.Y., 1972, Chapter XIII.
(23) P. W. Atkins and D. Kivelson, *J. Chem. Phys.*, **44**, 169 (1966).
(24) P. Debye, "Polar Molecules", Dover Publications, New York, N.Y., 1945.
(25) N. D. Chasteen and M. W. Hanna, *J. Phys. Chem.*, **76**, 3951 (1972).
(26) G. K. Fraenkel, *J. Chem. Phys.*, **42**, 4275 (1965).
(27) L. Libertini and O. H. Griffith, *J. Chem. Phys.*, **53**, 1359 (1970).
(28) S. A. Goldman, G. V. Bruno, and J. H. Freed, *J. Phys. Chem.*, **76**, 1858 (1972).
(29) R. Lefebve and J. Maruani, *J. Chem. Phys.*, **42** 1480 (1965).
(30) R. C. McCalley, E. J. Shimshick, and H. M. McConnell, *Chem. Phys. Lett.*, **13**, 115 (1972).
(31) "Handbook of Chemistry and Physics", 56th ed, R. C. Weast, Ed., Chemical Rubber Publishing Co., Cleveland, Ohio, 1974.
(32) C. F. Polnaszek, G. V. Bruno, and J. H. Freed, *J. Chem. Phys.*, **58**, 3185 (1973).
(33) C. F. Polnaszek, Ph.D. Thesis, Cornell University, Ithaca, N.Y., 1975.
(34) S. A. Goldman, G. V. Bruno, and J. H. Freed, *J. Chem. Phys.*, **59**, 3071 (1973).

COMMUNICATIONS TO THE EDITOR

Combustion of Carbon. Effect of Sulfur Dioxide

Publication costs assisted by Brookhaven National Laboratory

Sir: Although sulfur dioxide is generated in most combustion processes involving carbonaceous fuels, not much attention has been paid to its effect on combustion. However, it has been found that, below 500 °C, SO_2 retards the oxidation reaction of carbon by O_2; and a sulfoxy species was found on the carbon surface which was held responsible for the retardation.[1] In this report, we present the observation of a prominent transient effect caused by SO_2 at higher temperatures.

In the mechanism of the C–O_2 reaction, which is not thoroughly understood, surface oxides are formed upon collision of oxygen molecules and some oxide species thus formed are quite thermally stable and they do not contribute significantly to the rate of combustion. The surface sites capable of forming oxides, with various thermal stabilities, amount to only a few percent of the total surface area measured by BET N_2 adsorption method.[2] The surface oxides are formed preferentially on the edge carbon atoms rather than on the basal planes.[3,4] With SO_2 present in the gas phase, at temperatures higher than 500 °C, SO_2 does not seem to affect the steady-state (at constant SO_2 partial pressures) combustion rate.[1] However, upon changing the SO_2 partial pressure in the gas phase, a strong transient effect is observed and it will be shown here that the effect is caused by the interaction of SO_2 with the "stable" surface oxides.

The carbon used was a petroleum coke with the following analyses: L_c = 32 Å; L_a = 17 Å; d spacing = 3.458 Å; BET surface area at 0% burn-off (N_2 adsorption) = 3.2 m^2/g; impurities in ppm: Fe, 250; Ca, 200; V, 170; Al, 140; Si, 80; Na, 60; Ni, 20; Mg, 16; Pb, 16; Cu, 10; K, 6; and traces of others. Reaction rate at a total pressure of 1 atm was measured gravimetrically and is expressed in fractional weight loss per unit time based on the instantaneous sample weight. The experimental methods have been described elsewhere.[1,5] The particle size was in the range of 590–840 μm.

In Figure 1, retardation of the rate at 500 °C by SO_2 is shown. Steady rates were restored upon changing the SO_2 concentration, as shown by the solid line. Rates with

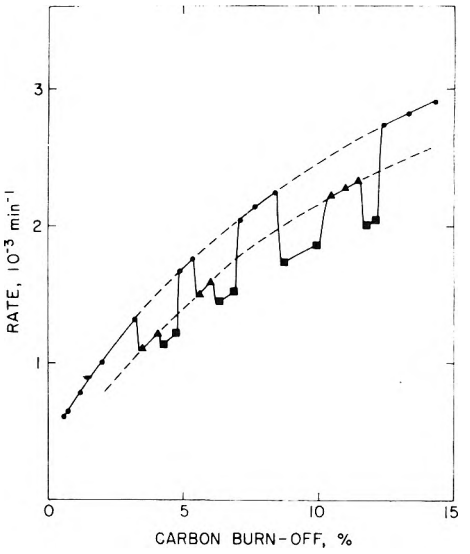

Figure 1. Effect of SO_2 concentration on the oxidation rate at 500 °C (total pressure = 1 atm) with 15% O_2 in N_2 and with the following SO_2 concentrations: 0% (●); 1% (▲), and 3% (■). Dashed curves represent rates with constant gas composition.

constant gas concentrations (0 and 1% SO_2) were also measured and are shown by the dashed line. At higher temperatures, however, transient perturbations of the rates were observed upon changing the SO_2 concentration. As shown in Figure 2, a transient increase of the rate occurred upon increasing the SO_2 concentration and a transient decrease occurred upon decreasing the SO_2 concentration. More important, in either case, the rate returned to a steady value after the transient perturbation, and the steady rate did not differ from the rate wherein no SO_2 exists (the dashed line). The magnitude of the transient effect increases with temperature. A "control experiment" was also performed in which O_2 was shut off after a few percent carbon burn-off, and SO_2 was subsequently introduced into the system and its concentration varied thereafter. As shown in Figure 3, no transient perturbation due to the change of SO_2 concentration occurred once the oxidized surface had been exposed to SO_2.

In all the experiments with SO_2, condensed elemental

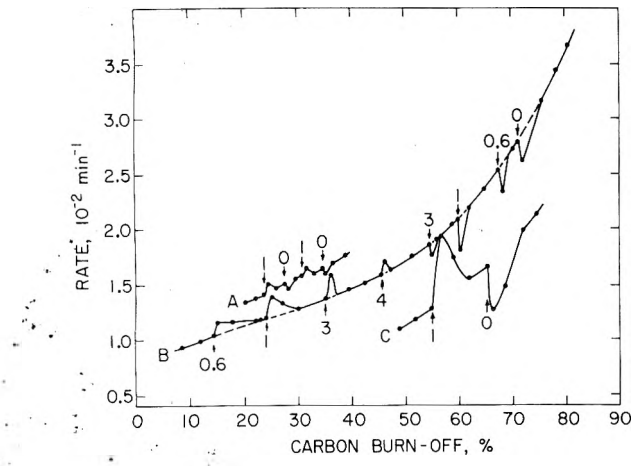

Figure 2. Effect of changing SO_2 concentration on the oxidation rate at higher temperatures (total pressure = 1 atm). Arrows indicate where the SO_2 concentration is changed to a new level denoted by a number in percent (it is held constant until a further change): (A) 600 °C and 5% O_2 in N_2, (B) 700 °C and 2% O_2 in N_2; and (C) 800 °C and 1% O_2 in N_2.

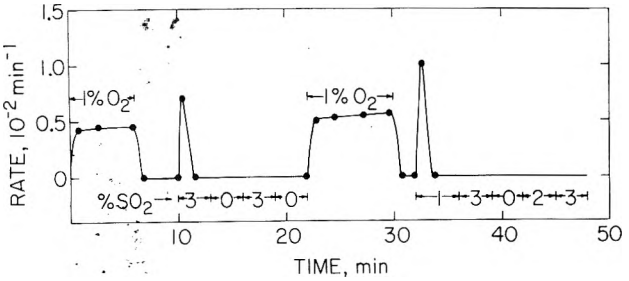

Figure 3. Reaction of SO_2 with stable surface oxides at 800 °C in flowing N_2.

sulfur was found on the cooler walls downstream of the reactor. Gas samples were analyzed by mass spectrometry during the transient perturbations (which lasted for several minutes) in the experiments the results of which are presented in Figures 2 and 3. The analyses showed that SO_2 was partially consumed and the gaseous products were mainly CO_2 and a small amount of COS. Other sulfur compounds and CO were not detected and are assumed to be negligible. The major differences in the analytical results for the two cases, i.e., in Figures 2 and 3, were that quantities of the sulfur deposit and the net SO_2 consumption for the latter case were much greater. Presumably most of the sulfur formed in the former case was oxidized in the gas phase by oxygen. A solid-phase analysis was also made for the sulfur content in the "control experiment" and it showed a gain of 0.1%; it increased from 1.7 to 1.8%.

From the above, it is clear that SO_2 interacts with the thermally stable surface oxides, dissociates and removes CO_2, releases S and COS resulting in a net weight loss of carbon. Although the reaction mechanisms involved are obviously very complex, the following represents the major reactions that are consistent with the observations:

$$C(O) + SO_2 \rightarrow CO_2(g) + C^*(SO) \quad (1)$$

$$C^*(SO) + C(O)_m \rightarrow C^*O_2(g) + S(g) + C_f \quad (2a)$$

$$C^*(SO) \rightarrow COS(g) + C_f \quad (2b)$$

$$C_f + O_2 \rightarrow C(O) + \ldots \quad (3)$$

$$C_f + SO_2 \xrightarrow{\text{slow}} CO + CO_2 + S + C(S \text{ species}) \quad (4)$$

The parentheses indicate the adsorbed state, the asterisk indicates the new surface site, and the subscript f denotes the free site. The subscript m indicates a mobile oxygen which remains in the surface force field but is energetic enough to jump from site to site, and which is believed to be important in the C–O_2 mechanism.[6,7] Reaction 2a is thought to be more important than reaction 2b. Reaction 3 could serve as a chain propagator until a stable species, e.g., an oxide, sulfide, or sulfoxide, is formed. This probably explains why the transient perturbations are longer when O_2 is present; especially when the surface is first exposed to SO_2 (Figure 2), and the transients are always shorter when SO_2 is not present in the gas phase (Figure 3). Reaction 4 has been studied and it proceeds quite slowly as compared to rates measured in this study.[8,9]

The fact that a steady-state rate is restored at each SO_2 concentration indicates that an equilibrium is reached between the gas phase and surface species involving sulfur. Results shown in Figure 3, however, indicate the lack of such an equilibrium. Therefore, O_2 in the gas phase must be involved in the equilibrium. The nature of the equilibrium and the interactions between SO_2 and the surface oxides, in general, is far from being understood at this point.

Results presented in this report are qualitative. Further work is in progress in our laboratory and the results should also shed some light on the carbon combustion mechanism. In passing, it should be noted that a similar phenomenon has also been observed with a nuclear graphite (ash content <100 ppm) in our laboratory and the involvement of the impurities does not seem likely. It is also noted that the suddenness in changing the SO_2 concentration seems to affect the intensities of the spikes. All the changes reported in this work were made by switching premixed gas flows.

Acknowledgment. We thank Mr. R. Smol for the entire experimental work and Drs. J. W. Sutherland and C. R. Krishna for helpful discussions. The carbon sample was kindly supplied and characterized by the Physical Chemistry Division of Alcoa Laboratories. This work was performed under the auspices of the Office of Molecular Sciences, Division of Physical Research, U.S. Energy Research and Development Administration, Washington, D.C.

References and Notes

(1) R. T. Yang and M. Steinberg, *Carbon*, **13**, 411 (1975).
(2) N. R. Laine, F. J. Vastola, and P. L. Walker, Jr., *J. Phys. Chem.*, **67**, 2030 (1963).
(3) G. R. Hennig, *Proc. Conf. Carbon, 5th*, **1**, 143 (1962).
(4) E. J. Evans, R. J. M. Griffiths, and J. M. Thomas, *Science*, **171**, 174 (1971).
(5) R. T. Yang and M. Steinberg, *J. Phys. Chem.*, **80**, 965 (1976).
(6) P. L. Walker, Jr., F. J. Vastola, and P. J. Hart in "Fundamentals of Gas-Surface Interactions", H. Saltzburg, J. N. Smith, and R. Rogers, Ed., Academic Press, New York, N.Y., 1967, p 307.
(7) H. Marsh and A. D. Foord, *Carbon*, **11**, 421 (1973).
(8) W. O. Stacy, F. J. Vastola, and P. L. Walker, Jr., *Carbon*, **6**, 917 (1968).
(9) H. Abramowitz, R. Insinga, and Y. K. Rao, *Carbon*, **14**, 84 (1976).

Department of Applied Science
Brookhaven National Laboratory
Upton, New York 11973

Ralph T. Yang*
Meyer Steinberg

Received December 20, 1976

Absolute Infrared Intensity Measurements of Fluoroform (CHF_3) Fundamentals

Sir: We should like to report here some recent measurements of the absolute integrated molar absorption

TABLE I: Summary of Reported Integrated Molar Absorption Coefficients, $A_i = \Gamma_i \nu_i$ (km mol^{-1}), for the Fundamental Vibrations of Fluoroform

Band	ν_i, cm^{-1}	A_i, km mol^{-1} This work	Ref 3	Ref 2	Best estimate
ν_1(CH)	3035	23.5 ± 1.9	24.8 ± 0.7	25.4 ± 1.4	24.6 ± 1.1[a]
ν_2, ν_5(CF)	1150	540 ± 100	690 ± 2.0	860 ± 30	620 ± 80[b]
$\nu_3(\delta CF_2)$	700	14.6 ± 1.5	13.2 ± 0.4	15.0 ± 1.5	14.3 ± 1.1[a]
$\nu_4(\delta CH)$	1377	87.6 ± 6.1	87.5 ± 2.4	97.5 ± 2.9	87.6 ± 4.3[b]
$\nu_6(\delta CF_2)$	507.5	49.2 ± 3.4	46 ± 1.4	57.7 ± 3.1	49 ± 2.0[a]
ΣA_i		670 ± 80	820 ± 20	1010 ± 30	750 ± 80 (756)[c]

[a] Average of the three values. [b] Average of the values from this work and those from SMK, ref 3. [c] Calculated value; taken from ref 4.

coefficients[1]

$$\Gamma_i = (1/nl)\int \ln (I_0/I)\, d(\ln \nu)$$

for the six fundamental vibrations of CHF_3. There have been two previous studies[2,3] of these properties; however, it is still difficult enough to make accurate intensity measurements that it is worth repeating them, especially for molecules (such as the freons) that are of such potential interest as atmospheric pollutants.[4] We report here just the experimental results; an analysis of the significance of these results will be presented elsewhere.[5]

We have used the Wilson–Wells technique[6] as modified by Penner and Weber[7] in our study. The metal (brass) gas cell (about 3.28 ±.0.01 cm pathlength) with 1-cm thick KBr windows (based on a design by Dickson[8]) was filled to a known measured partial pressure of fluoroform, and then pressurized to a total pressure of 15 atm by the addition of prepurified N_2 gas. The CHF_3 was from Linde Specialty Gas Division of the Union Carbide Corp., and the prepurified N_2 was from Air Reduction Co. The minimum purity of CHF_3 was claimed to be 98%; no impurities in either CHF_3 or N_2 were detected in the infrared spectra. The pressures of CHF_3 were read on an open-ended mercury manometer or on a Cartesian diver pressure gauge (Gilmont Instruments) depending on whether the pressure was greater than or less than, respectively, 20 Torr. The N_2 pressure was adjusted using an ordinary reducing valve. The spectra were measured on an Perkin-Elmer Model E-14 single beam grating spectrometer with spectral slit widths of about 1 cm^{-1}. The spectrum of the empty cell was recorded; the cell was then filled with the sample, pressurized, and the spectrum recorded again. In case the background and sample spectra did not coincide in regions of no absorption, a correction (gain change) was applied to bring them together. The scans were repeated several times. The data were read and converted to values of $\ln (I_0/I)$ at known wavenumbers and integrated numerically by the trapezoid rule using a programmable calculator. Errors in the numerical integration are much less than experimental error due to shifting background.

The integrated areas were plotted in a Beer's law plot vs. nl, the product of concentration and pathlength. A least-squares fit to the data produced the results given in Table I. We have listed there the values of $A_i = \Gamma_i \nu_i$, with uncertainties corresponding approximately to the value of 2σ (twice the standard deviation) calculated from the scatter about the Beer's law plots. We have also listed the values of A_i reported by Morcillo, Herranz, and Biarge[2] and those reported more recently by Saëki, Mizuno, and Kondo[3] for comparison. For each band we have also indicated our "best estimate" of the correct intensity obtained by averaging the date as described below.

In comparing the three measurements, we find that they are all in reasonably good agreement if allowance is made for what we believe are unrealistically low experimental uncertainties (estimated to a lower confidence level than ours) given by the others workers. For ν_1, ν_3, and ν_6 all three measurements agree within the experimental uncertainties; the "best estimates" are just the average of the three values with uncertainties that overlap the three different measurements. We are in close agreement with Saëki, Mizuno, and Kondo[3] (SMK) on the intensity of ν_4 but differ considerally from Morcillo, Herranz, and Biarge (MHB).[2] Our "best estimate" for the intensity of this band is the average of our value and that found by SMK.[3] Similarly, we believe our agreement on the intensity of the overlapped (ν_2, ν_5) pair with SMK[3] is within the respective experimental uncertainties, although again we differ from MBH.[3] Again, we average our result with that from SMK to obtain our "best estimate".

Although we shall discuss these results elsewhere,[5] it is worth pointing out here the remarkable agreement between the sum of the "best estimate" intensity values and the value predicted in ref 4, using effective changes[9] $\xi_C = 2.64e$ (obtained by linear interpolation between ξ_C for CH_4 and ξ_C for CF_4 as described in ref 4), $\xi_F = 1.06e$, and $\xi_H = 0.15e$.

Acknowledgment. We are grateful to the National Science Foundation for Grant No. CHE 74-21471 for partial financial support of this work. We are also grateful to Mr. Philip Bennett for preliminary measurements on this system.

References and Notes

(1) For definitions and discussion of details of the method see (a) J. Overend in "Infrared Spectroscopy and Molecular Structure", M. Davies, Ed., Elsevier, Amsterdam, 1963, p 345 *ff*; and (b) W. B. Person and D. Steele, "Molecular Spectroscopy", Vol. 2, The Chemical Society, London, 1974, p 357 *ff*.
(2) J. Morcillo, J. Herranz, and J. F. Biarge, *Spectrochim. Acta*, **15**, 110 (1959).
(3) S. Saëki, M. Mizuno, and S. Kondo, *Spectrochim. Acta, Part A*, **32**, 403 (1976).
(4) For example, see the discussion by W. B. Person, S. K. Rudys, and J. Newton, *J. Phys. Chem.*, **79**, 2525 (1975).
(5) J. H. Newton, R. A. Levine, and W. B. Person, to be published.
(6) E. B. Wilson, Jr., and A. J. Wells, *J. Chem. Phys.*, **14**, 578 (1946).
(7) S. S. Penner and D. Weber, *J. Chem. Phys.*, **19**, 807 (1950).
(8) A. D. Dickson, Ph.D. Thesis, University of Minnesota, 1955.
(9) W. T. King, G. B. Mast, and P. P. Blanchette, *J. Chem. Phys.*, **56**, 4440 (1972).

Department of Chemistry
University of Florida
Gainesville, Florida 32611

Robert A. Levine
Willis B. Person*

Received December 8, 1976

An Ionic Scale for the Partial Molal Heat Capacities of Aqueous Electrolytes from Chemical Models

Publication costs assisted by the Université de Sherbrooke

Sir: The determination of individual ionic contributions to the properties of electrolyte solutions has generally lead

to important advances in our understanding of ionic hydration. Since models and theories describing solvation phenomena attempt to predict single ion properties, experimental data on single ions become of highest relevance. Indeed the determination of ionic values for conductance, standard free energy and entropy, and limiting partial molal volumes have greatly improved our basic knowledge of the relative behavior of anions and cations in aqueous solution.[1,2]

The fundamental importance of single ion thermodynamic data make it desirable to reach for every function useful in characterizing ionic solvation. It quickly becomes apparent, however, that much in the same way as the theoretical prediction, single ion data for the second pressure or temperature derivatives of the free energy are difficult to extract in any reliable way. For example, the limiting partial molal heat capacity of electrolytes $\bar{C}_p°$, which is particularly sensitive to solvation effects, could not be satisfactorily resolved into its ionic components. So far, two types of approaches have been attempted involving either a rigourous treatment of ionic entropies of limited accuracy, or an intuitive breakdown of accurate heat capacity data.

Following the first type of approach, Criss and Cobble[3] have assigned partial molal ionic entropies in aqueous solutions as function of temperature, based on a "correspondance principle" for like-charge ions. From these data, the authors obtain an ionic scale of $\bar{C}_p°$ which yields $\bar{C}_p°(H^+) = 28$ cal mol^{-1} K^{-1}.

The "intuitive" approaches usually involve extrathermodynamic assumptions, such as, for example, $\bar{C}_p°(K^+) = \bar{C}_p°(F^-)$. Using the latter assumption, Noyes[4] tabulated an ionic scale leading to $\bar{C}_p°(H^+) = -14.5$ cal mol^{-1} K^{-1}. Another extrathermodynamic method, which has been found accurate for limiting partial molal volumes, can be devised from the data for homologous tetraalkylammonium salts.[5] A plot of $\bar{C}_p°$ data for R_4NBr salts as function of the molecular weight of the cation (or number of carbon atoms) can be extrapolated to give an estimate of $\bar{C}_p°(Br^-)$. This approach yields $\bar{C}_p°(H^+)$ as 30 cal mol^{-1} K^{-1}.[6,7] Although the agreement with the result derived from ionic entropies is good, it was believed fortuitous due to the rather different hydration effects associated with the lower and higher homologues in the R_4NBr series, i.e., Me_4N^+ and Bu_4N^+.[6]

We submit below still another extrathermodynamic method based on the following hypothesis: given a pair of analogous neutral and ionic quaternary compounds (e.g., R_4C and $R_4Y^+X^-$) with R substituents appropriate to effectively mask the charge on the central atom of R_4Y^+, then $\bar{C}_p°(R_4C) \equiv \bar{C}_p°(R_4Y^+)$. Following this assumption, $\bar{C}_p°(X^-)$ and the corresponding ionic scale is directly obtained from the experimental data for the neutral and ionic analogues.

As a first set of model compounds to test this hypothesis, we have chosen pentaerythritol $(HOCH_2)_4C$ and the salt tetrakis(hydroxymethyl)phosphonium chloride. The choice of polyol type compounds was suggested from solubility requirements for the neutral solute and also from the results of earlier investigations of $\bar{V}°$ and $\bar{C}_p°$ of such solutes in water.[8] Comparison among data for various alcohols and polyols showed that the –OH group cancels the anomalous positive $\bar{C}_p°$ contribution associated with the solvation of hydrophobic methyl or methylene groups. Hence, provided the –ROH groups (in the present case, $-CH_2OH$) effectively screen the charge of the central atom, the nature of the hydrophilic surfaces of the cationic and neutral polyol will be similar, and their $\bar{C}_p°$ can be compared in absence of the particular hydrophobic effects.

TABLE I: Limiting Apparent Molal Volume and Heat Capacity of Analogous Solutes at 25 °C

	$\phi_v° = \bar{V}°$,[b] cm^3 mol^{-1}	$\phi_c° = \bar{C}_p°$,[b] cal K^{-1} mol^{-1}	Concn range, m	No. of data points
$(HOCH_2)_4C$	101.90 ± 0.02 (101.81)[a]	80.2 ± 0.5 (78.6)[a]	0–0.4	7
$(HOCH_2)_4PCl$	124.78 ± 0.01	42.0 ± 0.2	0.1–2.0	16

[a] Reference 8. [b] Uncertainties quoted are standard deviations; for $(HOCH_2)_4PCl$, the standard deviation was calculated from data in the range 0.1–2.0 m.

The density (d) and volumetric specific heat (σ) of aqueous solutions of $(HOCH_2)_4C$ and $(HOCH_2)_4P^+Cl^-$ have been measured using flow techniques described in details elsewhere,[9,10] and capable of the following precision: $d \pm 2 \times 10^{-6}$ g cm^{-3} and $\sigma \pm 2 \times 10^{-5}$ cal K^{-1} cm^{-3} or ±0.2% of $(\sigma - \sigma_0)$. Pentaerythritol was recrystallized several times from ethanol and dried in a vacuum oven at 50 °C; the phosphonium salt was recrystallized twice from 2-propanol immediately before use and dried under P_2O_5 in vacuo. Chloride analysis of the latter showed >99.7% purity.

The solutions were prepared by weight following usual precautions.[6,8] Because of weak acid ionization of $(HOCH_2)_4P^+Cl^-$ (or minor acid impurities), the data at concentration lower than 0.1 m exhibited deviations much greater than the standard deviation. The consequences of such deviations on ϕ_v^0 and ϕ_c^0 should not be too serious, however, since the limiting values could be extrapolated from data in the range 0.1–2.0 m which showed accurate linearity. Furthermore, the magnitudes of the deviations were verified by adding 0.02–0.05 m HCl to minimize the effect of acid ionization.

The apparent molal volumes ϕ_v and heat capacities ϕ_c were calculated and plotted as described in earlier reports[6,8] to obtain the infinite dilution data reported in Table I.

The ϕ_v^0 and ϕ_c^0 values obtained here for pentaerythritol differ somewhat from those reported in a previous study.[8] This is due, in part, to the difficulty in assessing the purity of this compound especially with regards to contamination by dipentaerythritol. For the ϕ_c data, the discrepancy may be further understood since the polyhydroxy compounds have a marked effect on the volumetric specific heats and since our accuracy is limited at best to ±0.2% on the differential measurement $(\sigma - \sigma_0)$. However, the results reported in Table I were reproduced using two different batches of pentaerythritol, so we can safely presume that they are more accurate than the earlier data.

A straightforward application of our working hypothesis to the data in Table I yields $\bar{V}°(Cl^-) = 22.88$ cm^3 mol^{-1} and $\bar{C}_p°(Cl^-) = -36.7$ cal K^{-1}. From corresponding data for HCl ($\bar{V}° = 18.1$ cm^3 mol^{-1} [11] and $\bar{C}_p° = -29.4$ cal K^{-1} mol^{-1},[12] we obtain:

$$\bar{V}°(H^+) = -4.8 \pm 0.1 \text{ cm}^3 \text{ mol}^{-1}$$

and

$$\bar{C}_p°(H^+) = 7.3 \pm 1.0 \text{ cal K}^{-1} \text{ mol}^{-1}$$

The agreement of the $\bar{V}°(H^+)$ obtained here with the value of –5.4 cm^3 mol^{-1} established through various independent methods[2] is quite remarkable. On the other hand, the value of 7 cal K^{-1} mol^{-1} for $\bar{C}_p°(H^+)$ is roughly centered between the extremes obtained under previous assumptions: –14 to +31 cal K^{-1} mol^{-1}.

Although, from a unique set of data, it would be premature to conclude on the accuracy of the method for deriving ionic scales of $\bar{V}°$ and $\bar{C}_p°$, it is interesting that

we find $\bar{C}_p°(H^+)$ still large and positive. This situation implies that $\bar{C}_p°$ of common cations and anions are vastly different; for example, $\bar{C}_p°$ of alkali and halide ions would be of opposite signs.

From the preliminary results, the approach followed here suffers no obvious inconsistency and appears promising in supplying independent estimates of ionic partial molar volumes and heat capacities. The hypothesis is being further investigated with other analogous pairs of ionic and neutral compounds, with particular attention to two limiting aspects. In a first part, we should elucidate how the residual charge on the –ROH substituent of the cation will affect the derived ionic values. On the other hand, since it is known that $\bar{V}°$ of quaternary ions depends on the nature of the central atoms (differences in bond lengths[13]), we should establish the dependence of the ionic scales on this parameter.

Acknowledgment. The authors gratefully acknowledge financial assistance from the National Research Council of Canada through an operation grant and a scholarship to one of us (J.C.M.).

References and Notes

(1) D. R. Rosseinsky, *Chem. Rev.*, **65**, 467 (1965).
(2) J. E. Desnoyers and C. Jolicoeur in "Modern Aspects of Electrochemistry", B. E. Conway and J. O'M. Bockris, Ed., Plenum Press, New York, N.Y., 1969, Chapter 1.
(3) C. M. Criss and J. W. Cobble, *J. Am. Chem. Soc.*, **86**, 5390 (1964).
(4) R. M. Noyes, *J. Am. Chem. Soc.*, **86**, 941 (1964).
(5) B. E. Conway, R. E. Verrall, and J. E. Desnoyers, *Trans. Faraday Soc.*, **62**, 2738 (1966).
(6) C. Jolicoeur, P. R. Philip, G. Perron, P. A. Leduc, and J. E. Desnoyers, *Can. J. Chem.*, **50**, 3167 (1972).
(7) C. Shun, I. Worsley, and C. M. Criss, private communication.
(8) C. Jolicoeur and G. Lacroix, *Can. J. Chem.*, **54**, 624 (1976).
(9) P. Picker, E. Tremblay, and C. Jolicoeur, *J. Solution Chem.*, **3**, 377 (1974).
(10) P. Picker, P. A. Leduc, P. R. Philip, and J. E. Desnoyers, *J. Chem. Thermodyn.*, **3**, 631 (1971).
(11) Reference 2, p 26.
(12) J. L. Fortier, P. A. Leduc, and J. E. Desnoyers, *J. Solution Chem.*, **3**, 323 (1974).
(13) F. J. Millero, *J. Phys. Chem.*, **75**, 280 (1971).

Department of Chemistry
Université de Sherbrooke
Sherbrooke, Quebec J1K 2R1, Canada

Carmel Jolicoeur*
Jean-Claude Mercier

Received December 20, 1976

Termolecular Complexes of Trinitrobenzene and 5-Methoxyindole

Sir: It has been suggested that some of the observed anomalies concerning the calculated values of association constants for the formation of 1:1 complexes between π electron donors (D) and acceptors (A) are due to the presence in solution of termolecular complexes as well as the more familiar bimolecular complexes.[1-4] AD_2 is the termolecular complex reported since in the solutions usually studied the total concentration of donor ($[D]_0$) is greater than the total concentration of acceptor ($[A]_0$). In this paper we shall describe a study of the interaction of 5-methoxyindole with trinitrobenzene (TNB) in 1,2-dichloroethane that was performed using a variety of ratios of $[A]_0$ to $[D]_0$ in order to be able to observe different species of complexes. Thus when $[D]_0 \sim [A]_0$ AD should be the only complex present in solution if the solutions are dilute and the association constants for formation of the termolecular complexes are less than that for the bimolecular complex, while if the ratio is $[A]_0 >> [D]_0$ AD and A_2D will be the predominant species and if $[D]_0 >> [A]_0$ the major species present will be AD and AD_2. The equations for the formation of these complexes are

$$A + D = AD$$
$$AD + D = AD_2 \quad \text{(excess D)}$$
$$AD + A = A_2D \quad \text{(excess A)}$$

If this model is correct and proper account is taken of the termolecular species, experimental values of the association constants determined for AD (K_{AD}) should be the same when separately evaluated for each of the different ranges of concentration since AD is the complex species common to all the solutions.

The TNB 5-methoxyindole complex was chosen for this work because of a study on it and other substituted indole TNB complexes by Sung and Parker in which they assumed that only AD was present.[5] The values of K_{AD} that they gave differ considerably when results obtained for $[D]_0 >> [A]_0$ are compared with those obtained for $[A]_0 >> [D]_0$. Further indication that these compounds may form termolecular complexes can also be seen from the almost 100% variation in K_{AD} values obtained using the NMR spectral lines of different protons in the same complex.

A recent review by Foster has discussed the methods used to obtain the association constant from either the optical density (OD) at the peak of the charge transfer band or the upfield shift of a NMR line in one component caused by the other component (Δ).[1] In solutions where the ratio $[D]_0/[A]_0 = n$ is close to one and $[AD] << [A]_0$, $[A]_0$ and OD are related to the values of K_{AD} and the absorption coefficient of AD (ϵ_{AD}) by

$$\frac{[A]_0}{OD} = \frac{1}{nK_{AD}\epsilon_{AD}}\frac{1}{[A]_0} + \frac{n+1}{n}\frac{1}{\epsilon_{AD}} \tag{1}$$

For a series of solutions with a constant value of n, a plot of $[A]_0/OD$ vs. $1/[A]_0$ is linear and K_{AD} and ϵ_{AD} can be evaluated from the slope and intercept determined by a standard least-squares treatment. When $[A]_0 >> [D]_0$ or $[D]_0 >> [A]_0$ and only 1:1 complexes are assumed to be present the scatchard equation (eq 2) can be used to

$$\frac{OD}{[A]_0[D]_0} = -K_{AD}\frac{OD}{[A]_0} + K_{AD}\epsilon_{AD} \quad \text{for } [D]_0 >> [A]_0 \tag{2a}$$

$$\frac{OD}{[A]_0[D]_0} = -K_{AD}\frac{OD}{[D]_0} + K_{AD}\epsilon_{AD} \quad \text{for } [A]_0 >> [D]_0 \tag{2b}$$

evaluate K_{AD} and ϵ_{AD}. Both eq 2a and 2b are linear equations, so K_{AD} and ϵ_{AD} can be determined from the least-squares values of the slopes and intercepts of plots of $OD/[A]_0[D]_0$ vs. $OD/[A]_0$ or $OD/[D]_0$. When the formation of termolecular complexes (either AD_2 or A_2D) is taken into account eq 3 is applicable. K_{AD_2} and K_{A_2D} are

$$\frac{OD}{[A]_0[D]_0} = -K_{AD}(1 + K_{A_2D}[A]_0)\frac{OD}{[A]_0} + K_{AD}\epsilon_{AD} + \epsilon_{A,D}K_{AD}K_{A,D}[A]_0 \quad \text{for } [A]_0 >> [D]_0 \tag{3a}$$

$$\frac{OD}{[A]_0[D]_0} = -K_{AD}(1 + K_{AD_2}[D]_0)\frac{OD}{[D]_0} + K_{AD}\epsilon_{AD} + \epsilon_{AD_2}K_{AD}K_{AD_2}[D]_0 \quad \text{for } [D]_0 >> [A]_0 \tag{3b}$$

the formation constants for the reaction of AD with excess D or excess A. These last equations unlike eq 2a and 2b

TABLE I: Association Constants, Absorption Coefficients, and Chemical Shifts for 5-Methoxyindole–TNB Complexes in CH_2ClCH_2Cl at 33 °C

Concn ratio	Equation used	Method	K_{AD} (kg of solution/mol)	ϵ_{AD}		
$[A]_0 \sim [D]_0$	1	UV	4.8 ± 0.8	910 ± 180		
$[D]_0 > [A]_0$	2	UV	1.62 ± 0.06	2040 ± 20		
$[A]_0 > [D]_0$	2	UV	2.02 ± 0.13	1580 ± 40		
$[D]_0 > [A]_0$	3	UV	4.3 ± 0.6	800 ± 100	$K_{AD_2} = 1.0 \pm 0.3$	$\epsilon_{AD_2} = 1800 \pm 200$
$[A]_0 > [D]_0$	3	UV	4.5 ± 0.6	670 ± 100	$K_{A_2D} = 0.9 \pm 0.3$	$\epsilon_{A_2D} = 2230 \pm 200$
$[D]_0 > [A]_0$	2	NMR	1.43 ± 0.04	$\Delta_{AD} = 1.20 \pm 0.02$ ppm		
$[D]_0 > [A]_0$	3	NMR	4.6 ± 0.6	$\Delta_{AD} = 0.4 \pm 0.1$ ppm	$K_{AD_2} = 0.7 \pm 0.2$	$\Delta_{AD_2} = 1.4 \pm 0.2$ ppm

are not linear. In order to obtain values of the four parameters a least-squares procedure adapted from Wolberg[6] was used. For NMR data eq 2 and 3 can be used with Δ replacing $OD/[A]_0$ when $[D]_0 >> [A]_0$ or $OD/[D]_0$ when $[A]_0 >> [D]_0$. The differences between the chemical shift of a given proton in the complexes and the same proton in the free component (Δ_{AD}, Δ_{A_2D}, or Δ_{AD_2}) replace the appropriate values of ϵ.

The charge transfer peak of the complex is at 415 nm and it does not appear to vary in wavelength as the ratio of $[A]_0$ to $[D]_0$ changes over a very wide range. Therefore all the absorption readings were taken at this wavelength. Since the curvature predicted by eq 3 is not very pronounced, it is necessary to have values of OD for many solutions that cover a wide range of concentrations. Thus 16 solutions with a ratio of $[A]_0$ to $[D]_0$ ranging from 8 to 180 were used for one set of data while 23 solutions with a ratio of $[D]_0$ to $[A]_0$ from 4.5 to 150 were used for the other set.

At first glance it appears that the data fits eq 2a or 2b well, with only a small curvature in the linear plots. The regression coefficients for linear plots using all the data points are 0.955 for $[D]_0 >> [A]_0$ and 0.967 for $[A]_0 >> [D]_0$. The values of K_{AD} and ϵ_{AD} obtained from the two plots (Table I, lines 2 and 3) do not agree with each other. More importantly, neither sets of K_{AD} and ϵ_{AD} values agree with the values obtained using eq 1 on data from solutions with $[A]_0 \sim [D]_0$ (Table I, line 1). When the data for the solutions with an excess of one component are treated by eq 3a or 3b the parameters obtained have larger standard deviations than those obtained from eq 2a or 2b (Table I, lines 4 and 5). This increase in standard deviation is understandable since the regression coefficients indicate that the data fit the linear equations very well and using the termolecular model decreases the ratio of data to parameters by a half. Thus we cannot state that eq 3 gives a better fit of the data. However, within these limits the values of K_{AD} and ϵ_{AD} from eq 3a are in agreement with those given by eq 3b. Significantly, both sets of values are also in agreement with the data obtained from $[A]_0 \sim [D]_0$. From these results it is clear that both termolecular complexes exist in these solutions at different conditions.

Further evidence for the presence of AD_2 in solutions with $[D]_0 >> [A]_0$ was obtained from measurements of the chemical shifts of the protons in TNB. A linear plot of Δ vs. $\Delta/[D]_0$ has only a slight curvature with a high regression coefficient (0.981, 16 points), however, the value of K_{AD} obtained from eq 2 with these data (Table I, line 6) does not agree with the K_{AD} values obtained using the UV measurements. When these data are treated with eq 3 (Table I, line 7) the values of K_{AD} and K_{AD_2} obtained are in reasonable agreement with the values obtained from the UV data on the basis of termolecular species being present.

Due to the limited sensitivity of NMR measurements, data for solutions in which $[A]_0 \sim [D]_0$ could not be obtained. Also, attempts to follow the NMR spectra of the donor protons in solutions with $[A]_0 >> [D]_0$ were unsuccessful because the donor has a complex multiplet spectra. Addition of A caused the multiplets due to various donor protons to widen as well as move upfield. Thus it was impossible to obtain accurate values of Δ since changes in $[A]_0$ would cause one multiplet to overlap another. The only clear cut observation that can be made from the NMR data for $[A]_0 >> [D]_0$ is that the protons at the 2 and 3 positions in D were the ones most affected by the acceptor. This could indicate that there is a greater interaction at these position, in agreement with previous theoretical[7] and experimental suggestions.[7,8]

Acknowledgment. This work was partially supported by an NSF undergraduate research participation program, Grant No. SM176-03971.

References and Notes

(1) R. Foster in "Molecular Complexes", Vol. 2, R. Foster, Ed., Crane, Russak & Co., New York, N.Y., 1974, Chapter 3.
(2) C. C. Thompson, Jr., and Y. E. Ho, *J. Chem. Soc., Chem. Commun.*, 609 (1973).
(3) B. Dodson, R. Foster, A. A. S. Bright, M. I. Foreman, and J. Gorton, *J. Chem. Soc. B*, 1283 (1971).
(4) A. A. S. Bright, J. A. Chudek, and R. Foster. *J. Chem. Soc., Perkin Trans. 2*, 1256 (1975).
(5) M. T. Sung and J. A. Parker, *Proc. Natl. Acad. Sci., U.S.A.*, **69**, 1196 (1972).
(6) J. R. Wolberg, "Prediction Analysis", Van Nostrand, Princeton, N.J., 1976, Chapters 3 and 4.
(7) (a) A. Szent-Györgyi and I. Isenberg, *Proc. Natl. Acad. Sci., U.S.A.*, **46**, 1334 (1960); (b) A. Szent-Gyorgi, I. Isenberg, and J. McLaughlin, *ibid.*, **47**, 1089 (1961).
(8) (a) R. Foster and P. Hanson, *Trans. Faraday Soc.*, **60**, 2189 (1964); (b) R. Foster and C. A. Fyfe, *J. Chem. Soc. B*, 926 (1966).

Chemistry Department
University of North Dakota
Grand Forks, North Dakota 58201
Norman Kulevsky*
Sheila Specker

Received November 22, 1976

Vibrational Relaxation of Water at High Temperatures[1]

Publication costs assisted by the U.S. Air Force Office of Scientific Research

Sir: Several years ago we carried out a theoretical study of the ν_2 deexcitation of H_2O based on a model of vibration-to-rotation (VR) energy transfer.[2] The model is based on the rapid rotational motion of colliding molecules and is expected to describe the relaxation process at higher temperatures, but no experimental data were available at such temperatures for a rigorous test of the model. However, Kung and Center[3] recently reported the high temperature shock-tube measurements on the relaxation

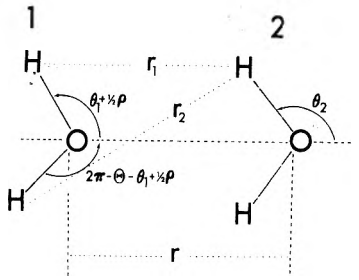

Figure 1. Interaction model and collision coordinates for $H_2O + H_2O$.

rates of H_2O, so a rigorous test of the model is now possible. In this note we shall reexamine the model developed in I for the ν_2 relaxation and show the temperature dependence of the deexcitation probability at high temperatures (1000–4000 K).

For the colliding molecules undergoing rotational motion, we define the interaction coordinates as in Figure 1. In this case the internal states of the colliding molecules are perturbed by the repulsive interaction of peripheral hydrogen atoms belonging to different molecules at close range. We consider molecule 1 to be in the ν_2 excited state (010) and its energy is transferred to molecule 2 intermolecularly through the VR process, while the molecules undergo translational motion. The collision model and the construction of the interaction potential have been represented in I in detail. For r significantly larger than d, we can approximate the interatomic distances as $r_1 = r - d\cos(\theta_1 + {}^1/_2\rho) + d\cos\theta_2 \simeq r - d\cos\theta_1 + d\cos\theta_2 + {}^1/_2 d\rho\sin\theta_1$ and $r_2 = r - d\cos(2\pi - \Theta - \theta_1 + {}^1/_2\rho) + d\cos\theta_2 \simeq r - d\cos\Theta\cos\theta_1 + d\sin\Theta\sin\theta_1 - {}^1/_2 d(\sin\Theta\cos\theta_1 + \cos\Theta\sin\theta_1)\rho + d\cos\theta_2$. Here the factor ${}^1/_2$ in ${}^1/_2\rho$ is introduced because both OH bonds of molecule 2 are bending in and out symmetrically to and from the axis which bisects the H–O–H angle; this factor was left out from I. Furthermore, the other angle of molecule 1 (i.e., $2\pi - \Theta - \theta_1 + {}^1/_2\rho$) is different from that defined in I. With these angles, we note that the angle of the instantaneous H–O–H bond of the molecule is $\Theta - \rho$ as it should. As shown in Figure 1, we take the same directional convention for both molecules, which is different from that shown in I. Also note that the angle ρ can be defined such that the instantaneous H–O–H bond angle is $\Theta + \rho$, but this would not change the result presented in this note. We now express the overall interaction energy in terms of these two interatomic distances in the exponential form $U(r, \rho, \theta_1, \theta_2) = D[(e^{l-r_1/a} + e^{l-r_2/a}) - 2(e^{l/2-r_1/2a} + e^{l/2-r_2/2a})]$, where D, a, and l are potential parameters; l does not appear in the final expression. The θ_1 average[2,4] of this function is

$$U(r,\rho,\theta_2) = A\exp\left(l - \frac{r}{a} - \frac{d}{a}\cos\theta_2\right) - B\exp\left(\frac{1}{2} - \frac{r}{2a} - \frac{d}{2a}\cos\theta_2\right) - \frac{Dd}{2a}\left[(I_1 - I_2)\exp\left(l - \frac{r}{a} - \frac{d}{a}\cos\theta_2\right) - (I_1' - I_2')\exp\left(\frac{l}{2} - \frac{r}{2a} - \frac{d}{2a}\cos\theta_2\right)\right]\rho \quad (1)$$

where $A = D[(a/d)\sinh(d/a) + I_0]$ and $B = 2D[(2a/d)\sinh(d/2a) + I_0']$. The functions Is, as well as the primed functions, are integrals over θ_1 and are already defined in I.

The energy transfer probability for the VR process can be given in the form

$$P_{010}^{000} = \hbar^{-2}[\langle 000|\rho|010\rangle]^2(Dd/2a)^2\left[\int_{-\infty}^{\infty}\left[(I_1 - I_2)\exp\left(l - \frac{r}{a} - \frac{d}{a}\cos\theta_2\right) - (I_1' - I_2')\exp\left(\frac{l}{2} - \frac{r}{2a} - \frac{d}{2a}\cos\theta_2\right)\right]\exp(i\omega t)\,dt\right]^2 \quad (2)$$

To evaluate the vibrational matrix element $\langle 000|\rho|010\rangle$ we used the method of symmetry coordinates which was first introduced by Howard and Wilson[5] and subsequently was used widely for the study of vibrations of polyatomic molecules.[6,7] Using this method, we determine the change ρ of the equilibrium angle and evaluate the matrix element as[8] $\langle 000|\rho|010\rangle = 1.56(\hbar/2M\omega d^2)^{1/2}$. Using the translational $r(t)$ and rotational $\theta_2(t)$ trajectories given in ref 4, we obtain

$$P_{010}^{000}(E_r, E_0) = \left(\frac{2c\omega}{\hbar M}\right)\left(\frac{\pi I_C a}{d^2}\right)^2(1+\alpha)^4 \times\left[\frac{D(I_1 - I_2)}{A}\right]^2\left[1 - \left(\frac{I_1' - I_2'}{I_1 - I_2}\right)\left(\frac{A}{2I_C}\right)\right]^{1/2} \times\left(\frac{1}{\omega\alpha_0}\right) - \frac{\tau_r E_0}{\mu\omega a^2}\Bigg]^2\exp(-2\omega\tau_r) \quad (3)$$

with

$$\tau_r = \left(\frac{\pi I_C}{2E_r}\right)^{1/2}\sum_{i=0}^{\infty}\frac{\Gamma({}^1/_2 + i)}{\Gamma(1+i)}\frac{\alpha_i}{E_r^{\,i}}$$

$\alpha_0 = (1+\alpha)a/d$, $\alpha_{1/2} = -B\alpha_0/2A^{1/2}$, $\alpha_1 = 0$, $\alpha_{3/2} = B^3\alpha_0/16A^{3/2}, \ldots$, $\alpha = 0.5(3a/d)^2[1 + (2a/d)^2/3]$. Here E_r is the initial rotational kinetic energy, I_C is the moment of inertia along the principal axis C, and $c = (1.56)^2$. Note that the term containing E_0, the initial translational energy, in the preexponential part determines the effect of the translational motion on the ν_2 relaxation. For simplicity, we express the preexponential part of eq 3 in the form $G[1 - K - \tau_r E_0/\mu\omega a^2]^2$. The thermal average of eq 3 over Boltzmann distributions of the initial translational and rotational energies gives[2,4]

$$P_{010}^{000}(T) = \left(\frac{4\pi\chi}{3kT}\right)^{1/2} G\left[(1-K)^2 - 2(1-K)\frac{\tau_r^* kT}{\mu\omega a^2} + 2\left(\frac{\tau_r^* kT}{\mu\omega a^2}\right)^2\right]\exp\left[-\frac{3\chi}{kT} + \frac{4g(D\chi)^{1/2}}{\pi kT} + \frac{16g^2 D}{3\pi^2 kT} + \frac{\hbar\omega}{2kT}\right] \quad (4)$$

where $g = [(2a/d)\sinh(d/2a) + I_0']/[(a/d)\sinh(d/a) + I_0]^{1/2}$, τ_r^* is τ_r given in eq 3 evaluated at $E_r^* = \chi - (8g/3\pi)(D\chi)^{1/2}$, and $\chi = [(I_C/2d^2)^{1/2}(1+\alpha)\pi\omega akT]^{2/3}$. The preexponential part is somewhat different from that given in I because of the differences in the interatomic distances and because of the presence of the factor c. Also note that the factor g is slightly different from the corresponding factor appearing in the exponential part in I. These corrections lead to significantly large transition probabilities than those given in I at higher temperatures. The quantity in the squared brackets of the preexponential part represents the effect of the translational motion on the ν_2 relaxation.

To calculate the transition probability we use the following molecular constants:[9,10] $d = 0.956$ Å, $\nu_2 = 1594$ cm^{-1}, and $D = 356k$; the potential parameter a has already been evaluated in I.[11] Calculated probabilities are plotted in

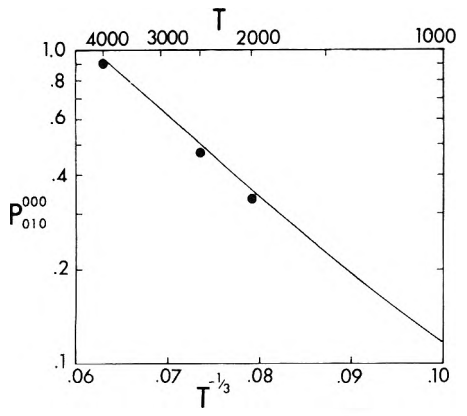

Figure 2. Plot of the deexcitation probability $P^{000}_{010}(T)$ as a function of $T^{-1/3}$. Experimental points at 2000, 2500, and 4000 K are taken from ref 3.

Figure 2; the probability increases with temperature showing a linear dependence of log $P^{000}_{010}(T)$ on $T^{-1/3}$ at higher temperatures. The slight deviation from the linearity at lower temperatures is in part due to the contribution of molecular attraction which is determined by the second and third terms in the exponent of eq 4. Probabilities at higher temperatures are quite large; e.g., at 2000, 2500, and 4000 K, they are 0.35, 0.64, and 0.93, respectively, which are consistent with the experimental data by Kung and Center.[3] At 2000, 2500, and 4000 K, Kung and Center reported the deexcitation rate constants 1.2×10^{-10}, 1.9×10^{-10}, and 4.6×10^{-10} cm^3/molecule s, respectively. The corresponding deexcitation probabilities[12] based on the collision diameter[10] 2.72 Å are 0.33, 0.47, and 0.91; see Figure 2. As the temperature decreases, the transition probability given by eq 4 becomes small due to the slowing down of both rotational and translational motion; at 1000 K it is 0.11.

In summary we may state that due to rapid rotational motion, the vibrational energy can be efficiently transferred to rotational motion of colliding molecules at high temperatures. During rotation, the colliding molecules also undergo translational motion, so a part of the vibrational energy is transferred to the translational motion. Therefore, the model used here includes the important contribution of the translational motion of the VR process. Since the rotational speed, as well as the translational motion, increases with temperature, the deexcitation probability also increases with temperature in a "normal" fashion; i.e., a positive temperature dependence. The calculation presented above shows that over the wide temperature range of 1000–4000 K, the change in the probability is less than one order of magnitude.

Acknowledgment. I am indebted to Dr. R. T. V. Kung and Dr. R. D. Center for making available their experimental data on rate coefficients at several different temperatures.

References and Notes

(1) This work was supported by the U.S. Air Force Office of Scientific Research, AFOSR 77-3163. Theoretical Chemistry Group Contribution No. 1083.
(2) H. K. Shin, *J. Phys. Chem.*, **77**, 346 (1973); hereforth referred to as I.
(3) R. T. V. Kung and R. E. Center, *J. Chem. Phys.*, **62** 2187 (1975).
(4) H. K. Shin, *J. Phys. Chem.*, **75**, 1079 (1971).
(5) J. B. Howard and E. B. Wilson, Jr., *J. Chem. Phys.*, **2**, 620 (1934).
(6) G. Herzberg, "Infrared and Raman Spectra", Van Nostrand, Princeton, N.J., 1945, pp 168–172.
(7) M. Karplus and R. N. Porter, "Atoms and Molecules", W. A. Benjamin, New York, N.Y., 1970, pp 511–517.
(8) The change ρ of the equilibrium angle due to the bending motion can be expressed in terms of the symmetry coordinates S_1 and S_2 as $\rho d = -2(1 + 2m_H/m_O)S_1 \sin(\Theta/2) - 2S_2 \cos(\Theta/2)$. The symmetry coordinates can finally be expressed as functions of the normal coordinates Q_1 and Q_2 or vice versa; i.e., $S_1 = a_{11}Q_1 + a_{12}Q_2$ and $S_2 = a_{21}Q_1 + a_{22}Q_2$, where the coefficient a's can be determined by a standard technique. For the present system for which only the bending mode matters, we can show that $S_1 = 0.921Q_2$ and $S_2 = -0.068Q_2$. Therefore, we find $\langle 000|\rho|010\rangle = 1.56 \cdot (\hbar/2M\omega d^2)^{1/2}$ where M is the effective reduced mass of H_2O associated with the bending mode ν_2; here $\omega = 2\pi\nu_2$.
(9) G. Herzberg, "Electronic Spectra of Polyatomic Molecules", Van Nostrand, Princeton, N.J., 1967, p 585 for d and ν_2.
(10) J. O. Hirschfelder, C. F. Curtiss, and R. B. Bird, "Molecular Theory of Gases and Liquids", Wiley, New York, N.Y., 1964, p 227 for D.
(11) In ref 1, the values for a for 300–2000 K are given. At 2500, 3000, and 4000 K, the values are 0.18, 0.18, and 0.17 Å, respectively.
(12) The rate constant is expressed as $k = ZP^{000}_{010}(T)$, where $Z = (1/2)[2^{1/2}\pi\sigma^2 n_0(8kT/\pi\mu)^{1/2}] = 7.9 \times 10^{-12} T^{1/2}$ cm^3/molecule s; here σ is the collision diameter, n_0 the number of molecules per cubic centimeter at 1 atm.

Department of Chemistry
University of Nevada
Reno, Nevada 89557

Hyung Kyu Shin

Received February 18, 1977

BETTER BET ON THE RABBIT

In the fable, the tortoise wins.
Of course, everybody knows it didn't really happen that way.
That's why they call it a fable.
No two ways about it. . .
THE RACE IS TO THE SWIFT.

To keep current on developments in the fast-moving discipline of physical chemistry, you need a journal that publishes up-to-date articles, communications, and symposia. Biweekly—now *that's* up to date. And you'll get biweekly information in. . .

THE JOURNAL OF PHYSICAL CHEMISTRY.

Swift is fine, but it's not nearly enough for an authoritative publication of ACS. You'll find more than 20 papers in every issue, covering spectroscopy, thermodynamics, reaction kinetics, and other areas of experimental and theoretical physical chemistry.
Would you like to be a little bit ahead of the rest of your field—the people who *don't* use the Journal? Then, just . . . *Complete, clip, and mail the coupon below.* Now?

- **new concepts**
- **new techniques**
- **new interpretations**

. . . plus reports on classical areas

The editors of the Journal of Physical Chemistry strive to select material that is useful in the classical areas of chemistry as well as in modern structural quantum mechanical areas. Start your subscription now. We'll do the rest.

Another service of ACS

The Journal of Physical Chemistry
American Chemical Society **1977**
1155 Sixteenth Street, N.W.
Washington, D.C. 20036

Yes, I would like to receive the JOURNAL OF PHYSICAL CHEMISTRY at the one-year rate checked below:

	U.S.	Foreign and Canada	Latin America
ACS Member *	☐ $24.00	☐ $ 34.00	☐ $ 33.00
Nonmember	☐ $96.00	☐ $106.00	☐ $105.00

Bill me ☐ Bill company ☐ Payment enclosed ☐

Air freight rates are available on request.

Name _____

Street _____ Home ☐ Business ☐

City _____ State _____ Zip _____

Journal subscriptions start in January '77.
Allow 60 days for your first copy to be mailed.
* NOTE: Subscriptions at ACS member rates are for personal use only.

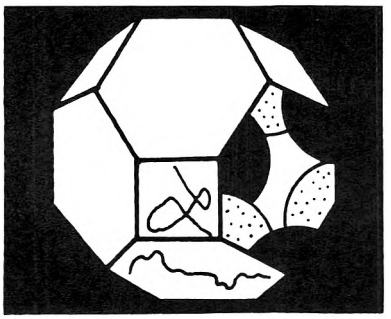

Molecular Sieves—II

ACS Symposium Series No. 40

James R. Katzer, *Editor*
University of Delaware

The Fourth International Conference co-sponsored by the Divisions of Colloid and Surface Chemistry, Petroleum Chemistry, and Physical Chemistry of the American Chemical Society and by the University of Chicago.

The excellent interdisciplinary treatment of zeolites provided in this new volume will be of particular value to chemists and chemical engineers in academia as well as in research and development in chemical and petroleum industries.

The collection—timely and comprehensive in scope—contains 58 formal program papers from the Fourth International Conference on Molecular Sieves. Review papers as well as those describing original research results offer a wide range of chemical information in five key areas—structure, synthesis and modification, adsorption and diffusion, catalysis, and technology.

These chapters illustrate the shift in research emphasis from classical framework structural papers to those concerned with the location and properties of transition metal complexes in zeolites. Sensitive electronic, nuclear, and other probes used in investigating zeolite properties are also examined.

732 pages (1977) clothbound $30.00
LC 77-720 ISBN 0-8412-0362-8

SIS/American Chemical Society
1155 16th St., N.W./Wash., D.C. 20036

Please send _____ copies of *SS 40 Molecular Sieves—II* at $30.00 per copy.

☐ Check enclosed for $ _____ ☐ Bill me. Postpaid in U.S. and Canada, plus 40 cents elsewhere.

Name _____

Address _____

City _____ State _____ Zip _____

A Century of Chemistry

The Role of Chemists and the American Chemical Society

Herman Skolnik, *Chairman, Editorial Board;* Kenneth M. Reese, *Editor*

An illuminating portrait of the life and times of the world's largest scientific society devoted to a single discipline.

The book portrays the growth and activities of the ACS in the context of a century that saw two World Wars, the Great Depression, the Cold War, the Space Race, the environmental movement, and numerous scientific and engineering advances.

The volume traces the development of chemical science and technology in the framework of the 27 technical divisions of the Society. It includes a compact, 100-year record of ACS people and events.

Part One: Historical Perspectives, Chemical Education, Professionalism, Publications, Impact of Government, Public Affairs, Intersociety Relations, Governance, Headquarters Staff and Operations, ACS Divisions and their Disciplines. Part Two: The Record

468 pages (1976) $15.00 clothbound
LC 76-6126 ISBN 0-8412-0307-5

SIS/American Chemical Society
1155 16th St., N.W./Wash., D.C. 20036

Please send _____ copies of *A Century of Chemistry* at $15.00 per book.

☐ Check is enclosed for $ _____. ☐ Bill me. Postpaid in U.S. and Canada, plus 40 cents elsewhere.

Name _____

Address _____

City _____ State _____ Zip _____

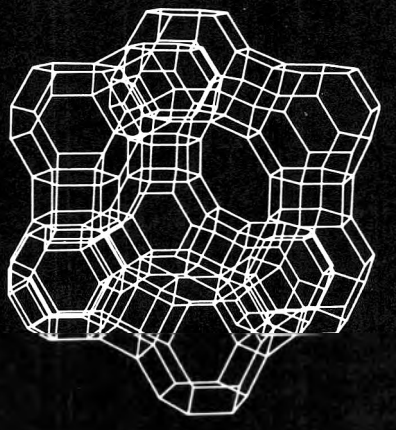

Zeolite Chemistry and Catalysis

ACS MONOGRAPH 171

Jule A. Rabo, *Editor*

A comprehensive overview of all important aspects of zeolite catalysis according to structure, chemistry and mechanism, and technology.

Chemists, material scientists, and chemical engineers working in the areas of catalysis and material science related to the petroleum and chemical industry will find this volume a useful and valuable addition to their reference library.

Specific topics include:

- origin and structure; IR studies of surfaces and surface reactions; stability and ultrastable zeolites
- salt occlusion in zeolite crystals; ESR studies; diffusion; hydrocarbon transformations; molecules containing hetero atoms; metal-containing zeolites
- shape selective catalysis; preparation and performance of cracking catalysts; hydrocracking, isomerization, and other industrial processes

796 pages (1976) clothbound $65.00
LC 76-17864 ISBN 0-8412-0276-1

SIS/American Chemical Society
1155 16th St., N.W./Wash., D.C. 20036

Please send _____ copies of *Zeolite Chemistry and Catalysis* at $65.00 per book.

☐ Check enclosed for $ _____. ☐ Bill me. Postpaid in U.S. and Canada, plus 40 cents elsewhere.

Name _____

Address _____

City _____ State _____ Zip _____